UCLA
UCLA Electronic Theses and Dissertations

Title
The role of iron and hepcidin in infection

Permalink
https://escholarship.org/uc/item/16x9x9q7

Author
Stefanova, Debora

Publication Date
2018

Peer reviewed|Thesis/dissertation

eScholarship.org Powered by the California Digital Library
University of California

UNIVERSITY OF CALIFORNIA

Los Angeles

The role of iron and hepcidin in infection

A dissertation submitted in partial satisfaction of the

requirements for the degree Doctor of Philosophy

in Molecular, Cellular and Integrative Physiology

by

Debora Chavdarova Stefanova

2018

ABSTRACT OF THE DISSERTATION

The role of iron and hepcidin in infection

by

Debora Chavdarova Stefanova
Doctor of Philosophy in Molecular, Cellular and Integrative Physiology
University of California, Los Angeles, 2018
Professor Elizabeta Nemeth, Chair

Iron is an essential trace nutrient for both higher organisms and bacteria. Consequently, hosts have evolved to sequester iron during infection, while pathogens have developed multiple iron acquisition systems to access iron pools in the host. Hepcidin, the master iron-regulatory hormone, is induced by inflammatory cytokines early during infections. Hepcidin lowers extracellular iron concentration by binding to and inhibiting the cellular iron exporter ferroportin. Using structural modeling and site-directed mutagenesis, we analyzed the structural basis of ferroportin interaction with hepcidin.

Hepcidin induction by inflammation causes a rapid decrease in plasma iron concentration (hypoferremia) accompanied by iron retention within target cells (macrophages, enterocytes, hepatocytes). This response to infection is highly conserved during vertebrate evolution. In the main part of this thesis, we show that hepcidin is essential for protection against extracellular Gram-negative bacterium *Yersinia enterocolitica*. At the

same inocula, hepcidin-deficient mice suffer 100% mortality while WT mice survive disease-free. We determine that it is the spontaneous iron overload of hepcidin-deficient mice that promotes susceptibility to infection. We find that hepcidin is not universally protective and plays no role in catheter-associated *Staphylococcus aureus* infection or in macrophage-tropic *Mycobacterium tuberculosis*. Surprisingly, infection with clinical isolates of *Escherichia coli*, which was not previously considered siderophilic, caused sepsis and 60% to 100% mortality in hepcidin deficiency and iron overload while WT mice suffered 0% mortality. Although the difference in survival was not as pronounced, similar results were obtained with another clinically common non-siderophilic pathogen: *Klebsiella pneumoniae*.

Furthermore, we found that the cause of increased susceptibility of hepcidin-deficient mice to certain Gram-negative pathogens (*Y. enterocolitica, K. pneumoniae, E. coli)* is the appearance in plasma of non-transferrin bound iron (NTBI), an iron species that stimulates the growth of these gram-negative bacteria. Endogenous hepcidin in wild-type mice or therapeutic administration of the hepcidin agonist minihepcidin to hepcidin-deficient mice eliminate NTBI and thus protect from infection-associated mortality in all 3 infection models.

We hypothesize that in future studies many more pathogens will manifest iron-dependent pathogenicity. With antibiotic resistance rising rapidly, understanding the role of iron and hepcidin in host defense can provide new tools for combating infections.

The dissertation of Debora Chavdarova Stefanova is approved.

James Tidball

Otto Yang

Tomas Ganz

Elizabeta Nemeth, Chair

University of California, Los Angeles

2018

Table of Contents

Biographical sketch ix

Overview: Introduction 1

1. Iron 2

2. Biological functions of iron 2

3. Iron distribution in the body 2

4. Iron species in the organism 4

4.1 Iron toxicity 4

4.2 Intracellular iron 4

4.3 Extracellular iron 5

4.3.1. Transferrin-bound iron 5

4.3.2 Non-transferrin bound iron (NTBI) 5

5. Iron transport 5

5.1 Systemic iron transport 6

5.2 Cellular iron transport 6

6. Hepcidin 6

6.1 Hepcidin nature and structure 7

6.2 Mechanism of action of hepcidin 7

6.3 Regulation of hepcidin production 8

6.3.1. Regulation by iron 8

6.3.2 Regulation by erythropoiesis 10

6.3.3 Regulation by inflammation 10

7. Hereditary hemochromatosis 11

8. Iron supplementation 12

9. Infection 13

9.1 Bacteria 13

9.2 Gram-positive bacteria 13

9.3 Gram-negative bacteria 13

9.4 Siderophilic pathogens 14

9.5 Yersinia enterocolitica 14

9.6 Klebsiella pneumoniae 15

9.7 Escherichia coli 15

9.8 Staphylococcus aureus 16

9.9 Mycobacterium tuberculosis 16

10. Iron and infection 16

10.1 Bacterial iron acquisition 17

10.2 Host defense and hepcidin 18

10.3 Nutritional immunity and the battle for iron 18

11. Minihepcidin 19

12. Summary 19

Reference list 20

CHAPTER 1: Endogenous hepcidin and its agonist mediate resistance to selected infections by clearing non-transferrin bound iron 26

Abstract 27

Introduction 27

Methods 27

Results 29

Discussion 37

References 38

Supplemental Materials and Methods 40

Supplemental References 46

Supplemental Figures 47

CHAPTER 2: Hepcidin-mediated iron sequestration protects against bacterial dissemination during pneumonia 58

Abstract 59

Introduction 59

Results 60

Discussion 65

Methods 66

References 69

Supplemental Figures 71

Supplemental Methods 75

CHAPTER 3: Hepcidin protects against lethal *E.coli* sepsis in mice inoculated with isolates from septic patients *(submitted manuscript)* 76

Introduction 77

Results 79

Discussion 93

Methods 95

Supplemental Data 101

Supplemental references 107

CHAPTER 4: Structure-function analysis of ferroportin defines the binding site and an alternative mechanism of action of hepcidin 111

Abstract 112

Introduction 112

Materials and Methods 113

Results 114

Discussion 120

References 122

Supplemental Methods 124

Supplemental Data 129

Supplemental References 146

Conclusion 148

BIOGRAPHICAL SKETCH

Education

Sofia University "Saint Kliment Ohridski" 2011-2012

Sofia, Bulgaria

Master of Science in Biophysics

Sofia University "Saint Kliment Ohridski" 2007-2011

Sofia, Bulgaria

Bachelor of Science in Molecular Biology

Fellowships

Dissertation Year Fellowship, UCLA 2017-2018

Publications

S. Aschemeyer, B. Qiao, **D. Stefanova**, E. Valore, A. Sek, T. Ruwe, K. Vieth, G. Jung, C. Casu, S. Rivella, M. Jormakka, B. Mackenzie, T. Ganz, E. Nemeth. *Structure-function analysis of ferroportin defines the binding site and an alternative mechanism of action of hepcidin.* Blood. 2018 Feb 22;131(8):899-910. doi: 10.1182/blood-2017-05-786590.

D. Stefanova, A. Raychev, J. Arezes, P. Ruchala, V. Gabayan, M. Skurnik, B.J. Dillon, M.A. Horwitz, T. Ganz, Y. Bulut and E. Nemeth, *Endogenous hepcidin and its agonist mediate resistance to selected infections by clearing non-transferrin-bound iron,* Blood, 2017 Jul 20; 130:245-257; doi: 10.1182/blood-2017-03-772715

K. Michels, Z. Zhang, A. Bettina, R. Cagnina, **D. Stefanova**, M. Burdick, S. Vaulont, E. Nemeth, T. Ganz, B. Mehrad, *Hepcidin-mediated iron sequestration protects against bacterial dissemination during Gram-negative pneumonia*, JCI Insight, 2017 Mar 23; 2(6): e92002

Abstracts and Presentations

Stefanova D*, Raychev A, Arezes J, Michels K, Dillon B, Horwitz M, Mehrad B, Ganz T, Nemeth E and Bulut Y, *Hepcidin protects against extracellular infections by eliminating*

non-transferrin-nound iron, Gordon Research Conference: Red Cells, Newport, Rhode Island, USA, June 2017, *poster presentation*

Stefanova D*, Raychev A, Arezes J, Michels K, Dillon B, Horwitz M, Mehrad B, Ganz T, Nemeth E and Bulut Y, *Hepcidin mediates host defense against gram-negative pathogens by controlling non-transferrin bound iron*; International BioIron Society Congress, Los Angeles, May 2017, *podium presentation*

Stefanova D, Raychev A, Michels K, Dillon B, Horwitz M, Mehrad B, Ganz T, Bulut Y, Nemeth E**, Hepcidin protects against extracellular infections by eliminating non-transferrin-bound iron*; American Society of Hematology annual meeting, San Diego, CA, December 2016, *podium presentation by E. Nemeth,*

Stefanova D*, Raychev A, Michels K, Dillon B, Horwitz M, Mehrad B, Ganz T, Bulut Y, Nemeth E*, Hepcidin protects against extracellular infections by eliminating non-transferrin-bound iron*; UCLA Department of Medicine Research Day*,* October 2016, *poster presentation*

Stefanova D*, Arezes J, Raychev A, Gabayan V, Ganz T, Bulut Y, Nemeth E, *The role of iron and hepcidin in Yersinia enterocolitica infection*; Annual UCLA Molecular, Cellular and Integrative Physiology program retreat, February 2016, *podium presentation*

Stefanova D*, Arezes J, Raychev A, Gabayan V, Ganz T, Bulut Y, Nemeth E, *The role of iron and hepcidin in Yersinia enterocolitica infection*; International BioIron Society Congress, Hangzhou, China, September 2015, *podium presentation*

Stefanova D*, Arezes J, Gabayan V, Ganz T, Nemeth E**,** Bulut Y, *The role of iron and hepcidin in Yersinia enterocolitica infection*; Pediatric Academic Society Meeting, San Diego, CA, April 2015, *poster presentation*

Awards

Blood journal plenary paper and cover; article *"Endogenous hepcidin and its agonist mediate resistance to selected infections by clearing non-transferrin-bound iron"* was selected as plenary paper and as the journal cover for the edition; July 2017

Best Podium Presentation Award; International BioIron Society Congress, Los Angeles, USA, *May 2017*

***Abstract selected among Best of ASH*;** American Society of Hematology annual meeting, San Diego, CA, December 2016

Best Poster Presentation Award (4th place); UCLA Department of Medicine Research Day, October 2016

Best Podium Presentation Award; International BioIron Society Congress, Hangzhou, China, *September 2015*

OVERVIEW: IRON METABOLISM AND INFECTION

Introduction

1. Iron

Iron is a transition element belonging to group 8 elements. It can change its oxidation state from -2 to +6, but +2 (ferro) and +3 (ferri) are the most common ones[1] at currently prevailing atmospheric oxygen concentrations. Iron is the most abundant element by mass on Earth, distributed in the Earth's inner and outer core as well as crust[2]. However, despite being abundant on the Earth's surface, most of the iron is not bioavailable since it is readily oxidized to insoluble ferric iron[3].

2. Biological functions of iron

In biological systems, because of its ability to easily change its oxidation state, iron participates as a cofactor in many proteins performing vital functions[4]. Iron is an essential component of some complexes in the electron transport chain: iron-sulfur clusters[5] and iron-heme[6] in cytochromes directly take part in transporting electrons. In the core of hemoglobin, heme-coordinated iron binds oxygen for transport to tissues[7]. Furthermore, iron is required as a cofactor in multiple enzymes and other proteins that participate in DNA replication and repair, regulation of gene expression, as well as cell proliferation and differentiation[8].

3. Iron distribution in the body

The adult human organism contains about 4 g of iron most of which (2-3 g) is in hemoglobin in red blood cells. Another major compartment is the liver where iron is stored in ferritin (about 1 g) and released when needed. However, every cell in the organism requires iron for its vital functions including but not limited to energy metabolism, replication, differentiation etc. Humans absorb 1-2 mg of iron daily from the food through

enterocytes, and this balances out the1-2 mg of iron that is lost daily from the body as result of desquamation and minor bleeding[4,9]. Most of the daily iron requirement (20-25 mg) is needed for the synthesis of hemoglobin in new red blood cells. This iron is provided by the recycling of old red blood cells by splenic and hepatic macrophages *(Figure 1)*.

Regulation of iron metabolism is similar between humans and mice but there is a difference in the rates of absorption and recycling – while humans absorb minor amount of iron from food and depend mostly on recycling, mice absorb about half of their daily iron requirement from food and thus depend less on iron recycling. Consequently, it is significantly easier and requires less time to manipulate mouse body iron content through changes in dietary iron supply than it would for a human[10].

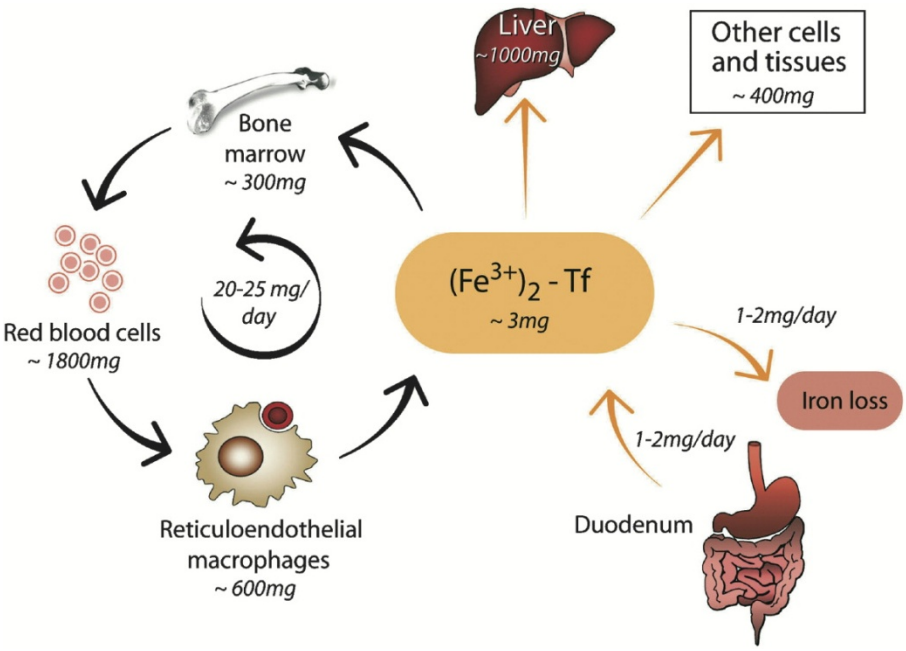


Figure 1. Iron distribution and utilization in the organism *(adapted from Hentze et al, Cell, 2004)*. The organism contains about 3-4g of iron, most of which is localized in red blood cells (around 1800mg) or stored in the liver (around 1000mg). Iron from recycled erythrocytes or from dietary absorption is transported towards the plasma from where it is directed towards tissues for utilization (mostly the bone marrow, requiring 20-25mg iron daily) or storage towards the liver. Minimal amounts of iron are lost daily (1-2mg) which is compensated for by dietary absorption.

4. Iron species in the organism

Iron, taken up from food or recycled from senescent red blood cells is transported through circulation towards different cell types based on their iron needs. In this process iron is bound to different carrier and storage proteins outside or inside the cell, and rarely remains “free” of such high affinity proteins.

4.1 Iron toxicity

Free iron is highly reactive and readily participates in Fenton’s reaction thus leading to the generation of free radicals[11] which can damage all types of biomolecules and consequently affect cellular and organismal functions[12]. As a result, under normal conditions iron is always complexed with proteins which act as chaperons and protect the organism from the highly reactive iron.

4.2 Intracellular iron

Intracellular iron is usually stored in ferritin, a 24-subunit protein that forms a nanocage which can encapsulate up to 4500 iron atoms[13]. Iron that is mobilized from ferritin or imported from the extracellular compartment is used for synthesis of prosthetic groups for ferroproteins (iron-sulfur clusters, heme etc.). Another iron species found inside cells is in the so-called labile iron pool (LIP). LIP is poorly defined due to its heterogeneity as well as difficulty of studying it. Generally LIP is a transition pool between extracellular iron and intracellular protein-bound iron. The chemical forms vary from iron associated with organic anions, through iron associated with polypeptides or membrane components. A common characteristic of LIP is that iron is loosely bound and is thus redox reactive[14].

4.3 Extracellular iron

Extracellular iron is formed as a result of iron efflux predominantly from enterocytes, macrophages and hepatocytes through ferroportin.

4.3.1 Transferrin-bound iron

Iron in the blood is usually bound to transferrin[15]. Transferrin is a two-domain protein and each domain can bind iron, thus yielding mono or diferric transferrin. The binding affinity of transferrin for iron[16] is very high with $Ka = 10^{20}\ M^{-1}$. Under normal physiologic conditions about 30% to 50% of plasma transferrin is bound to iron while the rest is unoccupied and available to bind surges of iron when needed.

4.3.2 Non-transferrin bound iron (NTBI)

In iron-loading conditions, the binding capacity of transferrin can be surpassed leading to the formation of non-transferrin bound iron[17] (NTBI). NTBI is heterogeneous but comprises mostly iron citrate and iron loosely bound to albumin[18]. Since NTBI is not tightly bound to any chaperone protein, it is highly reactive and is more readily available to pathogens. NTBI is taken up predominantly by the liver where the excess iron is stored but can also be taken up by other tissues such as the heart and adrenal glands leading to tissue iron overload and damage. Interestingly, NTBI is detectable in the blood of both humans and mice at transferrin saturation above 70% rather than at 100%[19]. NTBI concentration is likely determined by the kinetics of iron efflux combined with transferrin availability and ability of the liver to quickly deplete NTBI.

5. Iron transport

Once iron enters the organism, it is transported between different compartments for utilization, storage and recycling.

5.1 Systemic iron transport

Dietary iron is absorbed by enterocytes in the duodenum from where it flows out of the cells through the sole known iron exporter ferroportin. Once released into circulation iron is bound by the carrier protein transferrin and distributed to the cells that require iron[9]. In terms of quantity, most of the iron is utilized by the bone marrow for red blood cells synthesis. However, every cell in the organism requires iron.

5.2 Cellular iron transport

Most cells have a receptor for transferrin (TfR1) and can take up mono- or preferably diferric transferrin from the circulation[20]. Once inside the cell, iron is trafficked either for synthesis of ferroproteins or to ferritin for storage. Excess iron is released from the cell through the iron exporter ferroportin. The cells that handle the largest amounts of iron in the organism (enterocytes, hepatocytes, macrophages) have some specialized adaptations that allow them to perform their function. Enterocytes, for example, need to import ferric iron from the food so they have a ferrireductase duodenal cytochrome B on the apical membrane that reduces ferric to ferrous iron, which is then taken up by the divalent metal transporter 1 (DMT1). They also have an apical heme transporter to take up heme iron from meats[21]. Hepatocytes, which are responsible for iron storage in the organism, take up transferrin-bound iron through TfR1 but can also take up NTBI through the Zip14 transporter of divalent metals[22,23]. Similarly to other cells, hepatocytes store excess iron in ferritin. During the transfer of iron between cellular compartments labile iron pool (LIP) can be generated[14].

6. Hepcidin

Hepcidin is the master iron-regulatory hormone[24].

6.1 Hepcidin nature and structure

Despite changes in diet or blood loss, plasma iron concentrations are maintained quite stable in the range of 10 to 30 µM suggesting that there is homeostatic regulation. Hepcidin is the sole known iron regulatory hormone. It is a 25 amino acid peptide hormone with four disulfide bonds *(Figure 2)*. Hepcidin is produced by hepatocytes and secreted into circulation[25]. Other tissues have been shown to produce hepcidin, such as the heart[26] and the brain[27], which may play a role in local iron homeostasis but does not contribute significantly to systemic iron regulation. Hepcidin is a highly conserved molecule and the gene encoding it can be found in all vertebrate except possibly for most birds.

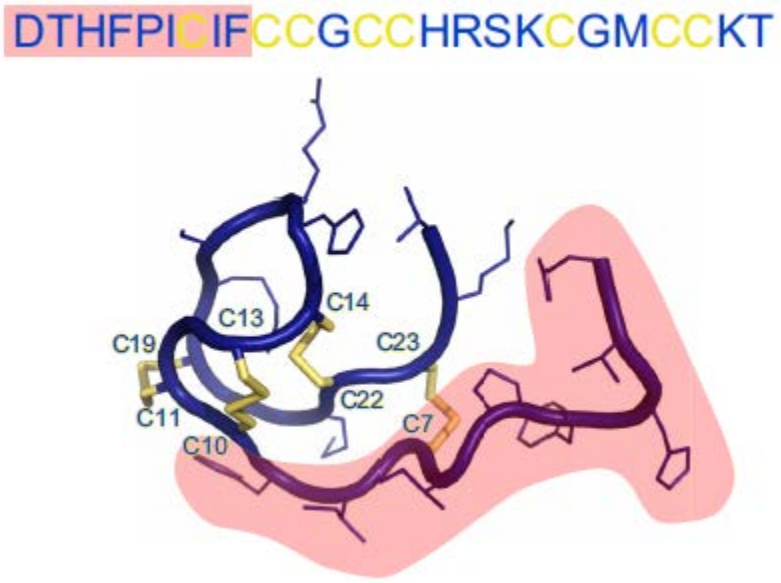


Figure 2. Hepcidin structure (adapted from Ganz, Physiol Rev, 2013). Hepcidin is 25 amino acid peptide hormone. It has 4 disulfide bonds in its structure (highlighted in yellow). The pink shading outlines the N-terminus which is required for hepcidin's biological activity.

6.2 Mechanism of action of hepcidin

Hepcidin is produced primarily by the liver and is released into the blood stream where it travels to target cells that express the iron transporter ferroportin. Hepcidin binds to ferroportin and causes ferroportin ubiquitination followed by internalization and degradation[28]. Consequently, iron efflux from the cell is inhibited leading to iron retention within cells and a decrease in extracellular iron concentration. Chapter 4 of this work

describes a novel mechanism of interaction between hepcidin and ferroportin that does not depend on internalization.

6.3 Regulation of hepcidin production

Hepcidin production is regulated transcriptionally by multiple stimuli, including iron, inflammation and erythropoiesis. There are, however, additional modes of hepcidin regulation, such as during pregnancy, that are currently being investigated[29].

6.3.1 Regulation by iron

Hepcidin production is regulated through feedback mechanisms by extracellular iron as well as tissue iron stores[30]. BMP6 is the main ligand that plays a role in this iron sensing feedback mechanism, although BMP2 also contributes. These BMPs are produced by sinusoidal endothelial cells in proportion to the iron content of the liver[31]. The BMPs reach the hepatocytes where they bind BMP receptors to phosphorylate SMAD1/5/8 which interact with SMAD4 to enter the nucleus and activate hepcidin transcription. The BMP-BMP receptor complex requires co-receptors among which hemojuvelin is absolutely essential *(Figure 3)*. Extracellular iron sensing is probably achieved through TfR2 or the TfR1/HFE complex binding holotransferrin, and interacting with the BMP receptor system to modulate its activity[32].

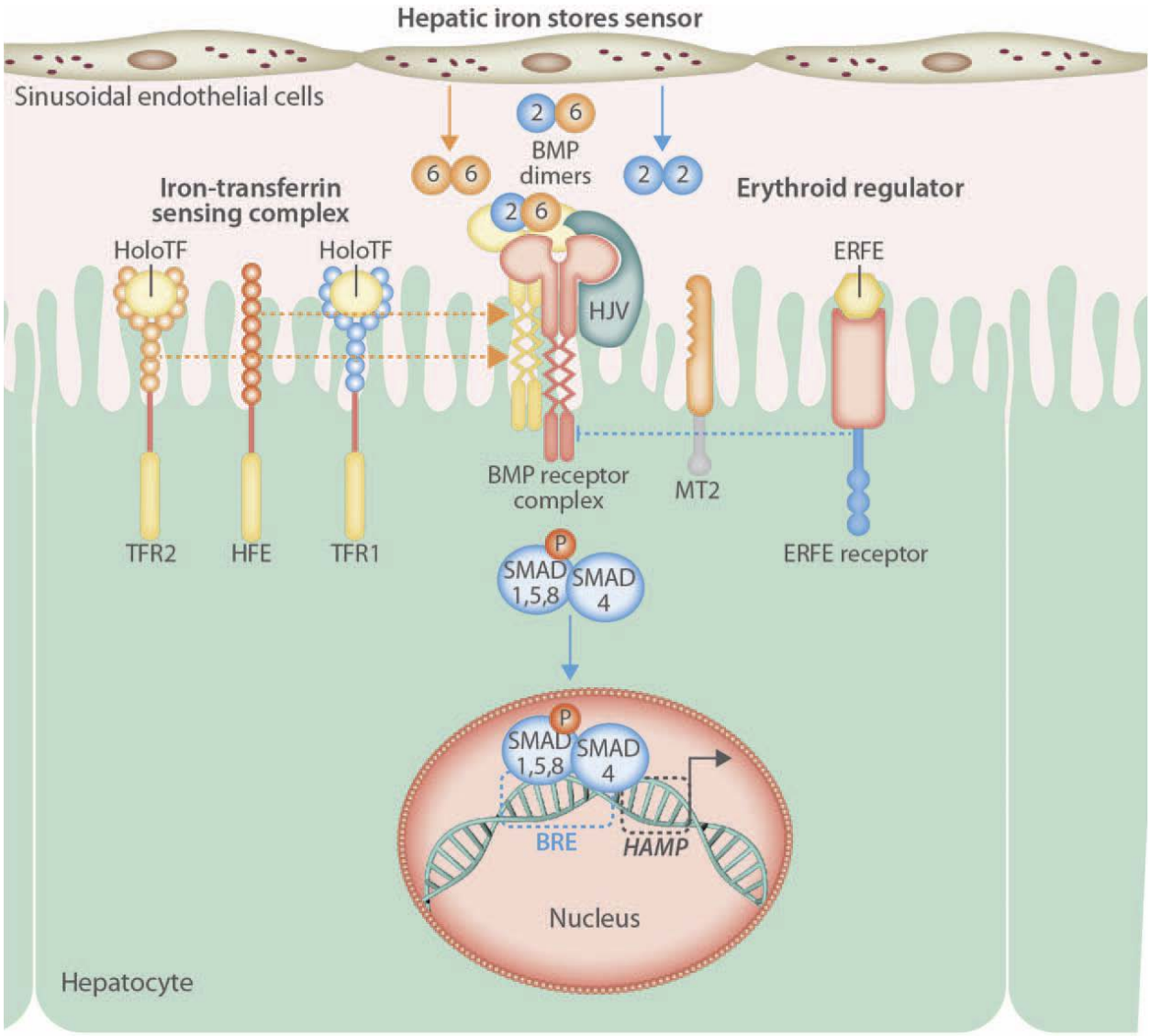


Figure 3. Regulation of hepcidin production (adapted from Coffey et al, HemaSphere, 2018). Hepcidin production is regulated by intracellular iron as well as by extracellular (holotransferrin). In conditions of iron overload, the concentration of holotransferrin increases, accompanied by increased production of BMP 6 and 2 by sinusoidal endothelial cells. The secreted BMPs form a complex with BMP receptors, hemojuvelin and other coreceptors. Consequently, BMPR activation leads to SMAD 1/5/8 phosphorylation which interact with SMAD4, enter the nucleus and activate hepcidin transcription. Erythropoiesis decreases hepcidin production through the action of the hormone erythroferrone which decreased SMAD 1/5/8 phosphorylation through unknown receptor and signaling pathways.

6.3.2 Regulation by erythropoiesis

Erythropoiesis requires a large proportion of the total iron flow for hemoglobin synthesis. In conditions of stress erythropoiesis, such as after phlebotomy, hepcidin production is suppressed to allow for higher iron flux into the plasma from where iron is distributed to erythropoietic tissues (mostly bone marrow). Hepcidin suppression is in response to erythropoietic iron demand is mediated by the hormone erythroferrone which is produced by the bone marrow[33].

6.3.3 Regulation by inflammation

Hepcidin was discovered as an antimicrobial peptide whose blood concentration was greatly increased by severe infection leading to significant excretion of hepcidin in the urine. However, later studies determined that even though hepcidin structurally resembles antimicrobial peptides and is induced by infection, it does not have direct antibacterial properties at physiological concentrations. Hepcidin production is induced by inflammation in IL-6 dependent manner through STAT-3 pathway *(Figure 4)* in response to both bacterial and viral pathogens[34]. Hepcidin upregulation inhibits iron efflux through ferroportin and leads to iron retention within target cells (with macrophages mostly affected) and rapid decrease in plasma iron concentration (hypoferremia). Hepcidin-induced hypoferremia is a highly conserved response to infection present in all vertebrates except for possibly most birds. Hypoferremia is hypothesized to be a mechanism of innate immunity to limit iron availability for pathogens[35]. In this thesis, the significance of this mechanism and the spectrum of pathogens affected is studied. However, in conditions of chronic inflammation, prolonged hepcidin upregulation restricts

iron availability for erythropoiesis and eventually leads to anemia known as anemia of inflammation[36].

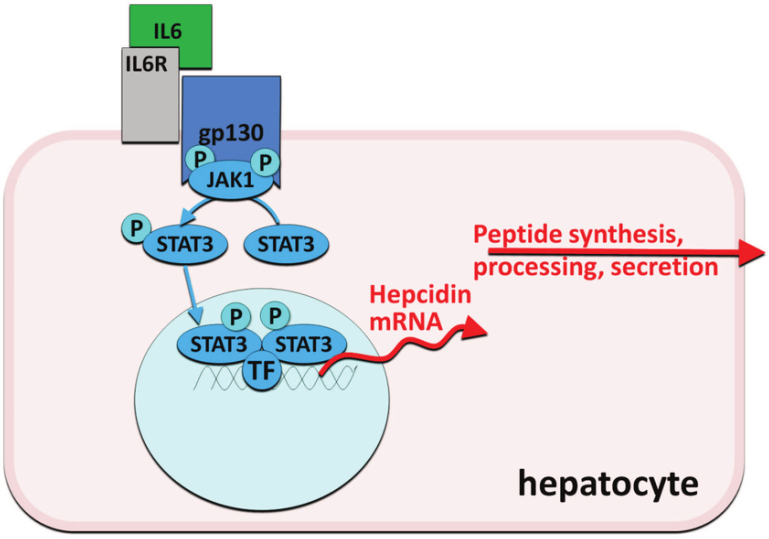


Figure 4. Hepcidin regulation by inflammation (adapted from Ganz and Nemeth, Hematology Am Soc Hematol Educ Program, 2011). During inflammation IL6 binds its receptor and activates the JAK-STAT3 pathway to stimulate hepcidin transcription

7. Hereditary hemochromatosis

Hereditary hemochromatosis (HH) is a genetic disease caused by hepcidin deficiency which results from mutations in some of the genes encoding hepcidin regulators or in the hepcidin gene itself. Consequently, the organism cannot properly regulate dietary iron absorption, and iron accumulates in tissues over time due to the inability of verterbrates to compensate by increasing iron excretion[37]. Excess iron deposition eventually leads to tissue damage and organ dysfunction. Hereditary hemochromatosis is classified into several types. The most severe is juvenile HH, usually caused by mutations in hepcidin or hemojuvelin, and leads to cardiomyopathies and endocrinopathies in late childhood/early adulthood[38]. Adult forms of HH are less severe and usually caused by mutations in the HFE gene, which are quite common in northern European people. Diagnosis of adult forms of HH is usually a result of laboratory testing targeted for health

maintenance or diagnosis of other conditions since HH patients rarely develop iron overload sufficient to cause symptoms or signs of disease on its own. Occasionally some patients develop cirrhosis or liver cancer. However, HH patients have been shown to be more susceptible to multiple infections, some of which preferentially cause systemic infection and/or sepsis in this population[39,40,41,42].

8. Iron supplementation

Anemia is one of the most prevalent health problems worldwide, affecting 1.62 billion people (WHO, 2008), and is most commonly caused by iron deficiency. The treatment for iron-deficiency anemia is iron supplementation which can be oral or intravenous (IV). Oral supplementation is easy, inexpensive and poses few risks. However, in some cases oral iron supplementation is either ineffective as a result of hepcidin upregulation, which blocks dietary iron absorption[43], or not rapid enough for the specific medical situation. Alternatively, iron can be administered IV, and in these preparations, iron is surrounded by a carbohydrate shell. IV iron preparations are taken up by macrophages where the complexes are processed and iron released into circulation. IV iron supplementation always leads to transient increase in serum iron concentration and the potential for formation of NTBI, and can even result in iron overload because of the large iron doses administered[44]. It is not surprising that IV iron has been associated with higher infection risk[45-47], which has led to guidelines that warn of the risks of IV iron therapy.

9. Infection

Infection is the invasion of the host organism by foreign microorganisms (bacteria, parasites, viruses) followed by their replication and dissemination in tissues, which eventually causes disease.

9.1 Bacteria

Bacteria are unicellular prokaryotic microorganisms that inhabit all ecosystems on Earth. Bacteria are usually very small, much smaller than a eukaryotic cell, measuring a few micrometers in length. Bacteria grow in various shapes from spheres (cocci) through rods (bacilli) to associations of multiple bacteria forming a shape that resembles a bunch of grapes. Bacterial shape is one of the characteristics used for their classification. Another important characteristic is the structure of the bacterial wall which determines whether a bacterium is Gram-positive, Gram-negative or falls in neither category.

9.2 Gram-positive bacteria

The designation of bacteria as Gram-positive or Gram-negative is based on their microscopic appearance after subjecting them to the Gram-stain test. Gram-positive bacteria retain the crystal violet dye because their cell wall is thicker and thus appear purple after the staining. The cell wall of Gram-positives is made of plasma membrane, small periplasmic space and a thick peptidoglycan layer. The most common Gram-positive pathogens in humans are *Streptococci* and *Staphylococci*[48].

9.3 Gram-negative bacteria

Gram-negative bacteria have a thinner cell wall which is why they do not retain crystal violet dye and are eventually stained pink with the counterstain. Their cell wall is made of plasma membrane, larger periplasmic space, thin peptidoglycan layer and outer

membrane where lipopolysaccharides (LPS) are found. When LPS is released from bacteria by the immune cells, it can cause an overwhelming reaction toxic for the organism, known as septic shock. The best known Gram-negative bacterium is *Escherichia coli* but other common ones include species such as *Yersinia*, *Pseudomonas*, *Klebsiella*, *Vibrio* etc[49].

9.4 Siderophilic pathogens

Siderophilic literally means iron-loving pathogens. This is a group of pathogens that do not cause serious disease in patients with normal iron status but cause severe overwhelming disease in iron-loaded patients[50]. Classical siderophilic pathogens are rare, with two characteristic exemplars: *Vibrio vulnificus*, which causes sepsis in iron-loaded hosts with 50% mortality[51], and *Yersinia enterocolitica*[52]. The molecular mechanism thought to underlie their dependence on host iron is the lack of production of small molecule iron chelators (siderophores) by the bacteria. Because of the absence of siderophores, it is thought that these bacteria are inefficient at stealing iron from host ferroproteins. This thesis demonstrates that more pathogens than previously realized, including clinically common ones, may fall into the siderophilic category and furthermore, that siderophilicity is not always defined by the lack of siderophore production.

9.5 Yersinia enterocolitica

Yersinia enterocolitica is a food-borne Gram-negative extracellular pathogen which causes self-limited gastro-intestinal infections in healthy people. However, in patients who are immunocompromised or iron-overloaded, *Y. enterocolitica* can cause systemic infection affecting multiple organs including the spleen and liver, with mortality rate up to 50%[52]. In a retrospective multicenter study, underlying iron overload was found in 40%

of *Yersinia* bacteremia patients[42], which combined with the higher incidence of septicemia in patients treated with the bacterial siderophore-derived iron chelator deferoxamine suggests a role for iron in the systemic spread of *Yersinia enterocolitica*.

9.6 Klebsiella pneumoniae

Klebsiella pneumoniae is a Gram-negative bacterium, commonly associated with hospital-acquired infections[53] including pneumonia, bloodstream infections, surgical site infections and meningitis (CDC), with mortality rates in severe infections as high as 70%[54]. Recently, the incidence of infections with multidrug resistant strains has increased immensely[55], while novel hypervirulent strains are spreading[56] that are capable of causing systemic infection in healthy people, with devastating sequelae. As was shown in the last few years, iron-acquisition related genes are a critical determinant of the associated hypervirulence.

9.7 Escherichia coli

Escherichia coli, the most common pathogenic Gram-negative bacterium, is among the most frequent causes of hospital-acquired infections, ranging from gastrointestinal through urinary tract infections to bacteremia and sepsis[57]. Sepsis is a leading cause of mortality affecting around 750 000 people in the USA alone each year and reaching mortality rates as high as 30% to 50%[58]. Hepcidin was recently shown to be a critical determinant of outcome in a urinary tract infection model, with HKO mice showing higher bacterial burden.

9.8 Staphylococcus aureus

Staphylococcus aureus is a Gram-positive bacterium present as a commensal in about 30% of the population (CDC). In most humans it is harmless but in people with

compromised or weakened immune system, such as hospitalized patients, it can cause severe infections including bacteremia, pneumonia, endocarditis, osteomyelitis etc. Medical device associated infections comprise 60-70% of all hospital acquired infections[59] and are usually caused by biofilms, with *Staphylococcus aureus* being a leading cause among these[60]. Recently, some *in vitro* studies supported a role for iron in *Staphylococcus aureus* biofilm formation[61].

9.9 Mycobacterium tuberculosis

Mycobacterium tuberculosis is the causative agent of tuberculosis. Tuberculosis (TB) is the second most deadly infection after HIV with more than 8 million new cases and 1 million deaths in 2010, mostly in the developing world (WHO). *M. tuberculosis* usually affects the lungs but can spread to other tissues leading to extrapulmonary tuberculosis, a condition common in immunocompromised or HIV co-infected patients. Recently it was shown that macrophage iron overload worsens tuberculosis outcome[62]. Iin agreement with that, hepcidin, which promotes iron retention within macrophages, was found to be an independent co-morbidity factor in TB/HIV co-infected patients[63]. However, *M. tuberculosis* can acquire iron from multiple sources including heme, ferritin and using siderophores.

10. Iron and infection

Multiple studies have shown that increased iron availability is linked to bacterial growth and pathogenicity[64,65]. Extensive *in vitro* data suggests that high iron concentration promotes growth of both extracellular and intracellular bacteria[66-68]. Administration of iron supplementation to infants in Africa and South Asia lead to unexpected serious adverse effects and mortality associated with malaria, gastrointestinal and respiratory infections[45-

[47]. In addition, hereditary hemochromatosis patients, who are iron-overloaded as a result of hepcidin deficiency, have been shown to be more susceptible to multiple infections.

10.1 Bacterial iron acquisition

Iron is required for vital processes which renders it essential for nearly all living organisms, including pathogens. However, iron in the host organism is rarely free but rather is chaperoned by high affinity proteins. Consequently, microbes needed to evolve efficient iron acquisition systems that can “steal” iron from these high affinity interactors[69]. The most common microbial strategy is the production and secretion of siderophores[70]. Siderophores are molecules that have even higher affinity for iron than many host ferroproteins and can thus extract iron from transferrin, ferritin or other sources. The siderophore carrying iron is then taken up through special receptors in the bacterium cell wall. Siderophore production, however, comes at a metabolic cost and siderophores can be readily utilized by competitor bacteria. *E. coli*, *K. pneumoniae*, *M. tuberculosis*, *S. aureus* and some serotypes of *Y. enterocolitica* (O8 studied in this work) can all produce siderophores. Another strategy some pathogens employ is direct utilization of host ferroproteins: some bacteria have receptors for transferrin-bound iron[71], others can utilize iron from ferritin and yet others take up heme or hemoglobin. Thus the battle for iron between host and pathogen is multifaceted and can sometimes be the determinant of infection outcome.

10.2 Host defense and hepcidin

Host defense mechanisms can be divided into early and late immune responses. Innate immunity, responsible for the early phase, is not specific to the pathogen and includes inflammation, complement, neutrophil and macrophage recruitment as well as

involvement of NK (natural killer) cells. Inflammation drives hepcidin upregulation in an IL-6 dependent manner thus rapidly decreasing plasma iron concentration[34]. Such hypoferremia of inflammation is hypothesized to be a mechanism of innate immunity to limit iron availability and thus limit bacterial replication[72]. In this thesis, we studied the significance of hepcidin-mediated hypferremic response, as well as its pathogen targets. If the pathogen is not cleared by innate immunity, adaptive immune response is mounted, which is specific for the pathogen and thus very effective but requires a longer period of time to activate sufficiently.

10.3 Nutritional immunity and the battle for iron

Nutritional immunity is a strategy of the organism to limit a critical nutrient in order to inhibit bacterial replication. Since zinc and iron are quite scarce in the human organism, but required for vital processes, it is mostly the sequestration of these metals that has been studied in the context of nutritional immunity. Iron is tightly bound to proteins, and inflammation during infection further decreases iron concentration in the extracellular compartment in hepcidin-dependent manner. However, pathogens secrete siderophores in an attempt to steal iron from the host ferroproteins. The host immune system has evolved further to produce lipocalin-2 which can bind bacterial siderophores, while bacteria, on the other hand, have evolved to take up iron from multiple other sources. Thus the battle for iron between host and pathogen happens on multiple levels and both sides constantly evolve to gain the upper hand[73].

11. Minihepcidin

Minihepcidins are synthetic hepcidin analogues based on the N-terminus of hepcidin which is required for its biological activity. Minihepcidins are, however, significantly

smaller (7 to 9 aminoacids) and are designed to contain unnatural aminoacids to inhibit proteolysis and increase their stability in blood plasma. In addition, some minihepcidins are PEGylated or acylated in order to decrease their clearance by the kidneys *(Figure 5)*. Altogether, these chemical modifications render minihepcidin more potent and with significantly longer half-life than endogenous hepcidin. Similarly to hepcidin, minihepcidin binds ferroportin and causes its ubiquitination, internalization and degradation thus decreasing iron efflux towards the blood[74]. At the doses used in this work, minihepcidin effect on serum iron can be detected up to 24h post injection.

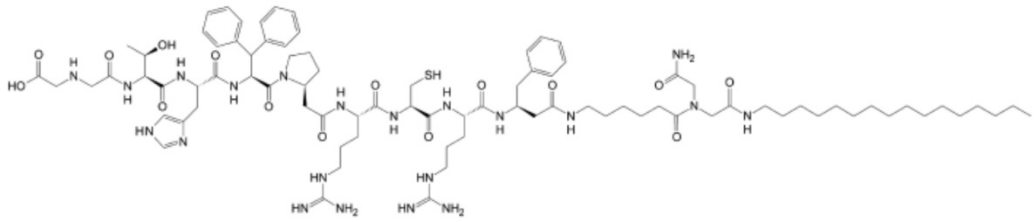


Figure 5 Chemical structure of minihepcidin PR73 (adapted from Chua et al, Bioorganic & Medicinal Chemistry Letters, 2015)

12. Summary

This work contributes towards understanding the role of iron in infection. Chapter 1 shows an extensive study of the role of iron and hepcidin in infection with extracellular, intracellular and biofilm forming pathogens leading to the conclusion that hepcidin is essential for protection against extracellular siderophilic Gram-negative *Yersinia enterocolitica*. The protective role of hepcidin is to clear non-transferrin bound iron (NTBI) from circulation. Chapter 2 shows that hepcidin plays a role in infection with non-siderophilic *Klebsiella pneumoniae*, although the effect on mortality is not as dramatic as in *Yersinia enterocolitica* model. Chapter 3 definitively shows that hepcidin deficiency and iron overload promote susceptibility to sepsis after infection with multiple clinical *E. coli*

isolates thus proving that clinically common pathogens such as *E. coli* behave as siderophilic, and can be targeted by manipulation of iron status by minihepcidin. Lastly, Chapter 4 provides evidence of a novel mechanism of interaction between hepcidin and ferroportin where ferroportin is not degraded but is rather occluded by hepcidin to inhibit iron export. Overall this work enhances our understanding of the role of hepcidin and iron in infection and provides insight into which pathogens could be therapeutically targeted by minihepcidin.

Reference list

1. Beard J, Dawson, H, Pinero, DJ. Iron metabolism: a comprehensive review. *Nutr Rev*. 1996;54(10):295-317.

2. Morgan J, Anders, E. Chemical composition of Earth, Venus, and Mercury. *Proc Natl Acad Sci U S A*. 1980;77(12):6973-6977.

3. Nakamori M, Hien, VT, Khan, NC, Lam, NT, Dung, NT, Uotsu, N, Shiomi, T, Okuhara, Y, Kise, M, Shigematsu, N, Yamamoto, S. Difructose anhydride III enhances bioavailability of water-insoluble iron in anemic Vietnamese women. *J Nutr Sci Vitaminol (Tokyo)*. 2010;56(3):191-197.

4. Ganz T, Nemeth E. Regulation of iron acquisition and iron distribution in mammals. *BiochimBiophysActa*. 2006;1763(7):690-699.

5. Johnson D, Dean, DR, Smith, AD, Johnson, MK. Structure, function, and formation of biological iron-sulfur clusters. *Annu Rev Biochem*. 2005;74:247-281.

6. Liu J, Chakraborty, S, Hosseinzadeh, P, Yu, Y, Tian, S, Petrik, I, Bhagi, A, Li, Y. Metalloproteins Containing Cytochrome, Iron–Sulfur, or Copper Redox Centers. *Chem Rev*. 2014;114(8):4366-4469.

7. Mairbäurl H, Weber, RE. Oxygen transport by hemoglobin. *Compr Physiol*. 2012;2(2):1463-1489.

8. Zhang C. Essential functions of iron-requiring proteins in DNA replication, repair and cell cycle control. *Protein Cell*. 2014;5(10):750-760.

9. Ganz T. Systemic iron homeostasis. *Physiol Rev*. 2013;93(4):1721-1741.

10. Ganz T, Nemeth E. Hepcidin and iron homeostasis. *BiochimBiophysActa*. 2012;1823(9):1434-1443.

11. Wardman P, Candeias, LP. Fenton chemistry: an introduction. *Radiat Res*. 1996;145(5):523-531.

12. Pietrangelo A. Mechanisms of iron hepatotoxicity. *J Hepatol*. 2016;65(1):226-227.

13. Wang W, Knovich MA, Coffman LG, Torti FM, Torti SV. Serum ferritin: Past, present and future. *BiochimBiophysActa*. 2010;1800(8):760-769.

14. Kakhlon O, Cabantchik, ZI. The labile iron pool: characterization, measurement, and participation in cellular processes. *Free Radic Biol Med*. 2002;33(8):1037-1046.

15. Huebers HA, Finch CA. The physiology of transferrin and transferrin receptors. *PhysiolRev*. 1987;67(2):520-582.

16. Aisen P, Leibman, A, Zweier, J. Stoichiometric and site characteristics of the binding of iron to human transferrin. *J Biol Chem*. 1978;253(6):1930-1937.

17. Brissot P, Ropert, M, Le Lan, C, Loréal, O. Non-transferrin bound iron: a key role in iron overload and iron toxicity. *Biochim Biophys Acta*. 2012;1820(3):403-410.

18. Hider RC, Silva AM, Podinovskaia M, Ma Y. Monitoring the efficiency of iron chelation therapy: the potential of nontransferrin-bound iron. *Ann N Y Acad Sci*. 2010;1202:94-99.

19. Piga A, Longo F, Duca L, et al. High nontransferrin bound iron levels and heart disease in thalassemia major. *AmJHematol*. 2009;84(1):29-33.

20. Hentze MW, Muckenthaler MU, Andrews NC. Balancing acts: molecular control of mammalian iron metabolism. *Cell*. 2004;117(3):285-297.

21. Duck K, Connor, JR. Iron uptake and transport across physiological barriers. *Biometals*. 2016;29:571-591.

22. Pinilla-Tenas JJ, Sparkman BK, Shawki A, et al. Zip14 is a complex broad-scope metal-ion transporter whose functional properties support roles in the cellular uptake of zinc and nontransferrin-bound iron. *AmJ PhysiolCell Physiol*. 2011;301(4):C862-C871.

23. Morgan EH, Baker E. Iron uptake and metabolism by hepatocytes. *FedProc*. 1986;45(12):2810-2816.

24. Park CH, Valore EV, Waring AJ, Ganz T. Hepcidin, a urinary antimicrobial peptide synthesized in the liver. *JBiolChem*. 2001;276(11):7806-7810.

25. Nemeth E, Ganz T. The role of hepcidin in iron metabolism. *Acta Haematol*. 2009;122(2-3):78-86.

26. Merle U, Fein E, Gehrke SG, Stremmel W, Kulaksiz H. The iron regulatory Peptide hepcidin is expressed in the heart and regulated by hypoxia and inflammation. *Endocrinology*. 2007;148(6):2663-2668.

27. Zechel S, Huber-Wittmer, K, von Bohlen und Halbach, O. Distribution of the iron-regulating protein hepcidin in the murine central nervous system. *J Neurosci Res*. 2006;84(4):790-800.

28. Nemeth E, Tuttle MS, Powelson J, et al. Hepcidin regulates cellular iron efflux by binding to ferroportin and inducing its internalization. *Science*. 2004;306(5704):2090-2093.

29. Sangkhae V, Nemeth, E. Regulation of the Iron Homeostatic Hormone Hepcidin. *Adv Nutr*. 2017;8(1):126-136.

30. Zhao N, Zhang AS, Enns CA. Iron regulation by hepcidin. *J Clin Invest*. 2013;123(6):2337-2343.

31. Canali S, Zumbrennen-Bullough, KB, Core, AB, Wang, CY, Nairz, M, Bouley, R, Swirski, FK, Babitt, JL. Endothelial cells produce bone morphogenetic protein 6 required for iron homeostasis in mice. *Blood*. 2017;129(4):405-414.

32. D'Alessio F, Hentze MW, Muckenthaler MU. The hemochromatosis proteins HFE, TfR2, and HJV form a membrane-associated protein complex for hepcidin regulation. *J Hepatol*. 2012;57(5):1052-1060.

33. Kautz L, Jung G, Valore EV, Rivella S, Nemeth E, Ganz T. Identification of erythroferrone as an erythroid regulator of iron metabolism. *NatGenet*. 2014;46(7):678-684.

34. Rodriguez R, Jung,CL, Gabayan, V, Deng, JC, Ganz, T, Nemeth, E, Bulut, Y. Hepcidin Induction by Pathogens and Pathogen-Derived Molecules Is Strongly Dependent on Interleukin-6. *Infection and Immunity*. 2014;82(2):745-752.

35. Arezes J, Jung, G, Gabayan, V, Valore, E, Ruchala, P, Gulig, PA, Ganz, T, Nemeth, E, Bulut, Y. Hepcidin-induced hypoferremia is a critical host defense mechanism against the siderophilic bacterium *Vibrio vulnificus*. *Cell Host Microbe*. 2015;17(1):47-57.

36. Kim A, Fung E, Parikh SG, et al. A mouse model of anemia of inflammation: complex pathogenesis with partial dependence on hepcidin. *Blood*. 2014;123(8):1129-1136.

37. Ganz T, Nemeth E. Hepcidin and disorders of iron metabolism. *AnnuRevMed*. 2011;62:347-360.

38. Pietrangelo A. Hereditary hemochromatosis--a new look at an old disease. *The New England Journal of Medicine*. 2004;350(23):2383-2397.

39. Christopher GW. *Escherichia coli* bacteremia, meningitis, and hemochromatosis. *Arch Intern Med*. 1985;145(10):1908.

40. Gerhard GS, Levin KA, Price GJ, Wojnar MM, Chorney MJ, Belchis DA. *Vibrio vulnificus* septicemia in a patient with the hemochromatosis HFE C282Y mutation. *ArchPathol Lab Med*. 2001;125(8):1107-1109.

41. Manso C, Rivas, I, Peraire, J, Vidal, F, Richart, C. Fatal *Listeria* meningitis, endocarditis and pericarditis in a patient with haemochromatosis. *Scand J Infect Dis*. 1997;29(3):308-309.

42. Piroth L, Meyer, P, Bielefeld, P, Besancenot, JF. Yersinia bacteremia and iron overload. *Rev Med Interne*. 1997.

43. Moretti D, Goede, JS, Zeder, C, Jiskra, M, Chatzinakou, V, Tjalsma, H, Melse-Boonstra, A, Brittenham, G, Swinkels, DW, Zimmermann, MB. Oral iron supplements increase hepcidin and decrease iron absorption from daily or twice-daily doses in iron-depleted young women. *Blood*. 2015;126(17):1981-1999.

44. Cançado R, Muñoz, M. Intravenous iron therapy: how far have we come? *Rev Bras Hematol Hemoter*. 2011;33(6):461-469.

45. Soofi S, Cousens, S, Iqbal, SP, Akhund, T, Khan, J, Ahmed, I, Zaidi, AK, Bhutta, ZA. Effect of provision of daily zinc and iron with several micronutrients on growth and morbidity among young children in Pakistan: a cluster-randomised trial. *Lancet*. 2013;382.

46. Zlotkin S, Newton, S, Aimone, AM, Azindow, I, Amenga-Etego, S, Tchum, K, Mahama, E, Thorpe, KE, Owusu-Agyei, S. Effect of iron fortification on malaria incidence in infants and young children in Ghana: a randomized trial. *JAMA*. 2013;310:9.

47. Manno D, Siame, J, Larke, N, Baisley, K, Kasonka, L, Filteau, S. Effect of multiple micronutrient-fortified food on mild morbidity and clinical symptoms in Zambian infants: results from a randomised controlled trial. *Eur J Clin Nutr*. 2011;65:3.

48. Woodford N, Livermore, DM. Infections caused by Gram-positive bacteria: a review of the global challenge. *J Infect* 2009;S1:S4-s16.

49. Kaye K, Pogue, JM. Infections Caused by Resistant Gram-Negative Bacteria: Epidemiology and Management. *Pharmacotherapy*. 2015;35(10):949-962.

50. Weinberg ED. Iron availability and infection. *Biochimica et Biophysica Acta (BBA) - General Subjects*. 2009;1790(7):600-605.

51. Horseman M, Surani, S. A comprehensive review of Vibrio vulnificus: an important cause of severe sepsis and skin and soft-tissue infection. *Int J Infect Dis*. 2011;15(3):9.

52. Rabson A, Hallett, AF, Koornhof, HJ. Generalized Yersinia enterocolitica infection. *J Infect Dis*. 1975.

53. Kuehn B. Nightmare bacteria on the rise in US hospitals long- term care facilities. . *JAMA*. 2013;309.

54. Morgan ME HC, Cooke RW. Klebsiella infection in a neonatal intensive care unit: role of bacteriological surveillance. *J Hosp Infect*. 1984;5:9.

55. Quale JM LD, Bradford PA, Visalli M, Ravishankar J, Flores C, Mayorga D, Vangala K, Adedeji A. Molecular epidemiology of a citywide outbreak of extended-spectrum -lactamase-producing Klebsiella pneumoniae infection. . *Clin Infect Dis*. 2002;35:7.

56. Shon A, Bajwa, RP,Russo,TA. Hypervirulent(hypermucoviscous) Klebsiella pneumoniae: a new and dangerous breed. *Virulence*. 2013;4:9.

57. Kaper J, Nataro, JP, Mobley, HLT. PATHOGENIC ESCHERICHIA COLI. *Nature Reviews Microbiology*. 2004;2:123-140.

58. Angus D, Linde-Zwirble, WT, Lidicker, J, Clermont, G, Carcillo, J, Pinsky, MR. Epidemiology of severe sepsis in the United States: analysis of incidence, outcome, and associated costs of care. *Crit Care Med*. 2001;29:1303-1310.

59. Bryers J. Medical biofilms. . *Biotechnol Bioeng*. 2008.

60. Kwiecinski J, Na, M, Jarneborn, A, Jacobsson, G, Peetermans, M, Verhamme, P, Jin, T. Tissue plasminogen activator coating on surface of implants reduces *Staphylococcus aureus* biofilm formation. *Appl Environ Microbiol* 2015;82(1):394-401.

61. Lin MH, Shu JC, Huang HY, Cheng YC. Involvement of Iron in Biofilm Formation by *Staphylococcus aureus*. *PLoS ONE*. 2012;7(3):e34388.

62. Boelaert J, Vandecasteele, SJ, Appelberg, R, Gordeuk, VR. The effect of the host's iron status on tuberculosis. *J Infect Dis*. 2007.

63. Armitage A, Moran, E. HIV-Associated Tuberculosis: Does the Iron-Regulatory Hormone Hepcidin Connect Anemia With Poor Prognosis? *Journal of Infectious Diseases* 2015;213(1):3-5.

64. Khan F, Fisher, MA, Khakoo, RA. Association of hemochromatosis with infectious diseases: expanding spectrum. *International journal of infectious diseases*. 2007;11:6.

65. Michels K, Nemeth, E, Ganz, T, Mehrad, B. Hepcidin and Host Defense against Infectious Diseases. *PLoS Pathog*. 2015;11.

66. Tam S, Lee, CJ, Winter, RE. Hemin Utilization Is Related to Virulence of Streptococcus pneumoniae. *Infection and Immunity*. 1993.

67. Chlosta S, Fishman DS, Harrington L, et al. The iron efflux protein ferroportin regulates the intracellular growth of Salmonella enterica. *Infect Immun*. 2006;74(5):3065-3067.

68. Singh PK, Parsek MR, Greenberg EP, Welsh MJ. A component of innate immunity prevents bacterial biofilm development. *Nature*. 2002;417(6888):552-555.

69. Wandersman C, Delepelaire P. BACTERIAL IRON SOURCES: From Siderophores to Hemophores. *Annual Review of Microbiology*. 2004;58(1):611-647.

70. Miethke M, Marahiel, MA. Siderophore-Based Iron Acquisition and Pathogen Control. *Microbiol Mol Biol Rev*. 2007;71:38.

71. Barber MF, Elde NC. Escape from bacterial iron piracy through rapid evolution of transferrin. *Science*. 2014;346(6215):1362-1366.

72. Drakesmith H, Prentice AM. Hepcidin and the iron-infection axis. *Science*. 2012;338(6108):768-772.

73. Skaar E. The Battle for Iron between Bacterial Pathogens and Their Vertebrate Hosts. *PLoS Pathog*. 2010;6(8):e1000949.

74. Preza GC, Ruchala P, Pinon R, et al. Minihepcidins are rationally designed small peptides that mimic hepcidin activity in mice and may be useful for the treatment of iron overload. *J ClinInvest*. 2011;121(12):4880-4888.

CHAPTER 1

Endogenous hepcidin and its agonist mediate resistance to selected infections by clearing non-transferrin bound iron

Plenary Paper

blood

RED CELLS, IRON, AND ERYTHROPOIESIS

Endogenous hepcidin and its agonist mediate resistance to selected infections by clearing non–transferrin-bound iron

Deborah Stefanova,[1] Antoan Raychev,[2] Joao Arezes,[3] Piotr Ruchala,[2] Victoria Gabayan,[2] Mikael Skurnik,[4] Barbara J. Dillon,[2] Marcus A. Horwitz,[2] Tomas Ganz,[2,5] Yonca Bulut,[6,*] and Elizabeta Nemeth[2,*]

[1]Molecular, Cellular, and Integrative Physiology Graduate Program and [2]Department of Medicine, David Geffen School of Medicine, University of California Los Angeles (UCLA), Los Angeles, CA; [3]Medical Research Council (MRC) Human Immunology Unit, MRC Weatherall Institute for Molecular Medicine, University of Oxford, Oxford, United Kingdom; [4]Department of Bacteriology and Immunology, University of Helsinki, Helsinki, Finland; and [5]Department of Pathology and [6]Department of Pediatrics, David Geffen School of Medicine, UCLA, Los Angeles, CA

Key Points

- In mouse models, hepcidin participates in innate immunity by controlling NTBI.
- NTBI-dependent infections can be treated with hepcidin agonists in mouse models of hereditary hemochromatosis or parenteral iron overload.

The iron-regulatory hormone hepcidin is induced early in infection, causing iron sequestration in macrophages and decreased plasma iron; this is proposed to limit the replication of extracellular microbes, but could also promote infection with macrophage-tropic pathogens. The mechanisms by which hepcidin and hypoferremia modulate host defense, and the spectrum of microbes affected, are poorly understood. Using mouse models, we show that hepcidin was selectively protective against siderophilic extracellular pathogens (*Yersinia enterocolitica* O9) by controlling non–transferrin-bound iron (NTBI) rather than iron-transferrin concentration. NTBI promoted the rapid growth of siderophilic but not nonsiderophilic bacteria in mice with either genetic or iatrogenic iron overload and in human plasma. Hepcidin or iron loading did not affect other key components of innate immunity, did not indiscriminately promote intracellular infections (*Mycobacterium tuberculosis*), and had no effect on extracellular nonsiderophilic *Y enterocolitica* O8 or *Staphylococcus aureus*. Hepcidin analogs may be useful for treatment of siderophilic infections. (*Blood*. 2017;130(3):245-257)

Introduction

During infections, inflammatory signals potently stimulate the production of the iron-regulatory hormone hepcidin,[1] causing iron sequestration in macrophages and decreased plasma iron concentrations.[2] Hypoferremia is hypothesized to limit iron availability for growth of extracellular microbes but iron retention in macrophages is thought to promote the growth of macrophage-tropic pathogens.

Hereditary hemochromatosis patients, who are iron-overloaded as a result of hepcidin deficiency, are more susceptible to infections with *Escherichia coli*,[3] *Vibrio vulnificus*,[4] *Listeria monocytogenes*,[5] and *Yersinia enterocolitica*.[6,7] Patients with transfusional iron overload are also at increased risk of infections.[8] Conversely, an association between elevated hepcidin and tuberculosis disease progression was reported.[9] The mechanisms by which hepcidin and iron regulation contribute to host defense remain largely unexplored in mammalian models of infection. We previously showed that hepcidin is critical for mouse survival in *V vulnificus* infection,[10] but extremely rapid lethality (12 hours) prevented detailed analysis of the mechanisms involved, and the relevance for clinically more common infections was unknown.

In this study, we comprehensively examine the role of hepcidin and iron in innate immunity, using a broad range of murine infection models, conditions of genetic or iatrogenic iron overload or iron depletion, as well as studies of iron-dependent growth of bacteria ex vivo. We examined infections with extracellular *Y enterocolitica* (siderophilic and nonsiderophilic strains) and *Staphylococcus aureus*, as well as intracellular *Mycobacterium tuberculosis*. We note that the term "siderophilic" is loosely defined and is not based on molecular characterization of the organisms. Rather, it generally applies to microbes whose virulence is enhanced in iron-overloaded hosts, with *V vulnificus* and certain strains of *Y enterocolitica* considered the classic examples.

We propose that the primary host defense function of hepcidin is not to decrease extracellular iron concentration (ie, transferrin-bound iron) but to eliminate non–transferrin-bound iron (NTBI). NTBI is a heterogeneous group of iron species that appears in circulation when the binding capacity of transferrin is exceeded, such as in iron-overload conditions. NTBI encompasses ferric citrate, acetate, and iron loosely bound to albumin,[11] and may be more readily utilizable by pathogens than transferrin-bound iron. We also explore the therapeutic potential of hepcidin agonists in treating infections that are exacerbated by NTBI.

Methods

Details are provided in supplemental Materials and methods (see supplemental Data, available on the *Blood* Web site).

Submitted 9 March 2017; accepted 29 April 2017. Prepublished online as *Blood* First Edition paper, 2 May 2017; DOI 10.1182/blood-2017-03-772715.

*Y.B. and E.N. contributed equally to this study.

The online version of this article contains a data supplement.

There is an Inside *Blood* Commentary on this article in this issue.

The publication costs of this article were defrayed in part by page charge payment. Therefore, and solely to indicate this fact, this article is hereby marked "advertisement" in accordance with 18 USC section 1734.

© 2017 by The American Society of Hematology

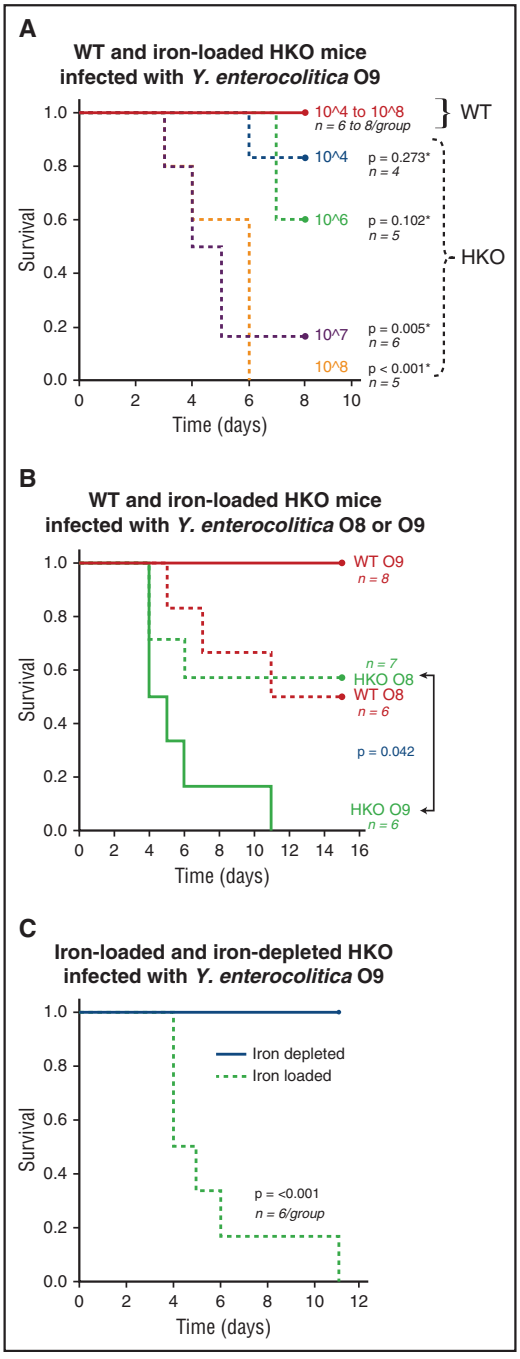


Figure 1. Hepcidin deficiency and resulting iron overload promote mortality from siderophilic but not nonsiderophilic *Y enterocolitica*. (A) Survival after oral infection with increasing doses of siderophilic *Y enterocolitica* O9 (10^4-10^8 CFUs per mouse) of WT mice with normal iron status or naturally iron-loaded HKO mice. *Comparison of HKO to WT mice infected with the same dose. (B) Survival curve for WT or naturally iron-loaded HKO mice infected through oral gavage with 10^8 CFUs per mouse *Y enterocolitica* serotype O9 (siderophilic) or O8 (nonsiderophilic). (C) Survival of naturally iron-loaded or dietary iron-depleted HKO mice after oral infection with 10^8 CFUs per mouse *Y enterocolitica* O9. Infection with siderophilic O9 bacteria resulted in significantly greater mortality than infection with nonsiderophilic O8 bacteria in iron-loaded HKO mice. Survival is defined in "Methods." Statistical comparison of survival was performed using multifactorial Kaplan-Meier log-rank analysis.

Bacterial organisms

We used *Y enterocolitica* O9 strain Ruokola/71, *Y enterocolitica* O8 strain WA (ATCC 27729), *S aureus* (strain Xen36 derived from the bacteremia isolate ATCC 49525), and *M tuberculosis* (Erdman strain).

Animal models

All animal studies were approved by the University of California Los Angeles (UCLA) Office of Animal Research Oversight. All mouse strains were on a C57BL/6 background: C57BL/6 wild-type (WT) mice, hepcidin-1 knockout mice (HKO), LysEGFP mice (enhanced green fluorescent protein [EGFP] insertion into lysozyme M locus[12]), and HKO/LysEGFP mice. Iron depletion of HKO mice was achieved with a 4-ppm Fe diet for 6 to 8 weeks, and iron loading of WT mice was achieved by intraperitoneal (IP) injection of 20 mg of iron dextran. For minihepcidin treatment, each mouse received 100 nmol PR73[10] or solvent by IP injection daily. Researchers were not blinded as to which treatment group each mouse belonged.

***Y enterocolitica* strains.** O9 (10^4-10^8 colony-forming units [CFUs] per mouse) and O8 (10^8 CFUs per mouse) were administered by oral gavage or IP injection.

Bioluminescent S aureus. Catheters incubated in 10^7 CFU/mL *S aureus* were inserted under the skin, and mice imaged over 7 days with IVIS 200 from Xenogen Inc.

M tuberculosis. Mice were challenged by aerosol with 30 CFU per mouse, and euthanized 5 and 10 weeks later.

Assessment of animal survival

As prescribed by animal use regulations at UCLA, death was not used as an end point. Rather, the mice were euthanized when showing characteristics predictive of imminent mortality, including rapid weight loss combined with cessation of water and food intake, loss of grooming, and immobility despite stimulation.

NTBI assessment by eLPI

NTBI refers to a heterogeneous group of iron complexes in circulation. To measure the NTBI content of mouse and human plasma, we used an "enhanced labile plasma iron" (eLPI) assay. The eLPI assay is an adaptation of a published protocol[13] based on catalytic conversion on nonfluorescent dihydrorhodamine to fluorescent rhodamine, in the presence and absence of the iron chelator deferiprone, but with an inclusion of a mild metal-mobilizing agent, nitriloacetate.

In vitro assay for *Y enterocolitica*

Human plasma was incubated with 0 to 60 μM ferric ammonium citrate (FAC), and mixed with concentrated liquid agar to produce 90% plasma agar plates. *Y enterocolitica* (5×10^3 CFUs) was plated on plasma agar, and bacterial growth assessed using a dissecting microscope.

In vitro assay for *V vulnificus*

V vulnificus (1×10^3 CFU/mL) were grown for 10 hours in a plated reader, in 250 μL of human plasma supplemented with 0 to 100 μM of either FAC, holotransferrin, or apotransferrin, and optical density at 600 nm measured.

Additional methods

Histopathology, CFU count, analysis of LysEGFP mice, measurement of iron parameters, gene expression, and hepcidin enzyme-linked immunosorbent assay are described in supplemental Materials and methods.

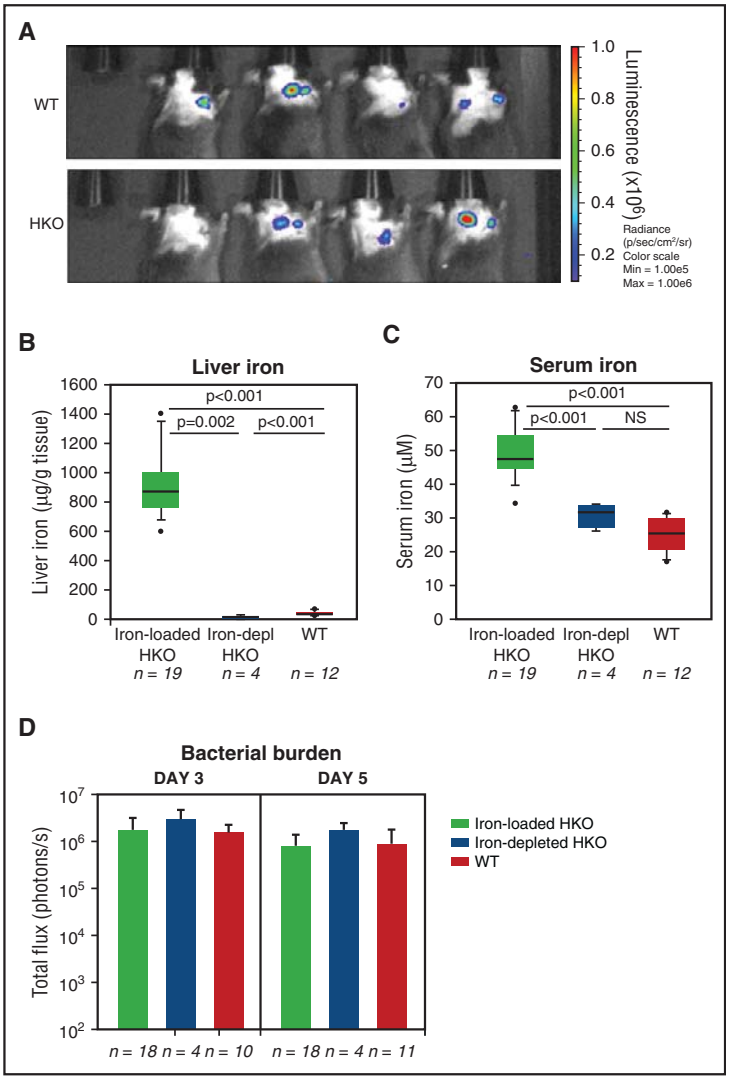


Figure 2. Hepcidin deficiency and iron overload do not alter susceptibility to catheter-associated infection with gram-positive *S aureus*. (A) A 0.5-cm catheter piece was incubated for 15 minutes at 10^7 CFU/mL bioluminescent *S aureus* and implanted under the skin of mice. Infection burden was assessed by in vivo bioluminescence imaging every other day starting on day 1 after surgery. Representative images from day 3 are shown. (B-C) Liver and serum iron in iron-loaded and iron-depleted HKO mice and WT mice. (D) Bacterial burden as measured by total luminescence flux was maximal on days 3 and 5, but similar between iron-loaded HKO, iron-depleted HKO, and WT mice. Statistical analysis was performed using the Student *t* test (B: ID HKO vs WT; C) or Mann-Whitney *U* test (the rest). Max, maximum; Min, minimum; NS, not significant.

Statistics

Statistical analysis was performed with SigmaPlot using the Student *t* test and Mann-Whitney rank sum (for normally and nonnormally distributed data), 2-way analysis of variance (time-course analysis), Kaplan-Meier and log-rank tests (survival), and the χ^2 test (tissue abscess analysis).

Results

Hepcidin prevents mortality from siderophilic but not nonsiderophilic *Y enterocolitica*

HKO mice have much higher baseline liver and serum iron concentrations than WT mice (supplemental Figure 1). We first compared the survival of WT and HKO mice after oral infection with *Y enterocolitica* O9 (10^4-10^8 CFU per mouse), a siderophilic serotype that causes severe infection in patients with iron overload.[14,15] Survival outcomes were dramatically different: HKO mice suffered inoculum-dependent mortality, reaching 100% in the 10^8 CFU group by day 6, but WT mice had 0% mortality after any of the inocula (Figure 1A).

We next studied *Y enterocolitica* O8, a strain with a high pathogenicity island, a genomic region encoding siderophore systems,[14] thought to render it more virulent than O9 in healthy organisms and less dependent on ambient iron.[14,16] As expected, in healthy WT mice, the O8 strain caused greater mortality than the O9 strain (Figure 1B), but there was no difference in mortality between WT and iron-overloaded HKO mice, indicating the infection outcome was unaffected by iron overload. However, O8-induced lethality was much lower than that of O9 in iron-loaded HKO (Figure 1B). Thus, an iron-rich environment makes siderophilic *Y enterocolitica* more virulent than the nonsiderophilic strain, perhaps because the smaller genome allows faster replication and avoids the increased metabolic costs of siderophore production and uptake.

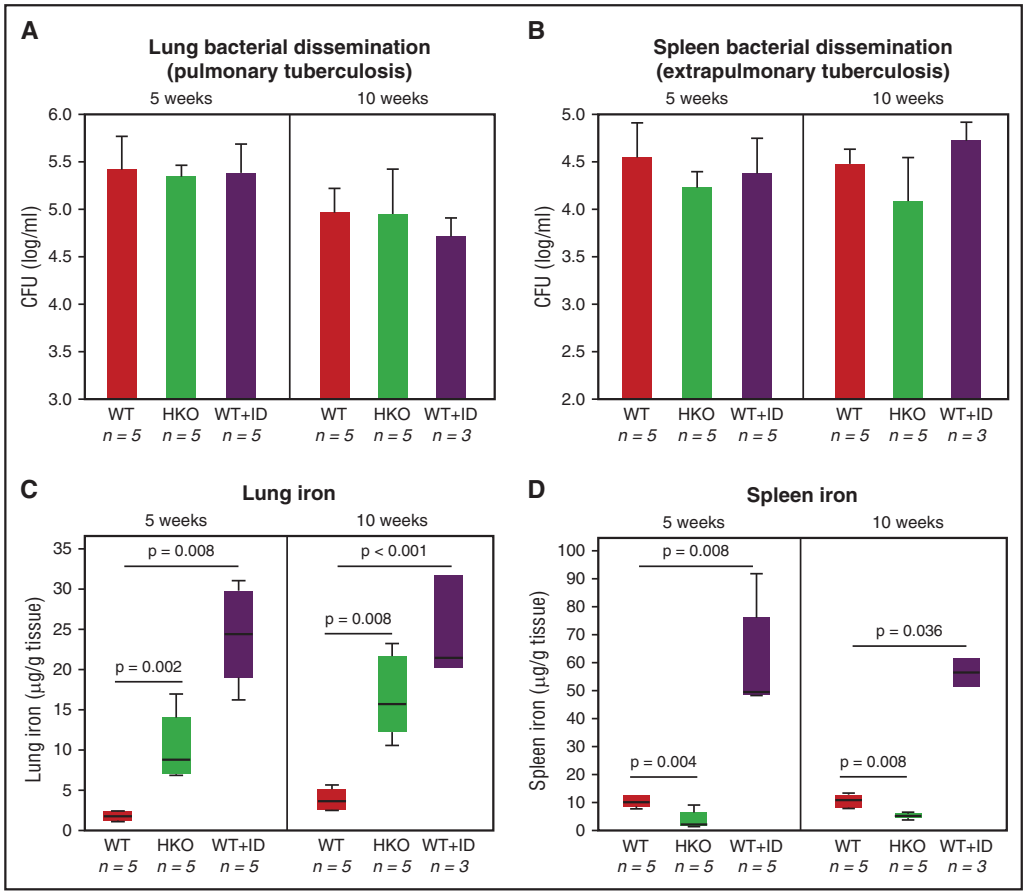


Figure 3. *M tuberculosis* infection is not affected by hepcidin deficiency or iron loading in mice. Control WT mice, naturally iron-loaded HKO mice, and parenterally iron-loaded WT mice (iron-dextran injection, WT + ID) were infected with 30 CFUs of *M tuberculosis* (aerosol). After 5 and 10 weeks, there was no difference between the 3 groups of mice in pulmonary (A) or extrapulmonary (B) bacterial burden as assessed by tissue CFUs. (C-D) Lung and spleen iron concentration. Statistical analysis: Student *t* test if data were normally distributed (C: WT vs HKO 5 weeks, WT vs WT+ID 10 weeks; D: WT vs HKO, 5 weeks) and Mann-Whitney *U* test if they were not normally distributed.

To determine whether the susceptibility of the HKO mice to the siderophilic O9 strain was a consequence of their baseline iron overload or any direct, iron-independent, antimicrobial effect of hepcidin, we compared the survival of iron-loaded and iron-depleted HKO mice after infection with 10^8 CFU *Y enterocolitica* O9. In contrast to the 100% mortality in the iron-loaded HKO group, iron-depleted HKO mice were completely protected (Figure 1C). The dietary iron depletion regimen was effective, as confirmed in a parallel set of mice by measuring liver and serum iron (supplemental Figure 1). Therefore, hepcidin protects the host from severe siderophilic *Y enterocolitica* infection not through direct effects of the hepcidin peptide on microbes, but by controlling systemic iron availability.

Hepcidin deficiency and iron overload do not promote catheter-associated infection with *S aureus*

S aureus commonly causes catheter-associated infections,[17] and its biofilm formation in vitro was reported to be enhanced by iron.[18] We developed a catheter-associated infection model with luminescent *S aureus*, and monitored bacterial burden over the entire time course by in vivo imaging (Figure 2A) in naturally iron-loaded HKO, dietary iron-depleted HKO mice, and WT mice. Liver and serum iron measurements for each group are shown in Figure 2B-C. Luminescence signal as a measure of bacterial burden was maximal between days 3 and 5, and infection was mostly cleared by day 7. None of the mice developed systemic infection and no mortality occurred. We did not observe any difference in bacterial burden as a function of iron loading or hepcidin deficiency (Figure 2D). These results indicate that iron availability and hepcidin production do not modulate catheter-associated infection with *S aureus* in vivo.

M tuberculosis infection in mice is not affected by hepcidin and iron status

It was previously reported that β2m-deficient mice, which have liver iron overload and aberrant major histocompatibility complex type I expression, develop greater *M tuberculosis* burden that WT mice, which can be reversed by treatment with lactoferrin.[19] We tested whether hepcidin and macrophage iron loading promotes the growth of macrophage-tropic intracellular bacteria in vivo. Using a mouse model of pulmonary *M tuberculosis* infection (aerosol-delivered 30 CFUs per lung), we compared 3 mouse groups: control

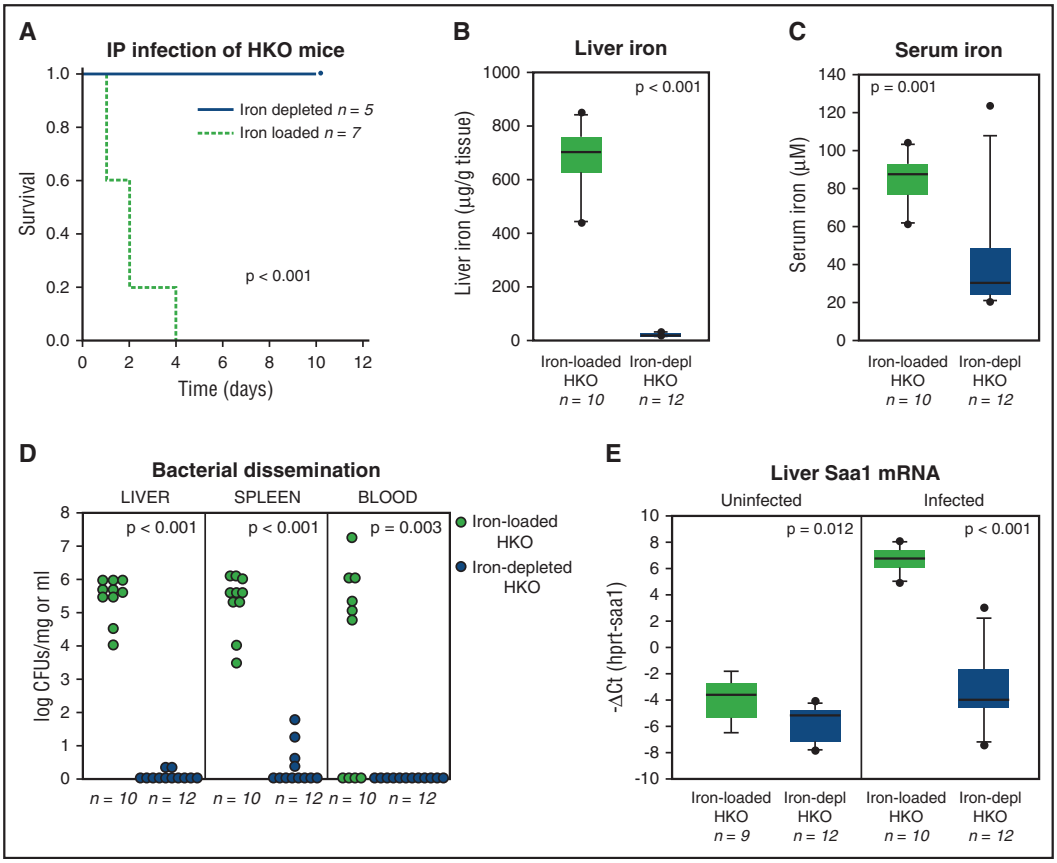


Figure 4. Iron overload promotes rapid growth and dissemination of *Y enterocolitica* O9. (A) Survival of naturally iron-loaded or dietary iron-depleted HKO mice after IP infection with 10^8 CFU *Y enterocolitica* O9 is comparable to that after oral infection (Figure 1C) indicating that intestinal bacterial translocation is not the critical iron-dependent step. (B-H) Iron-loaded or iron-depleted (depl) HKO mice were orally infected with 10^8 CFUs per mouse *Y enterocolitica* O9. (B-C) Liver and serum iron concentrations confirmed iron loading and iron depletion of HKO mice. (D) Iron-loaded HKOs had dramatically increased bacterial dissemination to the liver, spleen, and blood as assessed by tissue CFUs, and consequently (E) much higher liver Saa1 mRNA expression compared with iron-depleted HKOs. (F-H) Hematoxylin and eosin (H&E) and staining with antibody (Ab) specific for *Y enterocolitica* O9 of tissue sections from the liver, spleen, and Peyer patches of iron-loaded (in green rectangles) or iron-depleted (in blue rectangles) HKO mice; ×10 magnification. Arrows point to bacterial abscesses. Survival is defined in "Methods." Statistical analysis of survival curves (A) was performed using multifactorial Kaplan-Meier log-rank analysis. Statistical analysis in panels B through E was performed using the Student *t* test for normally distributed data (D: spleen CFUs; E) and the Mann-Whitney *U* test for data that were not normally distributed. ΔCt, Δcycle threshold; hprt, hypoxanthine-guanine phosphoribosyltransferase.

WT mice, HKO mice which have systemic iron overload but low macrophage iron content due to uncontrolled iron export through ferroportin, and WT mice injected with iron dextran which causes macrophage iron loading. Bacterial burden in the lung (Figure 3A) and the spleen (Figure 3B) was assessed 5 and 10 weeks after *M tuberculosis* challenge, but no significant difference in CFUs was detected between the 3 groups of mice at either time point. Lung iron content was higher in HKO mice and iron-dextran WT mice compared with control WT mice (Figure 3C). Spleen iron content, an indicator of macrophage iron loading, was lower in HKO mice compared with WT controls as expected, and higher in iron-dextran WT mice (Figure 3D). We conclude that hepcidin deficiency and macrophage iron status do not appreciably alter the outcome of *M tuberculosis* infection in mice.

Hepcidin protects against mortality from siderophilic *Y enterocolitica* by controlling baseline iron levels

We used the *Y enterocolitica* O9 infection model to analyze in detail how hepcidin and iron participate in host defense. We hypothesized that in WT mice exposed to *Yersinia*, an early induction of hepcidin and consequent hypoferremia may account for their resistance to infection. Surprisingly, oral infection of WT mice with 10^8 CFU per mouse did not cause any significant change in serum iron (supplemental Figure 2A), or hepatic expression of the inflammatory marker Saa1 (supplemental Figure 2B), and serum hepcidin levels were only marginally increased in infected mice (supplemental Figure 2C). None of the infected mice developed signs of disease. Thus, in WT mice with normal baseline iron levels, *Y enterocolitica* infection was already effectively controlled, without eliciting a systemic inflammatory response, presumably because any bacteria that crossed the intestinal barrier could not multiply rapidly in the absence of accessible iron, and therefore did not cause systemic infection. However, when *Y enterocolitica* was administered intraperitoneally in WT mice at the same dose, we observed an increase in serum hepcidin and Saa-1 as well as hypoferremia (supplemental Figure 3), indicating that the expected inflammatory response is mounted when high bacterial numbers are present in the systemic circulation. Thus, normal iron levels maintained by physiologic hepcidin concentration may be

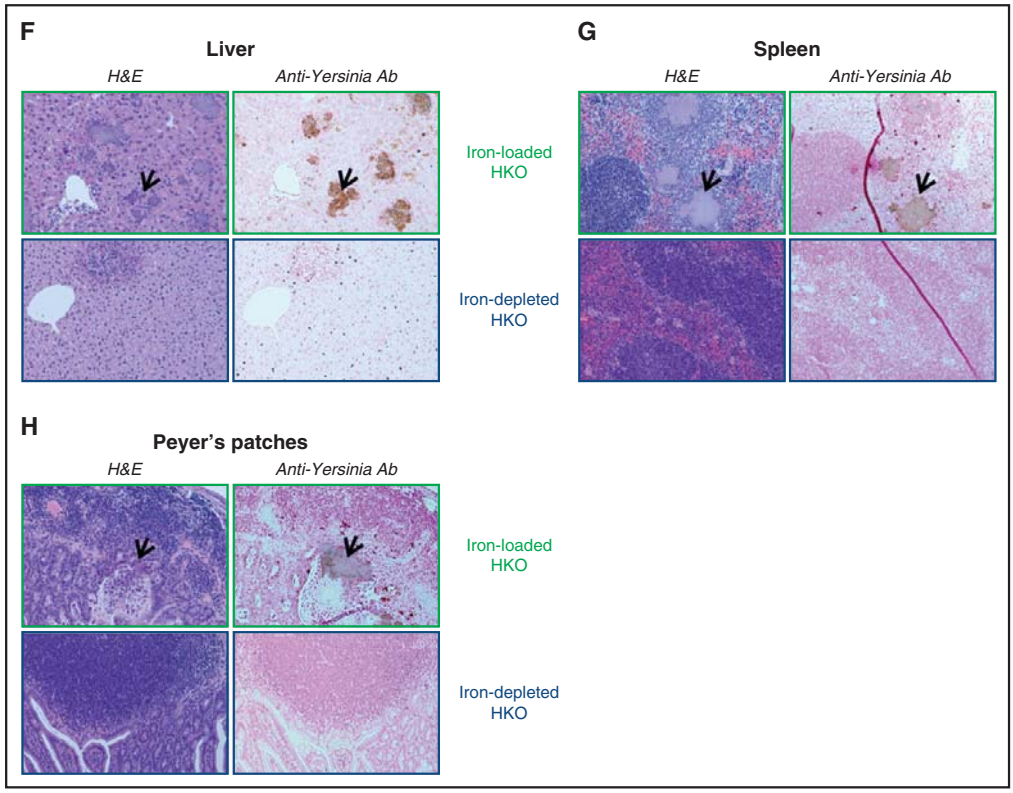


Figure 4. (Continued).

sufficient to protect healthy mice from severe yersiniosis, even without a reactive hepcidin increase or hypoferremia.

High mortality of iron-loaded HKO mice could hypothetically result from 2 separate mechanisms: (1) iron overload could promote the intestinal translocation of *Y enterocolitica* via an unknown mechanism, seeding the blood and allowing systemic infection to proceed or (2) high iron availability could promote the rapid growth of bacteria that reached the circulation, without affecting their intestinal translocation. We bypassed the intestine by injecting the pathogen intraperitoneally into iron-loaded or iron-depleted HKO mice. Similarly to oral infection (Figure 1C) but more rapidly, IP *Y enterocolitica* O9 (10^8 CFU per mouse) caused 100% mortality in the iron-overloaded group (Figure 4A) whereas iron-depleted HKO mice again had 0% mortality. Similar dependence of oral vs IP infection outcome on iron status of the mice suggests that high iron levels promote the growth of bacteria once they reach systemic circulation rather than affect their intestinal translocation.

Iron overload promotes rapid metastatic growth of *Y enterocolitica* O9 without affecting initial neutrophil recruitment and bacterial killing

To confirm that iron availability affects bacterial growth in vivo, we measured CFUs in blood and organs in iron-loaded and iron-depleted HKO mice after oral *Y enterocolitica* O9 infection (10^8 CFU per mouse). Measurements of liver (Figure 4B) and serum iron concentration (Figure 4C) confirmed that the mice were markedly iron-loaded or efficiently iron-depleted, as intended. Bacterial CFUs were dramatically increased in the liver, spleen, and blood of iron-loaded compared with iron-depleted HKOs (Figure 4D). We also measured expression of liver Saa1, an acute-phase protein produced by hepatocytes and used as a sensitive marker of inflammation in mice. In agreement with the widespread infection in iron-loaded animals, Saa1 messenger RNA (mRNA) was highly induced only in the iron-loaded group whereas iron-depleted groups had Saa-1 mRNA levels comparable to those of uninfected mice (Figure 4E). Furthermore, histological analysis of the liver, spleen, and Peyer patches (an important entry site for *Y enterocolitica*), and staining of tissue sections with an antibody specific for the O9 strain, revealed multiple large bacterial abscesses only in iron-loaded mice (Figure 4F-H).

Iron could promote metastatic bacterial infection by altering host defenses at the site of entry, affecting bacterial dissemination in blood and bacterial attachment in tissues, or modulating the multiplication of bacteria that have entered the organism. We first examined the effect of iron and hepcidin on host defense response at the site of infection and on early bacterial dissemination to blood. We used WT or HKO mice that have EGFP-expressing neutrophils and macrophages (LysEGFP and HKO/LysEGFP), and confirmed that these mice show the same difference in survival and iron loading as WT and HKO mice not carrying LysEGFP (supplemental Figure 4). The 2 groups of mice were injected intraperitoneally with 10^8 CFUs per mouse *Y enterocolitica* O9, and 6 hours later, bacterial killing was assessed by measuring CFUs

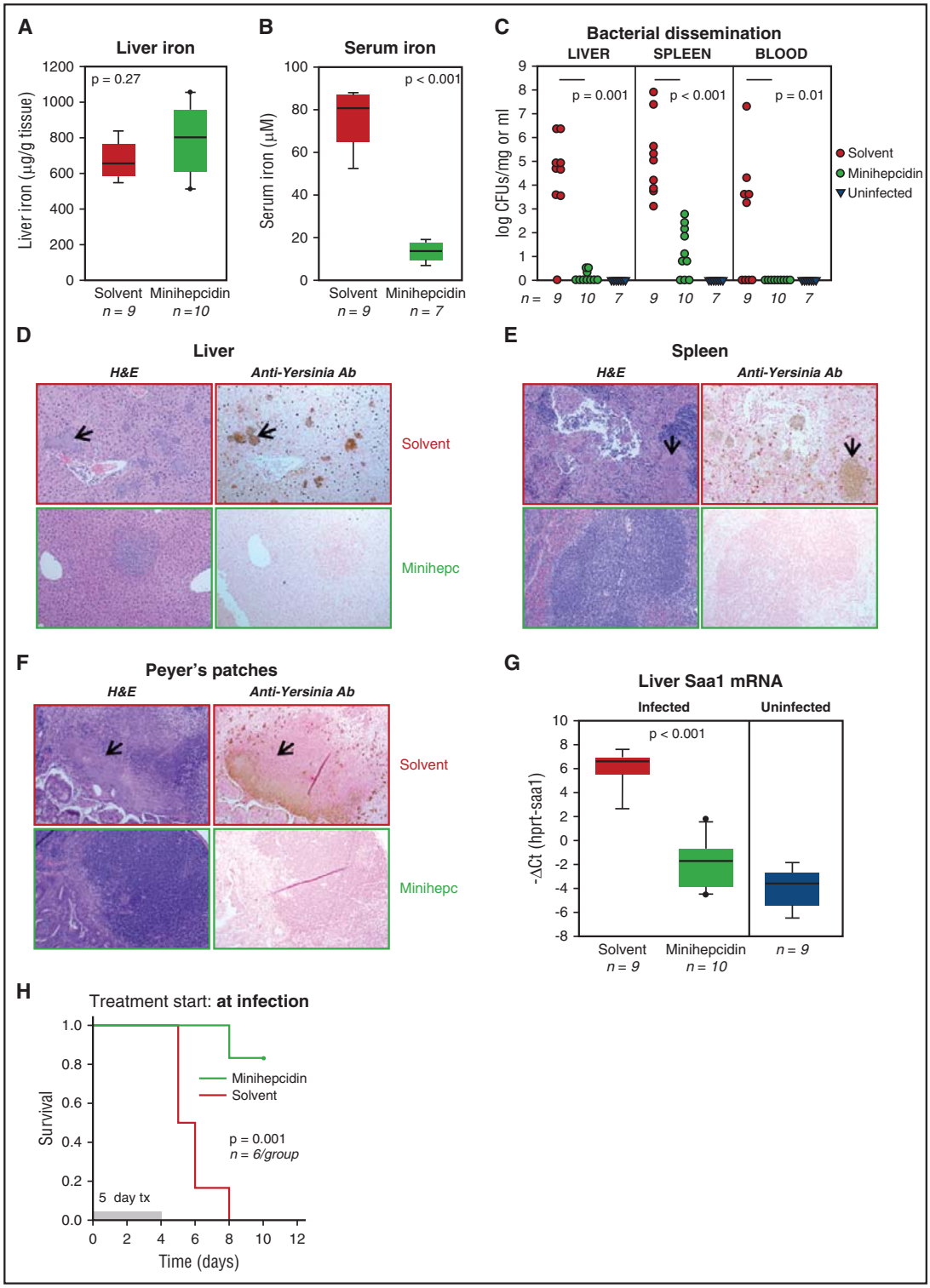

A
Liver iron
Liver iron (µg/g tissue)
p = 0.27
Solvent
Minihepcidin
n = 9
n = 10
B
Serum iron
Serum iron (µM)
p < 0.001
Solvent
Minihepcidin
n = 9
n = 7
C
Bacterial dissemination
LIVER
SPLEEN
BLOOD
log CFUs/mg or ml
p = 0.001
p < 0.001
p = 0.01
Solvent
Minihepcidin
Uninfected
n = 9 10 7 9 10 7 9 10 7
D
Liver
H&E
Anti-Yersinia Ab
Solvent
Minihepc
E
Spleen
H&E
Anti-Yersinia Ab
F
Peyer's patches
H&E
Anti-Yersinia Ab
Solvent
Minihepc
G
Liver Saa1 mRNA
Infected
Uninfected
-ΔCt (hprt-saa1)
p < 0.001
Solvent
Minihepcidin
n = 9
n = 10
n = 9
H
Treatment start: at infection
Survival
Minihepcidin
Solvent
p = 0.001
n = 6/group
5 day tx
Time (days)

Figure 5.

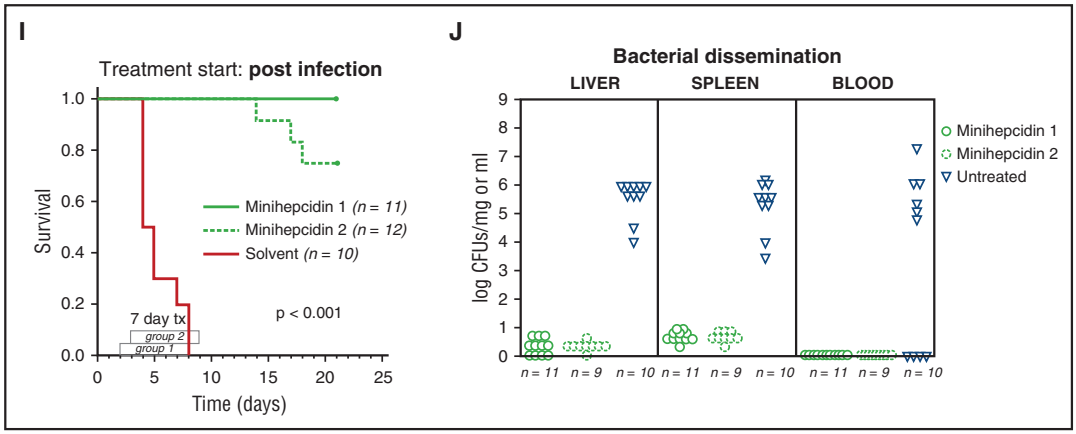


Figure 5. (Continued).

in peritoneal fluid. Early bacterial dissemination to blood was assessed by blood CFUs, and neutrophil recruitment to the IP cavity was assessed by counting the total number of cells as well as the GFP-expressing cells in the peritoneal lavage fluid. There was no difference in bacterial burden in peritoneal fluid or in blood (supplemental Figure 5A), or in the number of GFP^+ (supplemental Figure 5B) or total cells (supplemental Figure 5C), in peritoneal fluid between WT mice and mice lacking hepcidin.

To further assess the initial dissemination and attachment of bacteria in target tissues, iron-loaded or iron-depleted HKO mice were injected intraperitoneally with 10^8 CFUs per mouse *Y enterocolitica* O9 and 6 hours later CFUs were assayed in liver, spleen, and blood. No difference in initial bacterial spread and adhesion to target tissues was observed between iron-depleted and iron-loaded mice (supplemental Figure 5D). Iron measurements for these mice are shown in supplemental Figure 6.

Together, these results indicate that the innate immune response to *Y enterocolitica* infection is not affected by hepcidin deficiency and iron overload.

High extracellular iron concentration promotes *Y enterocolitica* O9 virulence and is therapeutically targetable by minihepcidins

Iron-overloaded mice that were susceptible to yersiniosis had both high serum iron and high liver (but not spleen) tissue iron concentrations. Because *Y enterocolitica* is an extracellular pathogen, we hypothesized that *Y enterocolitica* O9 virulence would be suppressed by low extracellular iron concentrations, even if tissue iron concentrations remained high. We treated iron-loaded HKO mice with a synthetic hepcidin analog minihepcidin PR73[10] or solvent 2 hours before oral infection with 10^8 CFUs per mouse of *Y enterocolitica* O9, and then daily for 5 days. Mice from the solvent-treated group were euthanized when showing signs of imminent mortality, including rapid weight loss combined with changes in behavior and appearance (days 3, 4, and 6). Matching numbers of minihepcidin-treated animals were euthanized at the same time points for comparative analysis of CFUs and iron parameters. As expected, the short-term treatment with minihepcidins did not affect liver iron stores (Figure 5A) but reduced serum iron concentration (Figure 5B). The treatment nearly completely ablated bacterial dissemination to the liver, spleen, and blood (Figure 5C-F). Accordingly, hepatic expression of the inflammatory marker Saa1 was increased only in solvent-treated HKO mice that had disseminated infection, but Saa1 expression in minihepcidin-treated mice was comparable to uninfected mice (Figure 5G). In a replicate experiment, survival of mice was likewise dramatically different: whereas all of the solvent-treated mice died by day 8, minihepcidin-treated mice showed >80% survival (Figure 5H). Thus, high extracellular iron concentrations are essential for *Y enterocolitica* O9 virulence.

To test the therapeutic potential of manipulating extracellular iron concentrations in *Y enterocolitica* infection, iron-loaded HKO mice were orally infected with 10^8 CFU bacteria on day 0, and minihepcidins or solvent treatment started 2 or 3 days after they were infected, when the disease signs were already apparent and mortality started occurring. In contrast to the solvent-treated group where 100% mortality was reached by day 8, the survival rates in minihepcidin-treated groups by day 21 were 100% when PR73 treatment was initiated on day 2 and 70% when treatment was initiated on day 3 (Figure 5I). Confirming the remarkable efficacy of even the delayed treatment, tissue bacterial burden 3 weeks after the infection was low to absent (Figure 5J).

Figure 5. High extracellular iron promotes *Y enterocolitica* O9 virulence, and lowering of plasma iron by minihepcidin treatment prevents mortality. (A-H) Iron-loaded HKO mice were orally infected with 10^8 CFUs of *Y enterocolitica* O9 and treated with solvent or minihepcidin (Minihepc; 100 nmol). Minihepcidin treatment did not alter liver iron (A) but lowered serum iron (B) and prevented bacterial dissemination to the liver, spleen, and blood (C). (D-F) H&E or anti–*Y enterocolitica* antibody staining of tissue sections from the liver, spleen, and Peyer patches of solvent-treated (in red rectangles) or minihepcidin-treated (in green rectangles) HKO mice; ×10 magnification. Arrows point to bacterial abscesses. (G) Liver Saa1 mRNA expression. (H) Survival curves. (I-J) Iron-loaded HKO mice were orally infected with 10^8 CFUs per mouse *Y enterocolitica* O9 and treated with solvent or minihepcidin for 7 days starting on day 2 (Minihepcidin 1) or 3 (Minihepcidin 2) after infection. (I) Survival curve. (J) Bacterial dissemination and tissue burden for minihepcidin-treated groups was assayed at euthanasia (on day 21 after infection). Tissue CFUs of iron-loaded moribund HKO mice were used for comparison (D). Survival is defined in "Methods." Statistical analysis: The Student *t* test was used for normally distributed data (B; C: spleen CFUs; G) and the Mann-Whitney *U* test for data that were not normally distributed (A; C: liver and blood CFUs). Survival (H-I) was analyzed using Kaplan-Meier log-rank. tx, treatment.

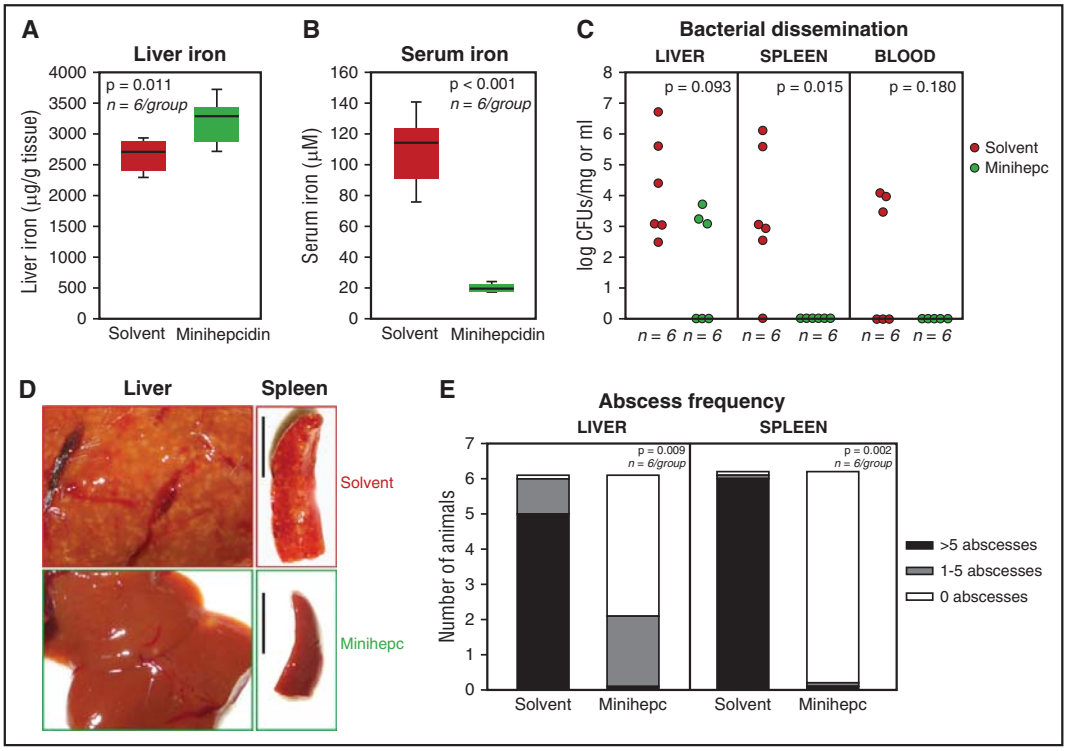


Figure 6. Minihepcidin treatment is beneficial even in mice with intact hepcidin regulation and iatrogenic iron overload. WT mice were iron loaded through IP injection of 20 mg of iron dextran on day −1, then orally infected with 10^8 CFUs of *Y enterocolitica* O9 on day 0 and treated with solvent or minihepcidin (100 nmol per day) for 10 days. (A-B) Liver and serum iron levels. (C) Bacterial dissemination to liver, spleen, and blood assessed by CFUs (whole liver and spleen). (D) Gross pathology of liver and spleen, with many abscesses visible in the tissues from solvent group. Scale bar, 1 cm. (E) Abscess proportion analysis (χ^2 test) showed abscess formation predominantly in solvent-treated animals, whereas minihepcidin treatment rescued the phenotype. Statistical analysis was done using the Student *t* test for normally distributed data (A; B; C: liver CFUs) and the Mann-Whitney *U* test for data that are not normally distributed (C). Data in panel F were analyzed using the χ^2 test.

Minihepcidin treatment is beneficial even in mice with intact hepcidin regulation and iatrogenic iron overload

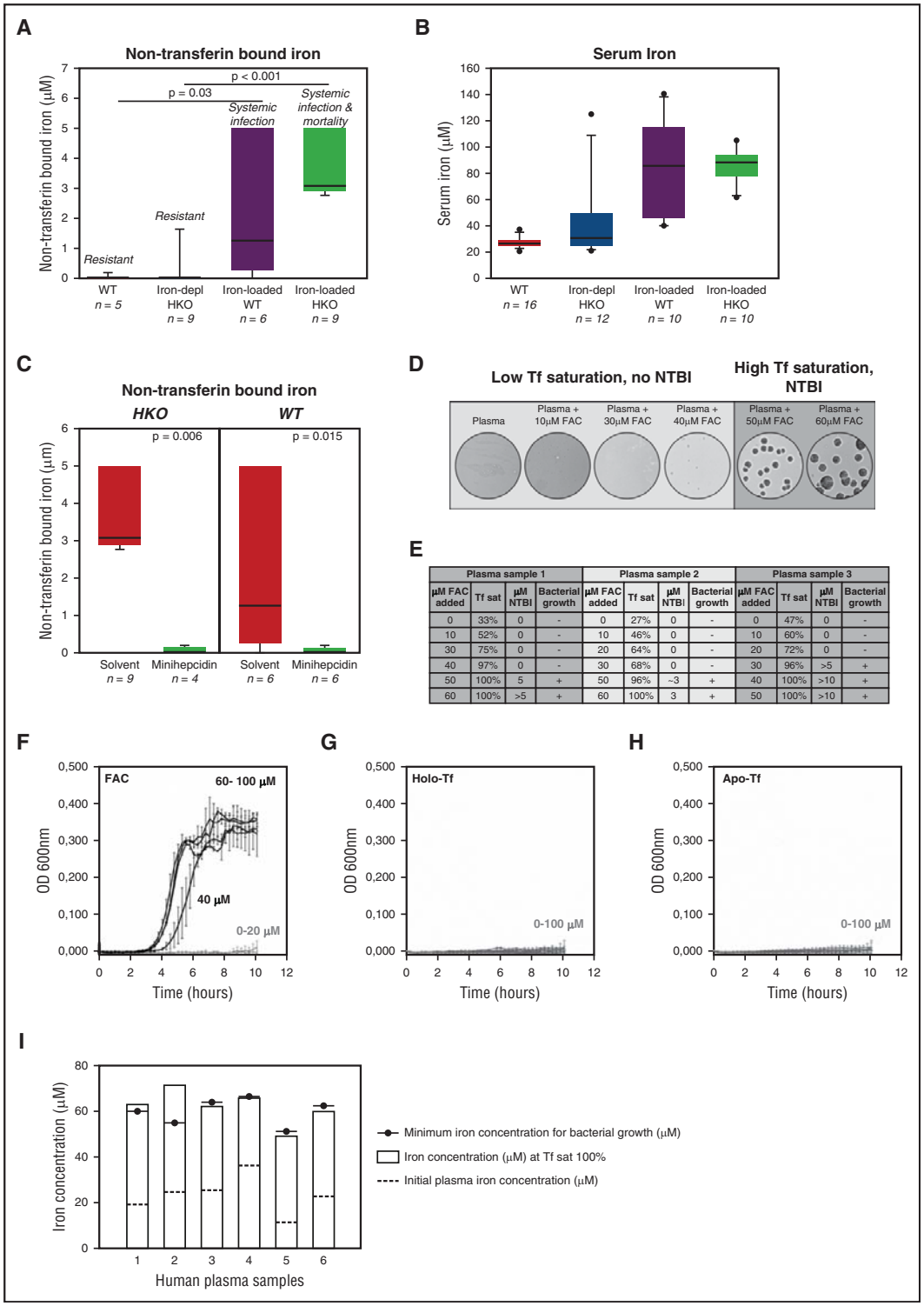
WT mice with normal iron levels do not develop systemic infection (Figure 1) but WT mice that are iron-loaded by parenteral administration of iron dextran do. We injected 20 mg of iron dextran 1 day before orally administering 10^8 CFU per mouse of *Y enterocolitica* O9. Although no mice died within 10 days after infection, the mice did develop systemic infection as evidenced by multiple abscesses in the liver (supplemental Figure 7).

To test the effect of minihepcidins in this model, we treated the iron-loaded infected WT mice with either solvent or minihepcidin daily for 10 days starting on the day of infection. Minihepcidin treatment slightly increased liver iron concentration (Figure 6A) but led to a dramatic drop in serum iron levels (Figure 6B) and almost completely ablated bacterial dissemination to the spleen, liver, and blood (Figure 6C). Minihepcidin treatment decreased weight loss (supplemental Figure 8A) and prevented the formation of tissue abscesses and organomegaly (supplemental Figure 8B; Figure 6D-E). Thus, minihepcidins may have therapeutic potential not only in patients with primary iron overload due to hepcidin deficiency (eg, hereditary hemochromatosis), but also in patients with iatrogenic iron overload (dialysis patients,[20] patients with hemolytic anemias,[21] transfused patients, etc) who still produce endogenous hepcidin.

Bacterial growth and associated mortality depend on NTBI

We observed that NTBI was only present in the serum of iron-loaded WT and HKO mice, but not in iron-depleted HKO or WT mice, paralleling the susceptibility to yersiniosis (Figure 7A). Minihepcidin treatment, which prevented yersiniosis, completely ablated NTBI in the blood of both iron-loaded HKO and parenterally iron-loaded WT mice (Figure 7C). To conclusively differentiate between the role of transferrin-bound iron and NTBI in the growth of *Y enterocolitica*, we developed a new in vitro assay using multiwell agar plates containing 90% human plasma supplemented with increasing concentrations of FAC (Figure 7D) generating increasing transferrin saturation. Using plasma from 3 separate donors, we showed that bacteria only grew in wells where the added iron exceeded the unsaturated iron-binding capacity of plasma and NTBI became detectable (Figure 7E).

Importantly, we observed an equivalent growth dependence on NTBI for another siderophilic bacterial species, *V vulnificus* (Figure 7F). We previously showed that *V vulnificus* bacterium became hypervirulent in iron-overloaded hepcidin KO mice that had high NTBI, and caused mortality within <24 hours.[10] Furthermore, *V vulnificus* was reported to grow rapidly in vitro in human serum with high transferrin saturation.[22] Here, we developed a liquid culture system using human plasma supplemented with different forms of iron



Plasma sample 1				Plasma sample 2				Plasma sample 3			
μM FAC added	Tf sat	μM NTBI	Bacterial growth	μM FAC added	Tf sat	μM NTBI	Bacterial growth	μM FAC added	Tf sat	μM NTBI	Bacterial growth
0	33%	0	-	0	27%	0	-	0	47%	0	-
10	52%	0	-	10	46%	0	-	10	60%	0	-
30	75%	0	-	20	64%	0	-	20	72%	0	-
40	97%	0	-	30	68%	0	-	30	96%	>5	+
50	100%	5	+	50	96%	~3	+	40	100%	>10	+
60	100%	>5	+	60	100%	3	+	50	100%	>10	+

Figure 7.

to identify which of the iron forms stimulated bacterial growth. *V vulnificus* growth was initiated in plasma only when a sufficient amount of FAC was added to saturate transferrin, at which point NTBI appears in the sample. Addition of holotransferrin or apotransferrin to the same human plasma sample did not promote the growth of *V vulnificus* (Figure 7G-H). Summarizing the results for 6 different human plasma samples, Figure 7I shows that for each plasma sample, *V vulnificus* growth was detected at iron concentrations where transferrin saturation neared 100%. Thus, the presence of NTBI appears to be essential for outgrowth of siderophilic pathogens in human plasma. In contrast, nonsiderophilic *Y enterocolitica* O8 did not show such dependence of colony formation on NTBI. Rather, similar numbers of bacterial colonies were observed in each plasma sample independently of NTBI presence (supplemental Figure 9), although the colony size increased slightly with total iron concentration.

Discussion

As an acute-phase reactant, hepcidin has long been suspected to play a role in innate immunity, but critical examination of its effect on infection outcomes has only begun.[10] Here, we comprehensively examined the role of hepcidin and iron in innate immunity using mouse models. We showed that hepcidin is essential for survival after infection with *Y enterocolitica* O9, a bacterium that causes severe illness in iron-overloaded humans. However, neither hepcidin nor variations in systemic iron loading had demonstrable effect on infections with *Yersinia* O8 strain or *S aureus* (Figures 1 and 2). This may be because the O8 strain can scavenge iron from multiple sources and is less sensitive to iron availability because it grows slower than 09,[14,16] and *S aureus* was shown to primarily use heme iron during infection initiation.[23] Also, hepcidin or macrophage iron loading did not promote growth of macrophage-tropic *M tuberculosis* in vivo (Figure 3). Many in vitro studies have established the general importance of iron for pathogen growth. Contrary to expectations, our studies demonstrate that over the pathophysiological range of iron concentrations in vivo, outcomes of many infections are not affected, likely because iron uptake mechanisms in those bacteria can compensate for the ambient changes in iron.

The protective role of hepcidin against the siderophilic O9 strain was related to its iron-regulatory function rather than direct antimicrobial activity, as iron depletion of HKO mice resulted in complete resistance to infection, equivalent to that of WT mice. Hepcidin deficiency and accompanying iron overload did not affect early innate immune responses we tested (supplemental Figure 5), as WT and iron-overloaded HKO mice infected by the peritoneal route showed a similar initial local inflammatory response, local bacterial killing, and early dissemination from the site of infection. As bacteria disseminate, an important determinant of the outcome of infection is the rate of bacterial multiplication in blood/extracellular fluid. *Y enterocolitica* O9 did not grow out on human plasma-agar plates unless enough ferric iron was added to saturate transferrin and generate NTBI (Figure 7D-E). Likewise, only mice that had NTBI in their blood were susceptible to systemic infection, whereas the groups that did not have detectable levels of NTBI were resistant to infection. Moreover, parenterally iron-overloaded WT mice with lower but detectable NTBI levels had a less severe illness and survived longer than hepcidin KO mice with higher NTBI concentrations. Analyzing all of the models together, serum NTBI concentrations below 2 μM correlated with nonlethal systemic infection whereas NTBI levels >2 μM associated with lethal *Y enterocolitica* O9 infection (supplemental Figure 11). We surmise that 1 or more iron species that appear when transferrin is saturated may be accessible to *Y enterocolitica* O9, which lacks the high-affinity iron-binding siderophore system. The presence of these NTBI species then stimulates rapid *Yersinia* growth and pathogenicity. We observed similar dependence on NTBI in another siderophilic pathogen, *V vulnificus*, which also exhibits hypervirulence in iron-overloaded patients. Like the O9 strain, other strains of *Y enterocolitica* most virulent in iron-overloaded patients generally lack known mechanisms for utilizing transferrin-bound iron or host ferroproteins. We hypothesize that bacteria that thrive in this niche trade off the fitness cost of dependence on NTBI against the cost of maintaining high-affinity siderophore systems or receptor-mediated ferroprotein uptake mechanisms. Because siderophilic bacteria are commonly zoonotic, we surmise that nonhuman hosts with extracellular NTBI exist, in which siderophilic strains have a fitness advantage over nonsiderophilic strains. The enhancement of bacterial outgrowth by NTBI in the plasma-agar assay could serve as a clinically useful predictor of NTBI-dependent pathogenicity in vivo for different bacterial species. It remains to be determined which specific forms of NTBI in circulation are capable of stimulating rapid growth of siderophilic pathogens.

Historically, the concept of iron-based nutritional immunity has focused on the reduction in plasma iron concentration or transferrin saturation during infection, not taking into account the inaccessibility of transferrin-bound iron to pathogens unless they are equipped with transferrin receptors[24] or high-affinity siderophores. We therefore propose that the prevention of NTBI production is the principal host defense function of hepcidin. During infections, the potential supply of iron into plasma increases because of macrophage scavenging of damaged erythrocytes and injured tissues. At the same time, erythropoietic demand for plasma iron decreases because of suppression of erythropoiesis by inflammatory cytokines. The 2 effects combine to raise plasma iron concentrations unless hepcidin is present. Indeed, in hepcidin KO mice, *Y enterocolitica* infection caused further increase in serum iron over already high baseline iron levels (supplemental Figure 10), and a similar increase in serum iron was observed in hepcidin KO inflamed with heat-killed *Brucella abortus*.[25] Viewed in this light, the inflammation-induced increase of hepcidin concentration may reduce the possibility that NTBI will be

Figure 7. Bacterial growth depends on NTBI. (A-E) *Y enterocolitica* and (F-I) *V vulnificus*. (A) NTBI and (B) serum iron measurements in WT, iron-depleted HKO, iron-loaded WT, and iron-loaded HKO mice. Presence of NTBI correlates with the severity of *Y enterocolitica* infection. (C) Minihepcidin treatment abolished NTBI in serum of iron-loaded WT and HKO mice. (D) Microscopy images (magnification ×4) of bacterial growth 24 hours after plating *Y enterocolitica* O9 (10^6 CFU/mL) on agar plates made of human plasma supplemented with 0 to 60 μM FAC. Bacterial growth was observed only in the samples with measurable NTBI (dark gray section). (E) Transferrin (Tf) saturation (sat), NTBI concentration, and bacterial growth on agar plates made from plasma of 3 different donors. Statistical analysis (A,C): Mann-Whitney *U* test. (F-I) *V vulnificus* (1×10^3 CFU/mL) were grown in vitro in human plasma supplemented with (F) 0 to 100 μM FAC, (G) 0 to 100 μM holo-Tf, or (H) 0 to 100 μM apo-Tf. *V vulnificus* growth was initiated only when 40 to 100 μM FAC was added to the plasma at which point transferrin saturation reached 100%. Bacteria did not grow in plasma supplemented with holo-Tf or apo-Tf. Each line represents mean (n = 3) ± standard deviation. (I) *V vulnificus* growth was measured in 6 different human plasma samples supplemented with a range of FAC. Black circle indicates the iron concentration at which *V vulnificus* growth was initiated. White bar shows plasma iron concentration at which transferrin saturation reached 100% for each sample. Dashed line indicates baseline plasma iron concentration for each human sample. *V vulnificus* growth in vitro in human plasma occurred only when transferrin was nearly completely saturated. OD, optical density.

generated, thus preventing NTBI-dependent growth and hypervirulence of siderophilic pathogens.

We propose that the term "siderophilic infection" should be redefined to specifically denote those organisms whose rate of growth is enhanced by NTBI. By this definition, siderophilic infections may be more common than is generally realized. In addition to *V vulnificus* and *Y enterocolitica* strains, *Klebsiella pneumoniae,* a common cause of pneumonia and sepsis, also manifested NTBI-enhanced pathogenicity in our mouse models.[26]

Clinical conditions that are characterized by the presence of NTBI, and therefore may be susceptible to more severe infections with NTBI-sensitive pathogens, include not only hereditary hemochromatosis and β-thalassemia, but also alcoholic liver disease, acute or chronic hepatic failure, stem cell transplantation, and chemotherapy-associated myelosuppression.[27] Importantly, NTBI levels >2 μM at the beginning of myelosuppression were associated with a higher risk of sepsis caused by gram-negative bacteria.[28]

Minihepcidins, synthetic hepcidin agonists, rapidly cause hypoferremia, desaturation of transferrin, and elimination of NTBI. In both iron-loaded hepcidin KO and iron-loaded WT mice, minihepcidin administration dramatically decreased the morbidity and mortality of infection (Figure 5), even when started 2 to 3 days after infection (hepcidin KO model), providing a realistic framework for future human trials. Minihepcidin treatment may be uniquely suited to rapidly deprive siderophilic bacteria of iron, a pharmacologic activity distinct from that of iron chelators. Deferoxamine has been associated with promoting bacterial growth in multiple studies,[29,30] whereas deferiprone at lower concentrations (data not shown) stimulated *Y enterocolitica* growth in vitro.

In summary, we propose that the function of hepcidin in innate immunity is to clear NTBI from plasma, and thereby inhibit the systemic spread of microbes whose outgrowth is enhanced by NTBI. Conversely, bacteria not dependent on NTBI appear to be unaffected by hepcidin or changes in systemic iron concentrations in our animal models. This paradigm shift implies that in vitro testing of microbial responses to NTBI may predict which infections can be treated with hepcidin agonists, and that doses of hepcidin agonists that consistently clear NTBI in vivo should be highly effective for the treatment of siderophilic infections. Testing of additional infection models is needed to determine whether hepcidin-mediated changes in transferrin saturation may also control the growth of other microbes. Our study was designed to provide a proof of concept for the relevance of hepcidin-mediated regulation of iron in multiple infection models in mice in vivo. We recognize that inbred animal models are an imperfect representation of complex human conditions,[31] and that the mechanisms and therapeutic applications proposed in our study will need further testing and refinement in human clinical studies.

Acknowledgments

The authors thank Dorine Swinkles for advice and assistance with establishing the method for NTBI quantitation.

This work was supported by funding from National Institutes of Health, National Institute of Diabetes and Digestive and Kidney Diseases grant R01 DK090554 (E.N., T.G.), Keryx Biopharmaceuticals grant 2015-0751 (E.N., T.G.), and a Will Rogers Foundation grant (T.G.).

Authorship

Contribution: D.S., J.A., M.A.H., T.G., Y.B., and E.N. designed the study; D.S., A.R., J.A., P.R., V.G., B.J.D., M.A.H., and Y.B. conducted experiments and analyzed data; M.S. provided reagents and consulted on *Yersinia* experiments; D.S., J.A., T.G., Y.B., and E.N. wrote the manuscript; and all authors contributed to the discussion of results and edited and approved the final manuscript.

Conflict-of-interest disclosure: E.N. and T.G. are consultants and shareholders of Intrinsic LifeSciences and Silarus Therapeutics, and consultants for La Jolla Pharmaceuticals. T.G. is a consultant for Keryx Pharmaceuticals. The remaining authors declare no competing financial interests.

Correspondence: Elizabeta Nemeth, David Geffen School of Medicine, University of California Los Angeles, CHS 37-055, Los Angeles, CA 90095-1690; e-mail: enemeth@mednet.ucla.edu.

References

1. Rodriguez R, Jung CL, Gabayan V, et al. Hepcidin induction by pathogens and pathogen-derived molecules is strongly dependent on interleukin-6. *Infect Immun.* 2014;82(2):745-752.
2. Nemeth E, Ganz T. Regulation of iron metabolism by hepcidin. *Annu Rev Nutr.* 2006;26:323-342.
3. Christopher GW. Escherichia coli bacteremia, meningitis, and hemochromatosis. *Arch Intern Med.* 1985;145(10):1908.
4. Gerhard GS, Levin KA, Price Goldstein J, Wojnar MM, Chorney MJ, Belchis DA. Vibrio vulnificus septicemia in a patient with the hemochromatosis HFE C282Y mutation. *Arch Pathol Lab Med.* 2001;125(8):1107-1109.
5. Manso C, Rivas I, Peraire J, Vidal F, Richart C. Fatal Listeria meningitis, endocarditis and pericarditis in a patient with haemochromatosis. *Scand J Infect Dis.* 1997;29(3):308-309.
6. Vadillo M, Corbella X, Pac V, Fernandez-Viladrich P, Pujol R. Multiple liver abscesses due to Yersinia enterocolitica discloses primary hemochromatosis: three cases reports and review. *Clin Infect Dis.* 1994;18(6):938-941.
7. Capron JP, Capron-Chivrac D, Tossou H, Delamarre J, Eb F. Spontaneous Yersinia enterocolitica peritonitis in idiopathic hemochromatosis. *Gastroenterology.* 1984;87(6):1372-1375.
8. Porter JB, Garbowski M. The pathophysiology of transfusional iron overload. *Hematol Oncol Clin North Am.* 2014;28(4):683-701.
9. Armitage AE, Moran E. HIV-associated tuberculosis: does the iron-regulatory hormone hepcidin connect anemia with poor prognosis? *J Infect Dis.* 2016;213(1):3-5.
10. Arezes J, Jung G, Gabayan V, et al. Hepcidin-induced hypoferremia is a critical host defense mechanism against the siderophilic bacterium Vibrio vulnificus. *Cell Host Microbe.* 2015;17(1):47-57.
11. Evans RW, Rafique R, Zarea A, et al. Nature of non-transferrin-bound iron: studies on iron citrate complexes and thalassemic sera. *J Biol Inorg Chem.* 2008;13(1):57-74.
12. Bernthal NM, Stavrakis AI, Billi F, et al. A mouse model of post-arthroplasty Staphylococcus aureus joint infection to evaluate in vivo the efficacy of antimicrobial implant coatings. *PLoS One.* 2010;5(9):e12580.
13. Esposito BP, Breuer W, Sirankapracha P, Pootrakul P, Hershko C, Cabantchik ZI. Labile plasma iron in iron overload: redox activity and susceptibility to chelation. *Blood.* 2003;102(7):2670-2677.
14. Carniel E. The Yersinia high-pathogenicity island: an iron-uptake island. *Microbes Infect.* 2001;3(7):561-569.
15. Bottone EJ. Yersinia enterocolitica: overview and epidemiologic correlates. *Microbes Infect.* 1999;1(4):323-333.
16. Schubert S, Rakin A, Heesemann J. The Yersinia high-pathogenicity island (HPI): evolutionary and functional aspects. *Int J Med Microbiol.* 2004;294(2-3):83-94.
17. Kwiecinski J, Na M, Jarneborn A, et al. Tissue plasminogen activator coating on surface of implants reduces Staphylococcus aureus biofilm formation. *Appl Environ Microbiol.* 2015;82(1):394-401.
18. Lin MH, Shu JC, Huang HY, Cheng YC. Involvement of iron in biofilm formation by Staphylococcus aureus. *PLoS One.* 2012;7(3):e34388.

19. Schaible UE, Collins HL, Priem F, Kaufmann SH. Correction of the iron overload defect in beta-2-microglobulin knockout mice by lactoferrin abolishes their increased susceptibility to tuberculosis. *J Exp Med*. 2002;196(11): 1507-1513.

20. Rostoker G, Vaziri ND, Fishbane S. Iatrogenic iron overload in dialysis patients at the beginning of the 21st century. *Drugs*. 2016;76(7):741-757.

21. Ware RE, de Montalembert M, Tshilolo L, Abboud MR. Sickle cell disease [published online ahead of print 31 January 2017]. *Lancet*. doi:10.1016/S0140-6736(17)30193-9.

22. Brennt CE, Wright AC, Dutta SK, Morris JG Jr. Growth of Vibrio vulnificus in serum from alcoholics: association with high transferrin iron saturation. *J Infect Dis*. 1991;164(5):1030-1032.

23. Skaar EP, Humayun M, Bae T, DeBord KL, Schneewind O. Iron-source preference of Staphylococcus aureus infections. *Science*. 2004;305(5690):1626-1628.

24. Cornelissen CN. Transferrin-iron uptake by Gram-negative bacteria. *Front Biosci*. 2003;8: d836-d847.

25. Kim A, Fung E, Parikh SG, et al. A mouse model of anemia of inflammation: complex pathogenesis with partial dependence on hepcidin. *Blood*. 2014;123(8):1129-1136.

26. Michels KR, Zhang Z, Bettina AM, et al. Hepcidin-mediated iron sequestration protects against bacterial dissemination during pneumonia. *JCI Insight*. 2017;2(6):e92002.

27. Brissot P, Ropert M, Le Lan C, Loréal O. Non-transferrin bound iron: a key role in iron overload and iron toxicity. *Biochim Biophys Acta*. 2012; 1820(3):403-410.

28. Belotti A, Duca L, Borin L, et al. Non transferrin bound iron (NTBI) in acute leukemias throughout conventional intensive chemotherapy: kinetics of its appearance and potential predictive role in infectious complications. *Leuk Res*. 2015;39(1): 88-91.

29. Arifin AJ, Hannauer M, Welch I, Heinrichs DE. Deferoxamine mesylate enhances virulence of community-associated methicillin resistant Staphylococcus aureus. *Microbes Infect*. 2014; 16(11):967-972.

30. Lesic B, Foulon J, Carniel E. Comparison of the effects of deferiprone versus deferoxamine on growth and virulence of Yersinia enterocolitica. *Antimicrob Agents Chemother*. 2002;46(6): 1741-1745.

31. Seok J, Warren HS, Cuenca AG, et al; Inflammation and Host Response to Injury, Large Scale Collaborative Research Program. Genomic responses in mouse models poorly mimic human inflammatory diseases. *Proc Natl Acad Sci USA*. 2013;110(9):3507-3512.

Supplemental Materials and Methods

Bacterial preparation

Clinical isolates *Yersinia enterocolitica* serotype O9 strain Ruokola/71 (kindly provided by Dr. Mikael Skurnik, University of Helsinki, Finland) and serotype O8 strain WA (ATCC 27729) were used for this study. The bacteria were stored as 35% glycerol stock at -80C and were cultured overnight (16-18 h) at room temperature (23 to 27C) in Luria Bertani broth (Becton Dickinson) before each experiment. On the day of the experiment, the bacteria were collected by centrifugation (7500 rcf for 5 min), washed with sterile buffer and suspended in sterile phosphate-buffered saline (PBS) to the required final concentration, using their wet weight as a measure of bacterial count (100mg = 10^{11} bacteria for serotype O9 and $7.8x10^{10}$ for serotype O8).

Bioluminescent *Staphylococcus aureus* (strain Xen36 derived from the bacteremia isolate ATCC 49525) was kindly provided by Prof. Nicolas Bernthal, Orthopedic hospital research center, UCLA [1]. Briefly, the strain contains lux ABCDE reporter cassette and thus continuously emits bioluminescence when the bacteria are metabolically active. The bacteria were stored as 35% glycerol stock at -80ºC and were cultured overnight in Trypticase™ soy broth (TSB, Becton Dickinson, BD) at 37ºC starting the night prior the experiment. On the following morning (the day of the experiment) the bacteria were collected by centrifugation (7500 rcf for 10min), washed once in TSB and twice in sterile PBS. Finally, the bacteria were resuspended in TSB with 0.5% glucose (Sigma) and concentration was adjusted to 10^7 CFU/ml (OD_{600} = 0.660 equals about $2x10^8$ CFU/ml). The suspension was then aliquoted (1ml) to sterile microtubes and transferred to the procedure room where catheters would be incubated and implanted by surgery.

A pretitered stock of *M. tuberculosis* (Erdman strain) was used for the mouse infection experiments. Stock was prepared by culturing bacteria passaged through guinea pig on Middlebrook 7H11 agar[2].

Animal models

All experiments involving animals, including infections with *Y. enterocolitica*, *S. aureus* and *M. tuberculosis* were approved by the University of California, Los Angeles (UCLA) Office of Animal Research Oversight. Researchers were not blinded as to which treatment group each mouse belonged.

The following mouse strains, all on C57BL/6 background, were used in infection experiments: C57BL/6 wild type (WT) mice (The Jackson Laboratory); hepcidin-1 knockout mice [3] (HKO); LysEGFP mice (kindly provided by Dr. Nicholas Bernthal from University of California, Los Angeles) and HKO/LysEGFP mice. LysEGFP mice have green fluorescent granulocytes and macrophages owing to EGFP insertion into lysozyme M locus [4]. All animals used in the experiments were bred in our vivaria.

The mice were fed either standard diet (containing 185 ppm Fe) or iron-deficient diet (4 ppm Fe, Envigo Teklad). In order to achieve substantial iron depletion, HKO mice were kept on 4 ppm Fe diet for 6 to 8 weeks prior to the experiment. Iron-loading of WT mice was achieved by intraperitoneal (IP) injection of 20 mg iron dextran (Sigma) per mouse one day before infection.

In dose-response experiments with *Y. enterocolitica* O9, mice were infected with 10^4 to 10^8 CFUs by oral gavage. Control mice were given sterile saline solution (Hospira). In some experiments, mice were infected with 10^8 CFUs per mouse by oral gavage or by intraperitoneal (IP) injection. The mice were fasted 2 h prior and 1 h post oral gavage. After infection, the mouse weight, appearance and behavior were monitored daily.

For *Yersinia enterocolitica* survival experiments the mice were euthanized using isoflurane (Clipper) when they showed signs of imminent death. These included rapid weight loss (>10%) combined with failure to consume food and water, loss of grooming and immobility despite stimulation.

For catheter associated *Staphylococcus aureus* infection, the catheters (BD Angiocath catheters 16GA x 3.25) were cut on the day of the experiment in sterile conditions (in biosafety hood using a sterile scalpel and on a sterile gauge) to 0.5 cm pieces. Each catheter piece was incubated in 1 ml of 10^7 CFU/ml *Staphylococcus aureus* (in TSB with 0.5% glucose) for 15 min at room temperature. During these 15 min, the mouse was anaesthetized using 2-3% isoflurane gas (Clipper) constantly flowing through a nose cone and eye ointment (company) was applied. The surgical area (upper right back) that was shaved the day before was cleaned three times consecutively with povidone-iodine pads (Professional Disposables, Inc., PDI) and alcohol pads (PDI). Sterile instruments were used to make a small incision (less than 0.5 cm) and the opposite tip of a sterile loop was used to create space for the catheter under the skin. Before insertion under the skin, the catheter was briefly washed in sterile PBS and the inside was rinsed using an insulin syringe with 100 µl sterile PBS to ensure that only bacteria attached to the catheter remain. After implantation, the incision site was sutured (Ethicon 662G ETHILON Suture, Reverse Cutting, FS-2 19mm 3/8 Circle, 18", 4-0), the mouse was injected subcutaneously with 1 mg/kg buprenorphine SR-LAB long acting narcotic and monitored until recovery of full mobility. The mice were single-housed to prevent obstruction of the surgery site by other mice, and were injected with buprenorphine SR every 72 h until the end of the experiment.

For *Mycobacterium tuberculosis* infection, 6-7 weeks old WT with normal iron status, iron-loaded WT (IP injected with 20 mg/mouse iron dextran, 4 days prior infection), or naturally iron-loaded HKO mice were challenged by aerosol with 30 CFU per mouse. The mice were euthanized and tissues were collected in two groups, respectively 5 and 10 weeks after infection.

Minihepcidin synthesis and preparation

Minihepcidin PR73 was synthesized by standard solid-phase Fmoc chemistry as previously described [5]. To dissolve PR73, the peptide and solvent DSPE-020 CN (NOF Corporation) were first separately dissolved in 70% ethanol (Gold Shield Chemical Co), then mixed and dried in a SpeedVac to remove the ethanol, and stored at 4 C for a maximum of 5 days. Lyophilized mixture was suspended in sterile water (Abbot Laboratories) immediately before use to a final concentration of 100 nmol PR73 per 100 µl injectate. Each mouse received 100 µl solvent or PR73 solution by IP injection.

Assessment of bacterial burden

Heparinized blood was collected using cardiac puncture, and a piece of the liver (~100 mg) and spleen (~50 mg) from each mouse was weighed and homogenized in sterile dH_2O. For some experiments (noted in the legend of the figure) the whole liver and spleen were homogenized, 50µl/75µl of the homogenate were weighed, sterile dH_2O was added and the mixture was processed. Each fluid was serially diluted 5 or 10-fold with sterile phosphate-buffered saline (PBS) containing 0.1% Tween-20 (Fisher), 5 µl of each dilution was plated on Luria-Bertani (LB) agar plates, and plates were incubated at room temperature (RT) for 24 h to 48 h. The colonies were counted using a dissecting microscope. For lung and spleen CFUs from mice infected with *Mycobacterium tuberculosis*, the whole organ was homogenized, the homogenate was serially diluted and 100 µl per plate were spread. The plates were incubated for 2.5 weeks and colonies number was counted.

For catheter associated *Staphylococcus aureus* infection, infection progression was assessed through *in vivo* bioluminescence imaging every other day starting on day 1 after surgery (imaging center in the California NanoSystems Institute at UCLA) with IVIS 200 from Xenogen Inc. The imaging settings were: 5min exposure, binning – medium, F/stop 1.2, photo binning – medium, F/stop 16, open filter, XFOV on, measure region of interest (ROI) – auto, 5% threshold. Both total flux and average radiance were quantified. In a small number of mice, for an unknown reason there was a complete lack of bioluminescent signal at all time points after catheter implantation and these animals were excluded from the final analysis since infection burden could not be evaluated.

Non-heme iron concentration measurements

Blood was collected by cardiac puncture, and serum obtained using separator tubes (BD). Iron concentration was measured by the colorimetric Iron SL assay (Sekisui Diagnostics) following the manufacturer's instructions. Serum samples with high hemolysis (as indicated by redness and high baseline absorbance) were not included in the analyzed data (as advised by the manufacturer's protocol). For liver iron

measurements, about 90% of the liver was homogenized, 75 µl from the homogenate was weighed and incubated in 1125 µl protein precipitation solution (0.53N HCl Fisher and 5.3% trichloroacetic acid, Fisher) at 100^0C for 60 min. After centrifugation to remove tissue debris, the supernatant was analyzed for iron concentration using Iron SL assay (Sekisui Diagnostics). Serial dilutions of Iron AA standard (RICCA Chemical Company) were used to generate standard curves.

Histopathology

Tissues (liver, spleen, ileum) for histopathology analysis were freshly collected and fixed in 10% formalin (Fisher) solution for 24 h, then paraffin-embedded and sectioned at the UCLA Translational Pathology Core Laboratory (TPCL). H&E staining was also performed by TPCL. For immunohistochemical analysis, the slides were stained with rabbit antibody specific for *Yersinia enterocolitica* O9*,* kindly provided by Dr. Mikael Skurnik (University of Helsinki, Finland) and visualized by Vectastain Elite ABC Kit, Rabbit IgG (Vector Laboratories) following the manufacturer's protocol. Peroxidase staining was developed using ImmPact DAB (Vector Laboratories) and fast nuclear red was used as counter stain.

Gene expression assessment

Total RNA was isolated from frozen liver using TRIzol Reagent (Life Technologies). cDNA was synthesized using iScript cDNA Synthesis Kit (Bio-Rad) following the manufacturer's protocol. Quantitative real-time PCR was performed using Sso Advance SYBR Green Supermix (Bio-Rad) and CFX96 Touch Real-Time PCR Detection System (Bio-Rad), with following primer sequences for Saa1 (forward: AGTCTGGGCTGCTGAGAAAA; reverse: ATGTCTGTTGGCTTCCTGTG) and Hprt (forward: CTGGTTAAGCAGTACAGCCCCAA; reverse: CAGGAGGTCCTTTTCACCAGC). All samples were measured in triplicate. Saa1 expression was normalized to Hprt and results shown as $dCt = Ct_{Hprt}-Ct_{Saa1}$.

Hepcidin ELISA

Hepcidin protein concentration in the serum was determined as previously described [5] by ELISA using Ab2B10 (capture) and Ab2H4-HRP (detection) antibodies kindly provided by Amgen, and synthetic mouse hepcidin-25 was used to generate standard curves ranging from 400 pg to 3.2 pg/ml.

NTBI assessment by enhanced labile plasma iron assay (eLPI)

In a protocol adapted from Esposito et al [6], HBS (20 mM HEPES Sigma, 150 mM NaCl Fisher, pH=7.4) was iron-depleted by incubation with Chelex-100 chelating resin (Bio-Rad) for 1 h. Solution was filtered to remove resin particles and supplemented with 60 nM deferrioxamine (Sigma). Dihydrorhodamine 123 dihydrochloride salt (DHR) 50 mM stock solution in dimethylformamide (Biotium) was stored in the dark, at -20^{0}C and under nitrogen. Additional reagents included: 10 mM deferiprone (DFP) stock (Sigma), 40 mM ascorbic acid (AA) stock (Sigma) stored in the dark at -20^{0}C, 35 mM nitrilotriacetic acid (NTA) stock with pH=7 (Sigma) stored protected from light.

In order to construct the standard curve, plasma-like medium (PLM, 20mM HEPES Sigma, 150 mM NaCl Fisher, 120 µM sodium citrate, 40 µM ascorbic acid, 1.2 mM sodium phosphate dibasic, 10 mM sodium bicarbonate, 40 mg/ml bovine serum albumin, pH 7.4) was supplemented with ferric iron. Ferric iron was prepared as a mixture of 35 mM NTA (pH 7) and 10 mM ferrous ammonium sulphate (FAS, Sigma) incubated for 30 min at RT to allow for oxidation of Fe(II) to Fe(III) and then stored at 4C. The mixture of PLM and FAS/NTA was incubated at 37C for 30 min and then diluted in iron-free HBS to concentrations ranging from 5 to 0.41 µM. PLM that was not supplemented with iron was used as blank.

Before the start of each measurement, HBS was incubated with 0.5 mM NTA (final concentration) at 37C for 15-30 min. For LPI measurements, 5 to 20 µl of serum samples were pipetted in 4 to 6 separate wells of Multiplate PCR 96-well plate (BioRad) and then 140 µl/well of HBS/50 µM DHR/40 µM AA/0.5 mM NTA were added to half of the wells ("-DFP"). The remaining buffer was supplemented with DFP to final concentration 100 µM and 140 µl/well were added to the other half of the wells for each sample ("+DFP"). Changes in fluorescence were then detected for 40 min at 37C with a read every 2 min using CFX96 Touch Real-Time PCR Detection System (Bio-Rad) with FAM selected as fluorophore. The slope of fluorescence change between 15th and 40th minute was calculated for each sample, the replicates were averaged and the difference between "-DFP" and "+DFP" was used as a measure of LPI.

In vitro assay for iron-dependent growth of Yersinia enterocolitica on plasma-agar

Human plasma (from three separate donors) was inactivated for 30 min at 56C, centrifuged to remove precipitate and then incubated overnight (14-20 h) at 37 C with a range of ferric ammonium citrate (Sigma) concentrations. A few drops of hot concentrated liquid agar (12% agar dissolved in water, autoclaved and kept in the hot water from the autoclave to prevent premature solidification) were added to 2-4 ml plasma to produce 90% plasma agar plates. The plasma was kept at 56C to prevent immediate solidification of the agar drops and poured into a 12-well plate with 2 plates per condition. *Yersinia enterocolitica* was resuspended at 10^6 CFU/ml and 5 µl plated in

triplicates on each plasma agar well, incubated for 24-48 h at 37 C and bacterial growth assessed using a microscope.

Transferrin saturation

Transferrin saturation (Tf sat) of plasma samples used for *Y.enterocolitica in vitro* growth was determined by measuring the unsaturated iron binding capacity (UIBC) of non-supplemented plasma with UIBC kit (Sekisui) following the manufacturer's protocol. Plasma iron concentrations combined with UIBC were used to calculate Tf sat.

In vitro assay for iron-dependent growth of Vibrio vulnificus in human plasma liquid cultures

Deidentified human plasma samples (from six separate donors) were obtained from UCLA Clinical Laboratories, inactivated by heating, and plasma iron measured as described above. *V. vulnificus* ($1x10^3$ CFU/ml) were grown in 250 µl of human plasma supplemented with 0-100 µM of either ferric ammonium citrate (FAC), holo-transferrin or apo-transferrin, for 10 h at 37C with shaking (300 rpm) in a plated reader. Bacterial growth was measured every 15 min by quantification of the optical density at 600 nm.

Determination of GFP-expressing and total cell count at the site of infection in LysEGFP mice

LysEGFP mice were injected with 10^8 CFU/mouse *Y. enterocolitica* IP. Six hours later fluid from the peritoneum was collected through IP lavage. Briefly, after euthanasia the peritoneum of the mice was injected with ice-cold PBS containing 3mM EDTA, massaged gently and the fluid was aspirated using 20Ga needle (to prevent damaging the cells). The obtained fluid was tested for bacterial concentration (CFU count as described previously). In addition, cell infiltrate was assessed after a 10-fold dilution by counting the number of GFP cells as well as total cell number under the microscope using hemocytometer. Four squares were counted and averaged per each animal.

Statistics

All statistical analysis was performed using SigmaPlot and the samples were compared through Student's t test if the data were normally distributed or Mann-Whitney rank sum test if they were not normally distributed. Two-way ANOVA was used to compare kinetics of serum hepcidin concentration, serum iron concentration and liver Saa1 expression between infected and uninfected animals. Differences in survival were assessed using Kaplan-Meier survival curves and log-rank test. The results were considered statistically significant if p value was below 0.05. Chi-squared test was

performed to compare the presence or absence of abscesses in tissues from infected animals. Box plots with error bars are showing the median, 10th, 25th, 75th, and 90th percentiles. Bar graphs with error bars are showing the mean and standard deviations. Data for tissue bacterial burden measurements (CFUs/mg or ml) were log-transformed before they were subjected to statistical analysis and plotted on the graph (Fig. 3A, 3B, 4D, 5C, 5J, 6C, S5D). G*Power was used to calculate group sizes with effect size ρ = 0.9, α error prob = 0.05 and power (1-β err prob) = 0.80.

References

1. Pribaz J, Bernthal, NM, Billi, F, Cho, JS, Ramos, RI, Guo, Y, Cheung, AL, Francis, KP, Miller, LS. Mouse model of chronic post-arthroplasty infection: noninvasive in vivo bioluminescence imaging to monitor bacterial burden for long-term study. *J Orthop Res*. 2012;30(3):335-340.
2. Hwang A, Lee, B, Clemens, D, Dillon, BJ, Zink, JI, Horwitz, MA. pH-Responsive Isoniazid-Loaded Nanoparticles Markedly Improve Tuberculosis Treatment in Mice. *Small*. 2015;11(38):5066-5078.
3. Lesbordes-Brion JC, Viatte L, Bennoun M, et al. Targeted disruption of the hepcidin 1 gene results in severe hemochromatosis. *Blood*. 2006;108(4):1402-1405.
4. Bernthal N, Stavrakis, AI, Billi, F, Cho, JS, Kremen, TJ, Simon, SI, Cheung, AL, Finerman, GA, Lieberman, JR, Adams, JS, Miller, LS. A Mouse Model of Post-Arthroplasty Staphylococcus aureus Joint Infection to Evaluate In Vivo the Efficacy of Antimicrobial Implant Coatings. *PLoS ONE*. 2010;5(9):e12580.
5. Arezes J, Jung, G, Gabayan, V, Valore, E, Ruchala, P, Gulig, PA, Ganz, T, Nemeth, E, Bulut, Y. Hepcidin-induced hypoferremia is a critical host defense mechanism against the siderophilic bacterium *Vibrio vulnificus*. *Cell Host Microbe*. 2015;17(1):47-57.
6. Esposito B, Breuer, W, Sirankapracha, P, Pootrakul, P, Hershko, C, Cabantchik, ZI. Labile plasma iron in iron overload: redox activity and susceptibility to chelation. *Blood*. 2003;102(7):2670-2677.

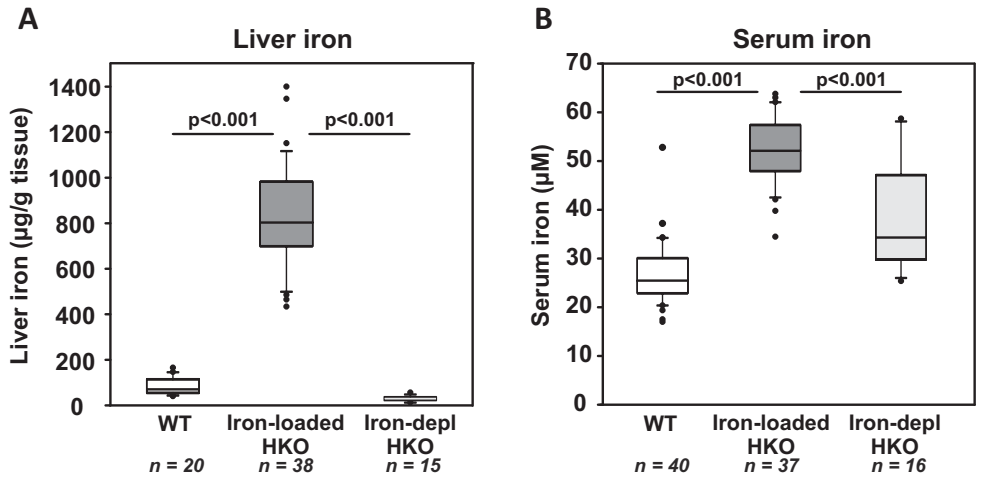


Figure S1. Hepcidin knockout mice are iron loaded at baseline compared to wild-type mice but can be efficiently iron depleted by low iron diet. (**A**) Liver iron and (**B**) serum iron concentration in WT mice, naturally iron-loaded HKO mice, and dietary iron-depleted HKO mice without systemic infection. Data from six independent experiments were combined. Statistical analysis was performed using Student's t-test for normally distributed data and Man-Whitney U test for data that were not normally distributed.

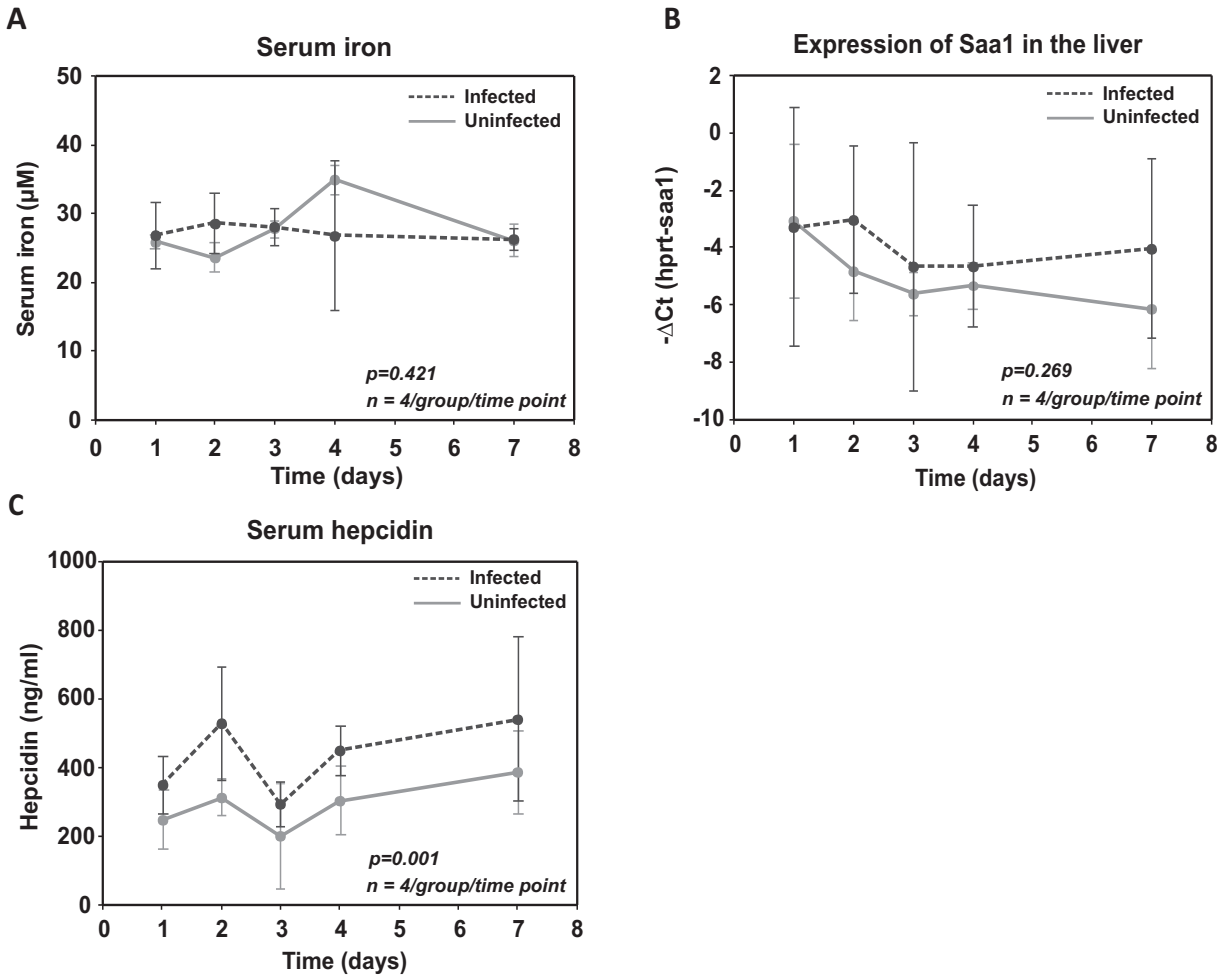


Figure S2. Oral infection with *Yersinia enterocolitica* O9 does not induce systemic inflammatory response. WT mice were either given saline (control) or infected with 10^8 CFU/mouse *Y. enterocolitica* O9 through oral gavage, and analyzed 1, 2, 3, 4 and 7 days after challenge. (**A**) Serum iron, and (**B**) liver Saa1 mRNA expression were not different between infected and uninfected groups. (**C**) Serum hepcidin only marginally increased in infected mice. Statistical analysis for comparison of uninfected to infected group was performed using two-way ANOVA.

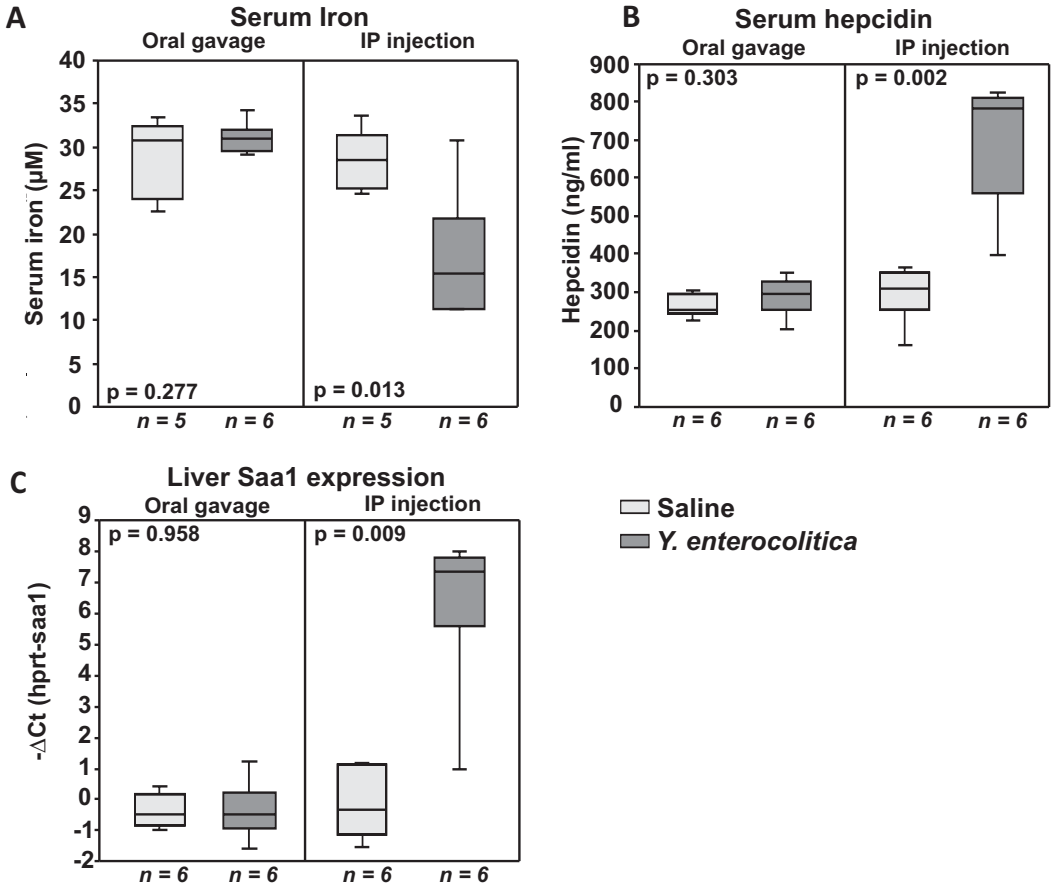


Figure S3. Oral exposure to *Y. enterocolitica* O9 does not generate systemic inflammation or increase hepcidin in healthy WT mice. Serum iron **(A)**, serum hepcidin (**B**) and liver Saa1 mRNA expression (**C**) 6h after oral or intraperitoneal (IP) infection of WT mice with 10^8 CFU *Y. enterocolitica* O9. Statistical analysis was performed using Student's t-test if data were normally distributed, or Mann-Whitney U test if they were not normally distributed.

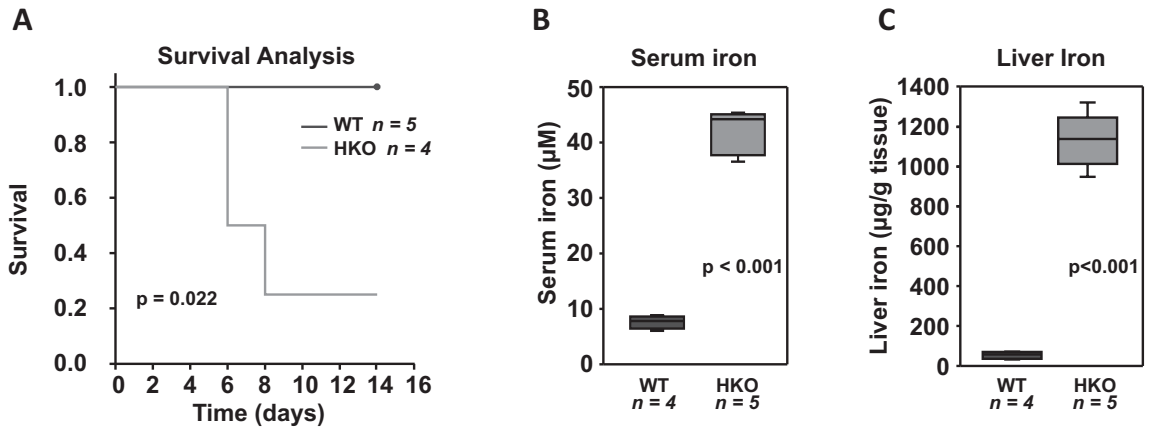


Figure S4. Susceptibility of LysEGFP mice to yersiniosis-associated mortality is promoted by hepcidin deficiency and iron loading. Mice with GFP-expressing neutrophils and macrophages (GFP inserted into the lysozyme M gene) were infected orally with 10^8 CFU/mouse *Y. enterocolitica O9*. Mice that are WT for hepcidin survived 100% while mice lacking hepcidin had only 30% survival (**A**). Serum iron (**B**) and liver iron (**C**) concentration correlated with the observed mortality. Student's t-test was used for normally distributed data and Mann-Whitney U test for data that are not normally distributed. Survival difference were analyzed using Kaplan-Meier log-rank test.

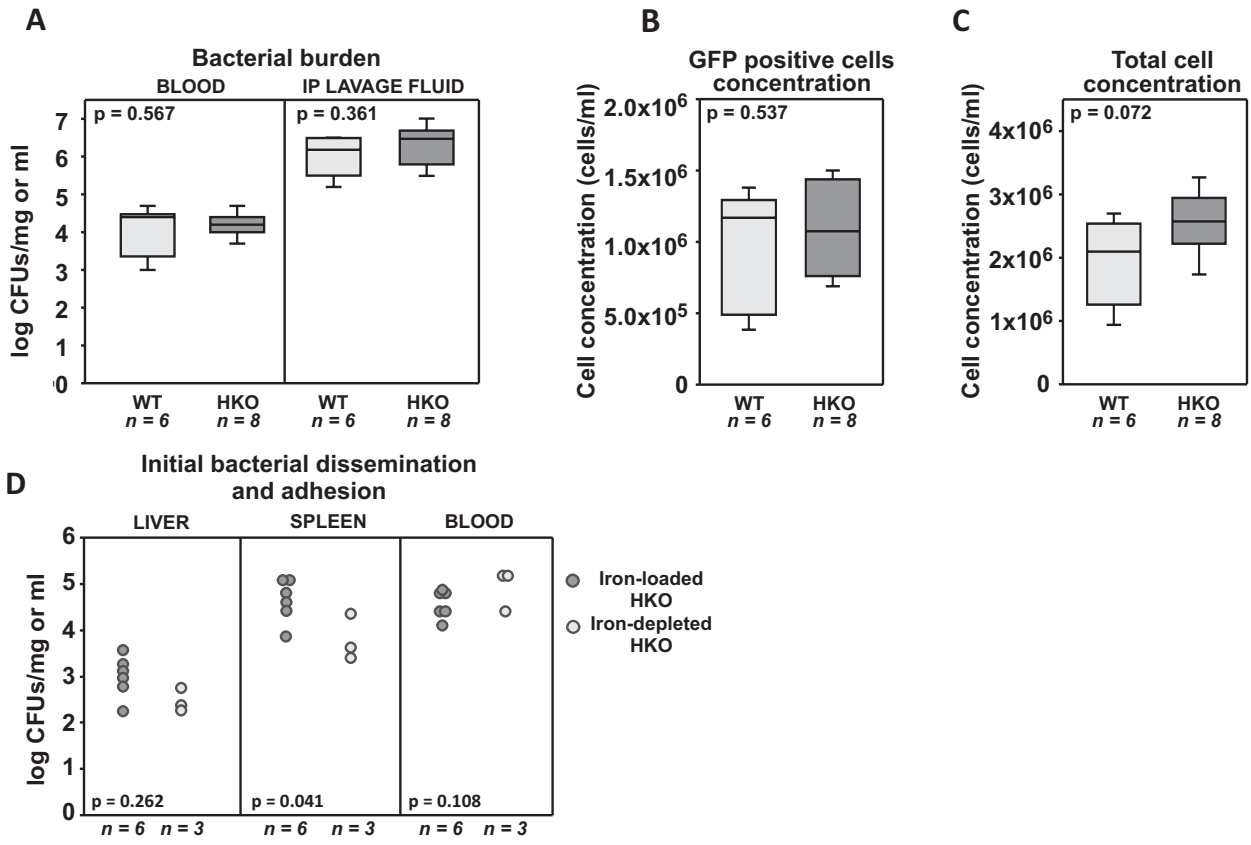


Figure S5. Hepcidin deficiency does not affect initial bacterial killing and immune cell recruitment to infection site nor initial bacterial attachment to target tissues. Mice with GFP-expressing neutrophils and macrophages (GFP inserted under lysozyme M promoter) that were either WT or KO for hepcidin were infected through IP injection with 10^8 CFU/mouse *Yersinia enterocolitica* O9. (A) Initial bacterial killing (CFUs from the fluid collected through IP lavage) and systemic spread (blood CFUs) did not differ between the two groups. (B and C) Hepcidin deficiency did not affect initial immune cell recruitment. (D) HKO mice (non GFP expressing) that were either naturally iron-loaded or iron-depleted (through diet and phlebotomy) were injected IP with 10^8 CFU *Yersinia enterocolitica* O9. Initial bacterial spread and adhesion to target tissues (liver, spleen and blood) was measured 6 h later and was equivalent between iron-loaded and iron-depleted HKOs. Statistical analysis was done using Student's t-test if data were normally distributed or Mann-Whitney U test if they were not.

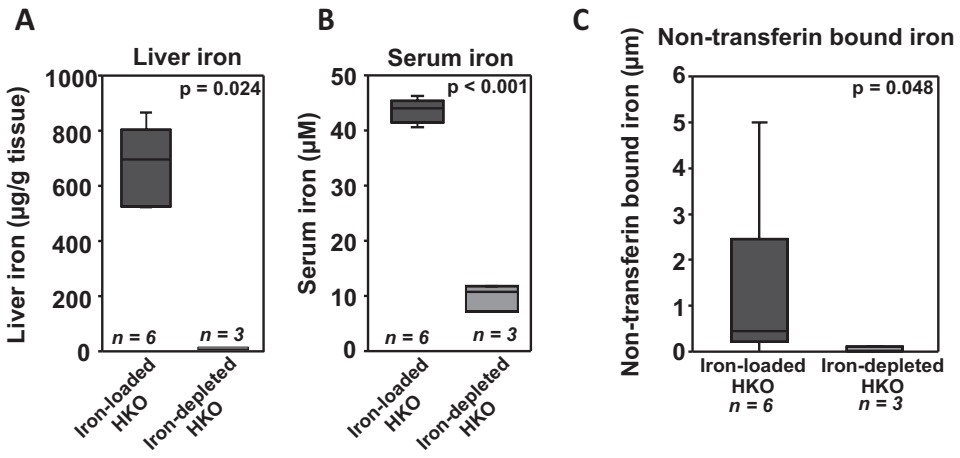


Figure S6. Iron overload does not affect initial bacterial adhesion to target tissues. HKO mice that were either naturally iron-loaded or iron-depleted (through diet and phlebotomy) were injected IP with 10^8 *Y. enterocolitica* O9. Despite large difference in liver iron (**A**), serum iron (**B**) and NTBI (**C**) between iron-loaded and iron-depleted groups, there was not difference in initial bacterial adhesion to target tissues (liver, spleen and blood, *Fig 5D*). Student's t-test was used for normally distributed data and Mann-Whitney U test for data that are not normally distributed.

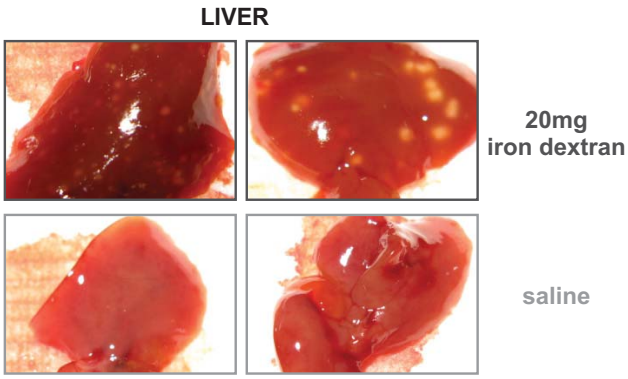


Figure S7. Parenterally iron-loaded WT mice develop systemic infection after oral administration of *Y. enterocolitica* O9. WT mice were iron-loaded by IP injection of 20mg iron dextran. Control mice were injected with the same volume of saline. Saline and iron dextran were administered one day before infection. The mice were orally infected with 10^8 CFU/mouse *Y. enterocolitica* O9. Gross pathology of the liver on day 13 revealed multiple abscesses in iron-loaded mice. Livers of two representative animals are shown for each condition.

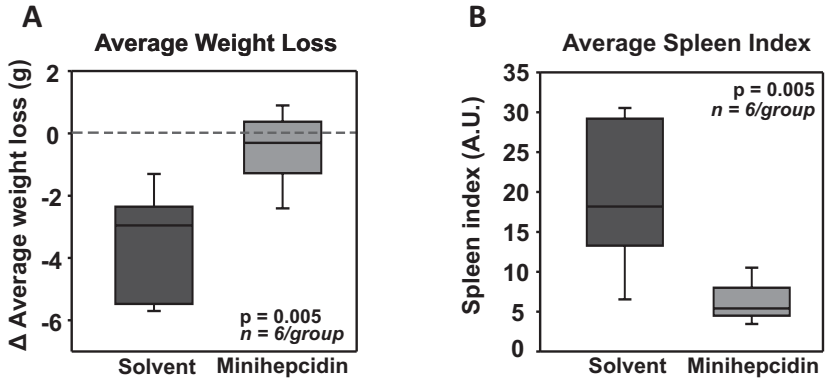
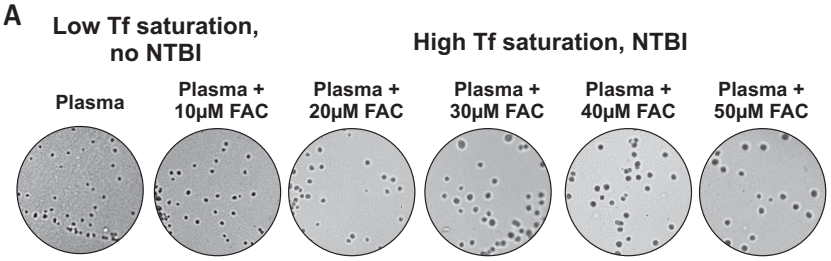


Figure S8. Minihepcidin treatment prevents weight loss and splenomegaly in infected iron-loaded WT mice. WT mice were iron-loaded by IP injection of 20mg iron dextran one day before infection, and were orally infected with 10^8 CFU/mouse *Y. enterocolitica* O9 and treated IP with solvent or 100 nmol minihepcidin for 10 days. Solvent-treated mice lost 2.5 to 5.7 g of weight (10% to 25% of their total weight) while minihepcidin treatment prevented the weight loss **(A)**. In addition, organomegaly in the target organs was observed with spleen index increasing up to 5-fold **(B)**. Student's t-test was used for normally distributed data and Mann-Whitney U test for data that were not normally distributed.

A



B

µM FAC added	Tf sat	µM NTBI	Bacterial growth
0	37%	0	+
10	51%	0	+
20	65%	>5	+
30	72%	>5	+
40	83%	>5	+
50	96%	>5	+

Figure S9. Growth of non-siderophilic *Yersinia enterocolitica* O8 does not depend on NTBI. *Yersinia enterocolitica* O8 (10^6 cfu/ml) was grown on 90% plasma agar that was pre-incubated at 37C for 20h alone or with a range of ferric ammonium citrate (FAC) concentrations. (**A**) Images represent bacterial growth as detected with light microscope after 22 h at 37C. Bacterial growth did not depend on high transferrin (Tf) saturation or NTBI (**B**).

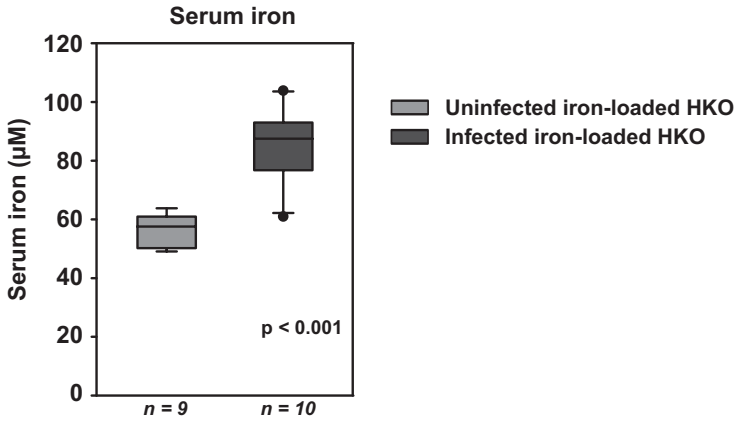


Figure S10. Serum iron increases in systemic infection of hepcidin-deficient mice. Naturally iron-loaded HKO mice were orally gavaged with saline (uninfected) or 10^8 CFU/mouse *Y. enterocolitica* O9 (infected). Samples from the infected animals were collected on day 3, 4 and 5 after infection upon developing severe disease signs. Matching numbers of uninfected animals were sacrificed at the same time points. Serum iron levels were significantly higher in the mice that developed severe systemic infection compared to the uninfected. Student's t-test was used for statistical comparison of the two groups.

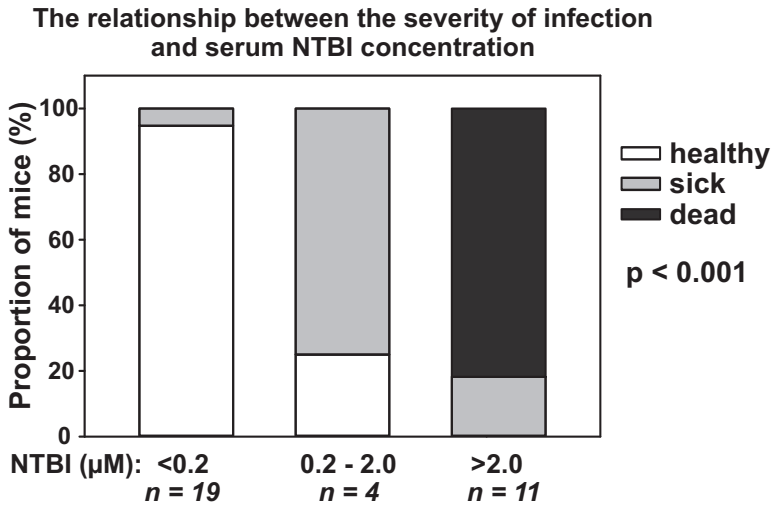


Figure S11. The relationship between infection outcomes and serum NTBI concentrations in mice. Mice were infected orally with 10^8 CFU/mouse *Y. enterocolitica* O9. Infection outcomes were represented as three distinct groups: "healthy" (no weight loss or ill appearance); "sick" (having severe systemic infection but no mortality within 10 days of infection); "dead" (animals euthanized when showing signs of imminent mortality). Data include animals from multiple experiments: iron-loaded WT mice, iron-loaded and iron-depleted HKO mice, solvent and minihepcidin treated animals. Chi square test was used for statistical analysis.

CHAPTER 2

Hepcidin-mediated iron sequestration protects against bacterial dissemination during pneumonia

JCI insight

RESEARCH ARTICLE

Hepcidin-mediated iron sequestration protects against bacterial dissemination during pneumonia

Kathryn R. Michels,[1] Zhimin Zhang,[2] Alexandra M. Bettina,[1] R. Elaine Cagnina,[2] Debora Stefanova,[3] Marie D. Burdick,[2] Sophie Vaulont,[4] Elizabeta Nemeth,[5] Tomas Ganz,[5] and Borna Mehrad[1,2,6]

[1]Departments of Microbiology, Immunology, and Cancer Biology, [2]Division of Pulmonary & Critical Care Medicine, Department of Medicine, University of Virginia, Charlottesville, Virginia, USA. [3]Departments of Molecular, Cellular, and Integrative Physiology, University of California, Los Angeles, California, USA. [4]INSERM U1016, Cochin Institute, Descartes University, Paris, France. [5]Department of Medicine, David Geffen School of Medicine, University of California, Los Angeles, California, USA. [6]Beirne B. Carter Center for Immunology, University of Virginia, Charlottesville, Virginia, USA.

Gram-negative pneumonia is a dangerous illness, and bacterial dissemination to the bloodstream during the infection is strongly associated with death. Antibiotic resistance among the causative pathogens has resulted in diminishing treatment options against this infection. Hepcidin is the master regulator of extracellular iron availability in vertebrates, but its role in the context of host defense is undefined. We hypothesized that hepcidin-mediated depletion of extracellular iron during Gram-negative pneumonia protects the host by limiting dissemination of bacteria to the bloodstream. During experimental pneumonia, hepcidin was induced in the liver in an IL-6–dependent manner and mediated a rapid decline in plasma iron. In contrast, hepcidin-deficient mice developed a paradoxical increase in plasma iron during infection associated with profound susceptibility to bacteremia. Incubation of bacteria with iron-supplemented plasma enhanced bacterial growth in vitro, and systemic administration of iron to WT mice similarly promoted increased susceptibility to bloodstream infection. Finally, treatment with a hepcidin analogue restored hypoferremia in hepcidin-deficient hosts, mediated bacterial control, and improved outcomes. These data show hepcidin induction during pneumonia to be essential to preventing bacterial dissemination by limiting extracellular iron availability. Hepcidin agonists may represent an effective therapy for Gram-negative infections in patients with impaired hepcidin production or signaling.

Introduction

Infections caused by aerobic Gram-negative bacteria are prevalent and dangerous. As a group, these organisms are the most common etiology of nosocomial infections, including most cases of hospital-acquired pneumonia, ventilator-associated pneumonia and healthcare-associated pneumonia, and they are important causes of morbidity and death in hospitalized patients (1). Dissemination of these organisms from the primary site of infection to the bloodstream is especially associated with mortality (2, 3). The progressive rise in antibiotic resistance among Gram-negative bacteria, particularly in the healthcare setting, has critically diminished the available treatment options for these infections. Better mechanistic understanding of the host-pathogen interplay during Gram-negative infections has the potential to lead to novel therapeutic strategies to augment the diminishing armamentarium of traditional antibiotics.

Iron is an essential component of many proteins and a required nutrient for nearly all organisms. In biological systems, free iron ions are present at extremely low concentrations, and the competition for iron between pathogens and the host is important to the outcome of many infections (4). While the iron acquisition mechanisms of aerobic Gram-negative bacteria are known to be essential to their virulence (5), the host mechanisms of iron restriction in these infections are incompletely defined.

Under homeostatic conditions, plasma iron is rapidly turned over with a half-life of < 1 hour, being continuously utilized in erythropoiesis and replenished by splenic macrophages that scavenge iron from senescent erythrocytes (6). The hormone hepcidin is the key regulator of plasma iron concentration that acts by mediating the degradation of the only known cellular iron exporter, ferroportin, thus trapping

Conflict of interest: EN and TG are inventors of minihepcidins, hold a patent on these peptides (US20120040894 A1), and are scientific founders and shareholders in Merganser Biotech, a company involved in the commercial development of minihepcidins.

Submitted: December 19, 2016
Accepted: February 9, 2017
Published: March 23, 2017

Reference information:
JCI Insight. 2017;2(6):e92002. https://doi.org/10.1172/jci.insight.92002.

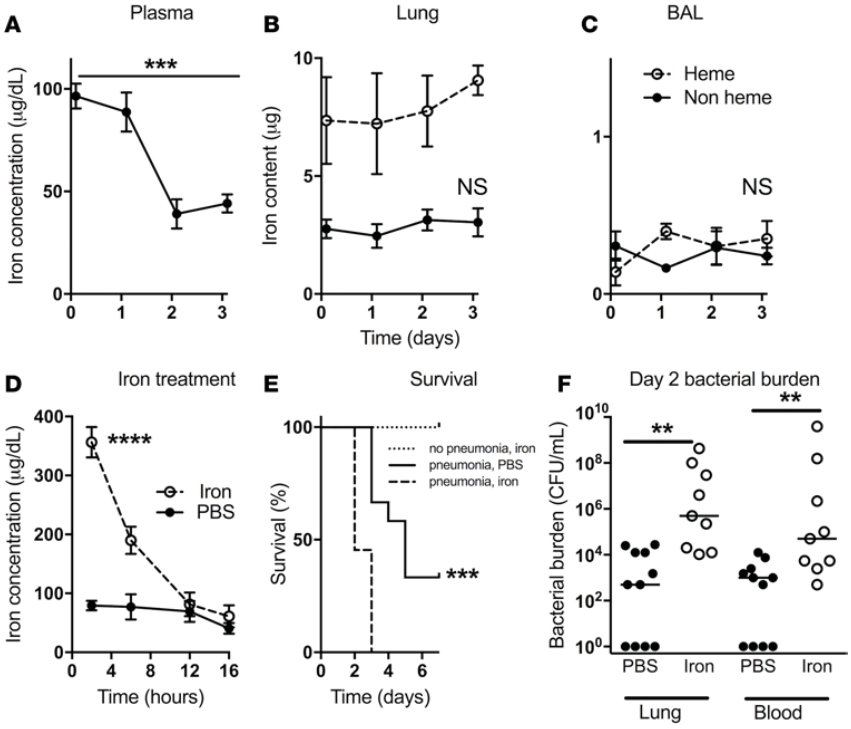


Figure 1. Iron availability during *Klebsiella* pneumonia. Time 0 represents uninfected animals. (**A**) Iron concentration in the plasma. (**B** and **C**) Calculated total iron levels in whole lung homogenate per mouse, and bronchoalveolar lavage fluid (BAL) recovered in a volume of 1 ml per mouse. Data shown as mean ± SE; n = 4–6 animals per time point, representative of 2 independent experiments; ***P < 0.001 (1-way ANOVA, multiple comparison for linear trend). (**D**) Plasma iron following i.p. injection with PBS or ferric ammonium citrate (iron) 30 minutes prior to intrapulmonary *K. pneumoniae* challenge. n = 6–8 per group per time point, combined result of 2 experiments; ****P < 0.0001, two-way ANOVA. (**E**) Mice were treated with either PBS or ferric ammonium citrate (iron) 30 minutes prior to intrapulmonary *K. pneumoniae* challenge and again 24 hours thereafter. n = 6–12 per group, combined result of 2 experiments; ***P < 0.001 Mantel-Cox test. (**F**) Bacterial burden on day 2 of infection in mice treated with ferric ammonium citrate or PBS prior to intratracheal challenge with *K. pneumonia*. Horizontal lines represent median, and each circle represents 1 animal; animals with no detectable bacteria are reported to have a bacterial burden of 1 CFU on the logarithmic scale. n = 9–11, combined result of 2 experiments; **P < 0.01 Mann-Whitney U test.

iron inside cells and reducing extracellular iron (7). During homeostasis, hepcidin is induced by elevated extracellular and intracellular iron levels via SMAD4 signaling, and is inhibited by anemia and hypoxia. During inflammation, hepcidin is induced as an acute-phase reactant by IL-6 and Activin B via STAT3 and SMAD4, respectively (8, 9). In the context of inflammation, hepcidin mediates acute hypoferremia, which is posited to be a defense mechanism against infectious disease; continual hepcidin production in this setting can infamously cause anemia of chronic inflammation. The role of hepcidin in disorders of iron metabolism is well established, but its contribution to antimicrobial host defenses is an emerging field. For example, hepcidin appears to protect the host against malaria but to promote the growth of pathogens that reside within the intracellular niche of macrophages (10). Hepcidin-mediated hypoferremia is essential for protection of the host against *Vibrio vulnificus* in a murine model (11), consistent with the clinical observation that individuals with iron-overload conditions are uniquely susceptible to this organism (12). In contrast, the role of hepcidin as a general defense against common bacterial infections, such as those caused by Enterbacteriaceae, remains unknown.

We reasoned that the bloodstream dissemination of microorganisms from the primary site of infection is a critical complication in Gram-negative bacterial infections. In the context of pneumonia, as well as other focal infections caused by aerobic Gram-negative bacilli, bacteremia is strongly associated with sepsis and death (13, 14). We therefore tested the hypothesis that hepcidin-mediated depletion of extracellular iron during Gram-negative pneumonia protects the host by limiting dissemination of bacteria to the bloodstream.

Results

Plasma iron is suppressed during bacterial pneumonia. We used a well-described model of *Klebsiella* pneumonia caused by a virulent strain of bacteria, delivered directly into the trachea of sedated experimental mice (15, 16). We first characterized the effect of *Klebsiella* pneumonia on iron metabolism in WT mice. As expected, plasma iron concentration decreased quickly in WT mice following infection (Figure 1A), similar to prior reports with acute inflammatory stimuli (9). To assess the availability of iron to bacteria in the lungs, we also measured heme-associated and non–heme-associated iron levels in whole lung homogenates (which includes both intra- and extracellular iron), and in the extracellular space, in the bronchoalveolar lavage (BAL) supernatant (Figure 1, B and C). We found that most lung iron was intracellular, and extracellular iron levels were low and did not change appreciably during infection.

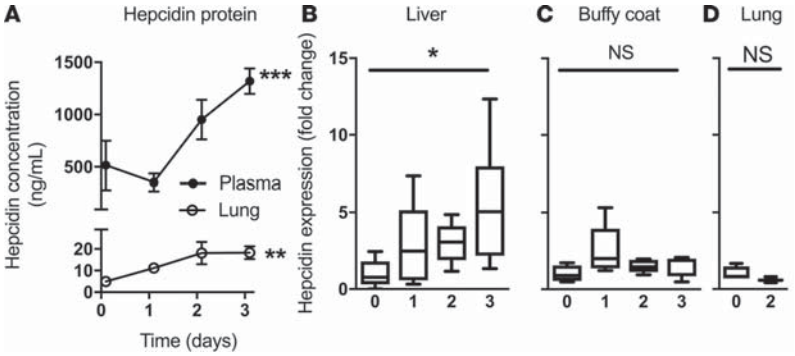


Figure 2. Hepcidin induction during *Klebsiella* pneumonia. Time 0 represents naive animals. (**A**) Hepcidin protein levels in the plasma and whole lung homogenate following infection. Data represent mean ± SEM. (**B**–**D**) Hepcidin mRNA in the liver, buffy coat, and lung normalized to GAPDH expression and then to day 0. Box and whisker plots show median (line within box), upper and lower quartiles (upper and lower box boundaries), and total range (bars); n = 4–6 animals per time point in each panel; *, **, and *** denote P values of <0.05, <0.01, and <0.001, respectively (1-way ANOVA, multiple comparison for linear trend for panels **A**–**C**, t test for panel **D**).

Increased iron availability worsens the outcome of infection. To determine whether iron availability influences host defense during the course of infection, we tested the effect of transient increase in extracellular iron availability, achieved by i.p. injection of ferric ammonium citrate, on the outcome of *Klebsiella* pneumonia. Mice treated with iron prior to intrapulmonary *K. pneumoniae* challenge developed transient elevation in plasma iron that resolved completely within 12 hours (Figure 1D) without influencing lung iron (Supplemental Figure 1; supplemental material available online with this article; https://doi.org/10.1172/jci.insight.92002DS1), consistent with prior studies indicating that excess iron is rapidly cleared from the blood and redistributed to the BM, spleen, and liver (6). This transient increase in iron availability during the first 24 hours after infection was associated with a markedly increased mortality from pneumonia associated with increased bacterial burden in the lung and the blood (Figure 1, E and F). Since WT mice developed hypoferremia upon infection with *K. pneumoniae,* and excess iron was associated with poor infection outcome, we hypothesized that endogenous iron regulation was important for controlling infection.

Hepcidin regulates plasma iron during bacterial pneumonia by an IL-6–dependent mechanism. To assess the role of hepcidin in mediating hypoferremia during pneumonia, we began by characterizing hepcidin expression during the infection. Infection resulted in a marked increase in hepcidin protein levels in plasma, in parallel with the development of hypoferremia (Figure 2A). Hepcidin protein concentration also increased in the

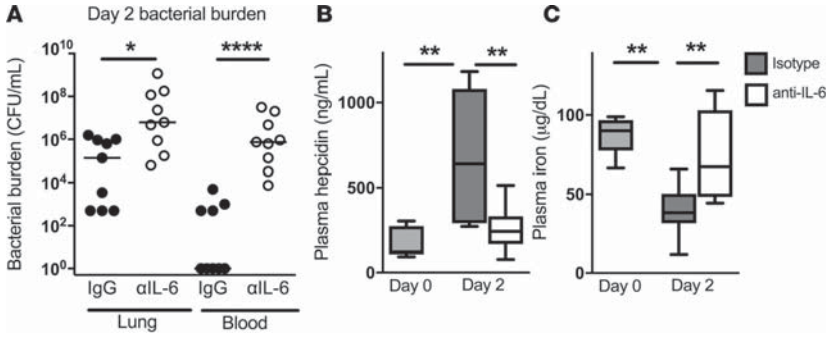


Figure 3. The role of IL-6 in hepcidin induction during *Klebsiella* pneumonia. (**A**) Animals were treated daily with an isotype control or IL-6 neutralizing monoclonal antibody and assessed for bacterial burden on day 2 of infection. Horizontal lines represent median, and each circle represents 1 animal; animals with no detectable bacteria are reported to have a bacterial burden of 1 CFU on the logarithmic scale; * and **** denote P values of <0.05 and <0.0001 by Mann-Whitney U test, respectively. (**B** and **C**) Plasma hepcidin protein and iron levels in uninfected and infected animals treated with isotype or IL-6 neutralizing antibody. Box and whisker plots show median (line within box), upper and lower quartiles (upper and lower box boundaries), and total range (bars) combined from 2 experiments; n = 8–9 animals per group; **P < 0.01, one way ANOVA Tukey post-test.

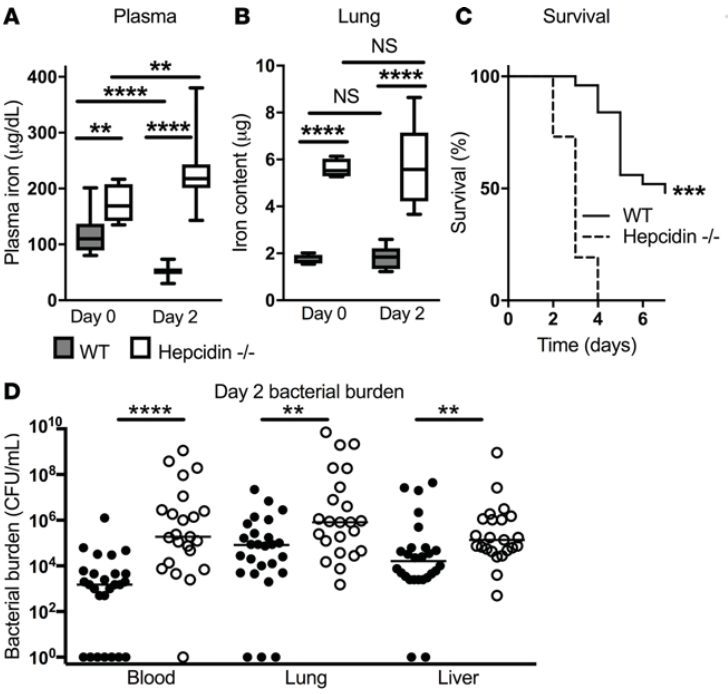


Figure 4. The role of hepcidin in *Klebsiella* pneumonia and dissemination. (**A** and **B**) Comparison of plasma or lung nonheme iron levels in WT and hepcidin$^{-/-}$ mice before and 2 days after infection. Box and whisker plots show median (line within box), upper and lower quartiles (upper and lower box boundaries), and total range (bars) of data from 2 experiments; n = 4–9 per group; ** and **** denote P values of <0.01 and <0.0001 by one-way ANOVA with Tukey post test, respectively. (**C**) Survival of WT and hepcidin$^{-/-}$ mice during pneumonia. n = 26–30 mice per group, combined from 3 independent experiments; ***P < 0.001 Mantel-Cox test. (**D**) Bacterial burden on day 2 of infection in WT and hepcidin$^{-/-}$ mice in indicated organs. Pooled data from 3 independent experiments; n = 23–26. Horizontal lines represent median and each circle represents one animal; animals with no detectable bacteria are reported to have a bacterial burden of 1 CFU on the logarithmic scale; ** and **** denote P values of <0.01 and <0.0001, respectively, using the Mann-Whitney U test.

lung but at relatively low concentrations (~15 ng in the entire lung, as compared with ~1,500 ng/ml of plasma on day 3; Figure 2A). The liver is the dominant source of hepcidin at baseline (17, 18), but hepcidin can be induced in leukocytes and airway epithelial cells in response to inflammatory stimuli under in vitro conditions (19–21). We thus measured hepcidin transcription in the liver, blood, and lungs during infection and found a robust induction of hepcidin mRNA in the liver (Figure 2B) but not in peripheral blood leukocytes or lungs (Figure 2, C and D), suggesting that liver is the main source of hepcidin during the infection and elevations in lung hepcidin protein likely represent extravasation from the blood.

The cytokine IL-6 is a key inducer of acute phase proteins in the liver and an important regulator of hepcidin expression in vivo (9). IL-6 is induced in the lungs in this model of pneumonia (22). We found that immunoneutralization of IL-6 resulted in higher blood and lung bacterial burden 2 days following infection (Figure 3A). In addition, IL-6 neutralization abrogated the increase in plasma hepcidin during the infection and eliminated the associated hypoferremia (Figure 3, B and C), indicating that hepcidin induction during pneumonia is dependent on IL-6.

Hepcidin mediates hypoferremia during bacterial pneumonia and is required for survival. Reduced availability of plasma iron in the context of acute inflammation can occur as a result of both hepcidin-dependent and -independent mechanisms (23–25). We therefore tested the contribution of hepcidin in regulation of plasma iron levels in the context of bacterial pneumonia. In contrast to reduction in plasma iron during infection in WT mice, plasma iron in hepcidin-deficient mice became more elevated during the infection (Figure 4A), indicating that hepcidin is essential for controlling plasma iron levels following infection. Consistent with reports of tissue iron overload in hepcidin-deficient mice (18, 26), we found elevated lung iron levels in hepcidin-deficient as compared with WT mice, but these values did not change over the infection period (Figure 4B).

We next assessed the contribution of hepcidin-mediated iron sequestration to host defense against *K. pneumoniae* and found that hepcidin-deficient animals were markedly more susceptible to bacterial pneumonia, demonstrating 100% mortality compared with 50% mortality in WT controls (Figure 4C), comparable to mice treated with exogenous iron during infection (Figure 1, D and E). Hepcidin-deficient mice exhibited 23% greater incidence of bacteremia and > 100-fold higher median blood bacterial concentration, as well as ~10-fold higher bacterial burden in the lungs and liver as compared with WT mice (Figure 4D).

Since the hepatocytes in hepcidin-deficient animals are iron loaded, we reasoned that the increase of iron in infected hepcidin$^{-/-}$ mice could originate from greater release of iron from damaged hepatocytes. We therefore quantified alanine aminotransferase and aspartate aminotransferase in the blood of infected mice to assess liver damage and found neither enzyme to be elevated in hepcidin$^{-/-}$ as compared with WT mice in the context of infection (Supplemental Figure 2), arguing against disproportionate

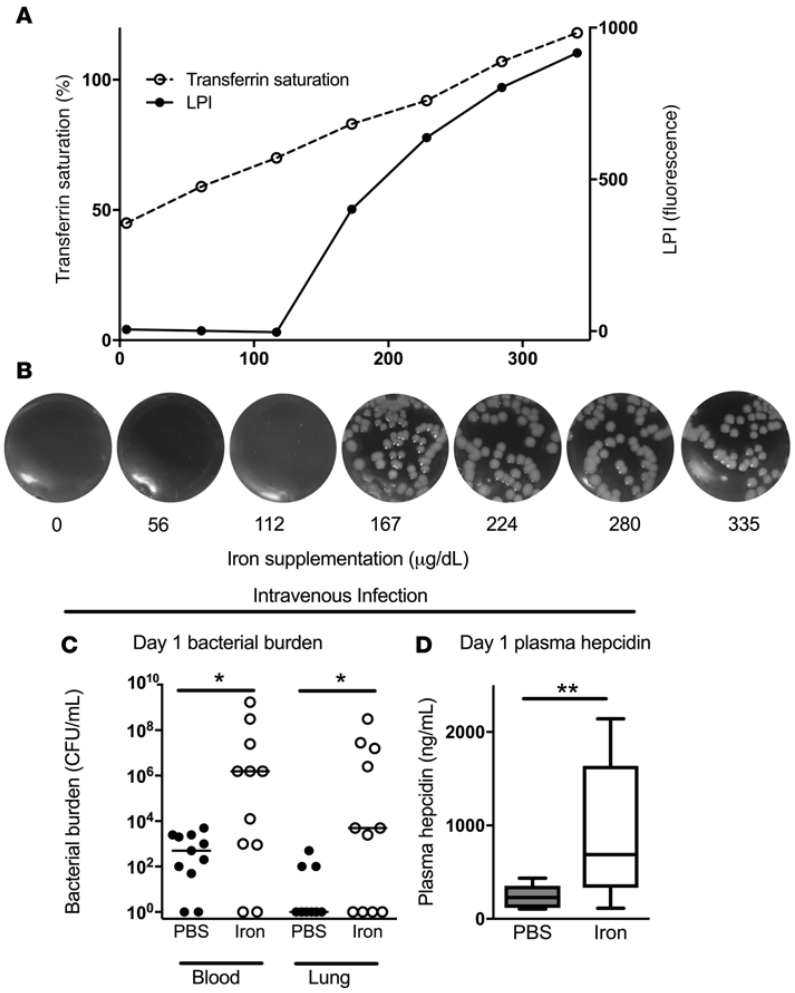


Figure 5. Effect of iron on *Klebsiella* growth in vitro and in vivo. (**A**) Human plasma was supplemented with ferric ammonium citrate and assayed for transferrin saturation and the presence of labile plasma iron (LPI). Transferrin saturation values of >100% represent complete saturation of transferrin iron-binding sites in the presence of additional, unbound ferric iron ions. (**B**) Agar plates composed of 90% human plasma were supplemented with ferric ammonium citrate and inoculated with *K. pneumoniae*. Plates were monitored for occurrence of bacterial growth. Representative data from 3 independent plasma agar preparations. (**C** and **D**) Bacterial burden and plasma hepcidin protein in WT mice treated with either PBS or iron citrate 30 minutes prior to i.v. challenge with *K. pneumoniae*. Lungs and blood were harvested after 24 hours. Box and whisker plots show median (line within box), upper and lower quartiles (upper and lower box boundaries), and total range (bars). n = 11 mice per group, combined form 2 experiments; $^{*}P < 0.05$, Mann-Whitney U test; $^{**}P < 0.01$, t test.

hepatic injury as a contributor to worse outcomes in hepcidin-deficient hosts.

In order to assess whether the beneficial effects of hepcidin are dependent on iron, we used established protocols to induce severe iron-deficiency in hepcidin-deficient mice (27). We found that iron-depleted hepcidin$^{-/-}$ animals did not develop hyperferremia during infection, had lower body iron stores than WT mice, and were no more susceptible to infection compared with WT mice (Supplemental Figure 3, A and B). Taken together, these data suggest that the hepcidin-mediated control of bacterial growth during infection is iron dependent.

Excess iron promotes the growth of K. pneumoniae in plasma. To assess whether the increased susceptibility of hepcidin-deficient mice to infection was attributable to increased bacterial growth in the high-iron environment of the plasma, we assessed the effect of iron supplementation on the in vitro growth of *K. pneumoniae* in human plasma. Supplementing agar composed of 90% human plasma with ferric ammonium citrate at physiologically relevant concentrations incrementally raised the transferrin saturation of the sample, resulting in the appearance of non–transferrin-associated labile pool iron (Figure 5A). The appearance of labile pool iron at transferrin saturation greater than 70% is consistent with prior reports (28, 29). *K. pneumoniae* growth was suppressed in plasma but was permitted by iron supplementation, consistent with reports that transferrin inhibits bacterial growth (30) (Figure 5B). Interestingly, we found that, in plasma preparations from 3 independent donors, addition of ferric iron resulted in *K. pneumoniae* out-growth coincided with the appearance of labile iron in the plasma, rather than with the total amount of iron citrate added. These data suggest that ferric ammonium citrate supports *K. pneumoniae* growth in plasma by providing iron, rather than acting as a carbon or nitrogen source.

We next sought to test the hypothesis that, during in vivo infection, elevated plasma iron is sufficient to enhance growth of blood-borne bacteria. To test this, we subjected WT mice with an i.p. injection of PBS or ferric ammonium citrate prior to i.v. challenge with *K. pneumoniae*. After 24 hours, mice treated with ferric ammonium citrate had higher blood bacterial content than mice treated with PBS, indicating that

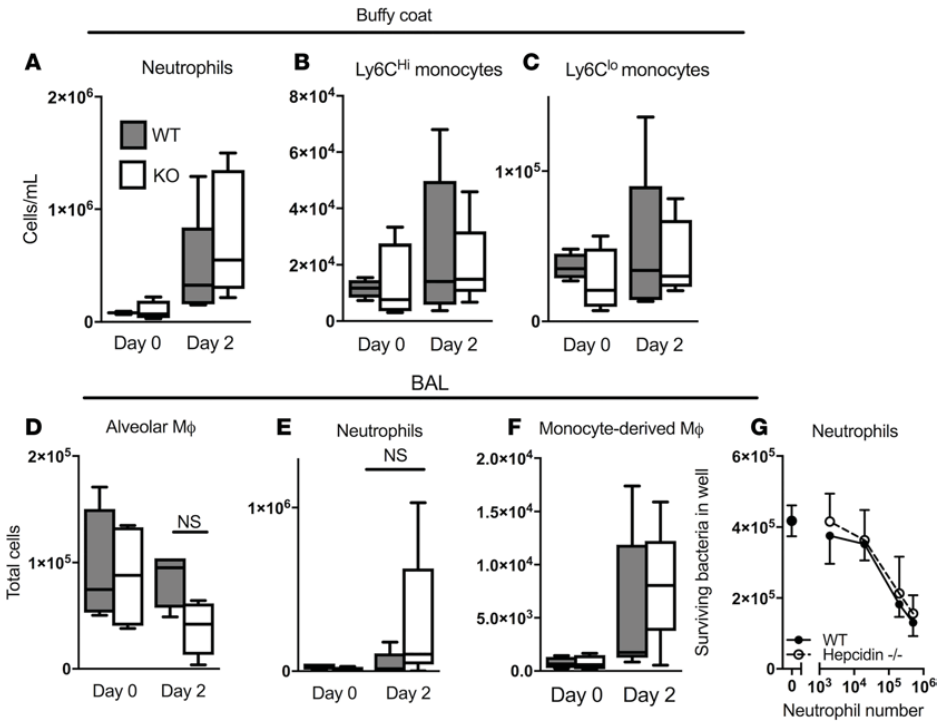


Figure 6. Leukocytes responses during *Klebsiella* pneumonia. (**A**–**F**) BAL and blood were harvested from WT and hepcidin$^{-/-}$ mice before and 2 days following infection. Box and whisker plots show median (line within box), upper and lower quartiles (upper and lower box boundaries), and total range (bars). *n* = 4–5 per group, one way ANOVA Tukey post-test. No significant differences were found for any WT to hepcidin$^{-/-}$ comparison. (**G**) Freshly isolated neutrophils from WT and hepcidin$^{-/-}$ mice were coincubated with 2 × 10^5 CFU of *K. pneumoniae* for 1 hour. Total surviving bacteria were enumerated from each well. *n* = 3 independent experiments per group; data were analyzed using a 2-way ANOVA, and no differences were found between groups

elevated plasma iron directly mediates increased growth of *K. pneumoniae* in the blood stream (Figure 5C). Interestingly, mice treated with ferric ammonium citrate also had higher bacterial burdens in the lungs. We interpret this as evidence that, in mice with increased bacteremia, bacterial seeding of the lung from the bloodstream contributes to higher lung bacterial content. Similar to prior reports (31), mice treated with iron also had marked elevation of plasma hepcidin as compared with mice treated with PBS in response to acute iron loading (Figure 5D), indicating that hepcidin induction alone is not sufficient to protect mice from fatal infection if plasma iron levels are high and supporting the hypothesis that the beneficial effects of hepcidin are mediated via induction of hypoferremia, rather than an iron-independent effect.

Hepcidin-deficient mice have intact cellular immunity against Klebsiella. Iron deficiency and iron overload have complex effects on immune responses (32), and phagocytes from iron-overloaded hosts may have altered antibacterial properties that could contribute to impaired host defenses of hepcidin-deficient mice independent of the effects of acute hyperferremia on bacteria. In order to assess the functionality of the innate immune response in hepcidin-deficient mice, we analyzed leukocyte populations in the blood and BAL (Figure 6, A–F). We found similar concentrations of circulating neutrophils, and Ly6C^{hi} and Ly6C^{lo} monocytes in WT and hepcidin-deficient mice at baseline and 2 days following infection. The number of BAL alveolar macrophages, neutrophils, and monocyte-derived macrophages were also similar between WT and hepcidin-deficient hosts, both at baseline and following infection, arguing against a defect in leukocyte quantity or recruitment in the absence of hepcidin. Since oxidative burst is an iron-dependent process, we compared the generation of reactive oxygen species in lung and blood leukocyte populations and found no difference between infected WT and hepcidin-deficient mice (Supplemental Figure 4). Similarly, neutrophils from WT and hepcidin-deficient mice exhibited comparable ex vivo bacterial killing (Figure 6G). While these data do

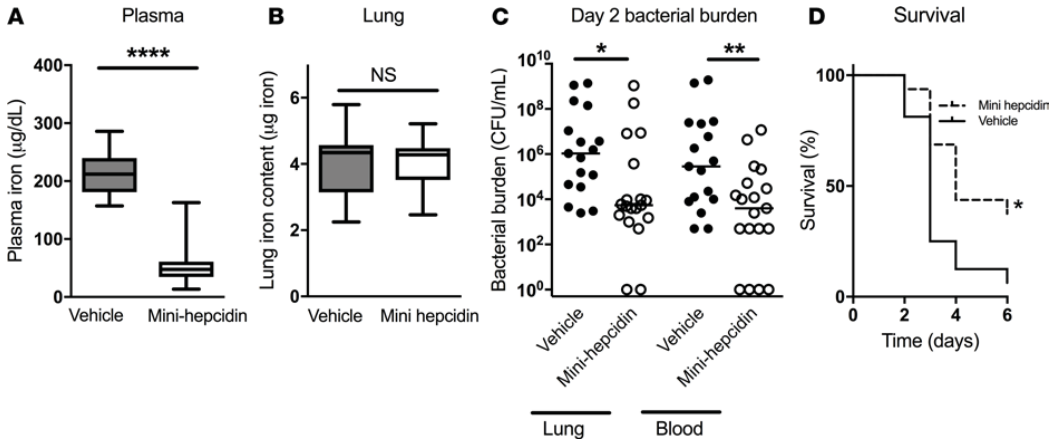


Figure 7. The effect of hepcidin agonist treatment in *Klebsiella* pneumonia in hepcidin-deficient mice. (**A** and **B**) Nonheme iron levels in the plasma and lung of vehicle-treated and minihepcidin-treated hepcidin-deficient mice. Box and whisker plots show median (line within box), upper and lower quartiles (upper and lower box boundaries), and total range (bars). n = 17–19 per group combined from 2 independent experiments; ****$P < 0.001$, t test. (**C**) Bacterial burden in blood and lungs. Horizontal lines represent median and each circle represents 1 animal; animals with no detectable bacteria are reported to have a bacterial burden of 1 CFU on the logarithmic scale; n = 17–19 per group, combined data from 2 experiments; * and ** denote P values <0.05 and <0.01 by Mann-Whitney U test, respectively. (**D**) Survival of hepcidin-deficient mice treated with either vehicle or hepcidin analogue days 0–5; n = 16 per group, combined result of 2 experiments; *$P < 0.05$ by Mantel-Cox test.

not formally exclude the possibility that hepcidin deficiency impairs the immune system in some other way, they suggest intact cellular innate immune mechanisms against *K. pneumoniae* in hepcidin$^{-/-}$ mice.

Restoring hypoferremia is sufficient to protect hepcidin-deficient mice from infection. Impaired hepcidin production is common in the clinical setting — for example, in patients with liver disease (33–36) — and our data suggests a mechanism by which these hosts may be predisposed to Gram-negative bacterial infections. As proof-of-principle of a potential therapeutic approach in this population, we assessed the effect of minihepcidin, a hepcidin analogue, on the outcome of *K. pneumoniae* infection in hepcidin-deficient hosts. We used a previously described synthetic peptide based on the 9 N-terminal amino acids of the hepcidin molecule, which are necessary and sufficient to induce the degradation of ferroportin (37, 38). Daily treatment with the hepcidin analogue beginning on the day of infection resulted in markedly lowered plasma iron levels in infected hepcidin-deficient mice as compared with vehicle-treated controls without affecting the total lung iron content (Figure 7, A and B), consistent with utilization of plasma iron in erythropoiesis (6). The treatment also resulted in > 99% reduction in median lung and blood bacterial burden in infected hepcidin-deficient mice and 40% reduction in mortality compared with vehicle alone (Figure 7, C and D). These data provide evidence that the acute induction of hypoferremia during infection in hepcidin-deficient hosts may represent a plausible therapeutic strategy.

Discussion

Although the competition for iron is thought to be a general feature of antimicrobial host response, the mechanisms and contribution of iron restriction in most infections are undefined. In particular, hepcidin-mediated hypoferremia has only been implicated in host defense against *V. vulnificus*, an organism with specific affinity for iron-overloaded hosts, but its role in defense against common pathogens and in normal hosts is not known (10). We showed that hepcidin was necessary for protection against bacterial dissemination in Gram-negative pneumonia and that treatment with iron citrate was sufficient to permit bacterial outgrowth in WT mice. Finally, we showed that treatment with minihepcidin restored hypoferremia and rescued iron-overloaded, hepcidin-deficient hosts from the infection. Taken together, these data suggest that hepcidin-mediated iron sequestration protects against Gram-negative pneumonia.

Our data suggest that the hepcidin-dependent protection was mediated by reducing plasma iron, as indicated by our observation that WT mice treated with iron citrate were susceptible to *K. pneumoniae* infection despite robust hepcidin induction (Figure 1, E and F) and that hepcidin-deficient mice were protected from

infection if starved of iron (Supplemental Figure 3B). While there may be iron-independent effects of ferric ammonium citrate administration that we have not accounted for, such as bacterial fermentation of citrate, we are encouraged that the phenotype of iron citrate–treated mice is remarkably similar to that of hepcidin$^{-/-}$ mice in terms of death and bacterial burden. Furthermore, we found that hepcidin-deficient mice treated with minihepcidin were robustly protected from infection despite having tissue iron overload, suggesting that restriction of iron in the plasma is sufficient for protection (Figure 7, C and D). Hepcidin exhibits antimicrobial activity against a broad array of pathogens in vitro, and an iron-independent direct microbicidal role for hepcidin has thus been suggested (17, 39, 40). Arguing against such a direct microbicidal role, we report plasma hepcidin levels at concentrations much lower than those required to mediate killing in vitro (39). Similarly, administration of a hepcidin analogue, which lacks the β-defensin motif required for its antimicrobial activity (37), rescued the phenotype of hepcidin-deficient mice (Figure 7, C and D).

Although hepcidin-independent mechanisms of hypoferremia have been reported after challenge with inflammatory stimuli (23, 25, 41), we found that hypoferremia during pneumonia was completely abrogated in hepcidin-deficient mice, and in fact, plasma iron levels became elevated following infection in hepcidin-deficient mice. Our use of an infectious agent, rather than sterile inflammatory stimuli used in other reports, may account for this difference. We speculate that this increase in plasma iron levels reflects decreases in iron consumption by cytokine-suppressed erythropoiesis (24) and release of iron from intracellular sources damaged by infection, such as the liver (42). We thus propose a model in which infections result in a tendency toward increased extracellular iron that benefits the pathogen, and the protective role of inflammation-mediated hepcidin induction is to counteract this phenomenon. Furthermore, while hepcidin can be produced by leukocytes, airway epithelial cells and other tissues(19–21), our results indicate that hepcidin is predominantly produced by the liver and circulates systemically in the context of bacterial pneumonia. Consistent with this, we observed that hepcidin induction was dependent on IL-6, similar to observations with other systemic inflammatory stimuli (43). In addition, we found that IL-6 neutralization disrupted host defense against *K. pneumoniae* (Figure 3A), in corroboration with previous reports (22). While IL-6 induces many acute phase reactants, such as C reactive protein, which are crucial to the innate immune response, we speculate that hepcidin induction may be a component of IL-6–mediated protection.

These data provide the host counterpart to the existing literature on the role of the bacterial siderophore system in the virulence of Gram-negative pathogens (30, 44). The hypervirulent strain of *K. pneumoniae* used in this study produces yersiniabactin, which supports bacterial growth in the respiratory tract, and glycosylated enterobactin, which promotes bacterial growth in the bloodstream by evading lipocalin-2, a host-derived molecule that sequesters nonglycosylated enterobactin and limits microbial iron uptake (45–49). Our findings indicate that even bacteria equipped with these high-affinity acquisition systems are susceptible to a host mechanism that limits iron availability in the host environment. As such, we speculate that these findings may be broadly applicable to infections caused by other phylogenetically related aerobic Gram-negative pathogens (50).

This work has several implications for future research. First, our results may have implications for the therapeutic use of hepcidin antagonists, which are currently under development for the treatment of anemia of inflammation. In this context, we posit that relieving the iron-restricted state could predispose some individuals to Gram-negative sepsis. Second, impaired hepcidin production is a feature of several common clinical entities, including alcohol intoxication and chronic liver disease (33–36), illnesses associated with striking susceptibility to Gram-negative bacteremia (51, 52). Our data suggest that impaired hepcidin production may represent an unappreciated mechanism predisposing these hosts to infection. Finally, hepcidin agonists may represent a novel therapeutic strategy in illnesses where hepcidin production is diminished, such as liver disease and hereditary hemochromatosis, and possibly more broadly in acquired iron-overload states.

Methods

Supplemental Methods are available online with this article.

Animals and in vivo procedures. C57BL/6 mice, purchased from the Jackson Laboratories. *Hepc1*$^{-/-}$ mice generated on a C57BL/6 background (26) — acquired from the University of California, Los Angeles, California, USA — were bred at the University of Virginia under specific-pathogen–free conditions for a minimum of 2 generations, and offspring were used in the experiments. To minimize any effect of differing microbiota between groups of animals, all animals were bred and maintained in the same room in the vivarium and used bedding from cages of breeders, and animals to be used in experiments were intermixed at weekly intervals. Age- and sex-matched male and female 6- to 12-week-old mice were used in experiments.

Standard rodent chow has artifactually high iron content that causes near-maximal expression of hepcidin at baseline in WT animals (43). To correct this, all animals were conditioned on a low-iron diet (2–4 ppm iron; Teklad diet TD.80396, Envigo) for 5–7 days prior to, and throughout the duration of, all experiments. In our pilot studies and published reports (43, 53), this protocol normalizes baseline hepcidin expression without inducing iron deficiency.

Experimental bacterial pneumonia was induced as previously described (15, 16), by intratracheal inoculation of 500–1,500 CFU of *K. pneumoniae* strain 43816 (American Type Culture Collection). In some experiments, 1,500 CFU of *K. pneumoniae* was delivered i.v. in 100 μl PBS. To induce transient hyperferremia without iron overload, 900 μg of ferric ammonium citrate in 100 μl PBS was delivered i.p., using a previously characterized protocol (54, 55). In some experiments, mice were given 1 mg anti–IL-6 antibody or isotype control i.p. 3 hours prior to and 24 hours following infection (clones MP5-20F3 and HRPN1, BioXcell). In other experiments, 100 nmol of the synthetic hepcidin analogue PR73 (manufactured in house), referred to as minihepcidin in text, or vehicle was administered via i.p. injection beginning 5 hours prior to infection and then every 24 hours until day 5 after infection. PR73 was synthesized using Fmoc solid-phase peptide synthesis and was solubilized for in vivo use with SL220 (a polyethylene glycosylated-phospholipid based solubilzer; NOF America Corporation) as previously described (11, 37, 38).

Tissue harvest and determination of bacterial burden. Animals were euthanized with an overdose of a ketamine/xylazine solution, blood was collected from the right ventricle into heparinized syringes, and pulmonary vasculature was perfused with 2 ml of 2 mM EDTA solubilized in PBS. The median liver lobe was collected for RNA analysis. Lungs and liver were homogenized in 1 ml PBS. BAL was performed by serially inflating the lungs via an intratracheal catheter with 1 ml of 2 mM EDTA solubilized in PBS and recovering the fluid 4 times (56). For bacterial enumeration, lung homogenates and blood were serially diluted in sterile water and cultured on blood agar plates, as previously described (57).

RNA, protein, and iron analysis. Tissue RNA was extracted using TRIzol and chloroform (Thermo-Fisher Scientific). Buffy coat RNA was extracted using a commercial kit (Qiagen). A commercial kit was used to synthesize cDNA (Promega). Hepcidin transcript was quantified by quantitative PCR in duplicate using SYBR green (Bioline). Expression was calculated using the ΔΔC(t) method normalized to glyceraldehyde 3-phosphate dehydrogenase, and then relative to hepcidin expression of uninfected animals. Primers were custom synthesized (Sigma Aldrich) as previously published (35): hepcidin 5′ TGCAGAAGAGAAGGAAGAGAGACA 3′ (forward) and 5′ CACACTGGGAATTGTTACAGCATT 3′ (reverse); glyceraldehyde 3-phosphate dehydrogenase 5′ TTCACCACCATGGAGAAGGC 3′ (forward) and 5′ GGCATGGACTGTGGTCATGA 3′ (reverse) (58). The thermal cycling conditions were as follows: 2 minutes at 95°C, 10 minutes at 95°C, 5 seconds at 95°C, and 10 seconds at 55°C for 40 cycles. Reactions were performed on a BioRad iQ5 Cycler. Protein concentration of hepcidin was quantified using a commercial ELISA kit (Intrinsic Life Sciences) according to the manufacturer instructions. Plasma iron was quantified with a commercial kit (Sekisui Diagnostics) according to manufacturer instructions with minor modifications — namely, samples were scaled to volume and centrifuged at 10,000 *g* for 10 minutes between steps to clear insoluble material. Transferrin saturation was determined by measuring the unsaturated iron binding capacity (UIBC) of each sample using a commercial kit (Sekisui Diagnostics). UIBC values were added to plasma iron values in each sample to calculate the total iron binding capacity (TIBC). Transferrin saturation was calculated as (plasma iron/TIBC) × 100%.

Tissue heme and nonheme iron levels were quantified using the ferrozine assay, as previously described (59–61). Whole lungs and left lateral lobe of the liver were homogenized in 1 ml of water. BAL was collected into 1 ml of 2 mM EDTA solubilized in PBS. Briefly, 100 μl sample were heated in 100 μl buffer containing 1 N hydrochloric acid and 10% trichloroacetic acid with (total iron) or without (nonheme iron) 2.25% $KMnO_4$ at 60°C for 2 hours. Samples were centrifuged at 16,000 *g* for 10 minutes to remove insoluble material and were incubated with 50 μl iron detection reagent (6.5 mM ferrozine, 6.5 mM neucoproine, 1 M L-ascorbic acid, 2.5 M ammonium acetate) for 10 minutes and then plated in duplicate and read at A_{590} nm on a Dynex Triad microplate reader (Dynex Technologies). Heme-iron values were calculated by subtracting nonheme iron values from total iron content. Labile plasma iron (LPI), the major component of non–transferrin-bound iron, was measured using a published protocol with minor modifications (62): briefly, HEPES buffered saline was iron-depleted by incubation with Chelex-100 chelating resin (Bio-Rad) for 1 hour, filtered, and supplemented with 60 nM deferrioxamine (Sigma-Aldrich). For LPI measurements, 10 μl of plasma samples were mixed with either 140 μl of HBS/50 μM dihydrorhodamine/40 μM ascorbic acid/0.5 mM nitriloacetic acid (–DFP) or 140 μl of the same buffer supplemented with 100 μM deferriprone (+DFP).

Changes in fluorescence were measured over 40 minutes, and the slope was calculated for each sample. The difference between –DFP and +DFP was used as a measure of LPI. The experiment was repeated a total of 3 times using different plasma donors with similar results.

Flow cytometry. Cell suspensions from blood and BAL fluid were prepared and analyzed by flow cytometry as previously described, with minor modifications (16, 63, 64). The following antibodies were used for surface antigen staining: anti–MHC-II APC (clone M5/114.15.2), anti–CD11b Pe-Cy7 (clone M170), and anti–CD115 APC (clone AF598) from eBioscience; anti–CD11c PerCP (clone HL3) and anti–CD64 brilliant violet 421 (clone X54-5/7.1) from BioLegend; and anti-CD16/CD32 (clone 2.4G2), anti–Ly6G PE (clone 1A8), and anti–CD45 AmCyan (clone 30-F11) from BD Biosciences. After extracellular staining, cells were washed in 1% FCS in PBS once and resuspended in the same buffer. Data were acquired on a FACS Canto II instrument using BD FACS Diva software (version 8.0; BD Biosciences) and analyzed with FlowJo software (version 8.8.6; Tree Star Inc.). The absolute cell number was calculated as the product of the cell type frequency (as determined by gating analysis) and the total number of cells in the sample (as determined by manually counting under a hemocytometer).

In vitro experiments. BM neutrophils were isolated by grinding the tibia, femur, pelvis, and spine from uninfected mice in a sterile mortar and pestle as previously described (15, 57), followed by positive selection using anti-Ly6G magnetic beads, according to the manufacturer's instructions (MACS; Miltenyi Biotec). Isolated populations were found to have > 90% viability by examination in trypan blue. Neutrophil bacterial killing was quantified using a published protocol with minor modifications (57). Briefly, *K. pneumoniae* was opsonized at a concentration of 8×10^6 CFU/ml in 20% fresh mouse serum and HBSS for 30 minutes at 37°C, washed once in cold water, once in HBSS, and resuspended in HBSS. Aliquots of 2×10^5 bacteria were added to sterile U-bottom 96-well plates and coincubated with 5×10^5, 2×10^5, 2×10^4, 2×10^3, or no neutrophils from WT or hepcidin-deficient mice in triplicate in a total volume of 200 μl HBSS. Samples were incubated in a humidified chamber with 5% CO_2 at 37°C for 1 hour. Number of surviving bacteria was determined by hypotonic lysis of neutrophils in cold water and serial dilution and culture.

Human plasma was inactivated (30 min at 56°C) and incubated overnight at 37°C with 0–60 μM ferric ammonium citrate (Sigma-Aldrich), followed by quantification of transferrin saturation and LPI. The samples were then used to generate 90% plasma agar solid media, poured in sterile 12-well tissue culture plates. *K. pneumoniae* was suspended at 1×10^4 CFU/ml and 5 μl plated in triplicates on plasma agar wells and incubated for 24 hours at 37°C; bacterial colonies were counted and photographed.

Statistics. Data were analyzed using Prism software (version 6.0, GraphPad Software). The Mantel-Cox test was used to analyze survival data. A one-way ANOVA with a post-test for linear trend was used to analyze change in a single parameter over time, and one-way ANOVA with a Tukey multiple comparison post-test was used to analyze differences between 3 or more groups. A 2-way ANOVA with Tukey multiple comparison post-test was used to compare changes over time between 2 groups. An unpaired, 2-tailed *t* test was used to compare 2 groups for RNA, protein, and iron levels. A Mann-Whitney *U* test was used to compare bacterial burden between groups. $P < 0.05$ was considered statistically significant.

Study approval. Animal experiments were performed in compliance with NIH Guide for the Care and Use of Laboratory Animals, The US Animal Welfare Act, and PHS Policy on Humane Care and Use of Laboratory Animals and was approved by the Institutional Animals Care and Use Committee at the University of Virginia (protocol 3571).

Author contributions

KRM, EN, TG, and BM conceived the project, designed experiments, and interpreted data; KRM, ZZ, AMB, REC, DS, and MDB performed experiments; KRM and DS generated the figures; SV, EN, and TG designed and contributed materials; and KRM and BM wrote the first draft of the manuscript. All authors revised the manuscript.

Acknowledgments

This work was supported by NIH grants R21AI117397 and R01HL098329-05 awarded to BM; and R01DK065029 awarded to TG. The funders had no role in study design, data collection and analysis, decision to publish, or preparation of the manuscript.

Address correspondence to: Borna Mehrad, P.O. Box 800546, Charlottesville, Virginia 22908, USA. Phone: 434.243.4845; E-mail: mehrad@virginia.edu.

1. Gaynes R, Edwards JR, National Nosocomial Infections Surveillance System. Overview of nosocomial infections caused by gram-negative bacilli. *Clin Infect Dis*. 2005;41(6):848–854.
2. Meatherall BL, Gregson D, Ross T, Pitout JD, Laupland KB. Incidence, risk factors, and outcomes of Klebsiella pneumoniae bacteremia. *Am J Med*. 2009;122(9):866–873.
3. Uslan DZ, et al. Age- and sex-associated trends in bloodstream infection: a population-based study in Olmsted County, Minnesota. *Arch Intern Med*. 2007;167(8):834–839.
4. Skaar EP. The battle for iron between bacterial pathogens and their vertebrate hosts. *PLoS Pathog*. 2010;6(8):e1000949.
5. Cassat JE, Skaar EP. Iron in infection and immunity. *Cell Host Microbe*. 2013;13(5):509–519.
6. Craven CM, Alexander J, Eldridge M, Kushner JP, Bernstein S, Kaplan J. Tissue distribution and clearance kinetics of non-transferrin-bound iron in the hypotransferrinemic mouse: a rodent model for hemochromatosis. *Proc Natl Acad Sci USA*. 1987;84(10):3457–3461.
7. Nemeth E, et al. Hepcidin regulates cellular iron efflux by binding to ferroportin and inducing its internalization. *Science*. 2004;306(5704):2090–2093.
8. Besson-Fournier C, et al. Induction of activin B by inflammatory stimuli up-regulates expression of the iron-regulatory peptide hepcidin through Smad1/5/8 signaling. *Blood*. 2012;120(2):431–439.
9. Nemeth E, Valore EV, Territo M, Schiller G, Lichtenstein A, Ganz T. Hepcidin, a putative mediator of anemia of inflammation, is a type II acute-phase protein. *Blood*. 2003;101(7):2461–2463.
10. Michels K, Nemeth E, Ganz T, Mehrad B. Hepcidin and Host Defense against Infectious Diseases. *PLoS Pathog*. 2015;11(8):e1004998.
11. Arezes J, et al. Hepcidin-induced hypoferremia is a critical host defense mechanism against the siderophilic bacterium Vibrio vulnificus. *Cell Host Microbe*. 2015;17(1):47–57.
12. Khan FA, Fisher MA, Khakoo RA. Association of hemochromatosis with infectious diseases: expanding spectrum. *Int J Infect Dis*. 2007;11(6):482–487.
13. Agbaht K, et al. Bacteremia in patients with ventilator-associated pneumonia is associated with increased mortality: A study comparing bacteremic vs. nonbacteremic ventilator-associated pneumonia. *Crit Care Med*. 2007;35(9):2064–2070.
14. Magret M, et al. Bacteremia is an independent risk factor for mortality in nosocomial pneumonia: a prospective and observational multicenter study. *Crit Care*. 2011;15(1):R62.
15. Barletta KE, Cagnina RE, Burdick MD, Linden J, Mehrad B. Adenosine A(2B) receptor deficiency promotes host defenses against gram-negative bacterial pneumonia. *Am J Respir Crit Care Med*. 2012;186(10):1044–1050.
16. Bettina A, et al. M-CSF Mediates Host Defense during Bacterial Pneumonia by Promoting the Survival of Lung and Liver Mononuclear Phagocytes. *J Immunol*. 2016;196(12):5047–5055.
17. Park CH, Valore EV, Waring AJ, Ganz T. Hepcidin, a urinary antimicrobial peptide synthesized in the liver. *J Biol Chem*. 2001;276(11):7806–7810.
18. Zumerle S, et al. Targeted disruption of hepcidin in the liver recapitulates the hemochromatotic phenotype. *Blood*. 2014;123(23):3646–3650.
19. Armitage AE, Pinches R, Eddowes LA, Newbold CI, Drakesmith H. Plasmodium falciparum infected erythrocytes induce hepcidin (HAMP) mRNA synthesis by peripheral blood mononuclear cells. *Br J Haematol*. 2009;147(5):769–771.
20. Chen QX, et al. Silencing airway epithelial cell-derived hepcidin exacerbates sepsis induced acute lung injury. *Crit Care*. 2014;18(4):470.
21. Nguyen NB, Callaghan KD, Ghio AJ, Haile DJ, Yang F. Hepcidin expression and iron transport in alveolar macrophages. *Am J Physiol Lung Cell Mol Physiol*. 2006;291(3):L417–L425.
22. Sutherland RE, Olsen JS, McKinstry A, Villalta SA, Wolters PJ. Mast cell IL-6 improves survival from Klebsiella pneumonia and sepsis by enhancing neutrophil killing. *J Immunol*. 2008;181(8):5598–5605.
23. Guida C, et al. A novel inflammatory pathway mediating rapid hepcidin-independent hypoferremia. *Blood*. 2015;125(14):2265–2275.
24. Langdon JM, et al. Hepcidin-dependent and hepcidin-independent regulation of erythropoiesis in a mouse model of anemia of chronic inflammation. *Am J Hematol*. 2014;89(5):470–479.
25. Armitage AE, et al. Induced Disruption of the Iron-Regulatory Hormone Hepcidin Inhibits Acute Inflammatory Hypoferraemia. *J Innate Immun*. 2016;8(5):517–528.
26. Lesbordes-Brion JC, et al. Targeted disruption of the hepcidin 1 gene results in severe hemochromatosis. *Blood*. 2006;108(4):1402–1405.
27. Nagababu E, Gulyani S, Earley CJ, Cutler RG, Mattson MP, Rifkind JM. Iron-deficiency anaemia enhances red blood cell oxidative stress. *Free Radic Res*. 2008;42(9):824–829.
28. Gosriwatana I, Loreal O, Lu S, Brissot P, Porter J, Hider RC. Quantification of non-transferrin-bound iron in the presence of unsaturated transferrin. *Anal Biochem*. 1999;273(2):212–220.
29. Breuer W, Ronson A, Slotki IN, Abramov A, Hershko C, Cabantchik ZI. The assessment of serum nontransferrin-bound iron in chelation therapy and iron supplementation. *Blood*. 2000;95(9):2975–2982.
30. Nassif X, Sansonetti PJ. Correlation of the virulence of Klebsiella pneumoniae K1 and K2 with the presence of a plasmid encoding aerobactin. *Infect Immun*. 1986;54(3):603–608.
31. Pigeon C, et al. A new mouse liver-specific gene, encoding a protein homologous to human antimicrobial peptide hepcidin, is overexpressed during iron overload. *J Biol Chem*. 2001;276(11):7811–7819.
32. Wang L, Cherayil BJ. Ironing out the wrinkles in host defense: interactions between iron homeostasis and innate immunity. *J Innate Immun*. 2009;1(5):455–464.
33. Georgopoulou U, Dimitriadis A, Foka P, Karamichali E, Mamalaki A. Hepcidin and the iron enigma in HCV infection. *Virulence*. 2014;5(4):465–476.
34. Nahon P, Nuraldeen R, Rufat P, Sutton A, Trautwein C, Strnad P. In alcoholic cirrhosis, low-serum hepcidin levels associate with poor long-term survival. *Liver Int*. 2016;36(2):185–188.
35. Harrison-Findik DD, Klein E, Crist C, Evans J, Timchenko N, Gollan J. Iron-mediated regulation of liver hepcidin expression

in rats and mice is abolished by alcohol. *Hepatology*. 2007;46(6):1979–1985.
36. Kessler SM, Barghash A, Laggai S, Helms V, Kiemer AK. Hepatic hepcidin expression is decreased in cirrhosis and HCC. *J Hepatol*. 2015;62(4):977–979.
37. Ramos E, et al. Minihepcidins prevent iron overload in a hepcidin-deficient mouse model of severe hemochromatosis. *Blood*. 2012;120(18):3829–3836.
38. Preza GC, et al. Minihepcidins are rationally designed small peptides that mimic hepcidin activity in mice and may be useful for the treatment of iron overload. *J Clin Invest*. 2011;121(12):4880–4888.
39. Krause A, et al. LEAP-1, a novel highly disulfide-bonded human peptide, exhibits antimicrobial activity. *FEBS Lett*. 2000;480(2-3):147–150.
40. Pigeon C, et al. A new mouse liver-specific gene, encoding a protein homologous to human antimicrobial peptide hepcidin, is overexpressed during iron overload. *J Biol Chem*. 2001;276(11):7811–7819.
41. Kim A, et al. A mouse model of anemia of inflammation: complex pathogenesis with partial dependence on hepcidin. *Blood*. 2014;123(8):1129–1136.
42. Kell DB, Pretorius E. Serum ferritin is an important inflammatory disease marker, as it is mainly a leakage product from damaged cells. *Metallomics*. 2014;6(4):748–773.
43. Nemeth E, et al. IL-6 mediates hypoferremia of inflammation by inducing the synthesis of the iron regulatory hormone hepcidin. *J Clin Invest*. 2004;113(9):1271–1276.
44. Podschun R, Ullmann U. Klebsiella spp. as nosocomial pathogens: epidemiology, taxonomy, typing methods, and pathogenicity factors. *Clin Microbiol Rev*. 1998;11(4):589–603.
45. Lawlor MS, O'connor C, Miller VL. Yersiniabactin is a virulence factor for Klebsiella pneumoniae during pulmonary infection. *Infect Immun*. 2007;75(3):1463–1472.
46. Lawlor MS, Hsu J, Rick PD, Miller VL. Identification of Klebsiella pneumoniae virulence determinants using an intranasal infection model. *Mol Microbiol*. 2005;58(4):1054–1073.
47. Bachman MA, Lenio S, Schmidt L, Oyler JE, Weiser JN. Interaction of lipocalin 2, transferrin, and siderophores determines the replicative niche of Klebsiella pneumoniae during pneumonia. *MBio*. 2012;3(6):6.
48. Bachman MA, Miller VL, Weiser JN. Mucosal lipocalin 2 has pro-inflammatory and iron-sequestering effects in response to bacterial enterobactin. *PLoS Pathog*. 2009;5(10):e1000622.
49. Bachman MA, et al. Klebsiella pneumoniae yersiniabactin promotes respiratory tract infection through evasion of lipocalin 2. *Infect Immun*. 2011;79(8):3309–3316.
50. Drancourt M, Bollet C, Carta A, Rousselier P. Phylogenetic analyses of Klebsiella species delineate Klebsiella and Raoultella gen. nov., with description of Raoultella ornithinolytica comb. nov., Raoultella terrigena comb. nov. and Raoultella planticola comb. nov. *Int J Syst Evol Microbiol*. 2001;51(Pt 3):925–932.
51. Gustot T, Durand F, Lebrec D, Vincent JL, Moreau R. Severe sepsis in cirrhosis. *Hepatology*. 2009;50(6):2022–2033.
52. Jong GM, Hsiue TR, Chen CR, Chang HY, Chen CW. Rapidly fatal outcome of bacteremic Klebsiella pneumoniae pneumonia in alcoholics. *Chest*. 1995;107(1):214–217.
53. Pak M, Lopez MA, Gabayan V, Ganz T, Rivera S. Suppression of hepcidin during anemia requires erythropoietic activity. *Blood*. 2006;108(12):3730–3735.
54. Duong-Nu TM, et al. All Three TonB Systems Are Required for Vibrio vulnificus CMCP6 Tissue Invasiveness by Controlling Flagellum Expression. *Infect Immun*. 2015;84(1):254–265.
55. Elin RJ, Wolff SM. The role of iron in nonspecific resistance to infection induced by endotoxin. *J Immunol*. 1974;112(2):737–745.
56. Mehrad B, et al. Transient lung-specific expression of the chemokine KC improves outcome in invasive aspergillosis. *Am J Respir Crit Care Med*. 2002;166(9):1263–1268.
57. Mehrad B, et al. The lupus-susceptibility locus, Sle3, mediates enhanced resistance to bacterial infections. *J Immunol*. 2006;176(5):3233–3239.
58. Guo Z, et al. Cutting edge: membrane lymphotoxin regulates CD8(+) T cell-mediated intestinal allograft rejection. *J Immunol*. 2001;167(9):4796–4800.
59. Grundy MA, Gorman N, Sinclair PR, Chorney MJ, Gerhard GS. High-throughput non-heme iron assay for animal tissues. *J Biochem Biophys Methods*. 2004;59(2):195–200.
60. Rebouche CJ, Wilcox CL, Widness JA. Microanalysis of non-heme iron in animal tissues. *J Biochem Biophys Methods*. 2004;58(3):239–251.
61. Oremland M, Michels KR, Bettina AM, Lawrence C, Mehrad B, Laubenbacher R. A computational model of invasive aspergillosis in the lung and the role of iron. *BMC Syst Biol*. 2016;10:34.
62. Esposito BP, Breuer W, Sirankapracha P, Pootrakul P, Hershko C, Cabantchik ZI. Labile plasma iron in iron overload: redox activity and susceptibility to chelation. *Blood*. 2003;102(7):2670–2677.
63. Barletta KE, Cagnina RE, Wallace KL, Ramos SI, Mehrad B, Linden J. Leukocyte compartments in the mouse lung: distinguishing between marginated, interstitial, and alveolar cells in response to injury. *J Immunol Methods*. 2012;375(1-2):100–110.
64. Misharin AV, Morales-Nebreda L, Mutlu GM, Budinger GR, Perlman H. Flow cytometric analysis of macrophages and dendritic cell subsets in the mouse lung. *Am J Respir Cell Mol Biol*. 2013;49(4):503–510.

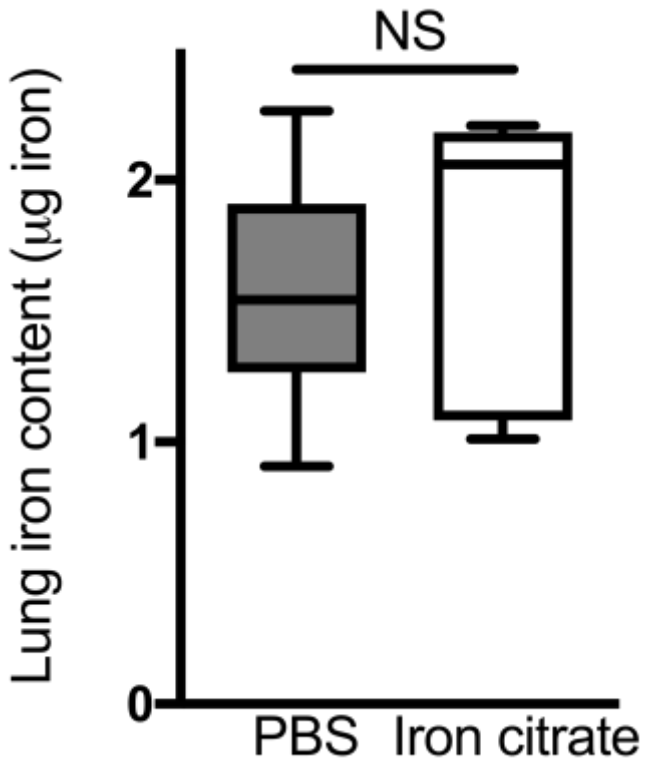


Figure S1. Lung iron content in wildtype mice treated with PBS or iron citrate. Mice were treated with either PBS or ferric ammonium citrate (iron) 30 minutes prior to intrapulmonary *K. pneumoniae* challenge and again 24 hours thereafter; lungs were harvested on day 2 of infection. Lung iron content was determined using the ferrozine assay. . Box and whisker plots show median (line within box), upper and lower quartiles (upper and lower box boundaries), and total range (bars); *n* = 6-5 per group; NS, not significant (*t*-test).

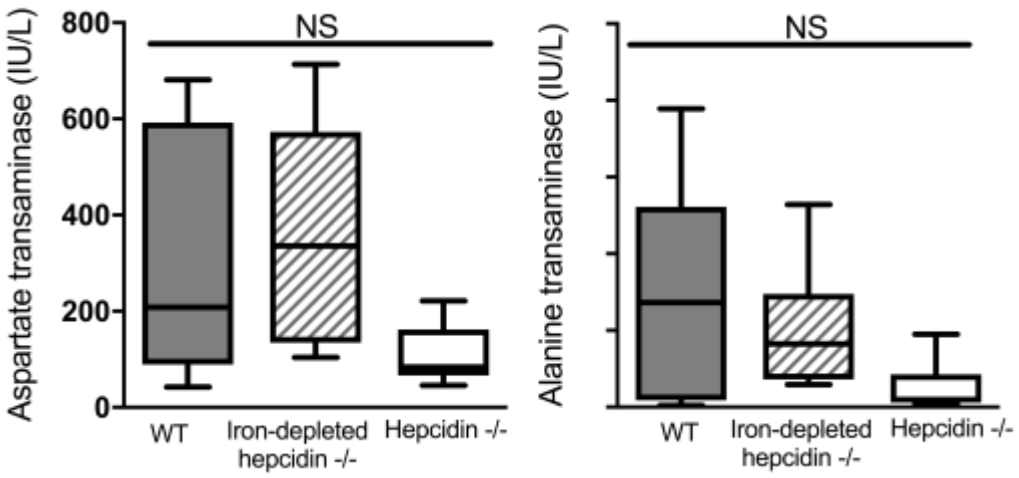


Figure S2. Aspartate transaminase (AST) and alanine transaminase (ALT) in wildtype and hepcidin -/- mice. Wildtype (WT) mice were maintained on standard diet, and hepcidin -/- mice were maintained on wither a prolonged iron-deficient diet (Iron depleted hepcidin -/-) or standard diet prior to intratracheal inoculation with *K. pneumoniae.* Samples were harvested on day 2 of infection. Box and whisker plots show median (line within box), upper and lower quartiles (upper and lower box boundaries), and total range (bars); *n*=6-9 per group; NS=not significant, one way ANOVA.

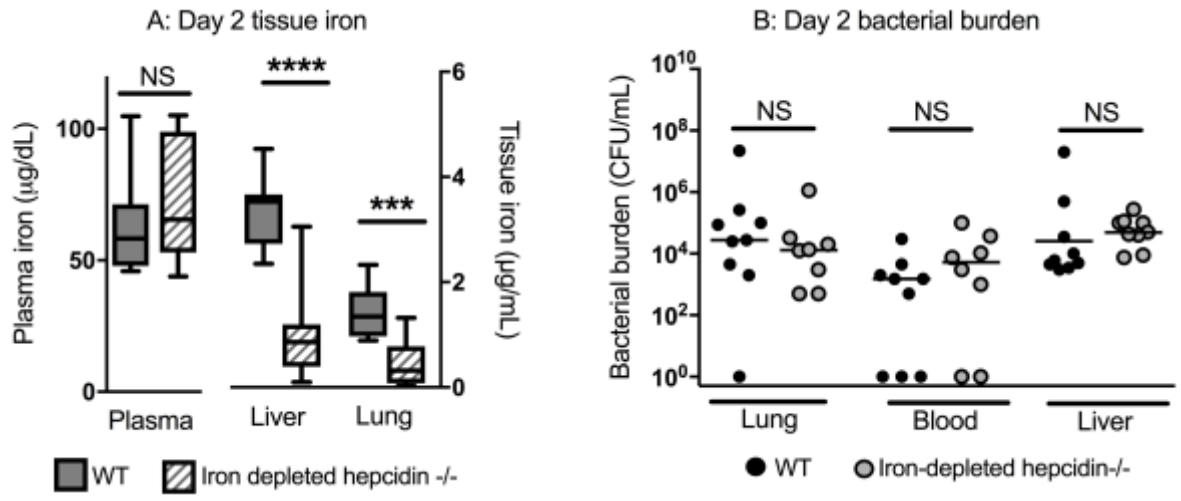


Figure S3. Iron-depleted hepcidin-/- mice are not susceptible to infection compared to wildtype mice. Wildtype (WT) mice maintained on standard diet and hepcidin -/- maintained on a prolonged iron-deficient diet were infected intratracheally with *K. pneumoniae* and samples were harvested on day 2 of infection. (A) Liver, lung, and plasma iron content in wildtype and iron-depleted hepcidin -/- mice. Box and whisker plots show median (line within box), upper and lower quartiles (upper and lower box boundaries), and total range (bars); *** and **** denote p <0.001 and p <0.0001 respectively; NS, not significant (*t*-test). (B): Lung, blood, and liver bacterial burden in wildtype and iron-depleted hepcidin -/- mice. Horizontal lines represent median and each circle represents one animal; animals with no detectable bacteria are reported to have a bacterial burden of 1 colony forming units on the logarithmic scale; NS, not significant (Mann-Whitney test). *N=8-9* per group in both panels.

Supplementary methods:

Iron depletion protocol: Hepcidin-deficient mice were weaned to iron deficient chow at 22 days of age for 3-4 weeks before use in experiments.

Determination of AST and ALT: Plasma AST and ALT were measured using commercial kits according to the manufacturer instructions (Liquid AST Reagent set and Liquid ALT Reagent Set; Pointe Scientific, Canton, MI).

Flow cytometry: Cell populations were isolated and stained as described in the main methods. After extracellular staining, cells were washed in FA buffer once and prepared for reactive oxygen species staining using DCFDA (2',7'–dichlorofluorescein diacetate) with a commercial kit (Abcam, Cambridge, UK) according to the manufacturer's instructions. Cells were stained using 2 µM DCDFA for 15 minutes at 37°C. TBHP (Tert-butyl-hydrogen peroxide) was added to a final concentration of 50 µM for stimulated cells. Cells were incubated for an additional 45 minutes at 37°C. Data were acquired immediately after incubation on a FACS Canto II instrument using BD FACS Diva software (version 8.0; BD Biosciences) and analyzed with FlowJo software (version 8.8.6; Tree Star, Ashland, Oregon).

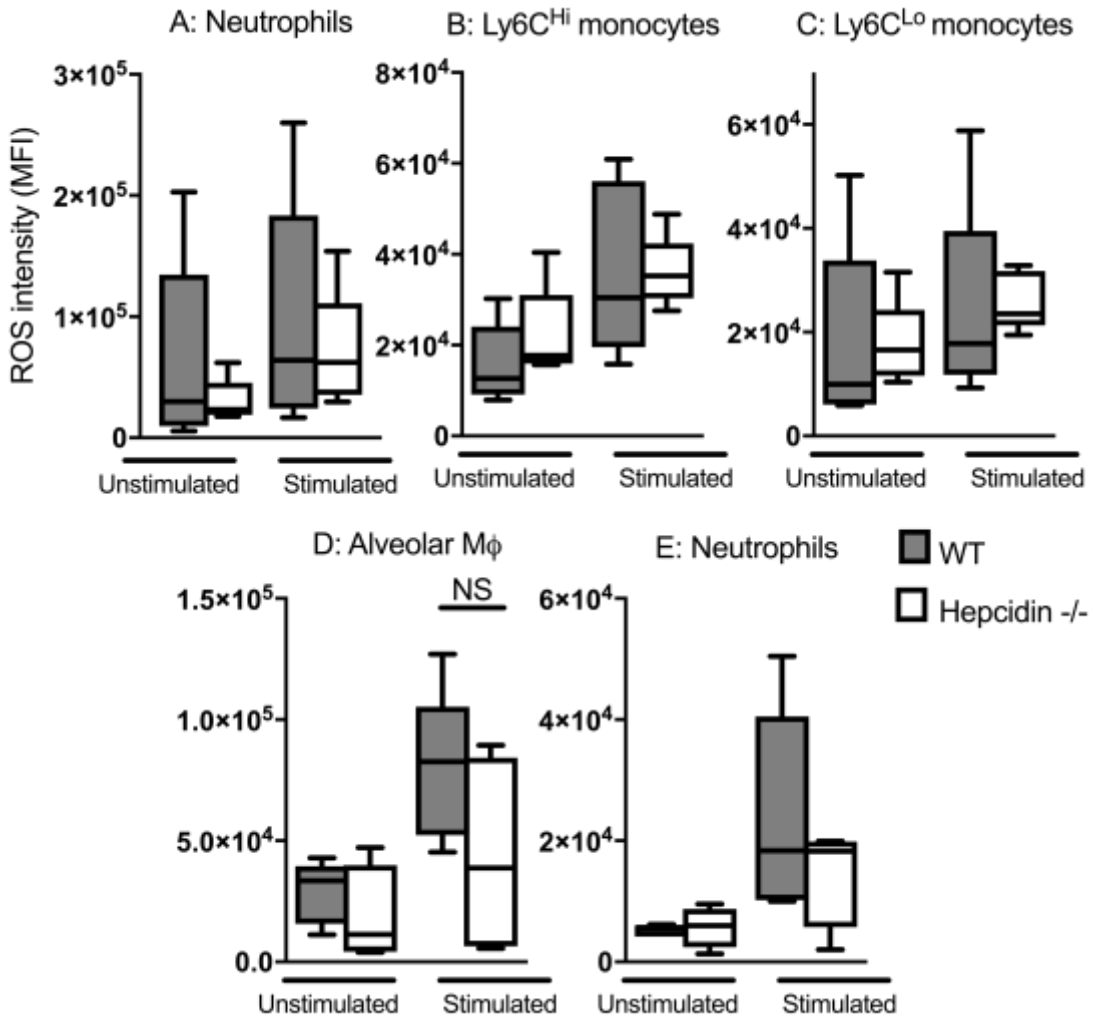


Figure S4. Reactive oxygen species (ROS) production in infected mice. ROS production in indicated cell types from in the blood and bronchoalveloar lavage fluid (BAL) of wildtype and hepcidin -/- mice 2 days following infection. Box and whisker plots show median (line within box), upper and lower quartiles (upper and lower box boundaries), and total range (bars); *n* = 4-5 per group; NS, not significant (*t*-test) for comparing ROS production between WT and hepcidin-/- mice.

CHAPTER 3

Hepcidin protects against lethal *E. coli* sepsis in mice inoculated with isolates from septic patients

(submitted manuscript)

Introduction

Iron is an essential trace element required for multiple vital functions such as oxygen transport, cellular respiration, DNA replication and repair, cell proliferation and differentiation[1]. Consequently, iron is critical for the survival of nearly all organisms including microbial pathogens. Host defense mechanisms evolved to target the iron dependence of invading microbes during infections, with multiple mechanisms acting to sequester iron from microbes[2]. Hepcidin is a hepatic peptide hormone that acts as the principal regulator of iron homeostasis, and orchestrates iron absorption and tissue distribution by inhibiting ferroportin-mediated cellular iron transport to plasma and extracellular fluid[3]. Hepcidin production is strongly induced by IL-6 and other inflammatory signals[4] thus causing iron sequestration in enterocytes and macrophages and rapid reduction in plasma iron levels. On the other side, pathogens have evolved to obtain iron from multiple sources even under limiting conditions, using such mechanisms as transferrin receptors[5], breakdown of ferroproteins including hemoglobin[6] and the secretion and reuptake of siderophores[7] which can “steal” iron from host molecules. However, these mechanisms, while effective, may impose a substantial metabolic burden on the invading pathogen. The battle for iron between the host and the invading pathogen can determine the outcome of infection[8].

Interventions or diseases that increase iron availability in the host have been linked to enhanced bacterial pathogenicity and increased susceptibility to infections[9-11]. Iron supplementation in human trials in South Asia and Africa was associated with increased risk of respiratory and gastrointestinal infections as well as malaria, leading to greater severity of infection and even mortality[12-15]. In addition, hereditary hemochromatosis

patients, who are iron-overloaded as a result of hepcidin deficiency, are highly susceptible to infections with several types of bacteria[16-19]. Intramuscular iron dextran administration was associated with increased *E. coli* sepsis in neonates[20].

We recently showed that hepcidin deficiency and iron overload dramatically increase infection-associated mortality in mouse models of infection with siderophilic bacteria *Yersinia enterocolitica*[21] or *Vibrio vulnificus*[22]. Studies with a strain of common Gram negative reference *Klebsiella pneumoniae* (ATCC 43816) revealed similar results although the effect of iron availability on survival after infection was less striking[23]. It is therefore not clear whether the enhancement of pathogenicity by excess iron is applicable to clinically common bacteria that cause sepsis in humans.

In each of these infections, the experimental evidence implicates non-transferrin bound iron (NTBI) as the iron species promoting infection. NTBI[24] appears in circulation when the binding capacity of the principal plasma iron-transport protein transferrin is exceeded transiently or chronically, as seen in conditions such as hereditary hemochromatosis or β-thalassemia, acute and chronic liver failure, hematopoietic stem cell transplantation, chronic parenteral iron administration and blood transfusions with older PRBCs (11)[25 26]. The molecular forms of NTBI include mainly ferric citrate but also ferric salts of other organic acids and iron loosely bound to albumin.

E. coli is a Gram-negative pathogen, which normally inhabits the gastrointestinal tract of humans and other animals without causing any adverse effects[27]. However, it is also among one of the most common causes of infections in hospitalized patients: ranging from gastrointestinal infections and urinary tract infections to bacteremia and sepsis[28]. Sepsis affects around 750 000 people in the United States every year and has high

mortality rate reaching 30% to 50%[29]. According to CDC, *E. coli* was the most commonly isolated pathogen from the blood of septic patients[30]. Even though *E. coli* is not considered a siderophilic pathogen there are a few reports suggesting a correlation between iron overload and susceptibility to *E. coli* infection[31,32] but the mechanistic connection has not been further explored.

Using randomly selected clinical isolates of *E. coli* from pediatric patients with sepsis, we now show in mouse models that iron overload, either from genetic hepcidin deficiency (hereditary hemochromatosis) or intravenous (IV) iron supplementation increases sepsis-associated mortality. Pathogenicity of *E. coli* is enhanced not by tissue iron overload but by the generation of a specific iron species, NTBI.

We demonstrate that hepcidin has a critical role in host defense against *E. coli* infections by clearing NTBI and that acute post exposure treatment of susceptible HKO mice with the hepcidin agonist PR73 abolishes NTBI and improves survival.

Results

Hepcidin deficiency promotes susceptibility to *E. coli* sepsis

Hepcidin-deficient mice had much higher susceptibility to *E. coli* infection compared to WT mice (*Table 3-1 and Supplemental Figure 3-1*). Most of the clinical *E. coli* isolates, 8 out of 10, caused mortality (60 to 100%) in naturally iron-loaded (IL) HKO mice within 24h of infection at doses where none of the WT mice developed signs of disease (no significant weight loss, *Supplemental Table 3-1*; no changes in appearance or activity). The remaining two *E.coli* isolates (isolate 9 and 10) were not pathogenic in mice since we observed very low mortality after infection of IL-HKO and WT mice even with high

bacterial doses. The mortality in mice did not correlate with ceftriaxone resistance of the bacteria.

Genetic as well as iatrogenic iron overload promote sepsis-associated mortality in *E. coli* infection model

From among the five isolates that caused rapid mortality in mice at the 10^4 CFU inoculum, we randomly selected isolate 1 (blood culture isolate from a patient with urosepsis) for more detailed characterization. Because they lack hepcidin, HKO mice develop spontaneous severe iron overload even when they are fed standard diet, modeling hereditary hemochromatosis in human patients. As shown in Table 3-1, *E. coli* isolate 1 caused 100% mortality in IL-HKO mice while none of the infected WT mice died (*Fig. 3-1A*). These results were validated using WT littermates of HKO mice (data not shown). Further analysis showed that hepcidin deficiency and associated iron overload promoted tissue bacterial dissemination: 16h after infection WT mice had undetectable CFUs while naturally iron-loaded HKO mice had 10^10 CFU/ml in their blood and 10^6 CFU/mg in their liver (*Fig. 3-1B*), indicating that the initial inoculum rapidly multiplied in the host. We then tested whether it was the iron overload that promoted susceptibility to *E. coli* infection rather than any other potential effect of hepcidin deficiency. In these experiments, iron-loaded HKO mice suffered 80% mortality within 24h of IP infection with 10^4 CFU/mouse *E. coli* (isolate 1). However, iron-depletion (ID) of HKO mice completely prevented infection-associated mortality with the same isolate (*Fig. 3-1C*) indicating that hepcidin deficiency promotes susceptibility to *E. coli* infection through iron overload. Accordingly, bacterial burden in tissues and blood was very high for iron- loaded HKO (IL-HKO) mice while bacteria were not detected in

Isolate number	**Diagnosis**	**Ceftriaxone-resistant**	**Dose (CFU/mouse)**	**%Mortality (HKO mice)**	**n**	**%Mortality (WT mice)**	**n**	***p value***
1	Urosepsis	no	10^4	100%	6	0%	6	***<0.001***
2	Liver failure	no	10^4	100%	6	0%	6	***<0.001***
3	Leukemia	no	10^4	100%	5	0%	6	***0.002***
4	Sickle cell disease	yes	10^4	100%	5	0%	5	***0.003***
5	Urosepsis	no	10^4	100%	5	0%	5	***0.003***
6	Congenital heart disease	no	10^6	100%	5	0%	5	***0.003***
7	Evan's syndrome	yes	10^6	100%	5	0%	3	***0.012***
8	Kidney, liver transplant	no	10^6	60%	5	0%	3	***0.05***
9	Liver and bowel transplant	no	10^6	30%	4	0%	3	***0.386***
10	End stage Renal disease	yes	10^7*	20%	5	0%	5	***0.371***

Table 3-1 Hepcidin deficiency promotes susceptibility to infection with clinical E. coli isolates*: List of clinical E. coli blood isolates obtained from the Ronald Reagan UCLA Medical Center. WT mice suffered 0% mortality and did not develop disease signs such as weight loss, change in appearance or decreased activity after infection with any of the isolates at the described doses. However, for 8 out of 10 isolates HKO mice suffered 60% to 100% mortality with the same inocula.*

**For isolate 10 we also tested 5x10^7 CFU/mouse dose and it caused 100% mortality in both WT and HKO mice.*

iron-depleted HKO (ID-HKO) mice (*Fig. 3-1D*).

Intravenous (IV) iron administration for iron deficiency is used quite commonly in chronically ill hospitalized patients especially if repletion is urgent or the oral route is not available because of the underlying disease processes. IV iron can cause iatrogenic iron overload in these patients and in some studies has been linked to higher infection rates[8]. Here we investigated whether IV iron supplementation affects *E. coli* sepsis. WT mice were injected with either 2-4 mg of IV iron sucrose (*Fig. 3-1E*) or 2 mg of IV iron dextran (*Fig 3-1F*) through the retroorbital plexus. Control animals received sterile saline injections. Four hours after IV iron administration the mice were infected intraperitoneally (IP) with 10^4 CFU/mouse *E. coli* (isolate 1). We observed 100% mortality in iron sucrose injected mice and 50% mortality in iron dextran injected mice (*Fig. 3-1E, F*) while all control animals survived, suggesting that iatrogenic iron loading also promotes susceptibility to sepsis-associated mortality in WT mice. We also tested IV iron injection alone without infection and did not observe any adverse effects of iron administration (data not shown). Another common cause of iron overload and possible transient increase of serum iron is red blood cell (RBC) transfusion especially when older packed RBCs are transfused. We developed a model in which WT mice were transfused through the

retroorbital plexus with 400 µl of fresh (3h old) mouse packed RBCs and 4h later were infected with *E. coli*. However, transfusion did not promote susceptibility to sepsis in this model (*Supplemental Figure 3-2*). It has been previously shown that a single transfusion only with old (>14 days old mouse PRBCs which is equivalent to >42 days old human packed RBCs) but not fresh packed RBCs promotes susceptibility[11] to infection which may explain our results. Furthermore, a single transfusion in our model introduced only a moderate amount of iron (~0.4 mg), most of which likely remained in RBC hemoglobin during the course of infection, and did not reflect the degree of clinical iron overload resulting from multiple transfusions over time[33].

In infected WT mice, early inflammatory response induces hepcidin and subsequent hypoferremia

We have previously shown that hepcidin is essential to protect from early mortality after infection with certain siderophilic ("iron-loving") pathogens such as *Yersinia enterocolitica and Vibrio vulnificus*[21,22]. Hepcidin has two important effects which are demonstrated respectively in the two models: 1) it controls baseline iron levels allowing local defenses to abort the initial infection without eliciting a systemic inflammatory response (in the case of oral administration of *Y. enterocolitica*), and 2) it induces inflammation-driven hypoferremia after the initial infection develops and thus further limits available iron for subsequent bacterial replication (seen after intraperitoneal injection of *Y. enterocolitica* and subcutaneous injection of *V. vulnificus*). To measure the inflammatory response in our *E. coli* model we injected WT mice IP with

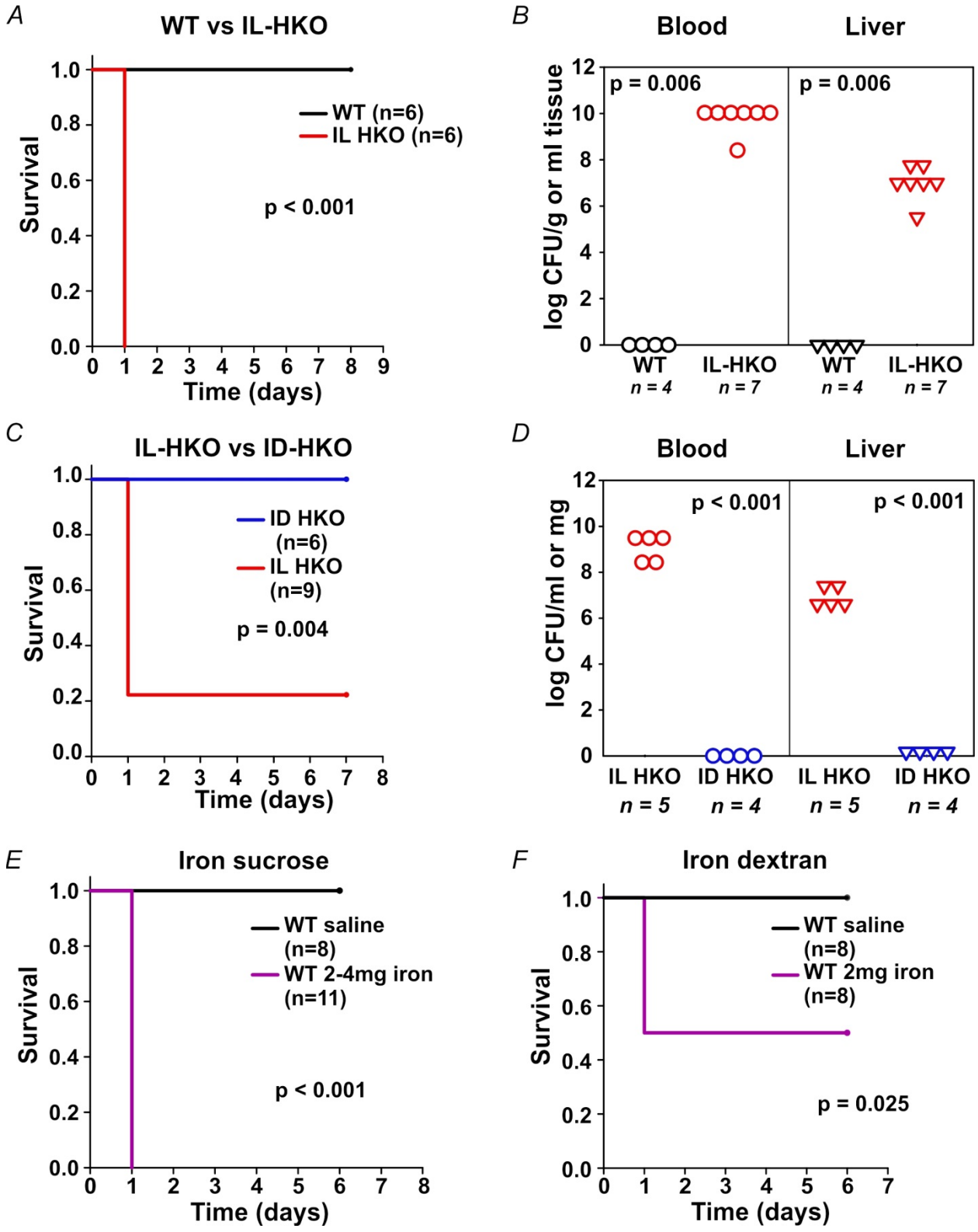

A
WT vs IL-HKO
Survival
Time (days)
WT (n=6)
IL HKO (n=6)
p < 0.001
B
Blood
Liver
log CFU/g or ml tissue
p = 0.006
p = 0.006
WT
IL-HKO
WT
IL-HKO
n = 4
n = 7
n = 4
n = 7
C
IL-HKO vs ID-HKO
Survival
Time (days)
ID HKO (n=6)
IL HKO (n=9)
p = 0.004
D
Blood
Liver
log CFU/ml or mg
p < 0.001
p < 0.001
IL HKO
ID HKO
IL HKO
ID HKO
n = 5
n = 4
n = 5
n = 4
E
Iron sucrose
Survival
Time (days)
WT saline (n=8)
WT 2-4mg iron (n=11)
p < 0.001
F
Iron dextran
Survival
Time (days)
WT saline (n=8)
WT 2mg iron (n=8)
p = 0.025

Figure 3-1 Genetic as well as iatrogenic iron overload enhances sepsis-associated mortality in a mouse model of E. coli infection *A) Survival and B) bacterial CFU in blood and liver after infection of wild type (WT, in black) or naturally iron-loaded hepcidin knockout (IL-HKO, in red) mice with 10^4 CFU/mouse E. coli (isolate 1). C) Survival and D) bacterial CFU in blood and liver after infection of IL-HKO (in red) or dietary iron-depleted HKO (ID-HKO, in blue) mice with 10^4 CFU/mouse E. coli (isolate 4). E) and F) Survival for WT mice that were injected IV with saline (in black) or with 2-4 mg iron sucrose (E, in purple) or 2 mg iron dextran (F, in purple) and 4h later infected IP with 10^4 CFU/mouse E. coli (isolate 1). Two separate experiments were combined for E and for F*.

saline (control) or 10^4 CFU/mouse *E. coli* (isolate 1) and collected tissues for analysis at 4h and 16h post infection (p.i.). As before, none of the infected WT mice suffered mortality or showed signs of illness. However, liver Saa1 mRNA, which is a marker of acute inflammation, was increased 64-fold both at 4h and 16h p.i (*Fig. 3-2A*) showing that an early systemic inflammatory response to the infection was mounted. Accordingly, hepcidin was induced as we detected 2-fold higher hepcidin protein (*Fig. 3-2B*) and 4-fold increased hepcidin mRNA (*Fig. 3-2C*) at 4h p.i. We often observe even greater hepcidin induction but the mice used in this experiment were 10-14 weeks old and their baseline hepcidin level was already very high, limiting the fold-increase. Hepcidin induction at 4h p.i. resulted in hypoferremia (*Fig. 3-2D*) detected at 16h p.i since it takes time for the plasma to become depleted of iron after iron efflux is inhibited by hepcidin. It has been previously reported that inflammation can induce hypoferremia independently of hepcidin[34] but this is not the case in our model since hepcidin-deficient mice do not have lower serum iron at 16h after infection with *E. coli* (*Supplemental figure 3*). Thus, even in mice that did not show any signs of illness, *E. coli* infection was sufficient to elicit a

systemic inflammatory response, increased hepcidin and hypoferremia.

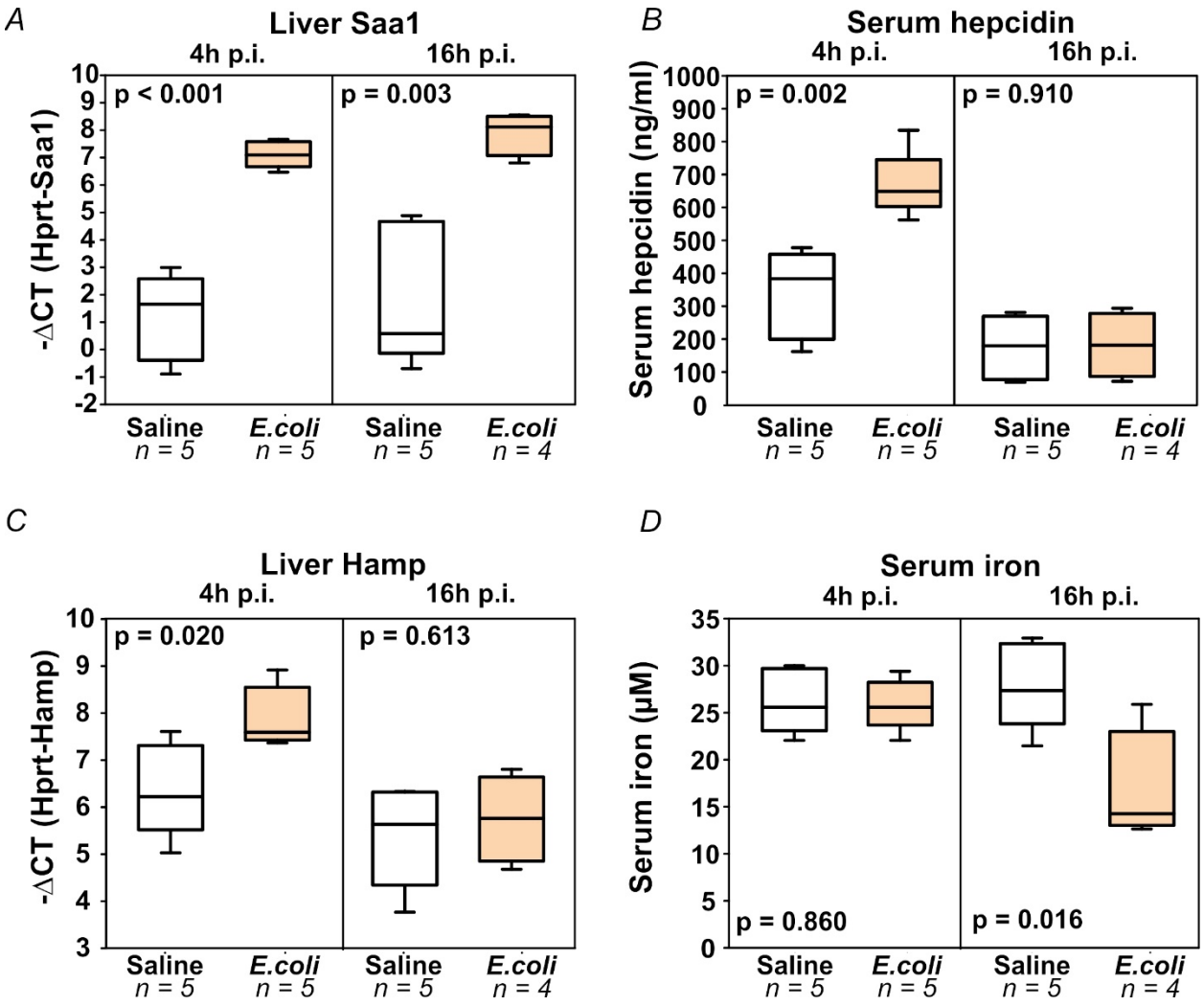


Figure 3-2 E. coli infection rapidly induces systemic inflammation, increases hepcidin and causes hypoferremia. *WT mice were injected IP with either saline (white boxes) or 10^4 CFU/mouse E.coli (isolate 1, orange boxes). Tissues were collected 4 and 16 hours post infection for analysis. A) We measured liver Saa1 as a marker of systemic inflammation, B) hepcidin protein, C) hepcidin mRNA and D) serum iron concentration. Inflammation induces the initial rise in serum hepcidin protein and mRNA followed by hypoferremia and a reactive decrease in hepcidin protein and mRNA.*

Minihepcidin PR73 prevents *E. coli* sepsis-associated mortality in HKO mice, a model of hereditary hemochromatosis

Our study so far showed that hepcidin is essential for protection against *E. coli* sepsis. We therefore tested for the therapeutic effect of the hepcidin agonist PR73 in infected mice. Naturally iron-loaded HKO mice were infected with 10^4 CFU/mouse *E. coli* (isolate 1) and treated IP with solvent (control) or 100 nmoles of PR73 at 3h and 24h post infection. As before, 100% of the control animals died within 24h of infection and solvent treatment. However, treatment with only two doses of minihepcidin was sufficient to completely prevent mortality after infection with isolate 1 (*Fig. 3-3A*). Similar results were obtained when using isolate 2 (*Supplemental Figure 3-4A*). This effect resulted from inhibition of bacterial dissemination and replication, as both blood and liver CFU were significantly decreased by the PR73 treatment (*Fig. 3-3B*): while control animals had on average 10^10 CFU/ml and 10^7 CFU/mg in their blood and liver respectively, minihepcidin treated animals had only 10^2 CFU/ml or mg in each tissue. Next, we asked whether minihepcidin treatment could be beneficial if started even later than 3h p.i. Since most of the mice become moribund by 16h p.i. we decided to administer the first minihepcidin dose at 10h p.i. However, at this time point the mice were already very sick and minihepcidin treatment was not beneficial (*Supplemental Figure 3-4B*). These results suggest that minihepcidin treatment prevents *E. coli* sepsis-associated mortality in a model of hereditary hemochromatosis but only if given early enough after infection.

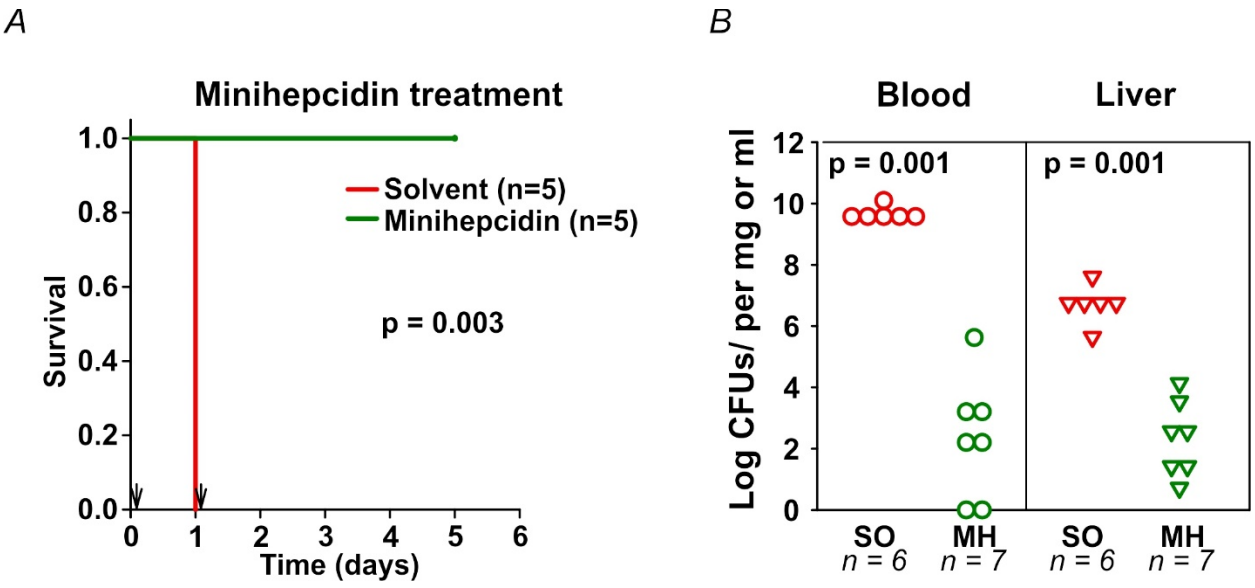


Figure 3-3 Minihepcidin prevents E. coli sepsis-associated mortality in a model of hereditary hemochromatosis*: Naturally iron-loaded HKO mice were infected IP with 10^4 CFU/mouse E. coli (isolate 1) and treated with solvent (in red) or 100 nmoles minihepcidin (in green) at +3 and +24h p.i. A) Survival was monitored and B) in two repeat experiments tissues were collected 16h p.i. to assess bacterial burden in the blood and liver.*

Increased non-transferrin bound iron promotes *E. coli* infection

Having shown that iron overload promotes susceptibility to *E. coli* infection and that endogenous hepcidin or exogenous minihepcidin are protective, we next asked which iron pool may be critical in promoting infection. We analyzed tissue iron (liver), extracellular iron (serum) and a specific extracellular iron species (non-transferrin bound iron, NTBI) in groups of mice that are susceptible to or protected from infection (*Fig. 3-4*).

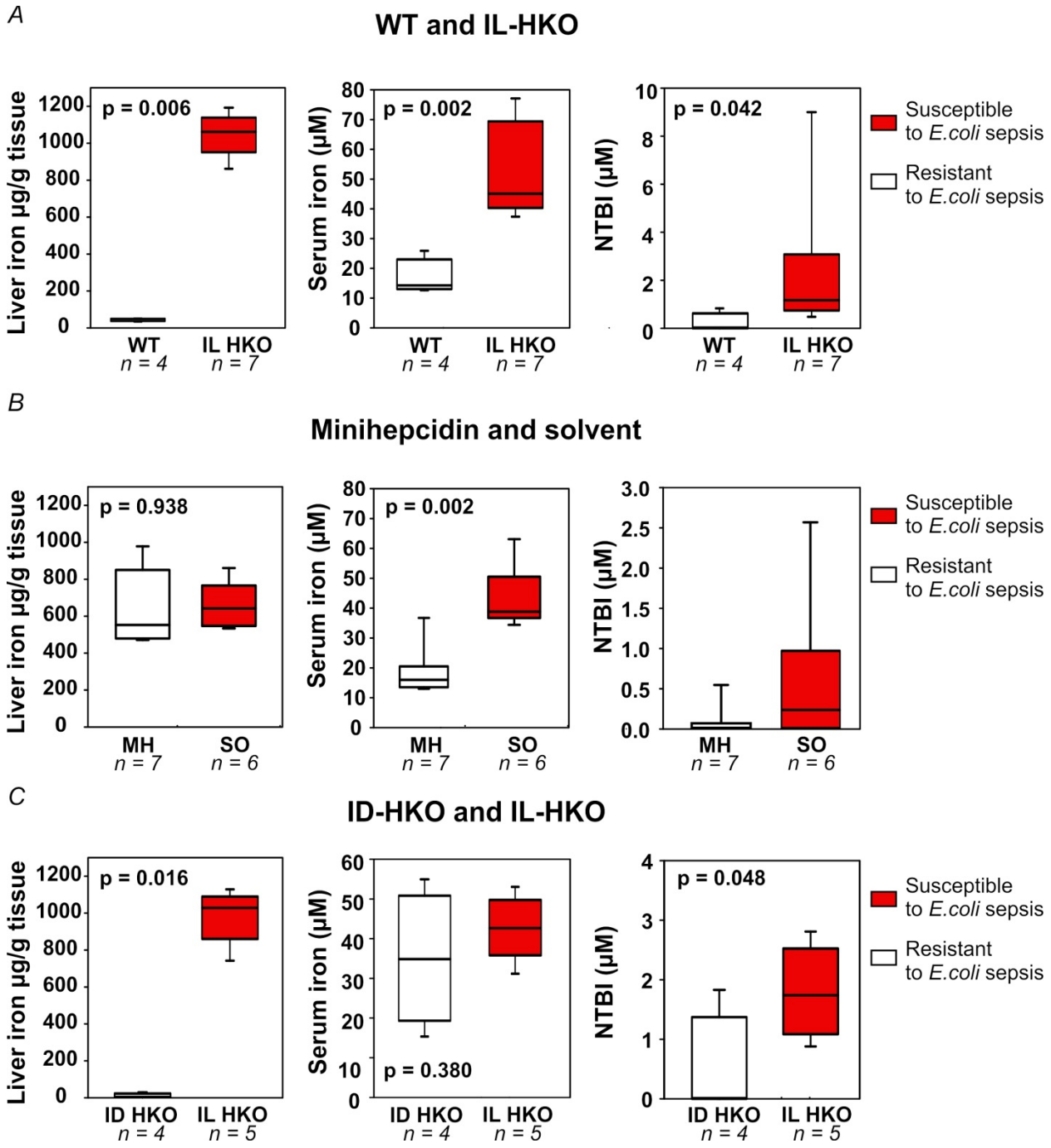
Comparing those parameters between resistant WT and susceptible iron-loaded HKO mice, we found that iron-loaded HKO mice had high liver iron, serum iron as well as NTBI (*Fig. 3-4A*) confirming that iron overload promotes susceptibility to infection.

To selectively deplete extracellular iron, we treated HKO mice with the minihepcidin PR73, a potent hepcidin agonist, at a dose that prevents sepsis-related disease signs and mortality. As expected, a single minihepcidin dose did not change liver iron but caused a significant drop in serum iron and NTBI concentration (*Fig. 3-4B*) suggesting the importance of extracellular rather than total body iron in promoting *E. coli* infection.

Lastly, we compared iron distribution in iron-depleted HKO and iron-loaded HKO mice. As expected, we found tissue iron levels to be higher in iron-loaded than iron-depleted HKO mice (*Fig. 3-4C*). As HKO mice lack the ability to lower their serum iron concentrations until their stores are completely iron-depleted, serum iron levels were comparable between the two groups and only NTBI was different. The generation of NTBI is not reflected solely in serum iron concentration but is also dependent on the kinetics of iron efflux from macrophages, hepatocytes and enterocytes, and the ability of the liver to rapidly clear NTBI. The differences in cellular iron content and therefore efflux likely account for the difference in NTBI concentration between the infection-susceptible iron-loaded and resistant iron-depleted groups. Altogether, the protective effects of iron depletion and minihepcidin treatment indicate that it is not primarily the tissue iron nor the serum iron level but NTBI that promotes susceptibility to *E. coli* sepsis.

To determine whether NTBI promotes *E. coli* growth in human plasma, we supplemented the plasma with increasing concentrations of iron. We added 0 to 60 µM ferric ammonium citrate, FAC, an iron species similar to the predominant component of NTBI[35] in order to gradually saturate transferrin thus increasing the concentration of transferrin-bound iron (Tf-Fe) and eventually leading to the formation of non-transferrin bound iron (NTBI). The plasma was solidified by the addition of agar, and *E. coli* (isolate 1) plated on the plasma

agar. We observed bacterial growth only in conditions where NTBI was present (*Fig. 3-4D and Supplemental Table 3-2*). When testing the other 9 isolates we observed two types of behavior (*Supplemental Table 3-3*): similarly to isolate 1, five out of the nine isolates grew only in conditions where NTBI was detectable. The other four isolates likewise failed to grow in plasma when iron was not supplemented, but did start growing already at lower FAC concentrations where we could not yet detect NTBI with our methodology. We hypothesize the plasma did not reach equilibrium with the added FAC so that a small amount of NTBI was present and was sufficient to promote bacterial growth for these isolates. The obtained results are heterogeneous, reflecting the expected heterogeneity of clinical isolates. However, for all isolates the additional iron accelerated bacterial colony formation within 24h incubation. Further incubation would not be relevant for our model since all of the mice die within 24h of infection. These data indicate that the ability of hepcidin to clear NTBI from circulation and extracellular fluid delays bacterial growth and this delay is an important determinant of infection outcome.


A
WT and IL-HKO
Liver iron µg/g tissue
p = 0.006
WT
n = 4
IL HKO
n = 7
Serum iron (µM)
p = 0.002
NTBI (µM)
p = 0.042
Susceptible to E.coli sepsis
Resistant to E.coli sepsis
B
Minihepcidin and solvent
p = 0.938
MH
n = 7
SO
n = 6
C
ID-HKO and IL-HKO
p = 0.016
ID HKO
n = 4
IL HKO
n = 5
p = 0.380
p = 0.048

D

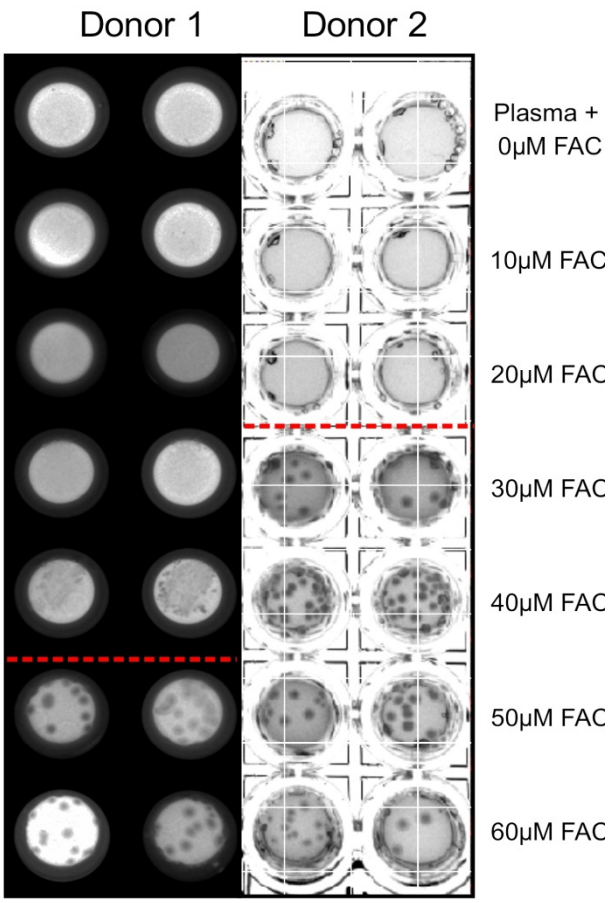


Figure 3-4 Non-transferrin bound iron (NTBI) rather than total iron promote susceptibility to E. coli sepsis*: Liver iron, serum iron and non-transferrin bound iron measurements for: (A) WT (white boxes) and IL-HKO (red boxes) mice, (B) IL-HKO (red boxes) and ID-HKO (white boxes) mice, (C) IL-HKO mice treated IP either with single dose solvent (red boxes) or 100 nmoles minihepcidin (white boxes) 14h prior tissue collection. All mice were infected IP with 10^4 CFU/mouse E. coli (isolate 1) and tissues were collected 14-16h post infection (p.i.). IL=iron-loaded; ID=iron-depleted. D) Human plasma was supplemented with 0 to 60 μM ferric ammonium citrate (FAC), and used to make agar plates. E. coli isolate 1 was plated and incubated for 38-41h at 37°C and bacterial CFUs documented by photography. Two separate experiments using different plasma donors are shown. Conditions below the red line had detectable NTBI.*

Discussion

During infection and inflammation, the plasma concentration of hepcidin is greatly increased, leading to sequestration of iron in macrophages and enterocytes with consequent hypoferremia[4]. We previously showed that this mechanism of innate immunity limits extracellular iron availability and inhibits the growth of siderophilic pathogens *Vibrio vulnificus*[22] and *Yersinia enterocolitica*[21], *in vitro* and in mice. However, hepcidin-induced hypoferremia is a highly conserved response to various infections of mammals raising the question of whether it acts against a broader set of bacteria than these relatively rare classical siderophilic pathogens. We therefore compared outcomes after infection of HKO mice and WT mice with 10 different clinical *E. coli* isolates. To our surprise, with most isolates, hepcidin-deficient mice rapidly developed overwhelming sepsis and suffered 100% mortality within 24h of infection at inoculum doses where 0% of wild type mice with normal iron metabolism died (*Table 1*). Thus, hepcidin is essential for protection against *E. coli* infection-associated mortality. The dramatic difference in survival was observed for 8 out of the 10 clinical isolates, while the remaining 2 isolates showed low virulence in mice, not causing significant mortality in either WT or HKO mice. These results suggest that hepcidin is an important component of innate immune response against a wider range of pathogens than heretofore appreciated. Using iron-depletion experiments, we showed that the protective effect of hepcidin is dependent on its effects on iron distribution rather than a direct antimicrobial effect. The hepcidin analogue PR73 completely protected the highly susceptible HKO mice with only two doses given at 3h and 24h post infection.

Hepcidin controls extracellular iron levels by occluding and degrading the iron transporter ferroportin. Inflammation resulting from administration of different PAMPs (pathogen associated molecular patterns) in mice was reported to decrease ferroportin expression independently of hepcidin[34] . In our hepcidin-deficient mice, however, this mechanism was not sufficient to alter plasma iron levels or protect mice from sepsis, indicating that in infection *in vivo*, hepcidin plays an essential and dominant role in controlling iron availability to pathogens.

Iron supplementation has been linked to increased infection rates in some human trials[12,13]. As a result, medical guidelines recommend avoiding IV iron in infected patients, although without strong evidence supporting causality[36]. In our model of *E. coli* infection, IV iron administration dramatically increased sepsis and mortality (Fig. 3-2) thus supporting the concern about iron supplementation in patients with infections. Moreover, parenteral iron administration may be linked to systemic oxidative stress-induced mortality in experimental murine sepsis models with heat-killed *E. coli*[37]. We cannot exclude the possibility that increased oxidative stress also contributes to mortality in our models of *E. coli* sepsis.

We suggest that assessing the infection status of patients should be an important consideration in the timing of iron therapy. Furthermore, as with the classical siderophilic bacteria[21], the iron species implicated in increased susceptibility to sepsis with clinical isolates of *E. coli* was NTBI. Apparently, NTBI, not tightly bound to chaperone proteins, is more readily available to pathogens, may allow them to acquire iron faster or with lower energy expenditure, thus allowing faster growth. *E. coli* has not been considered a classic siderophilic pathogen because, unlike *Y. enterocolitica* and *V. vulnificus,* its disease-

causing ability has not been clearly linked to iron availability. Furthermore, most *E. coli* isolates produce siderophores[38] and should be able to access iron from multiple sources. However, siderophore production incurs a high metabolic cost, and secreted siderophores are readily pirated by niche competitors. Many bacteria do not produce siderophores constitutively but induce production in response to environmental clues. The initial survival of bacteria entering the host may depend on relative rates of bacterial proliferation compared to bacterial clearance by host defense mechanisms. If NTBI is present during early phases of infection, the bacteria may rapidly replicate, overwhelming local defense mechanisms and causing severe infection and mortality such as we see in HKO mice and IV iron injected WT mice (*Table 3-1 and Fig 3-1*). In the absence of NTBI, the bacteria depend on the induction of more complex iron acquisition systems that require additional metabolic resources, slowing the initial proliferation of bacteria.

Our current understanding of the role of iron in infections is still limited and future studies may find that the disease-causing ability of many more bacterial species is enhanced by genetic or iatrogenic iron excess. In these settings, the manipulation of iron metabolism by hepcidin agonists early in the course of the disease could be an effective adjunctive treatment.

Methods

Bacterial preparation

Escherichia coli blood culture isolates collected in 2015 from hospitalized pediatric patients were kindly provided by the Pediatric Infectious Disease Division at UCLA, with brief patient histories in Table 1. 35% glycerol stock was prepared for each of the isolates,

aliquoted and stored at -80ºC. For infection experiments, an aliquot of the stock was thawed, 5 µl was inoculated in 5ml Luria Bertani broth (LB, Becton Dickinson BD) and cultured overnight at 37ºC (18-22h). Overnight culture (ON) was re-cultured (100µl of the ON culture in 5ml fresh LB) for 3h at 37ºC in order to reach exponential phase and then centrifuged at 7500rcf for 5min and re-suspended in sterile phosphate buffered saline (PBS). The bacteria were diluted to the desired concentration using OD_{600} as indicator of bacterial concentration (OD_{600} = 1 is equivalent to 1x10^9 CFU/ml)[39].

Animal models

All animal experiments performed for this study were approved by the UCLA Office of Animal Research Oversight. Wild type (WT) mice (The Jackson Laboratory) and hepcidin-1 knockout mice[40] (HKO), both on C57BL/6 background, were used for infection experiments. For survival experiments comparing HKO to WT mice, we used either WT and HKO littermates, or WT mice purchased from the Jackson Laboratory and acclimated to our vivarium for at least two weeks, with no difference in outcomes. At arrival to the vivarium the bedding was exchanged between purchased WT mice and resident HKO mice to partially account for differences in microbiome. The animals were fed ad libitum standard diet (185 ppm iron concentration). In order to achieve iron depletion of HKO mice, the animals were fed iron-deficient diet (4 ppm Fe, Envigo Teklad) for 5-6 weeks prior to the experiment. For some experiments WT mice were injected intravenously (IV) with iron sucrose or iron dextran: the animals were anaesthetized using isoflurane (Clipper) and then injected IV in the retroorbital plexus using 28Ga insulin syringe. The dose used was 2 or 4 mg iron sucrose (Venofer, American Regent Inc.) per mouse in 100

or 200 µl volume respectively, or 2 mg iron dextran (Sigma) in 100 µl per mouse. Iron administration was performed 4h prior to infection.

Mice were infected via intraperitoneal (IP) injection with different doses of *E. coli*. Animal wellbeing and behavior were monitored closely and mice euthanized by isoflurane (Clipper) when they showed symptoms of imminent mortality (decreased activity, weight loss, lack of grooming).

Preparation of minihepcidin

Minihepcidin PR73 was synthesized as previously described[22] using standard solid-phase Fmoc chemistry. Lyophilized minihepcidin was dissolved in 70% ethanol (Gold Shield Chemical Co) together with solvent DSPE-020 CN (NOF Corporation). The solution was dried in SpeedVac to decrease ethanol content. The dried product was stored at 4ºC until needed for experiment, when it was resuspended in sterile injection water (Abbot Laboratories). IP injections were administered at 100nmol PR73 in 100µl per mouse. Control animals were injected with solvent only (100µl IP).

Assessment of bacterial burden

Blood and liver were collected 13 to 18 hours post infection for bacterial burden measurement. Blood was collected through cardiac puncture, mixed with heparin to prevent coagulation, and serial 10-fold dilutions with sterile PBS prepared. The whole liver was collected, homogenized, and 50µl of the homogenate weighed and mixed with 200 µl sterile water. The resulting mixture was used for serial 10-fold dilutions with sterile PBS. For both blood and liver CFU assessment, 5µl from each dilution was plated on LB 1.5%

agar plates in duplicates. The plates were incubated at 37ºC for 15-16h and the number of colonies was counted using a dissecting microscope.

Measuring non-heme iron

The whole liver was dissected, homogenized and 75µl weighed. Then 1125µl protein precipitation solution (0.53N HCl Fisher and 5.3% trichloroacetic acid, Fisher) was added and the mixture was incubated at 100ºC for 1h. The samples were centrifuged and the supernatant was analyzed for iron concentration using the colorimetric Iron SL assay (Sekisui Diagnostics) following the manufacturer's instructions. Iron AA standard (RICCA Chemical Company) was used in serial dilutions to generate standard curve and determine iron concentration in the samples. For serum iron measurements, blood was collected through cardiac puncture and centrifuged in serum separator tubes (BD) to obtain serum samples. Their iron concentration was measured using the colorimetric Iron SL assay (Sekisui Diagnostics) following the manufacturer's instructions.

Gene expression assessment

TRIzol Reagent (Life Technologies) was used to isolate RNA from snap frozen liver samples. Then cDNA was synthesized using iScript cDNA Synthesis Kit (Bio-Rad) following the manufacturer's protocol. Sso Advance SYBR Green Supermix (Bio-Rad) and CFX96 Touch Real-Time PCR Detection System (Bio-Rad) were used to perform quantitative real-time PCR for the following genes: Saa1 (forward: AGTCTGGGCTGCTGAGAAAA; reverse: ATGTCTGTTGGCTTCCTGTG); Hprt (forward: CTGGTTAAGCAGTACAGCCCCAA; reverse: CAGGAGGTCCTTTTCACCAGC); Hamp (forward: TTGCGATACCAATGCAGAAGA reverse:

GATGTGGCTCTAGGCTATGTT). Hprt was used as the house-keeping gene and results in figures are shown as dCt = Ct_{Hprt}-Ct_{test}.

Hepcidin ELISA

Serum hepcidin protein concentration was measured by performing ELISA as previously described[22] with the following reagents: Ab2B10 (capture) and Ab2H4-HRP (detection) antibodies kindly provided by Amgen, synthetic mouse hepcidin-25 (standard curves ranging from 400 pg to 3.2 pg/ml).

Non-Transferrin bound iron (NTBI) assay

Non-transferrin bound iron concentration was measured as previously described[21] in a protocol adapted from Esposito et al[41]. All samples were frozen after collection and stored at -80ºC. Once thawed, the samples were measured in triplicates at 5 µl/well and never reused.

Bacterial growth in human plasma agar

Human plasma was inactivated by incubation at 56°C for 30min and centrifuged at 9200g to remove precipitated protein. Then 0µM to 60µM ferric ammonium citrate (FAC, Sigma) was added and the plasma was incubated ON at 37°C to allow for the iron to bind transferrin. The following day a few drops of hot 12% agar were added to the warm plasma and the mixture was quickly pipetted into a 96-well plate. *E. coli* isolates were cultured as described above, diluted to a concentration of 10^4 CFU/ml and 5µl plated in each well in duplicate. The bacteria were incubated for up to 42h at 37°C and bacterial growth photographed.

Statistics

Statistical analysis was performed using SigmaPlot. Survival was analyzed using Kaplan-Meier survival curves and log-rank test. For the rest of the data, student's t-test was used for normally distributed data and Mann-Whitney rank sum test was used for data that are not normally distributed. Box plots with error bars show the median, 10th, 25th, 75th, and 90th percentiles.

Authorship: DS, EN, TG and Yb designed the study; DS and AR performed experiments and analyzed data; SC, RH and JD provided clinical E.coli isolates as well as intellectual input; DS, EN, YB and TG wrote the manuscript and all authors contributed to results discussion

Acknowledgements: The authors want to thank Victoria Gabayan for her hard work on maintaining the hepcidin knockout mouse colony. The research was supported by the following grants R01DK107309 (to E.N.) and R01DK065029 (to T.G.).

Conflicts of interest: E.N. and T.G. are consultants and shareholders of Intrinsic LifeSciences and Silarus Therapeutics, and consultants for La Jolla Pharmaceutical Company and Keryx Pharmaceuticals. EN is a consultant for Protagonist Therapeutics. TG is a consultant for Fresenius-Vifor and Akebia.

Supplemental Data

		WT mice		HKO mice	
Isolate number	**Dose (CFU/mouse)**	**Average weight change 16-24h after infection**	**n**	**Average weight change 16-24h after infection**	**n**
1	10^4	-1.7%	6	-8.1%	6
2	10^4	-1.3%	6	-8.7%	6
3	10^4	-4.9%	4	-8.3%	4
4	10^4	0.5%	5	no data	
5	10^4	2.2%	5	no data	
6	10^6	0.0%	5	-10.3%	2
7	10^6	-1.3%	3	-7.3%	4
8	10^6	1.7%	5	-1.5%	5
9	10^6	-2.0%	3	-4.1%	4
10	10^7	-0.3%	5	-8.1%	5

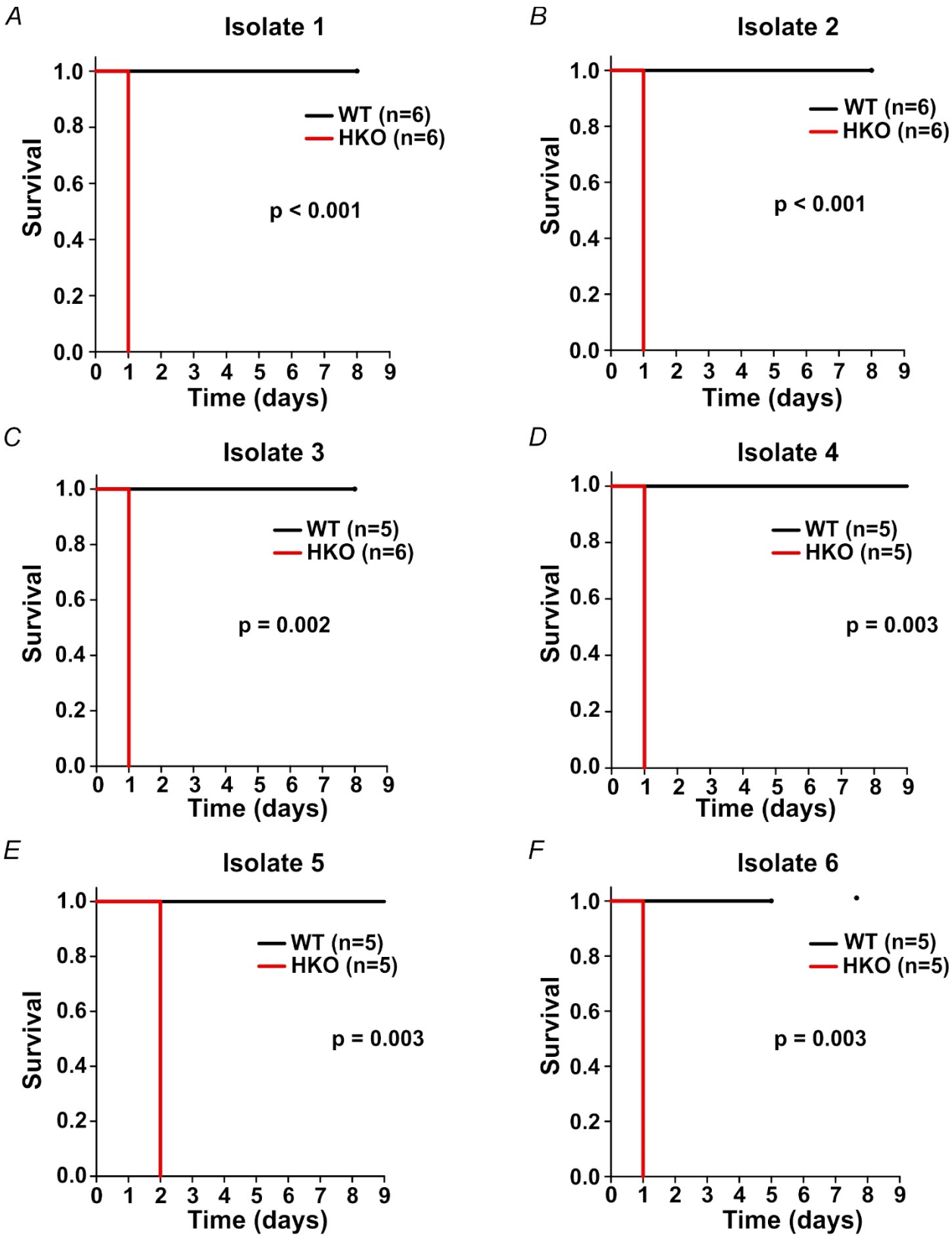
Supplemental Table 3-1 *WT mice and naturally iron-loaded HKO mice were infected IP with E. coli. Weight was recorded at the same time for WT and HKO mice: at the time of infection and 16 to 24h later. WT mice did not lose weight or lost weight within the error range (5%). For each isolate HKO mice lost more weight than WT mice. Not all mice were weighed because some were moribund and were euthanized.*

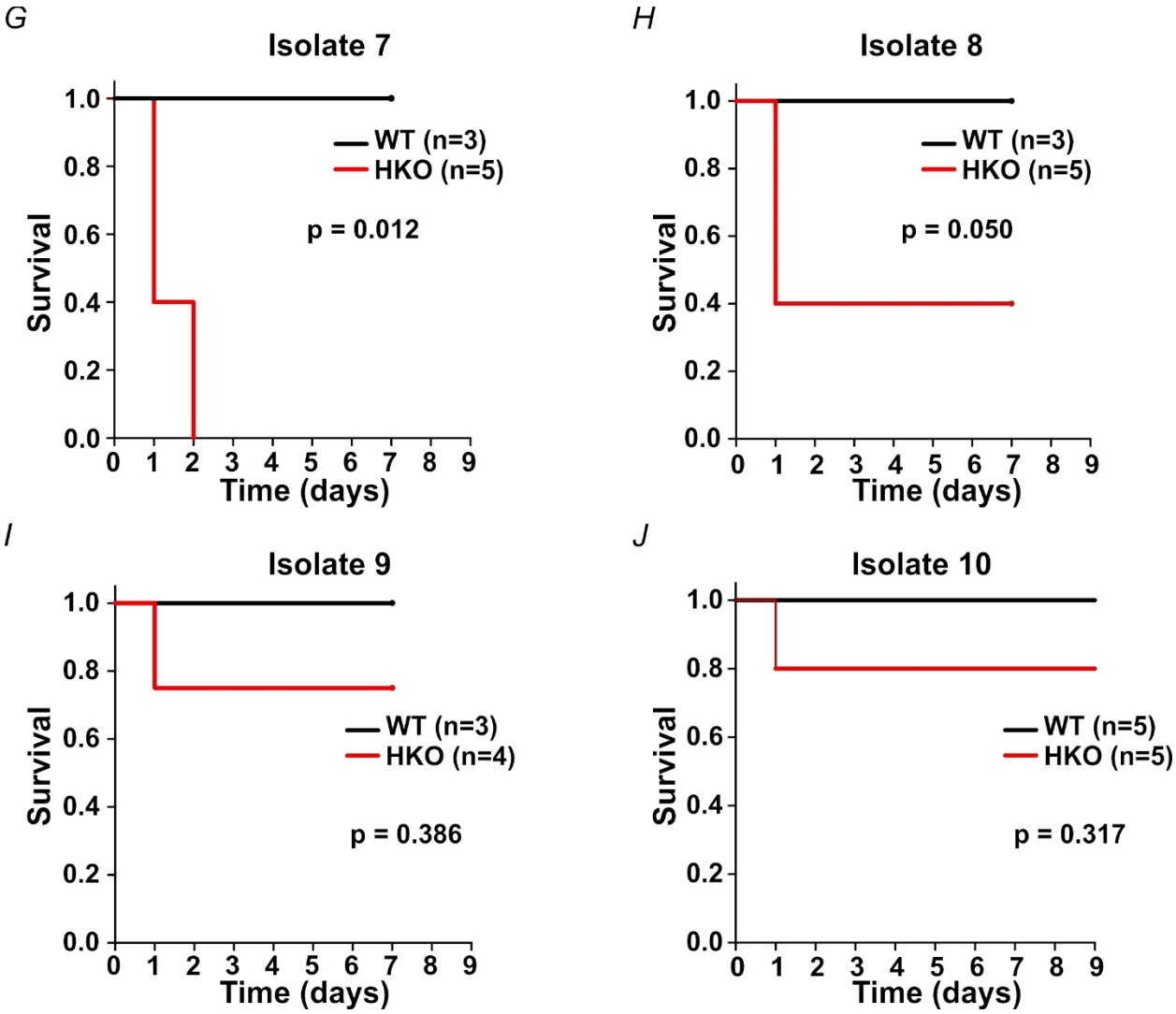
	Donor 1		Donor 2	
Sample ID	**Tf Sat**	**µM NTBI**	**Tf Sat**	**µM NTBI**
Plasma	30%	**0**	31%	**0**
10µM FAC	43%	**0**	47%	**0**
20µM FAC	58%	**0**	60%	**0**
30µM FAC	65%	**0**	76%	**~ 0.4**
40µM FAC	77%	**0**	96%	**3.2**
50µM FAC	89%	**2.7**	100%	**>5**
60µM FAC	100%	**>5**	100%	**>5**

Supplemental Table 3-2 *Human plasma was supplemented with 0 to 60µM ferric ammonium citrate (FAC), agar was added and E. coli isolate 1 was inoculated on the plasma agar. The table shows transferrin saturation (Tf Sat) and non-transferrin bound iron (NTBI) concentration for the different conditions at the start of the experiment. Two different plasma donors were used in separate experiments*

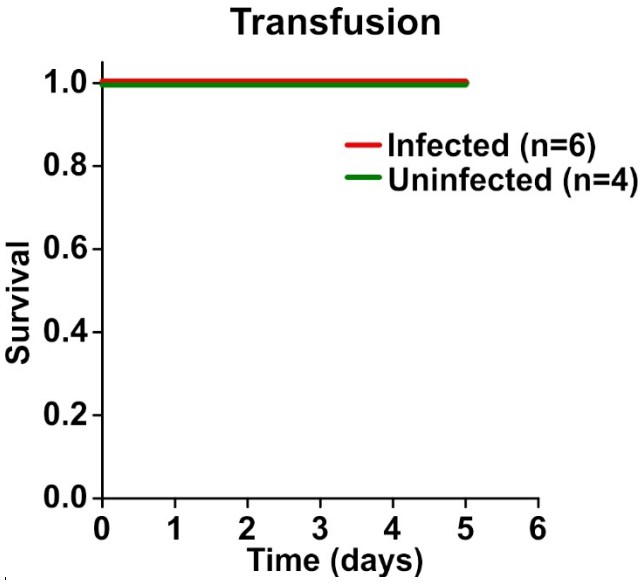
Isolate number	Growth in plasma (no added iron)	Growth in plasma (added iron but no NTBI)	Growth in plasma (with NTBI)
1	no	no	yes
2	delayed	yes	yes
3	no	no	yes
4	no	yes	yes
5	no	no	yes
6	no	no	yes
7	no	no	yes
8	delayed	yes	yes
9	no	yes	yes
10	no	no	yes

Supplemental Table 3-3 *Each of the isolates was inoculated in human plasma (agar or liquid) supplemented with 0 to 60µM FAC and bacterial growth was monitored for 22 to 41h. No growth means that no bacterial colonies or increase in OD600 were observed within the time frame of the experiment (40h and 22h respectively). Delayed growth designates lack of bacterial colonies at 22h of incubation but positive bacterial growth at 40h of incubation. Positive growth means that colonies were detected early in the experiment.*

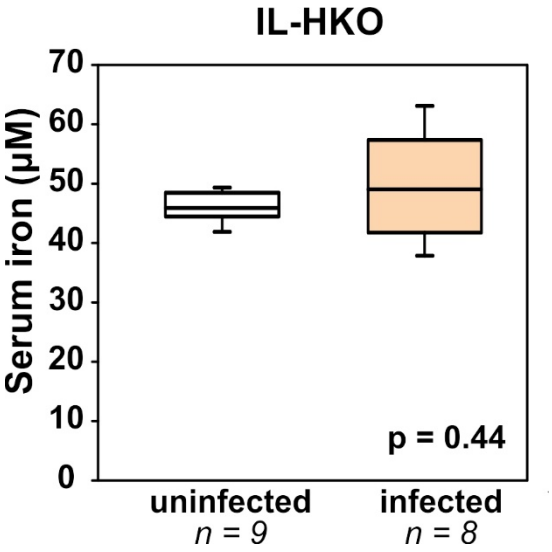

A
Isolate 1
WT (n=6)
HKO (n=6)
p < 0.001
B
Isolate 2
WT (n=6)
HKO (n=6)
p < 0.001
C
Isolate 3
WT (n=5)
HKO (n=6)
p = 0.002
D
Isolate 4
WT (n=5)
HKO (n=5)
p = 0.003
E
Isolate 5
WT (n=5)
HKO (n=5)
p = 0.003
F
Isolate 6
WT (n=5)
HKO (n=5)
p = 0.003
Survival
Time (days)



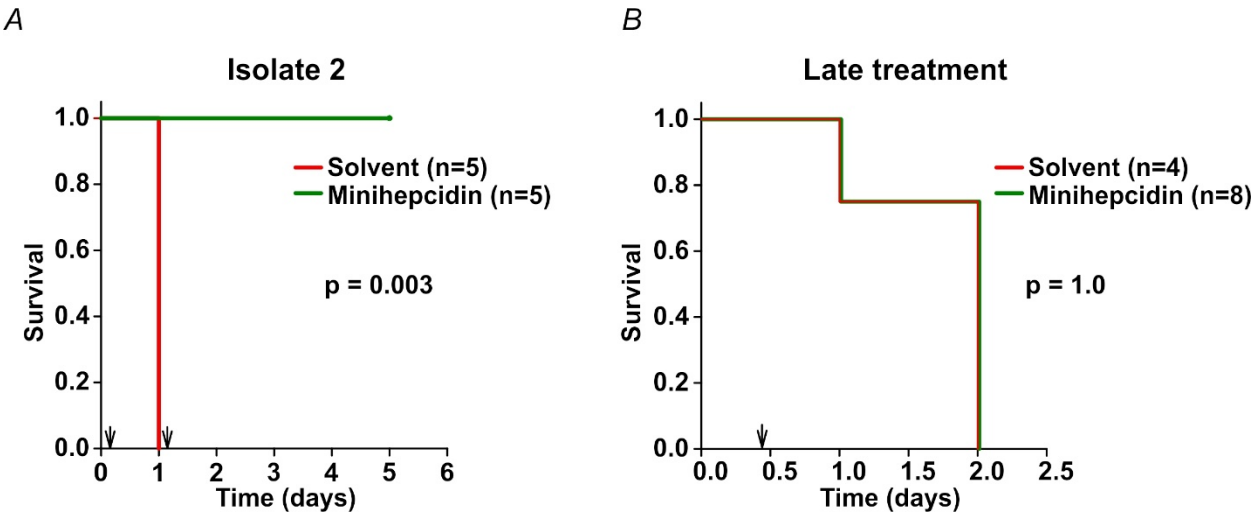
Supplemental Figure 3-1 *Wild type (WT) mice and naturally iron-loaded hepcidin knockout mice (HKO) were infected IP with different clinical E.coli isolates at the following doses: 10^4 CFU/mouse for isolates 1 through 5; 10^6 CFU/mouse for isolates 6 through 9 and 10^7 CFU/mouse for isolate 10. Survival was monitored. WT mice suffered 0% mortality and did not develop disease symptoms (no weight loss, no changes in appearance or behavior) after infection with any of the isolates. HKO mice suffered 100% mortality within 24h of infection with isolates 1 to 7, 60% mortality after infection with isolate 8 and no significant difference in mortality between WT and HKO mice was observed for isolates 9 and 10. Panel A was presented in the main body of the paper as Figure 1A*



Supplemental Figure 3-2 *WT mice were injected IV through the retroorbital plexus with 250-400µl fresh packed red blood cells (PRBCs). PRBCs were isolated the same day from mice with the same genotype and age. 4h post transfusion the mice were injected IP with either saline (uninfected) or 10^4 CFU/mouse E.coli (isolate 1). Survival was monitored but none of the mice suffered mortality.*



Supplemental Figure 3-3 *Naturally iron-loaded HKO mice were injected IP with 0.1ml saline or 10^4 CFU/mouse E.coli (isolate 1) and serum was collected for analysis 16h later. No significant difference was observed between infected and uninfected animals.*



Supplemental Figure3- 4 *A) Naturally iron-loaded HKO mice were infected IP with 10^4 CFU/mouse isolate 2 and treated with solvent (control) or 100nmol minihepcidin at 3h and 24h post infection (p.i.). Survival was monitored. 100% of control animals died by day 1, while minihepcidin treated animals suffered 0% mortality. B) Naturally iron-loaded HKO mice were infected IP with 10^4 CFU/mouse isolate 1 and treated with solvent (control) or 100nmol minihepcidin at 10h post infection. Survival was monitored. All of the mice died by day 2 p.i*

Reference list

1. Ganz T, Nemeth E. Regulation of iron acquisition and iron distribution in mammals. *BiochimBiophysActa*. 2006;1763(7):690-699.

2. Ganz TN, E. Iron homeostasis in host defence and inflammation. *Nat Rev Immunol*. 2015;15(8):500-510.

3. Park CH, Valore EV, Waring AJ, Ganz T. Hepcidin, a urinary antimicrobial peptide synthesized in the liver. *JBiolChem*. 2001;276(11):7806-7810.

4. Rodriguez R, Jung CL, Gabayan V, et al. Hepcidin Induction by Pathogens and Pathogen-Derived Molecules Is Strongly Dependent on Interleukin-6. *Infection and Immunity*. 2014;82(2):745-752.

5. Barber MF, Elde NC. Escape from bacterial iron piracy through rapid evolution of transferrin. *Science*. 2014;346(6215):1362-1366.

6. Wandersman C, Delepelaire P. BACTERIAL IRON SOURCES: From Siderophores to Hemophores. *Annual Review of Microbiology*. 2004;58(1):611-647.

7. Miethke M, Marahiel, MA. Siderophore-Based Iron Acquisition and Pathogen Control. *Microbiol Mol Biol Rev*. 2007;71:38.

8. Drakesmith H, Prentice AM. Hepcidin and the iron-infection axis. *Science*. 2012;338(6108):768-772.

9. Michels K, Nemeth, E, Ganz, T, Mehrad, B. Hepcidin and Host Defense against Infectious Diseases. *PLoS Pathog*. 2015;11.

10. Vento S, Cainelli F, Cesario F. Infections and thalassaemia. *LancetInfectDis*. 2006;6(4):226-233.

11. Prestia, K, Bandyopadhyay, S, Slate, A, Francis, RO, Francis, KP, Spitalnik, SL, Fidock, DA, Brittenham, GM, Hod, EA. Transfusion of stored blood impairs host defenses against Gram-negative pathogens in mice. *Transfusion*. 2014;54:2842-2851.

12. Sazawal S, Black RE, Ramsan M, et al. Effects of routine prophylactic supplementation with iron and folic acid on admission to hospital and mortality in preschool children in a high malaria transmission setting: community-based, randomised, placebo-controlled trial. *Lancet*. 2006;367(9505):133-143.

13. Zlotkin S, Newton, S, Aimone, AM, Azindow, I, Amenga-Etego, S, Tchum, K, Mahama, E, Thorpe, KE, Owusu-Agyei, S. Effect of iron fortification on malaria incidence in infants and young children in Ghana: a randomized trial. *JAMA*. 2013;310:9.

14. Soofi S, Cousens, S, Iqbal, SP, Akhund, T, Khan, J, Ahmed, I, Zaidi, AK, Bhutta, ZA. Effect of provision of daily zinc and iron with several micronutrients on growth and morbidity among young children in Pakistan: a cluster-randomised trial. *Lancet*. 2013;382.

15. Manno D, Siame, J, Larke, N, Baisley, K, Kasonka, L, Filteau, S. Effect of multiple micronutrient-fortified food on mild morbidity and clinical symptoms in Zambian infants: results from a randomised controlled trial. *Eur J Clin Nutr*. 2011;65:3.

16. Khan F, Fisher, MA, Khakoo, RA. Association of hemochromatosis with infectious diseases: expanding spectrum. *International journal of infectious diseases*. 2007;11:6.

17. Gerhard GS, Levin KA, Price GJ, Wojnar MM, Chorney MJ, Belchis DA. *Vibrio vulnificus* septicemia in a patient with the hemochromatosis HFE C282Y mutation. *ArchPathol Lab Med*. 2001;125(8):1107-1109.

18. Vadillo M, Corbella, X, Pac, V, Fernandez-Viladrich, P, Pujol, R. Multiple liver abscesses due to *Yersinia enterocolitica* discloses primary hemochromatosis: three cases reports and review. *Clin Infect Dis*. 1994;18(6):938-941.

19. Manso C, Rivas, I, Peraire, J, Vidal, F, Richart, C. Fatal *Listeria* meningitis, endocarditis and pericarditis in a patient with haemochromatosis. *Scand J Infect Dis*. 1997;29(3):308-309.

20. Barry D, Reeve, AW. Increased incidence of gram-negative neonatal sepsis with intramuscula iron administration. *Pediatrics*. 1977;60(6):908-912.

21. Stefanova D, Raychev, A, Arezes, J, Ruchala, P, Gabayan, V, Skurnik, M, Dillon, BJ, Horwitz, MA, Ganz, T, Bulut, Y and Nemeth, E. Endogenous hepcidin and its agonist mediate resistance to selected infections by clearing non-transferrin-bound iron. *Blood*. 2017;130(3):245-257.

22. Arezes J, Jung G, Gabayan V, et al. Hepcidin-induced hypoferremia is a critical host defense mechanism against the siderophilic bacterium Vibrio vulnificus. *Cell Host Microbe*. 2015;17(1):47-57.

23. Michels K, Zhang, Z, Bettina, AM, Cagnina, RE, Stefanova, D, Burdick, MD, Vaulont, S, Nemeth, E, Ganz, T, Mehrad, B. Hepcidin-mediated iron sequestration protects against bacterial dissemination during pneumonia. *JCI Insight*. 2017;2(6):e92002.

24. Brissot P, Ropert M, Le LC, Loreal O. Non-transferrin bound iron: A key role in iron overload and iron toxicity. *BiochimBiophysActa*. 2012;1820(3):403-410.

25. Brissot P, Ropert, M, Le Lan, C, Loréal, O. Non-transferrin bound iron: a key role in iron overload and iron toxicity. *Biochim Biophys Acta*. 2012;1820(3):403-410.

26. Hirano K, Morinobu, T, Kim, H, Hiroi, M, Ban, R, Ogawa, S, Ogihara, H, Tamai, H, Ogihara, T. Blood transfusion increases radical promoting non-transferrin bound iron in preterm infants. *Arch Dis Child Fetal Neonatal Ed*. 2001;84(3):F188-F193.

27. Tenaillon O, Skurnik, D, Picard, B, Denamur, E. The population genetics of commensal Escherichia coli. *Nature Reviews Microbiology*. 2010;8:207-217.

28. Kaper J, Nataro, JP, Mobley, HLT. PATHOGENIC ESCHERICHIA COLI. *Nature Reviews Microbiology*. 2004;2:123-140.

29. Angus D, Linde-Zwirble, WT, Lidicker, J, Clermont, G, Carcillo, J, Pinsky, MR. Epidemiology of severe sepsis in the United States: analysis of incidence, outcome, and associated costs of care. *Crit Care Med*. 2001;29:1303-1310.

30. Novosad S, Sapiano, MRP, Grigg, C, Lake, J, Robyn, M, Dumyati, G, Felsen, C, Blog, D, Dufort, E, Zansky, S, Wiedeman, K, Avery, L, Dantes, RB, Jernigan, JA, Magill, SS, Fiore, A, Epstein, L. Vital Signs: Epidemiology of Sepsis: Prevalence of Health Care Factors and Opportunities for Prevention. *Morbidity and Mortality Weeksly Report, US Department of Health and Human Services/Centers for Disease Control and Prevention*. 2016;65:864-869.

31. Christopher GW. *Escherichia coli* bacteremia, meningitis, and hemochromatosis. *Arch Intern Med*. 1985;145(10):1908.

32. Sydow M, Crozier, TA, Schauer, A, Burchardi, H. Septic shock with acute abdomen in idiopathic hemochromatosis. *Anasthesiol Intensivmed Notfallmed Schmerzther*. 1993;28(4):258-260.

33. Shander A, Sazama, K. Clinical consequences of iron overload from chronic red blood cell transfusions, its diagnosis, and its management by chelation therapy. *Transfusion*. 2010;50(5):1144-1155.

34. Guida C, Altamura S, Klein FA, et al. A novel inflammatory pathway mediating rapid hepcidin-independent hypoferremia. *Blood*. 2015;125(14):2265-2275.

35. Hider RC, Silva AM, Podinovskaia M, Ma Y. Monitoring the efficiency of iron chelation therapy: the potential of nontransferrin-bound iron. *Ann N Y Acad Sci*. 2010;1202:94-99.

36. Drüeke TB, Parfrey PS. Summary of the KDIGO guideline on anemia and comment: reading between the (guide)line(s). *Kidney International*. 2012;82(9):952-960.

37. Zager R, Johnson, AC, Hanson, SY. Parenteral iron therapy exacerbates experimental sepsis. *Kidney Int*;65(6):2108-2112.

38. Martin P, Tronnet S, Garcie C, Oswald E. Interplay between siderophores and colibactin genotoxin in Escherichia coli. *IUBMB Life*. 2017;69(6):435-441.

39. Myers J, Curtis, BS, Curtis, WR. Improving accuracy of cell and chromophore concentration measurements using optical density. *BMC Biophys*. 2013;6(1):4.

40. Lesbordes-Brion JC, Viatte L, Bennoun M, et al. Targeted disruption of the hepcidin 1 gene results in severe hemochromatosis. *Blood*. 2006;108(4):1402-1405.

41. Esposito B, Breuer, W, Sirankapracha, P, Pootrakul, P, Hershko, C, Cabantchik, ZI. Labile plasma iron in iron overload: redox activity and susceptibility to chelation. *Blood*. 2003;102(7):2670-2677.

CHAPTER 4

Structure-function analysis of ferroportin defines the binding site and an alternative mechanism of action of hepcidin

blood® Regular Article

RED CELLS, IRON, AND ERYTHROPOIESIS

Structure-function analysis of ferroportin defines the binding site and an alternative mechanism of action of hepcidin

Sharraya Aschemeyer,[1,2] Bo Qiao,[2] Deborah Stefanova,[3] Erika V. Valore,[2] Albert C. Sek,[3] T. Alex Ruwe,[4] Kyle R. Vieth,[4] Grace Jung,[2] Carla Casu,[5] Stefano Rivella,[5] Mika Jormakka,[6,7] Bryan Mackenzie,[4] Tomas Ganz,[1,2,8] and Elizabeta Nemeth[2]

[1]Molecular Biology Interdepartmental Doctoral Program, [2]Department of Medicine, and [3]Department of Molecular, Cellular, and Integrative Physiology, David Geffen School of Medicine, University of California, Los Angeles, Los Angeles, CA; [4]Department of Molecular and Cellular Physiology, University of Cincinnati College of Medicine, Cincinnati, OH; [5]Division of Hematology, Department of Pediatrics, Children's Hospital of Philadelphia, Philadelphia, PA; [6]Structural Biology Program, Centenary Institute, and [7]Faculty of Medicine, University of Sydney, Sydney, Australia; and [8]Department of Pathology, David Geffen School of Medicine, University of California, Los Angeles, Los Angeles, CA

KEY POINTS

- **Analysis of mutations causing nonclassical FD defined the hepcidin-binding site in the central cavity of Fpn.**
- **Hepcidin inhibits iron export through Fpn not only by causing Fpn endocytosis, but also by occluding the transporter.**

Nonclassical ferroportin disease (FD) is a form of hereditary hemochromatosis caused by mutations in the iron transporter ferroportin (Fpn), resulting in parenchymal iron overload. Fpn is regulated by the hormone hepcidin, which induces Fpn endocytosis and cellular iron retention. We characterized 11 clinically relevant and 5 nonclinical Fpn mutations using stably transfected, inducible isogenic cell lines. All clinical mutants were functionally resistant to hepcidin as a consequence of either impaired hepcidin binding or impaired hepcidin-dependent ubiquitination despite intact hepcidin binding. Mapping the residues onto 2 computational models of the human Fpn structure indicated that (1) mutations that caused ubiquitination-resistance were positioned at helix-helix interfaces, likely preventing the hepcidin-induced conformational change, (2) hepcidin binding occurred within the central cavity of Fpn, (3) hepcidin interacted with up to 4 helices, and (4) hepcidin binding should occlude Fpn and interfere with iron export independently of endocytosis. We experimentally confirmed hepcidin-mediated occlusion of Fpn in the absence of endocytosis in multiple cellular systems: HEK293 cells expressing an endocytosis-defective Fpn mutant (K8R), *Xenopus* oocytes expressing wild-type or K8R Fpn, and mature human red blood cells. We conclude that nonclassical FD is caused by Fpn mutations that decrease hepcidin binding or hinder conformational changes required for ubiquitination and endocytosis of Fpn. The newly documented ability of hepcidin and its agonists to occlude iron transport may facilitate the development of broadly effective treatments for hereditary iron overload disorders. (*Blood*. 2018;131(8):899-910)

Introduction

Iron homeostasis is maintained by the hepcidin-ferroportin (Fpn) axis, which controls intestinal absorption of iron, as well as internal iron recycling and systemic distribution. Fpn is the only known cellular iron exporter in vertebrates and is the conduit through which iron is delivered into plasma (reviewed in Drakesmith et al[1]). The main tissues expressing Fpn include duodenal enterocytes absorbing dietary iron, hepatic and splenic iron-recycling macrophages, and hepatocytes, which export stored iron when demand is high. Hepcidin is a systemically acting iron-regulatory peptide hormone and the only known natural Fpn ligand. Hepcidin binding to Fpn causes the ubiquitination, endocytosis, and degradation of the ligand-receptor complex, thereby decreasing iron supply to plasma.[2-4] Decreased Fpn activity, usually caused by high hepcidin levels, is manifested as an iron-restriction syndrome. The condition is exemplified by iron-refractory iron deficiency anemia (IRIDA) or anemia of inflammation,[5,6] in which iron accumulates in recycling macrophages and enterocytes, but may become insufficient in other tissues. The other extreme of the spectrum of iron disorders is exemplified by hereditary hemochromatosis or β-thalassemia intermedia.[7,8] In these disorders, Fpn is hyperactive, usually as a result of hepcidin deficiency, and leads to excessive iron absorption and toxic iron deposition in hepatocytes and other parenchymal cells, but relative iron depletion of macrophages. Understanding the mechanism of hepcidin-ferroportin interaction would allow improved targeting of this regulatory axis and development of novel treatments for iron disorders.

To study structural determinants of hepcidin-ferroportin interaction, we focused on Fpn mutations that cause ferroportin disease (FD), a rare, autosomal-dominant iron disorder. Specifically, we focused on nonclassical FD, which is characterized by hyperferritinemia with high transferrin saturation and iron overload

© 2018 by The American Society of Hematology

primarily in hepatocytes, thought to result from Fpn gain-of-function mutations.[9,10] In contrast, classical FD is characterized by hyperferritinemia with normal-to-low transferrin saturation that arises from Fpn mutations that cause decreased iron export (loss-of-function), and iron accumulates primarily in macrophages, which normally export very high amounts of iron after erythrophagocytosis.

We examined the structural and functional characteristics of clinical gain-of-function Fpn mutants associated with both hyperferritinemia and transferrin saturation >60% (Table 1[11-24]). Additional nonclinical mutants were generated to probe the hepcidin-binding region in greater detail.

Our study builds on 2 important technical advances: improved cellular modeling of Fpn mutants and updated structural Fpn data. To avoid the limitations of transiently transfected cells with large variations of Fpn expression between individual cells and mutants,[10,13,14,18,24-29] we established stable, inducible mammalian cell lines expressing wild-type (WT) or mutant Fpn from a defined genomic location, a Flp-In recombination locus. This allowed for a more accurate comparison and quantification of the mutation effects on iron export, Fpn stability, hepcidin binding, and hepcidin-induced Fpn ubiquitination and degradation, steps that were not individually assessed in earlier studies of hepcidin resistance.[10,13,14,18,24-29]

The lack of information about Fpn structure has also hampered understanding of hepcidin-Fpn interaction.[28,30-32] Recently, Taniguchi et al identified the prokaryotic protein, BdFPN, from the bacterium *Bdellovibrio bacteriovorus* as an ortholog of Fpn and obtained its structure by X-ray crystallography.[33] However, hepcidin itself and the hepcidin-binding site within Fpn are found only in vertebrates,[34] so in this context, the BdFPN structure can only serve as a modeling constraint. We therefore used the available structural data from related members of the major facilitator superfamily, including eventually BdFPN, and incorporated the experimental results from the Fpn mutant analysis to develop a new model of hepcidin-Fpn interaction, which segregates the Fpn residues important for hepcidin-induced conformational change from those critical for hepcidin binding. As predicted by the model, we also experimentally demonstrated that hepcidin can function by occluding Fpn and preventing iron export even in the absence of endocytosis.

Materials and methods

Site-directed mutagenesis

Human Fpn-GFP in the pGFP-N3 vector[27] was transferred into the pcDNA5/FRT/TO vector (Invitrogen). Single mutations were introduced using the QuikChange Lightning Site-Directed Mutagenesis Kit (Agilent Technologies) and confirmed by sequencing. Mutagenesis primers are listed in supplemental Table 1 (available on the *Blood* Web site).

Stably transfected inducible cell lines

All mutant human Fpn-GFP pcDNA5/FRT/TO vector constructs were verified by sequencing. Using the Flp-In T-Rex system (Invitrogen K5600-01), HEK293T cells were transfected with the pcDNA5/FRT/TO vector encoding WT or mutant Fpn and pOG44 vector. Stable cell lines were established according to the manufacturer's protocol. Doxycycline (dox) was used to induce expression of Fpn-GFP.

The characterization of these cell lines, including Fpn microscopy, Fpn cell surface localization, iron export as assessed by ferritin assay or radiolabeled iron export, hepcidin binding to Fpn, hepcidin-dependent ubiquitination of Fpn, Fpn stability, and hepcidin-dependent degradation of Fpn by western blotting, is described in the supplemental Methods.

Computational modeling

Structural models of human Fpn (hFpn) were generated using I-TASSER Iterative Threading ASSEmbly Refinement).[35,36] This server predicted the protein structure and function of hFpn by threading hFpn onto program-selected crystal structures of other members of the major facilitator superfamily (Protein Data Bank entries: 4IKV, 3WDO, 4AV3, and 4M64), either not including (Figure 2) or including (supplemental Figure 7) the BdFPN crystal structure (Protein Data Bank entry: 5AYM) as a template. The models without and with the BdFPN template were generated respectively on 18 June 2015 and 20 January 2016.

Functional expression of hFpn in *Xenopus* oocytes

The pOX(+) oocyte expression plasmid vectors containing human WT or K8R Fpn-GFP were used to synthesize RNA in vitro. RNA-injected *Xenopus* oocytes were incubated for 4 to 5 days before being used in functional assays. Oocytes were treated for 0 to 4 hours with 10 μM hepcidin before assaying iron efflux. Oocytes were injected with 50 nL of 5 μM ^{55}Fe, added as $FeCl_3$ (Perkin-Elmer Life Science Products). The first-order rate constants (k) describing iron efflux >30 minutes was determined,[37] and live-cell imaging of Fpn-GFP performed as described.[37]

Treatment of human red blood cells with hepcidin and hepcidin agonists

Human packed red blood cells (PRBCs) were obtained from the University of California, Los Angeles Department of Pathology and Laboratory Medicine. PRBC aliquots from 4 different donors were incubated in their citrate-phosphate-dextrose-adenine (CPDA-1) storage medium at 37°C for 24 hours in the presence of hepcidin (0.4 and 3.6 μM), PR73 (0.4 and 3.6 μM), or solvent. Samples were collected after 24 hours by centrifuging the PRBC at 5000 *g* for 8 minutes to obtain cell pellets. The supernatant was centrifuged again, and non–transferrin-bound iron (NTBI) was measured using enhanced labile plasma iron assay, as previously described.[38] For protein isolation, cell pellets were lysed, and membranes were pelleted and lysed in RIPA buffer. After electrophoresis and transfer, western blotting was performed using anti-ferroportin antibody (human anti-human ferroportin 38C8, Amgen) and developed with SuperSignal West Pico Chemiluminescent Substrate (Thermo Scientific).

Mouse treatment with hepcidin agonists

C57BL/6 mice were injected intraperitoneally with PR73 (2 60-nmol doses, 12 hours apart) or solvent, and analyzed 4 hours after the second injection. Th3 mice were injected subcutaneously with 50 nmol minihepcidin M009[39] and were analyzed over a time course of 0 to 36 hours after injection. We measured serum iron using a colorimetric assay, duodenal and splenic Fpn levels by western blotting, and serum hepcidin by enzyme-linked immunosorbent assay.

Additional details and methods can be found in the supplemental Methods and supplemental Figures 1-14.

Table 1. Nonclassical FD mutations

Mutant	Serum ferritin, μg/L	Transferrin saturation, %	Examples of pathological findings	References	Adult patients, n
WT	15-200 F 40-300 M	15-45 both M and F		11	
C326Y*	481-552F 4232-4326 M	94-80 F 96-100 M		11	2 F, 2 M
C326S*	Elevated	Elevated	Cirrhosis and arthritis	12	1 M†
Y501C*	43-199 F 568-642 M	35-64 F 94-104 M	Asthenia, arthralgia, and hepatomegaly	13	2 F, 2 M
D504N*	1514-1605 M	89-102 M	Hepatomegaly	14	2 M
N144D*	7500 F 10 510 M	99 M	Iron loading in hepatocytes and BDECs, cirrhosis	15	1 F, 1 M
V72F*	27-174 F 195-1091 M	31-35 F 53-81 M	Iron loading primarily in hepatocytes, but also in Kupffer cells, BDECs, and PTMs, fibrosis, and hepatic steatosis	16	2 F, 3 M
Y64N‡	176-513 F 647-2,812 M	47-86 F 91-98 M	Iron loading in Kupffer cells and hepatocytes, fatigue and tremors	17	3 F, 5 M
H507R‡	233 F 785-3751 M	46 F 93-100 M	Iron loading in hepatocytes, mild steatosis, and siderosis	18, 19	1 F, 3 M
S71F‡	5500	70	Uncharacterized	20	1§
G204S‡	4-5236 F 508-3755M	2-100 F 27-91 M	Mixed iron loading, but mainly hepatocytes heterogeneous phenotype	20, 21	3 F, 5 M
D270V‡	<1000 F 353-559 M‖	78 F 37-41 M‖	Fatigue, fibrosis, iron loading in hepatocytes and Kupffer cells, hepatitis C	22, 23	1 F, 1 M
S338R‡	1990 M	90 M	Iron loading in hepatocytes, Kupffer cells, and PTMs, mild steatosis	24	1 M

Based on the literature, the 12 Fpn mutations listed in the table are associated with elevated serum ferritin and transferrin saturation, although not every subject carrying the mutation had abnormal biochemical parameters or related pathology. Adult = ≥18 years.

BDEC, bile duct epithelial cell; F, female; M, male PTM, portal tract macrophage.

*Mutants in which hepcidin binding is impaired based on the results of our study; of these, C326Y, C326S, Y501C, D504N, and N144D were more severely impaired.

†Six descendants aged 8 to 16 had transferrin saturation 84-97%.

‡Mutants in which hepcidin binding is normal, but hepcidin-mediated ubiquitination is impaired based on the results of our study; of these, Y64N and H507R were most severely impaired, followed by S71F and G204S.

§Source did not cite sex.

‖The patient's parameters were recorded at 2 different times.

Results

Fpn-GFP mutants localize to cell membrane and export iron

We first examined whether the gain-of-function Fpn mutants (Table 1) were expressed on the cell membrane and exported iron. Mutants were visualized by microscopy to assess membrane localization. Green fluorescence was visible on the cell membrane for all mutants (supplemental Figure 1). To quantify the amount of Fpn present on the cell surface compared with the total Fpn amount, we performed cell-surface, thiol-specific biotinylation targeting the Fpn C326 residue. All mutants were expressed on the cell surface similarly to WT (quantitation shown in Figure 1A, representative western blots in supplemental Figure 2). As expected, C326S mutant showed essentially no biotinylation, confirming the specificity of the method. We next assessed the iron-exporting function of the mutants by measuring intracellular ferritin as an index of remaining cellular iron stores. All mutants exported iron as indicated by decreased intracellular ferritin concentration after induction of Fpn-GFP expression with dox, compared with cells not induced with dox (Figure 1B).

Gain-of-function Fpn-GFP mutants display hepcidin resistance because of either impaired hepcidin binding or altered hepcidin-induced conformational change of Fpn with consequently decreased hepcidin-induced ubiquitination

Resistance of Fpn mutants to downregulation by hepcidin is thought be an essential component of nonclassical FD pathogenesis and manifests as continued cellular iron export despite exposure to hepcidin concentrations that cause iron retention in cells expressing WT Fpn. We therefore measured intracellular ferritin as an indicator of iron retention in cells treated with or without hepcidin for 24 hours and observed by microscopy the localization of Fpn after 24 hours. Finally, we quantified the stability of WT and mutant Fpn over 24 hours by western blotting, as well as Fpn degradation after treatment with hepcidin for

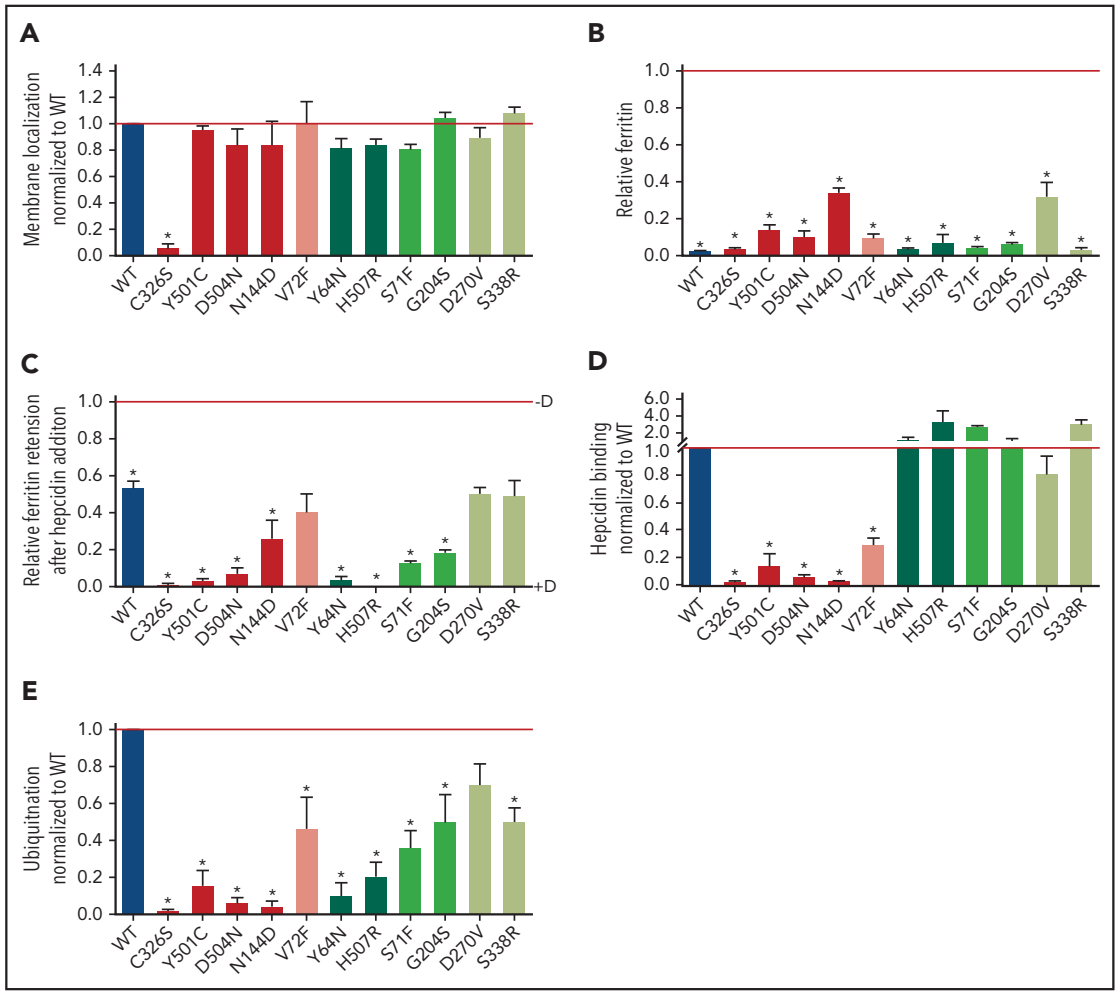


Figure 1. Fpn mutants have either impaired hepcidin binding or intact hepcidin binding but impaired hepcidin-dependent ubiquitination, leading to varying hepcidin resistance. (A) HEK293T cells stably transfected with hFpn-GFP mutants or WT were induced with dox (+D) to express Fpn, surface-thiol biotinylated for 30 minutes, immunoprecipitated with anti-GFP antibody (Ab), and immunoblotted with streptavidin-HRP or anti-GFP Ab. Band intensity was normalized to total GFP and then further normalized to WT Fpn on each blot. Because mutant data within each western blot were normalized to the WT sample on the same blot, the WT value is always 1 and is without error bars. WT is included in the graph only for visual reference. (B) hFpn-GFP mutants were induced overnight with dox and then incubated for 24 hours in the presence of 25 μM ferric ammonium citrate (FAC). The intracellular ferritin concentration was normalized to the total protein concentration. Ferritin was normalized to the uninduced sample (−D) for each cell line (uninduced = 1). Data shown are means ± standard errors of the means of 3 to 5 independent experiments. For statistical analysis, the 2-tailed 1-sample Student *t* test (normally distributed data) or the 2-tailed 1-sample signed rank test (data with nonnormal distribution) was used with 1 as the comparison. The false discovery rate (FDR) procedure was used to determine significance (*significant). (C) Expression of WT and mutant hFpn-GFP was induced overnight or not, and cells were then incubated for 24 hours with 25 μM FAC ± 1 μg/ml (0.4 μM) hepcidin. The intracellular ferritin concentration was normalized to the total protein concentration and expressed relative to uninduced cells (ie, maximal ferritin levels for each mutant, −dox). (D) HEK293T cells expressing WT and mutant hFpn-GFP were treated with N-terminally biotinylated hepcidin for 30 minutes, immunoprecipitated with anti-GFP Ab, run under nonreducing conditions, and immunoblotted with streptavidin-HRP or anti-GFP Abs. The streptavidin signal was first normalized to total GFP, and then mutant hepcidin binding values were expressed as a fraction of hepcidin binding to WT Fpn. Because mutant data within each western blot were normalized to the WT sample on the same blot, the WT value is always 1 and is without error bars. WT is included in the graph only for visual reference. (E) Fpn-GFP WT and mutants were treated with hepcidin for 30 minutes, immunoprecipitated with anti-GFP Ab, and immunoblotted with anti–poly-/monoubiquitin (FK2) Ab or anti-GFP Ab. The ubiquitination signal was first normalized to the GFP signal, and then the mutant ubiquitination was expressed as a fraction of WT Fpn ubiquitination. As in panel B, WT is included only for visual reference. For statistical analysis in panels B and C, the 2-tailed 1-sample Student *t* test was used wtih 1 as the comparison, and for panel A, the 2-tailed Student *t* test (normally distributed data) or the Mann-Whitney rank sum test (data with nonnormal distribution) was used with WT as the comparison. After the *P* values were obtained, the FDR procedure was used to determine significance (*significant). Data shown are means ± standard errors of the means of 3 to 6 independent experiments. Hepcidin-binding mutants are denoted by red shades and ubiquitination mutants by green shades. Severely impaired mutants are denoted by bolder colors. Severe impairment was defined as ≤25% of WT values based on assessing the values from panels C-E for mutants with impaired hepcidin binding and panels C and E for impaired hepcidin-induced conformational change mutants. Also, for panels A-E, red and dark green indicate severe mutations, medium green indicates mild mutation, and pink and light green indicates borderline mutations.

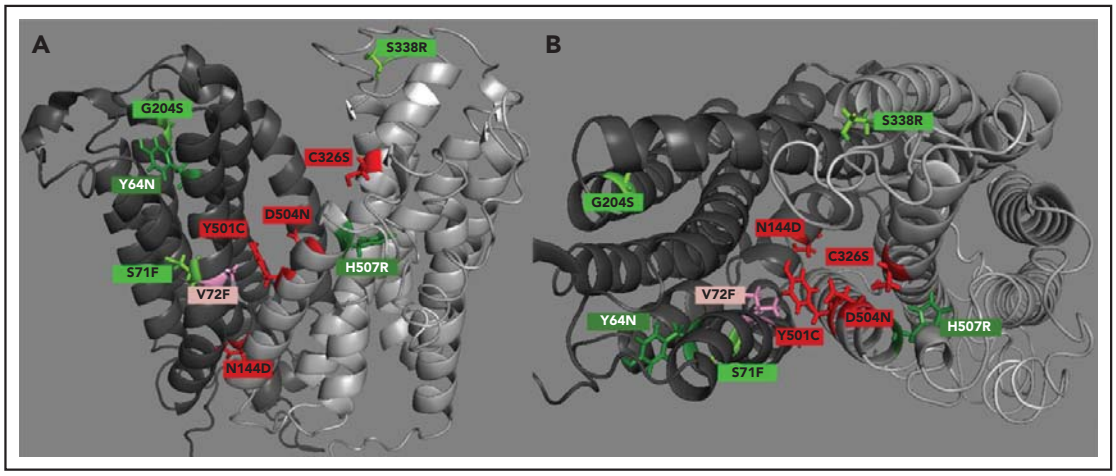


Figure 2. hFpn structure depicting clinically relevant mutant residues. (A) A side view of hFpn in its outward-facing state, with the N-terminus on the left and C-terminus on the right. (B) A top-down view of hFpn in its outward-facing state. D270V is not modeled because it is located in the unstructured intracellular loop of Fpn. The red/pink color denotes mutants with impaired hepcidin binding, and the green color denotes mutants with intact hepcidin binding, but variably impaired hepcidin-dependent ubiquitination. For simplicity, the mild and borderline mutants are labeled with the same light color.

24 hours. All clinical mutants, with the exception of V72F, D270V, and S338R, were functionally hepcidin resistant compared with WT as demonstrated by lower ferritin retention after hepcidin treatment (Figure 1C), and less Fpn-GFP degradation as assessed by both microscopy (supplemental Figure 1) and western blotting compared with WT (supplemental Figure 3A, representative blots and supplemental Figure 3B, quantitation). To detect milder resistance, we exposed V72F and D270V mutants to a lower hepcidin concentration for a shorter time and measured iron export using radioactive iron release for ≤10 hours. V72F and D270V indeed displayed mild hepcidin resistance compared with WT Fpn (supplemental Figure 4; S71F and C326S mutants were added as controls manifesting strong resistance). We also examined S338R using the radioactive iron export assay, but with higher hepcidin concentrations (supplemental Figure 4), and also observed mild, but significant resistance to hepcidin (with N144D and C326S serving as controls for medium-to-strong resistance).

Of note, several mutants (Y64N, H507R, D270V and S338R) had decreased stability at 24 hours compared with WT (supplemental Figure 3A,C), which could partially counteract hepcidin resistance in vivo, and modulate the patient phenotype.

Two potential mechanisms can explain the hepcidin-resistant phenotype of the clinical Fpn mutants as shown in Figure 1C: (1) decreased hepcidin binding to Fpn, or (2) decreased hepcidin-induced endocytosis of Fpn despite intact hepcidin binding. To determine if the Fpn-GFP mutants bind hepcidin, we treated mutant cell lines with biotinylated hepcidin for 30 minutes, immunoprecipitated Fpn with anti-GFP antibody, and detected bound hepcidin by immunoblotting with streptavidin-horseradish peroxidase (HRP), taking advantage of the stability of the hepcidin-ferroportin complex in nonreducing sodium dodecyl sulfate-polyacrylamide gel electrophoresis.[2,40] We identified 5 mutants that showed impaired hepcidin binding compared with WT (quantitation shown in Figure 1D and representative western blots in supplemental Figure 5): C326S, Y501C, D504N, N144D and V72F.

After hepcidin binding to Fpn, ubiquitination of several cytoplasmic lysines is required for endocytosis of Fpn.[3] To assess hepcidin-induced ubiquitination, we treated Fpn-GFP mutants with hepcidin, immunoprecipitated with anti-GFP antibody, and probed for ubiquitin with an antibody that recognizes both poly- and monoubiquitinated proteins. We identified 6 mutants that had normal hepcidin binding, but variably deficient hepcidin-induced ubiquitination: Y64N and H507R showed severe impairment in ubiquitination, and S71F, G204S, D270V, and S338R were less impaired (quantitation shown in Figure 1E and representative western blots in Figure S6).

The results shown in Figure 1D-E (hepcidin binding and Fpn ubiquitination, respectively) were used as the basis for color assignment in additional figures in this manuscript (Figure 2, supplemental Figures 3, 7, and 10): red/pink indicates mutants with impaired hepcidin binding, and light/dark green indicates mutants that bind hepcidin normally but have variably impaired ubiquitination. The intensity of the color denotes the severity of the impairment, where bold colors indicate severe impairment, lighter colors indicate mild impairment, and the lightest colors (V72F, D270V, and S338R) indicate borderline impairment.

Fpn-GFP mutants map out a hepcidin-binding site in the central cavity and reveal peripheral hindrance of conformation-dependent ubiquitination

We next mapped the mutations causing impaired hepcidin binding (C326S, Y501C, D504N, N144D, and V72F) or impaired hepcidin-dependent ubiquitination (Y64N, H507R, S71F, G204S, D270V, and S338R) onto a computational structural model of hFpn (Figure 2). All the mutations that decreased hepcidin binding localized within the main cavity of Fpn, implicating 4 helices in the hepcidin-binding site (helices 2, 4, 7, and 11). All of the mutations causing impaired Fpn ubiquitination localized to the periphery of Fpn at the helix-helix interfaces, suggesting that these substitutions interfere with appropriate conformational change after hepcidin binding. A second computational model (supplemental

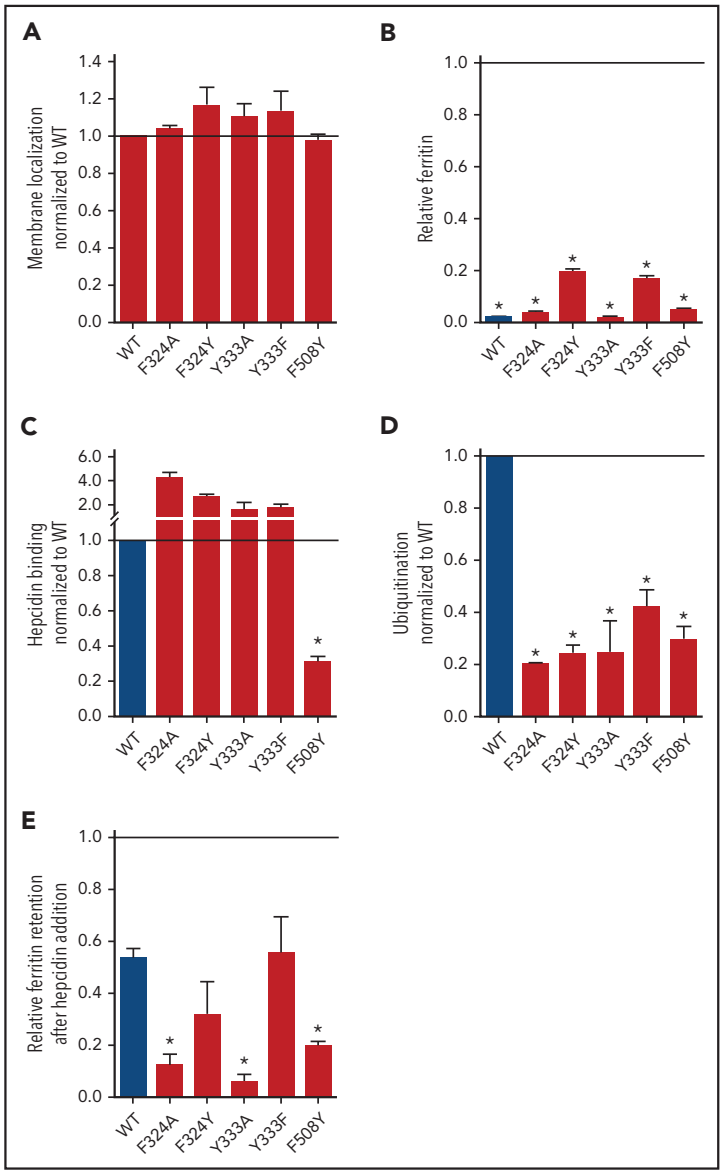


Figure 3. Analysis of nonclinical hFpn-GFP mutants. Cells expressing inducible nonclinical Fpn mutants were analyzed with the same approaches as those expressing clinical mutants. (A) All mutants were displayed on the cell membrane. Membrane localization was determined as in Figure 1A. (B) All mutants exported iron. Ferritin was determined as in Figure 1B by normalizing it to the uninduced (−dox) condition for each cell line (thus, uninduced ferritin levels = 1). (C) Hepcidin binding was determined as in Figure 1D. (D) Ubiquitination was determined as in Figure 1E. (E) Relative ferritin retention after hepcidin addition was determined as in Figure 1C. Data shown are means ± standard errors of the means of 3 to 6 independent experiments. For statistical analysis the 2-tailed 1-sample Student *t* test was used with 1 as the comparison for panels A-D, and the 2-tailed Student *t* test (normally distributed data) or the Mann-Whitney rank sum test (data with nonnormal distribution) was used with WT as the comparison for panel E. After the *P* values were obtained, the FDR procedure was used to determine significance (*significant).

Figure 7A-D), which included the crystal structure of BdFPN in the modeling, led to the same conclusion.

To refine the model of hepcidin binding to Fpn, we generated additional nonclinical mutations within helices 7 and 11 (supplemental Figure 7E) because our data suggest that these helices contribute most strongly to hepcidin binding. We tested F324A, F324Y, Y333A, Y333F, and F508Y with the same assays as clinical mutants, which showed that all were displayed on the membrane and exported iron (Figure 3A-B). Only F508Y exhibited impaired hepcidin binding, whereas the other mutants had impaired ubiquitination compared with the WT (Figure 3C-D). Ferritin retention as a marker of functional resistance to hepcidin showed that F508Y was strongly resistant despite its conservative amino acid substitution (Figure 3E; supplemental Figure 8), whereas for other residues, nonconservative substitutions (F324A and Y333A) were required for significant resistance (Figure 3E). Interestingly, even though F508Y bound hepcidin very poorly and failed to retain intracellular ferritin or radiolabeled iron, it was mostly degraded by 24 hours (supplemental Figure 9A-B), suggesting delayed internalization and degradation. The only unstable nonclinical mutant was F324A (supplemental Figure 9C), a ubiquitination-impaired mutant. Mapping the 5 nonclinical Fpn-GFP mutants onto our computational hFpn model (supplemental Figures 7 and 1) indicates that the deduced hepcidin-binding site may include F508. The model

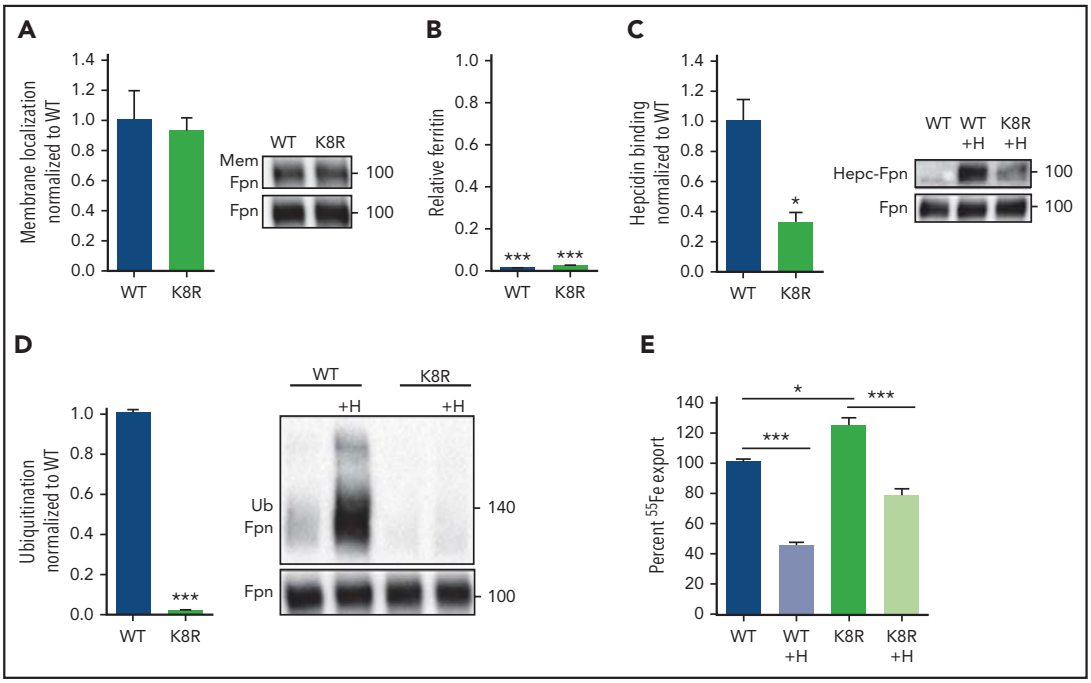


Figure 4. Iron export by the K8R mutant is inhibited by hepcidin despite the absence of ligand-induced ubiquitination. (A) Cells were treated as in Figure 1A. K8R localized to the cell membrane similarly to WT. (B) Cells were treated as in Figure 1B. K8R exported iron and decreased ferritin similarly to WT. For statistical analysis, the 1-sample Student *t* test with 1 as the comparison (normally distributed data) or the 1-sample signed rank test (data with nonnormal distribution) was used. (C) HEK293T cells expressing WT and mutant Fpn-GFP were treated with N-terminally biotinylated hepcidin for 30 minutes, immunoprecipitated with anti-GFP Ab, run under nonreducing conditions, and immunoblotted with streptavidin-HRP or anti-GFP Abs. Hepcidin bound less to K8R compared with WT. (D) Cells were treated as in Figure 1E. The K8R mutant was not ubiquitinated after hepcidin addition. For the statistical analysis in panels A, C, and D, the 2-tailed Student *t* test was used with WT as the comparison. (E) Cells were loaded with 2 mM ^{55}Fe-NTA for 48 hours, washed, replated, induced overnight, washed again, and then ±3 μg/ml hepcidin was added. Extracellular radioactivity was measured at 0, 2, 4, and 8 hours. The "uninduced" measurement at each time point was subtracted as background, and the slope for each sample was determined and used to calculate the percentage of iron export by normalizing the slopes to the untreated WT. For the statistical analysis in panel E, the 2-tailed Student *t* test (normally distributed data) and Mann-Whitney rank sum test (data with nonnormal distribution) were used with WT as the comparison. Data shown are means ± standard errors of the means of 3 to 4 biological replicates. ***$P < .001$; **$P < .01$; *$P < .05$. Hepc-Fpn, hepcidin complexed with Fpn; Mem, membrane.

also highlights the role of peripheral Fpn mutations in impeding ubiquitination and thereby causing variable resistance to hepcidin-induced Fpn endocytosis and degradation.

Characterization of K8R Fpn mutant and evidence of its occlusion by hepcidin and minihepcidin

Our structural Fpn model implies that hepcidin binding deep in the Fpn central cavity should impede iron export, even if hepcidin-induced endocytosis of Fpn is disabled. To test this, we designed an Fpn variant deficient in ligand-induced endocytosis through mutations that disable ubiquitination, but have a minimal effect on the intramembrane domains of Fpn. The cytoplasmic loop that connects the two 6-helix bundle lobes of Fpn contains lysines that undergo hepcidin-dependent ubiquitination,[3] so we generated a cell line stably expressing inducible K8R Fpn-GFP, in which 8 lysines of the loop were mutated to arginines (supplemental Figure 7E). K8R localized on the cell membrane (Figure 4A), exported iron similarly to WT as measured by the loss of intracellular ferritin after Fpn induction (Figure 4B), and bound hepcidin, though at about 30% of WT Fpn binding (Figure 4C). K8R had severely impaired hepcidin-induced ubiquitination as expected (Figure 4D), even at very high hepcidin concentrations (supplemental Figure 11).

Despite the complete loss of hepcidin-dependent ubiquitination, K8R ^{55}Fe export was still decreased by hepcidin treatment (Figure 4E). We compared ferritin retention and Fpn degradation in WT, C326S (a mutant that cannot bind hepcidin), and K8R in response to a range of hepcidin concentrations. After hepcidin addition, K8R Fpn retained ferritin in a dose-dependent manner, and higher hepcidin concentrations achieved maximal iron retention comparable with WT (Figure 5A). The C326S mutant was resistant to hepcidin-induced iron retention. The profound block of iron export through K8R was achieved despite impaired Fpn degradation, as determined by western blotting (Figure 5B), and despite the lack of degradation or punctate structures characteristic of endocytosis, as shown by microscopy (Figure 5C). PR73,[41] a minihepcidin that was engineered to bind to Fpn more strongly than hepcidin, was 10 times more potent than hepcidin in inducing ferritin retention without endocytic degradation of K8R Fpn (supplemental Figure 12).

We next tested whether hepcidin-mediated occlusion occurs in those clinical Fpn mutants that bind hepcidin strongly, but have impaired ubiquitination (Y64N and H507R). However, unlike in K8R Fpn, we could not dissociate occlusion from internalization in these mutants: Fpn-GFP underwent

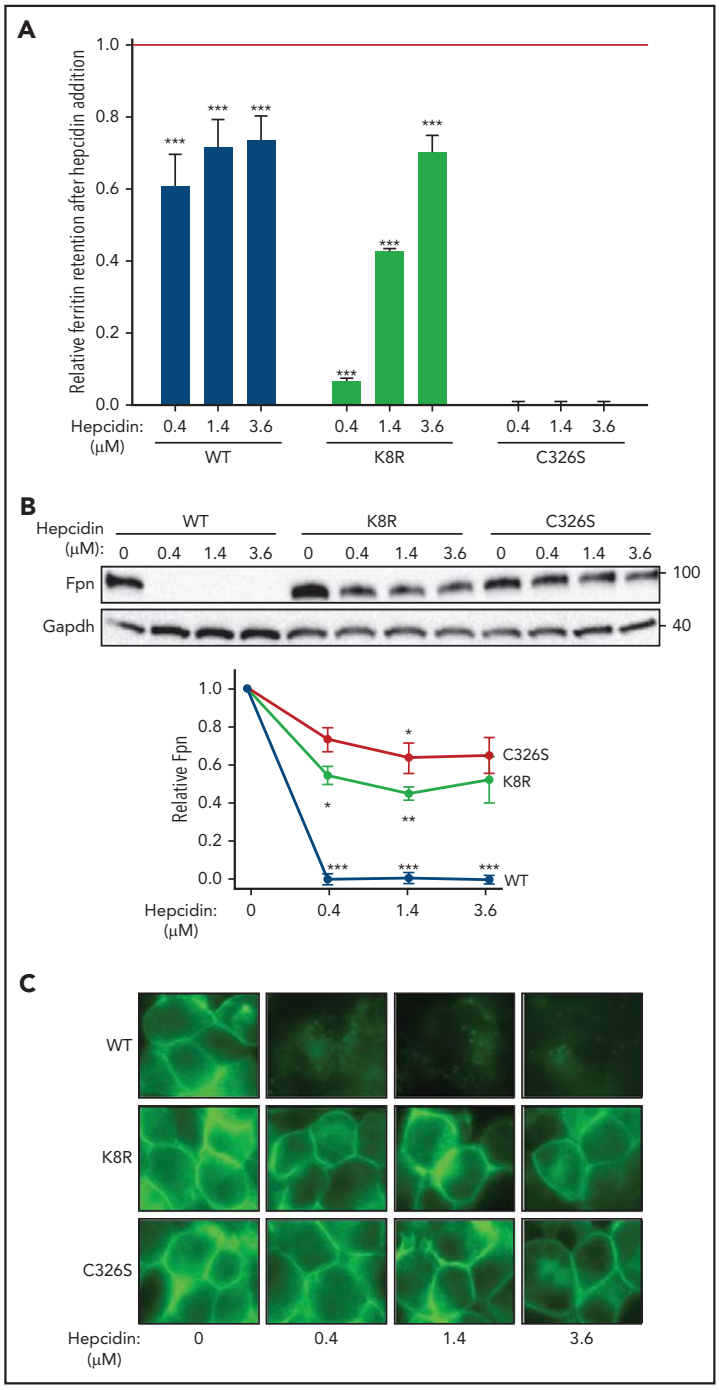


Figure 5. Evidence for Fpn occlusion by hepcidin. Cells expressing inducible nonubiquitinating K8R mutant were compared with those expressing WT Fpn or C326S mutant, which does not bind hepcidin. (A) Ferritin retention after hepcidin addition was determined as in Figure 1C. For the statistical analysis the 2-tailed Student *t* test was used with the respective untreated control for comparison. ***$P < .001$; **$P < .01$; *$P < .05$. (B) Lysates from panel A were analyzed by western blotting. Top: representative western blot. Bottom: densitometry of triplicate western blots. The Fpn signal was first normalized to glyceraldehyde-3-phosphate dehydrogenase, then expressed as a fraction of its respective untreated control (no hepcidin treatment). For the statistical analysis, the 2-tailed 1-sample Student *t* test was used with 1 as the comparison. ***$P < .001$; **$P < .01$; *$P < .05$. C) Microscopy of live cells from panel A after 24 hours (original magnification ×40). Data shown are the mean ± standard errors of the mean of 3 independent experiments.

endocytosis and degradation when treated with high concentrations of hepcidin (supplemental Figure 13A) or mini-hepcidin (supplemental Figure 13B-C). Although it remains to be explained why these clinical nonubiquitinating mutants are less severe than the K8R mutant, the finding has important implications because it suggests that patients carrying these mutations may benefit from treatment with pharmacological doses of hepcidin.

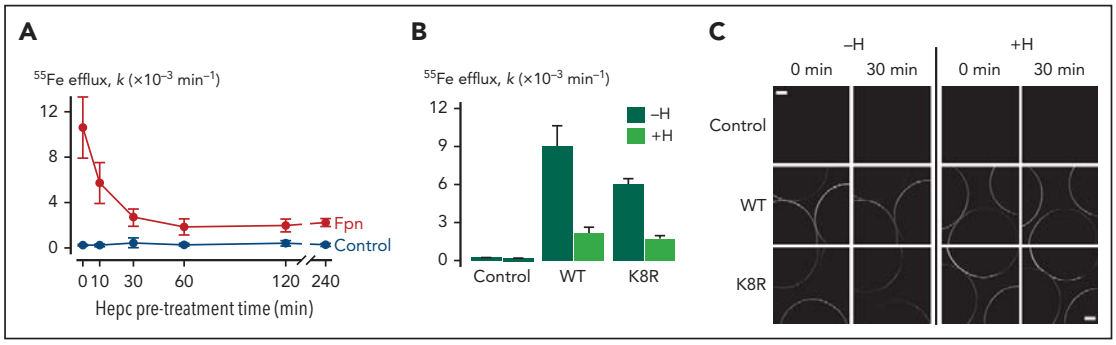


Figure 6. Effect of hepcidin on WT and mutant Fpn expressed in *Xenopus* oocytes. (A) First-order rate constants (k) describing ^{55}Fe efflux (assayed over 30 minutes) from control oocytes (gray) and oocytes expressing WT Fpn (black) pretreated with 10 μM hepcidin for 0 to 240 minutes (n = 8-12 per group). Two-way analysis of variance (ANOVA) revealed an interaction ($P < .001$); within Fpn, the 0- and 10-minute time points differed from all other time points ($P < .001$), and the 30- to 240-minute time points did not differ from one another ($P \geq .35$). (B) ^{55}Fe efflux in control oocytes and oocytes expressing WT or K8R Fpn that were untreated (−H) or pretreated for 30 minutes with 10 μM hepcidin (+H) (n = 9-12 per group). Two-way ANOVA revealed an interaction ($P < .001$). Percent inhibition of ^{55}Fe efflux by hepcidin did not differ between WT (76% ± 6%) and K8R (71% ± 3%) (means ± standard errors of the means) ($P = .47$). (C) Live-cell imaging of control oocytes and oocytes expressing WT or K8R Fpn before and after 30 minutes of treatment without hepcidin (−H) or with 10 μM hepcidin (+H) in the same oocyte preparation as used in panel B. Each frame captures portions of 3 oocytes, and the image plane approximately bisects the oocytes. Scale bars, 0.2 mm. Two-way ANOVA of the change in fluorescence intensity (ΔF) over time revealed a greater loss of fluorescence in untreated oocytes (−H) compared with hepcidin-treated (+H) ($P = .005$) and that ΔF did not differ between WT and K8R ($P = .75$).

Hepcidin occludes both WT and K8R Fpn in *Xenopus* oocytes

To further confirm that hepcidin can inhibit iron export without causing Fpn endocytosis but by occluding Fpn, we used *Xenopus* oocytes expressing WT or K8R Fpn-GFP. Oocytes expressing WT Fpn-GFP were pretreated with hepcidin for up to 4 hours to determine the time course of the hepcidin effect on iron export. In contrast to mammalian cells, in which hepcidin treatment results in a progressively greater inhibition of iron export for ≤10 hours, maximal inhibition of iron export in oocytes was observed after only 30 minutes of pretreatment (Figure 6A). We found that 30 minutes of hepcidin treatment inhibited ^{55}Fe efflux from oocytes expressing K8R Fpn to the same degree as it did for WT Fpn (Figure 6B). Live imaging of oocytes revealed that the 30-minute hepcidin treatment did not induce endocytosis of either WT or K8R Fpn (Figure 6C). Whereas some reduction in the intensity of GFP fluorescence at the oocyte perimeter was observed in WT and K8R oocytes over time (presumably due to photobleaching), hepcidin did not stimulate a loss of fluorescence from the oocyte perimeter either for WT or K8R. These data reveal that hepcidin can directly inhibit Fpn-mediated iron transport activity independently of Fpn internalization not only in the K8R mutant but also in WT Fpn.

Hepcidin occludes endogenous Fpn in mature red blood cells

In vivo, occlusion by hepcidin may be the critical mechanism of regulation of iron efflux in Fpn-expressing cells that lack endocytic machinery, such as mature red blood cells (RBCs).[42] To test this, we treated PRBCs ex vivo in a transferrin-free medium with hepcidin or minihepcidin for 24 hours. Although Fpn was not degraded even with high concentrations (3.6 μM) of hepcidin or PR73, iron export was dose-dependently decreased, as evidenced by the lower concentration of NTBI in the medium (Figure 7), confirming that hepcidin-mediated occlusion modulates iron export by endogenous Fpn in RBCs.

How much occlusion contributes to the regulation of iron fluxes in vivo is difficult to determine in the absence of a mouse model expressing a nonendocytosing Fpn. Because injection of synthetic full-length hepcidin in mice was previously shown to cause ferroportin degradation in the spleen and duodenum,[43-46] we probed for the presence of occlusion in vivo by injecting mice with minihepcidins, because these peptides occlude Fpn more efficiently than does native hepcidin. Minihepcidins were injected into WT or thalassemic mice, and serum iron and Fpn levels were assessed. Treatment of WT mice with 2 60-nmol injections of PR73 over 16 hours resulted in a dramatic decrease in serum iron (supplemental Figure 14A), however, no decrease in Fpn protein levels in the duodenum or the spleen were observed (supplemental Figure 14B-E). Likewise, a single injection of another minihepcidin, M009,[39] did not decrease spleen Fpn levels at 6, 12, 24, or 36 hours postinjection (supplemental Figure 14F), but caused a prolonged decrease of serum iron (supplemental Figure 14G). Transient suppression of endogenous hepcidin production was also observed in response to hypoferremia (supplemental Figure 14H). Thus, in the absence of detectable Fpn degradation, the profound effect of hepcidin agonists on serum iron was consistent with the mechanism of occlusion in both mouse models. Interestingly, in contrast to the lack of Fpn degradation in vivo, minihepcidins readily caused Fpn degradation in vitro (supplemental Figure 12B-C). The reasons for this differential effect of minihepcidins on Fpn endocytosis are not clear. It is possible that Fpn glycosylation and/or Fpn-interacting proteins differ between in vitro cellular models and tissues in vivo, which may differentially affect minihepcidin binding to Fpn, Fpn conformational change, and its endocytosis. The data suggest that serum iron rather than Fpn levels should be used as a more accurate measure of the activity of hepcidin and its agonists.

Discussion

In this study, we characterized the mechanisms by which known clinical Fpn mutations (Table 1) cause nonclassical FD and extended these findings to gain insight into the structural basis of

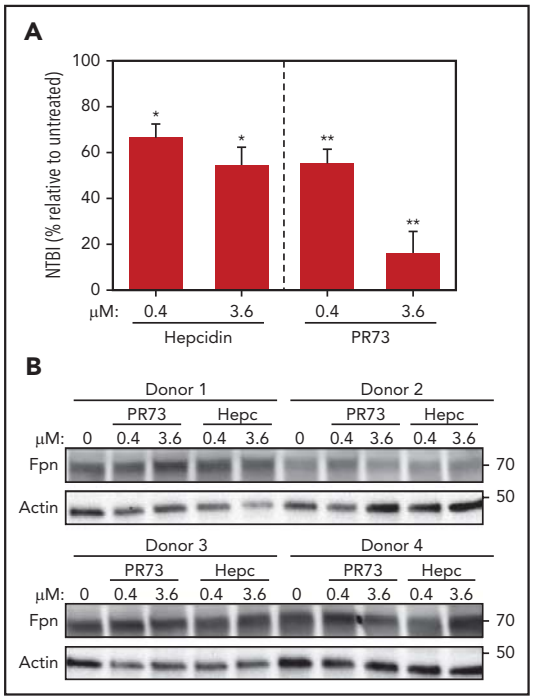


Figure 7. Hepcidin blocks iron export from human RBCs without degrading Fpn. Human PRBCs from 4 different donors were treated with hepcidin or PR73 for 24 hours at 37°C. (A) Iron export from PRBCs was assessed by measuring NTBI in the medium. For the statistical analysis, the 2-tailed 1-sample Student *t* test was used with 100% as the comparison. (B) Western blotting of Fpn and actin levels in PBRCs.

Fpn function and its regulation by hepcidin. Our cellular models revealed that nonclassical FD mutations cause resistance to hepcidin either by impairing the binding of hepcidin to Fpn or by altering hepcidin-induced conformational change and thereby impairing the ubiquitination required for endocytosis. Although all of the mutations were associated with a clinical phenotype of nonclassical FD, the mutants varied considerably in their degree of hepcidin resistance. In particular, V72F, D270V, and S338R showed only very mild hepcidin resistance in our cellular model, suggesting that additional factors may modify the phenotype of FD caused by these mutations. One such factor could be the decreased stability of some mutants, including Y64N, H507R, D270V, and S338R (supplemental Figure 3A,C). Such instability could decrease Fpn cell surface expression and iron export at baseline, perhaps accounting for the frequent reports of a mixed form of FD (Table 1) manifesting restriction of iron export leading to iron accumulation in Kupffer cells with simultaneous resistance to hepcidin leading to systemic and hepatic iron overload. The structural model also suggests that D270V and S338R may be mild because of their peripheral position on the Fpn structure: S338R is predicted to be located on an extracellular loop rather than at a helix-helix interface, and D270V in the long intracellular loop, where it may act by interfering with ubiquitination of a nearby lysine residue. Lastly, important modifiers that affect disease severity include sex, age, and comorbidities, such as alcohol abuse, obesity, and metabolic syndrome, which are all known to affect the iron status of patients with FD.[20,47] Although our cellular model faithfully documents profound hepcidin resistance in the more severe mutations, it lacks the complex cellular and systemic regulatory factors that could amplify the effects of the weakest mutations.

Our structural models indicate that hepcidin binding occurs within the main cavity of Fpn, where hepcidin interacts with as many as 4 different helices. Additionally, we conclude that peripheral amino acids, positioned at helix-helix interfaces, influence the hepcidin-induced conformational change that leads to the ubiquitination of Fpn. They may even affect Fpn conformation in the absence of hepcidin, which explains how some of the ubiquitination-impaired mutants (Y64N, H507R, D270V, S338R, and F324A), but none of the hepcidin binding-impaired mutants, are unstable. Although the alternative structure generated by adding BdFPN to the threading set displayed small differences from our earlier model (supplemental Figure 7), it did not alter the conclusions of our analysis.

Using the model as a guide to design informative nonclinical mutants, we examined F508Y, the nearest residue that could contribute to the binding site based on its location on helix 11 immediately above Y501 and D504. F508Y was a milder hepcidin-resistant mutant than Y501C and D504N, likely because the amino acid substitution we chose was very conservative. We previously showed that hepcidin binding to Fpn involves a disulfide-thiol interaction between hepcidin and Fpn C326 residue, because the isosteric C326S substitution results in the complete loss of hepcidin binding.[27,40] However, our current study implicates several additional residues on multiple helices in stabilizing the binding between the ligand and its receptor. We also examined F324 and Y333 Fpn residues, because we had previously noted that mutants at these locations did not internalize radiolabeled hepcidin.[40] In the present study, we found that these mutants bound hepcidin, but displayed impaired ubiquitination and endocytosis. Our proposed Fpn structural model is consistent with all our experimental data classifying residues as those involved in hepcidin binding versus those that affect the conformational change leading to the ubiquitination of Fpn. After we completed the cellular analyses and modeling, Praschberger et al described a partially hepcidin-resistant clinical Fpn mutant, A69T,[48] in a patient with iron-overloaded hepatocytes. Another group described a patient with the A69T mutation as having severe hyperferritinemia (6242 μg/L) and elevated serum transferrin saturation (95.4%).[49] According to our hFpn computational model, this mutation would be expected to affect hepcidin binding based on its location in the central cavity (supplemental Figure 7).

Chung et al previously observed that hepcidin treatment inhibited iron efflux in Caco-2 cells, but failed to decrease Fpn protein levels, and hypothesized that hepcidin could directly block iron export through Fpn in these cells.[44] Taniguchi et al.[33] similarly proposed Fpn occlusion by hepcidin based on the structure of the prokaryotic homolog BbFPN. Our refined models also predict that hepcidin binds to Fpn in the main cavity, and our mutagenesis data experimentally identified a patch of Fpn residues critical for hepcidin binding. Furthermore, we provide the first experimental evidence that hepcidin binding occludes Fpn and directly blocks iron export even without causing Fpn internalization. We report that the engineered Fpn mutant, K8R, shows severely impaired hepcidin-induced Fpn internalization and degradation, but its ability to export iron is completely inhibited by hepcidin, although requiring higher concentrations than WT. Furthermore, using *Xenopus* oocytes, which do not endocytose Fpn in response to

hepcidin, we show that hepcidin blocks iron export by occlusion of not only K8R, but also WT Fpn.

We surmise that high concentrations of hepcidin are necessary to demonstrate the occlusion of iron transport, because at lower concentrations, many Fpn molecules may not be stably occupied by hepcidin. If so, hepcidin-induced endocytosis serves to amplify the effect of transiently bound hepcidin. The relative contribution of Fpn occlusion and endocytosis may differ depending on the cell type, its endocytic machinery, and even Fpn glycosylation, perhaps explaining the reported differences between tissues in sensitivity to hepcidin and the discrepancies between the effects of hepcidin on iron export compared with endocytosis.[43] Indeed, we observed the effect of occlusion in mature human RBCs, a cell type that expresses high levels of Fpn,[42] but lacks endocytic machinery: hepcidin and minihepcidin decreased iron export from RBCs without affecting Fpn levels in these cells. Similarly, injection of WT or thalassemic mice with minihepcidins profoundly decreased serum iron without lowering Fpn protein levels in the duodenum or the spleen, suggesting that serum iron rather than Fpn degradation should be the primary readout of the activity of hepcidin and its agonists in vivo. The high potency of minihepcidin in inhibiting iron export by Fpn K8R suggests that assays of Fpn iron export and FPN endocytosis measure potentially distinct activities of hepcidin agonists, and that engineered hepcidin agonists may exert a therapeutic effect even in patients exhibiting Fpn resistance to hepcidin.

Acknowledgments

The authors would like to thank Tracey Rouault and Deliang Zhang for illuminating discussions related to ferroportin function in RBCs.

This work was supported by National Institutes of Health awards R01 DK107309 (E.N., M.J., and B.M.), R01 DK090554 (E.N. and T.G.), F31 HL129760 and T32 GM007185 (S.A.), and R01 DK095112 and R01 DK090554 (S.R.).

Authorship

Contribution: S.A., M.J., B.M., S.R., T.G., and E.N. designed the study; S.A., B.Q., E.V.V., A.C.S., T.A.R., K.R.V., D.S., G.J., C.C., S.R., and B.M. conducted the experiments and analyzed the data; S.A., M.J., B.M., T.G., and E.N. wrote the manuscript; and all authors contributed to the editing of the final manuscript.

Conflict-of-interest disclosure: E.N. and T.G. are consultants and shareholders of Intrinsic LifeSciences and Silarus Therapeutics and consultants for La Jolla Pharmaceuticals. T.G. is a consultant for Keryx Pharmaceuticals. B.M. is a recipient of a Vifor Pharma grant. S.R. is a member of the scientific advisory board and the recipient of a grant from Ionis Pharmaceuticals. The remaining authors declare no competing financial interests.

ORCID profile: T.G., 0000-0002-2830-5469.

Correspondence: Elizabeta Nemeth, Department of Medicine, David Geffen School of Medicine, University of California, Los Angeles, 10833 LeConte Ave, Center for Health Sciences 37-131, Los Angeles, CA 90095; e-mail: enemeth@mednet.ucla.edu.

Footnotes

Submitted 22 May 2017; accepted 30 November 2017. Prepublished online as *Blood* First Edition paper, 13 December 2017; DOI 10.1182/blood-2017-05-786590.

The online version of this article contains a data supplement.

There is a *Blood* Commentary on this article in this issue.

The publication costs of this article were defrayed in part by page charge payment. Therefore, and solely to indicate this fact, this article is hereby marked "advertisement" in accordance with 18 USC section 1734.

REFERENCES

1. Drakesmith H, Nemeth E, Ganz T. Ironing out ferroportin. *Cell Metab*. 2015;22(5):777-787.
2. Nemeth E, Tuttle MS, Powelson J, et al. Hepcidin regulates cellular iron efflux by binding to ferroportin and inducing its internalization. *Science*. 2004;306(5704):2090-2093.
3. Qiao B, Sugianto P, Fung E, et al. Hepcidin-induced endocytosis of ferroportin is dependent on ferroportin ubiquitination. *Cell Metab*. 2012;15(6):918-924.
4. Preza GC, Pinon R, Ganz T, Nemeth E. Cellular catabolism of the iron-regulatory peptide hormone hepcidin. *PLoS One*. 2013;8(3):e58934.
5. De Falco L, Sanchez M, Silvestri L, et al. Iron refractory iron deficiency anemia. *Haematologica*. 2013;98(6):845-853.
6. Fraenkel PG. Anemia of inflammation: a review. *Med Clin North Am*. 2017;101(2):285-296.
7. Pietrangelo A. Hereditary hemochromatosis–a new look at an old disease. *N Engl J Med*. 2004;350(23):2383-2397.
8. Origa R. β-Thalassemia. *Genet Med*. 2017;19(6):609-619.
9. Pietrangelo A. The ferroportin disease. *Blood Cells Mol Dis*. 2004;32(1):131-138.
10. Schimanski LM, Drakesmith H, Merryweather-Clarke AT, et al. In vitro functional analysis of human ferroportin (FPN) and hemochromatosis-associated FPN mutations. *Blood*. 2005;105(10):4096-4102.
11. Lok CY, Merryweather-Clarke AT, Viprakasit V, et al. Iron overload in the Asian community. *Blood*. 2009;114(1):20-25.
12. Sham RL, Phatak PD, West C, Lee P, Andrews C, Beutler E. Autosomal dominant hereditary hemochromatosis associated with a novel ferroportin mutation and unique clinical features. *Blood Cells Mol Dis*. 2005;34(2):157-161.
13. Létocart E, Le Gac G, Majore S, et al. A novel missense mutation in SLC40A1 results in resistance to hepcidin and confirms the existence of two ferroportin-associated iron overload diseases. *Br J Haematol*. 2009;147(3):379-385.
14. Callebaut I, Joubrel R, Pissard S, et al. Comprehensive functional annotation of 18 missense mutations found in suspected hemochromatosis type 4 patients. *Hum Mol Genet*. 2014;23(17):4479-4490.
15. Wallace DF, Clark RM, Harley HA, Subramaniam VN. Autosomal dominant iron overload due to a novel mutation of ferroportin1 associated with parenchymal iron loading and cirrhosis. *J Hepatol*. 2004;40(4):710-713.
16. Pelucchi S, Mariani R, Salvioni A, et al. Novel mutations of the ferroportin gene (SLC40A1): analysis of 56 consecutive patients with unexplained iron overload. *Clin Genet*. 2008;73(2):171-178.
17. Rivard SR, Lanzara C, Grimard D, et al. Autosomal dominant reticuloendothelial iron overload (HFE type 4) due to a new missense mutation in the FERROPORTIN 1 gene (SLC11A3) in a large French-Canadian family. *Haematologica*. 2003;88(7):824-826.
18. Mayr R, Griffiths WJH, Hermann M, et al. Identification of mutations in SLC40A1 that affect ferroportin function and phenotype of human ferroportin iron overload. *Gastroenterology*. 2011;140(7):2056-2063.e1.
19. Yamakawa N, Oe K, Yukawa N, et al. A novel phenotype of a hereditary hemochromatosis type 4 with ferroportin-1 mutation, presenting with juvenile cataracts. *Intern Med*. 2016;55(18):2697-2701.

20. Le Lan C, Mosser A, Ropert M, et al. Sex and acquired cofactors determine phenotypes of ferroportin disease. *Gastroenterology*. 2011; 140(4):1199-1207.e1-2.

21. Santos PC, Cancado RD, Pereira AC, et al. Hereditary hemochromatosis: mutations in genes involved in iron homeostasis in Brazilian patients. *Blood Cells Mol Dis*. 2011;46(4): 302-307.

22. Zaahl MG, Merryweather-Clarke AT, Kotze MJ, van der Merwe S, Warnich L, Robson KJ. Analysis of genes implicated in iron regulation in individuals presenting with primary iron overload. *Hum Genet*. 2004;115(4):409-417.

23. Lee PL, Gaasterland T, Barton JC. Mild iron overload in an African American man with SLC40A1 D270V. *Acta Haematol*. 2012; 128(1):28-32.

24. Wallace DF, Dixon JL, Ramm GA, Anderson GJ, Powell LW, Subramaniam VN. A novel mutation in ferroportin implicated in iron overload. *J Hepatol*. 2007;46(5):921-926.

25. Rice AE, Mendez MJ, Hokanson CA, Rees DC, Björkman PJ. Investigation of the biophysical and cell biological properties of ferroportin, a multipass integral membrane protein iron exporter. *J Mol Biol*. 2009;386(3):717-732.

26. Drakesmith H, Schimanski LM, Ormerod E, et al. Resistance to hepcidin is conferred by hemochromatosis-associated mutations of ferroportin. *Blood*. 2005;106(3):1092-1097.

27. Fernandes A, Preza GC, Phung Y, et al. The molecular basis of hepcidin-resistant hereditary hemochromatosis. *Blood*. 2009;114(2):437-443.

28. Wallace DF, Harris JM, Subramaniam VN. Functional analysis and theoretical modeling of ferroportin reveals clustering of mutations according to phenotype. *Am J Physiol Cell Physiol*. 2010;298(1):C75-C84.

29. Détivaud L, Island ML, Jouanolle AM, et al. Ferroportin diseases: functional studies, a link between genetic and clinical phenotype. *Hum Mutat*. 2013;34(11):1529-1536.

30. Liu XB, Yang F, Haile DJ. Functional consequences of ferroportin 1 mutations. *Blood Cells Mol Dis*. 2005;35(1):33-46.

31. Le Gac G, Ka C, Joubrel R, et al. Structure-function analysis of the human ferroportin iron exporter (SLC40A1): effect of hemochromatosis type 4 disease mutations and identification of critical residues. *Hum Mutat*. 2013; 34(10):1371-1380.

32. Bonaccorsi di Patti MC, Polticelli F, Cece G, et al. A structural model of human ferroportin and of its iron binding site. *FEBS J*. 2014; 281(12):2851-2860.

33. Taniguchi R, Kato HE, Font J, et al. Outward- and inward-facing structures of a putative bacterial transition-metal transporter with homology to ferroportin. *Nat Commun*. 2015; 6:8545.

34. Hilton KB, Lambert LA. Molecular evolution and characterization of hepcidin gene products in vertebrates. *Gene*. 2008;415(1-2): 40-48.

35. Roy A, Kucukural A, Zhang Y. I-TASSER: a unified platform for automated protein structure and function prediction. *Nat Protoc*. 2010;5(4):725-738.

36. Yang J, Yan R, Roy A, Xu D, Poisson J, Zhang Y. The I-TASSER Suite: protein structure and function prediction. *Nat Methods*. 2015;12(1):7-8.

37. Mitchell CJ, Shawki A, Ganz T, Nemeth E, Mackenzie B. Functional properties of human ferroportin, a cellular iron exporter reactive also with cobalt and zinc. *Am J Physiol Cell Physiol*. 2014;306(5):C450-C459.

38. Stefanova D, Raychev A, Arezes J, et al. Endogenous hepcidin and its agonist mediate resistance to selected infections by clearing non-transferrin-bound iron. *Blood*. 2017; 130(3):245-257.

39. Casu C, Oikonomidou PR, Chen H, et al. Minihepcidin peptides as disease modifiers in mice affected by β-thalassemia and polycythemia vera. *Blood*. 2016;128(2):265-276.

40. Preza GC, Ruchala P, Pinon R, et al. Minihepcidins are rationally designed small peptides that mimic hepcidin activity in mice and may be useful for the treatment of iron overload. *J Clin Invest*. 2011;121(12): 4880-4888.

41. Fung E, Chua K, Ganz T, Nemeth E, Ruchala P. Thiol-derivatized minihepcidins retain biological activity. *Bioorg Med Chem Lett*. 2015;25(4):763-766.

42. Zhang D-L, Wang J, Shah B, et al. Ferroportin protects red blood cells from oxidative stress and malaria infection by exporting free intracellular iron. Abstract from the Seventh Congress of the International BioIron Society (IBIS) Biennial World Meeting (BioIron 2017); 7-11 May 2017; Los Angeles, CA.

43. Chaston T, Chung B, Mascarenhas M, et al. Evidence for differential effects of hepcidin in macrophages and intestinal epithelial cells. *Gut*. 2008;57(3):374-382.

44. Chung B, Chaston T, Marks J, Srai SK, Sharp PA. Hepcidin decreases iron transporter expression in vivo in mouse duodenum and spleen and in vitro in THP-1 macrophages and intestinal Caco-2 cells. *J Nutr*. 2009;139(8): 1457-1462.

45. Zhang DL, Senecal T, Ghosh MC, Ollivierre-Wilson H, Tu T, Rouault TA. Hepcidin regulates ferroportin expression and intracellular iron homeostasis of erythroblasts. *Blood*. 2011;118(10):2868-2877.

46. Harrison-Findik DD, Schafer D, Klein E, et al. Alcohol metabolism-mediated oxidative stress down-regulates hepcidin transcription and leads to increased duodenal iron transporter expression. *J Biol Chem*. 2006;281(32): 22974-22982.

47. Olynyk JK, Knuiman MW, Divitini ML, Bartholomew HC, Cullen DJ, Powell LW. Effects of HFE gene mutations and alcohol on iron status, liver biochemistry and morbidity. *J Gastroenterol Hepatol*. 2005;20(9): 1435-1441.

48. Praschberger R, Schranz M, Griffiths WJ, et al. Impact of D181V and A69T on the function of ferroportin as an iron export pump and hepcidin receptor. *Biochim Biophys Acta*. 2014; 1842(9):1406-1412.

49. Ferbo L, Manzini PM, Badar S, et al. Detection of a rare mutation in the ferroportin gene through targeted next generation sequencing. *Blood Transfus*. 2016;14(6): 531-534.

SUPPLEMENTAL METHODS

Reagents were obtained from Sigma–Aldrich or Research Products International unless otherwise indicated.

Microscopy in mammalian cells

Cells were induced with 100 ng/ml dox overnight in 12-well poly-D-lysine coated plates (BD). Cells were washed with PBS, and treated with 25 μM ferric ammonium citrate (FAC), hepcidin (Peptide International) or PR73[15] for 24 hours (concentrations as indicated in figure legends). Cells were visualized with an epifluorescence microscope (Nikon Eclipse), and images were acquired with a 40x objective, SPOT camera, and SPOT Advanced Imaging Software (Diagnostic Instruments).

Fpn membrane localization in mammalian cells

Cells were seeded on 6-well poly-D-lysine coated plates (BD) and induced with 500 ng/ml doxycycline for 24 hours. Cells were washed 3x with PBS and treated with EZ-link maleimide PEG-2-biotin in PBS for 30 minutes at 4 ºC. Cells were then washed with 1x PBS, solubilized in RIPA (Boston BioProducts) with protease inhibitors, and Fpn-GFP was immunoprecipitated with anti-GFP Ab as described previously[16]. Blots were probed with Streptavidin-HRP (Pierce) and total Fpn was detected with anti-GFP Ab (Roche). To adjust for variations between individual Western blots, we normalized band intensity to WT Fpn sample within the same blot.

Ferritin assay

Cells were processed the same as in the microscopy section. After 24 hours of treatment, cells were washed with PBS and harvested in RIPA with protease inhibitors. Ferritin levels were determined by an ELISA assay (Ramco Laboratories) according to the manufacturer's instructions and were normalized to the total protein concentration in each sample (BCA assay, Pierce). To adjust for variations of the absolute ferritin values between multiple experiments, we expressed the measurements as the relative change in ferritin, according to the formula I/U, where I is the ferritin value for the induced cell line and U is the ferritin value for the uninduced cell line. For hepcidin or PR73-treated cells, we expressed the ferritin measurements as (H-I)/U or (P-I)/U, where H refers to the ferritin value for the induced cells treated with hepcidin and P refers to the ferritin value for the induced cells treated with PR73.

Hepcidin binding

Cells were treated with 3 μg/ml N-terminally biotinylated hepcidin (Peptides International) for 30 min at 37°C. Protein lysates were immunoprecipitated with anti-GFP Ab (Abcam)[16], run under non-reducing conditions, and blotted with Streptavidin-HRP (Pierce). Total Fpn

was blotted with anti-GFP Ab (Roche). To adjust for variations between Western blots, we normalized the values from Fpn mutants to those of WT Fpn within the same blot.

Immunoprecipitation and Western blotting for ubiquitination

Immunoprecipitation was performed as previously[16], except the gel-loading dye contained 5% 2-mercaptoethanol. To adjust for variations between Western blots, we normalized the mutant ubiquitination values to those of the WT within the same blot.

Radioactive iron export for clinical and nonclinical mutants

Adherent cells were loaded with 2 mM ^{55}Fe-NTA for 48 hours (prepared from $^{55}FeCl_3$, Perkin Elmer), washed 3x with medium, re-plated, induced overnight, washed 2x with medium, and then hepcidin was added to some wells. Aliquots of the medium were sampled for up to 10 hours to measure iron export. The “uninduced” measurement at each time point was subtracted as background. The slope of each line was determined and used to calculate the percent iron export by comparing the slopes to that of untreated WT.

Fpn Western blot

Protein was measured by BCA assay, 6x SDS-loading buffer was added to lysates which were then separated by SDS-PAGE on 4-20% Mini-PROTEAN TGX Precast Gels (BioRad), and transferred to PVDF membranes using Trans-Blot Turbo (Bio-Rad). Blocking was performed overnight at 4°C in 5% milk in TBST (50mM Tris-HCl, pH7.5, 150mM NaCl, 0.1% Tween 20). Anti-GFP (Roche) was used to detect Fpn and anti-GAPDH-HRP (Cell Signaling) were used for normalization.

Fpn stability Western blot

Cells were induced with 100 ng/ml doxycycline overnight in 12-well poly-D-lysine coated plates (BD). Next, the medium was removed, cells were washed 2x with 1xPBS, and the zero-time point sample harvested. The remaining wells were treated with 25 μM ferric ammonium citrate (FAC) either with or without 1 μg/ml hepcidin for 24 hours. The protein concentration was measured using the BCA assay and 25 μg of protein per sample was used for Western blots. Anti-GFP Ab (Roche) was used to detect FPN, and normalization was performed using an anti-GAPDH Ab or anti-actin Ab when specified.

Functional expression of hFpn in *Xenopus* oocytes

We performed laparotomy and ovariectomy on adult female *Xenopus laevis* frogs (Nasco) under 2-aminoethylbenzoate methanesulfonate anesthesia (0.2%, by immersion, to effect) following a protocol approved by the University of Cincinnati Institutional Animal Care and Use Committee. The pOX(+) oocyte expression plasmid vectors containing human WT or K8R Fpn-GFP were used to synthesize RNA *in vitro*. We examined the

functional expression of hFpn-GFP and K8R-hFpn-GFP in RNA-injected *Xenopus* oocytes as described[17] except for the following modifications. RNA-injected oocytes were stored at 17 ºC in modified Barths' medium (MBM) containing 50 mg.l^{-1} dox, and incubated 4–5 days before being used in functional assays.

We treated oocytes for 0−4 h with 10 μM hepcidin in MBM prior to assaying iron efflux. Oocytes were injected with 50 nl of 5 μM ^{55}Fe, added as Fe^{3+} $FeCl_3$ (Perkin-Elmer Life Science Products) in a vehicle of composition 250 mM KCl, 5 mM nitrilotriacetic acid trisodium salt, 4 mM 2-(*N*-morpholino)ethanesulfonic acid (GFS Chemicals). To initiate the efflux assay, we placed oocytes in efflux medium of composition 100 mM NaCl, 1 mM KCl, 2 mM $CaCl_2$, 1 mM $MgCl_2$, 0.5 mM bathophenanthroline disulfonic acid, 1 mM nitrilotriacetic acid trisodium salt, 50 μg.ml^{-1} human apotransferrin (R&D Systems), buffered with 2.5 mM 1,4-diethylpiperazine (Alfa Aeser) and approximately 2.5 mM 2-(*N*-morpholino)ethanesulfonic acid to obtain pH 7.5. We obtained the first-order rate constants (k) describing iron efflux over 30 min determined for individual oocytes as described[18]. Live-cell imaging of Fpn-GFP in oocytes before and after 30-min 10 μM hepcidin treatment was performed as described[17].

Iron export and Fpn Western in human red blood cells

Human packed red blood cells (PRBC, 1 to 10 days old) from four different donors were obtained from the Division of Transfusion Medicine, Department of Pathology and Laboratory Medicine, David Geffen School of Medicine, UCLA, Los Angeles, California. PRBCs were aliquoted and incubated in their storage medium (Anticoagulant Citrate Phosphate Dextrose Adenine Solution, USP, CPDA-1) at 37 ºC for 24 h in the presence of 0, 0.4 and 3.6 μM hepcidin or PR73. Samples were collected after 24 h by centrifuging the PRBC at 5,000 g for 8 min. The cell pellet was frozen at -80 ºC for further processing. The supernatant was centrifuged again at 5,000 g for 8 min and non-transferrin bound iron (NTBI) measured as previously described[18]. Briefly, we used an "enhanced labile plasma iron" (eLPI) assay, based on the catalytic conversion of nonfluorescent dihydrorhodamine to fluorescent rhodamine, in the presence and absence of the iron chelator deferiprone, and a mild metal-mobilizing agent, nitriloacetate.

To measure Fpn protein by Western blotting, cell pellets were lysed in 5 mM sodium phosphate buffer pH 8 with protease and phosphatase inhibitors (Halt protease and phosphatase inhibitors cocktail, Thermo Scientific) to obtain RBC ghost membranes. The membranes were pelleted at 10,000 g for 5 min at 4 C and washed three times in the same buffer. The resulting pellet was lysed in 80 μl RIPA lysis buffer (Chem Cruz, Santa Cruz) with protease and phosphatase inhibitors, by incubation for 15 min on ice and periodic vortexing. The samples were then centrifuged at 14,000 g for 15 min at 4 ºC and the supernatant was used to determine protein concentration using Pierce BCA Protein

Assay Kit (Thermo Scientific) following the manufacturer's protocol. 10 µg protein was loaded on a 4-20% protein gel (Mini Protean TGX gels, BioRad) (samples were not boiled and no reducing agent was added). Proteins were transferred to a Trans Blot Turbo nitrocellulose membrane (BioRad), the membrane was blocked for 1 h with 5% milk dissolved in Tris-buffered saline (Sigma) with 0.1% Tween 20 (TBST, Acros Organics), and incubated with primary antibody (human anti-human ferroportin 38C8, Amgen) overnight at 4 ºC at concentration 1 µg/ml, washed and incubated with secondary Goat anti-Human IgG (H+L) Horseradish Peroxidase Conjugate (BioRad) at dilution 1:3000. After washing, the membrane was incubated with Super Signal West Pico chemiluminescent substrate (Thermo Scientific) and imaged using ChemiDoc XRS+ imaging system (BioRad).

Mouse treatment with hepcidin agonists

C57BL/6 mice injected with PR73: Experiments were conducted in accordance with the guidelines by the National Research Council and were approved by the Animal Research Committee of the University of California, Los Angeles. 6-week old male C57BL/6 mice received two intraperitoneal injections 12 hours apart of either solvent SL220 (NOF Corporation) or 60 nmoles PR73 dissolved in SL220, and were analyzed 4 hours after the second injection.

th3 mice injected with minihepcidin M009: th3/+ mice received a single subcutaneous injection of M009[19] (~50 nmoles per mouse), and were analyzed over a time-course of 0-36 h after injection (n=3 per group).

Serum iron was determined as previously described,[20] using acid treatment followed by a colorimetric assay for iron quantitation (Sekisui Diagnostics, Charlottetown, Canada). Duodenum Fpn and spleen Fpn were determined by Western blotting as follows: spleen or duodenum was homogenized in lysis buffer, centrifuged, and the supernatant was collected. The protein concentration was determined using the Pierce BCA assay. Samples were run on a 4-15% SDS-PAGE gel without boiling or reducing agent. Once transferred onto nitrocellulose, the blot was blocked in Genscript blocking buffer for 5 minutes. The blot was incubated overnight with rat-anti-mouse Fpn (IC7 from Amgen) in WB-2 buffer from Genscript or monoclonal anti-actin antibody (Sigma) in 5% milk/TTBS overnight at 4 ºC. After incubation with secondary antibodies, the blots were imaged using chemiluminescence on ChemiDoc XRS+ imaging system (BioRad). Serum hepcidin was detected using a hepcidin ELISA immunoassay as previously described[21].

Statistical analysis

We set critical significance level, $\alpha = 0.05$, and expressed our data as mean, SEM for *n* observations. Statistical analyses employed the two-tailed t-test (normally distributed

data) or Mann-Whitney rank sum test (data with non-normal distribution), the two-tailed one-sample t-test (normally distributed data) or the two-tailed one-sample signed rank test (data with non-normal distribution) compared with a reference of 1, and 2-way analysis of variance (ANOVA). (SigmaPlot version 12.5, Systat Software). The unequal variance t-test was used when the samples failed the equal variance t-test. To account for the possibility of false positives due to multiple comparisons, we determined the significance for each mutant by using the false discovery rate (FDR) correction for multiple comparisons procedure. The significance threshold, α, was set at 0.05. To determine if an individual p-value is significant, the critical level for each comparison is first calculated by α/Ki, where Ki= the rank of the individual comparison (its ranking when compared to other mutants when ordered from highest to lowest p-value). If the individual P value (Pi) is less than the individual critical significance level then that mutant is significantly different from its comparator (designated by * in graphs). The first ranked value of Pi that is greater than its corresponding critical significance level is not significant and all comparisons with a higher Pi are not significant.

Table S1. Primers for site-directed mutagenesis of human Fpn-GFP

Mutation	Forward primer	Reverse primer
S71F	ctggtggtggcagggtttgttctggtcctg	caggaccagaacaaaccctgccaccaccag
V72F	ggtggcagggtcttttctggtcctggg	cccaggaccagaaaagaccctgccacc
G204S	tggctccccagtcatcagctgtggctttatttc	gaaataaagccacagctgatgactggggagcca
D270V	catctaatgggtgtgaaagtctctaacatccatgagctt	aagctcatggatgttagagactttcacacccattagatg
S338R	cactcagggactgaggggttccatcctcagt	actgaggatggaacccctcagtccctgagtg
Y501C	ggtgtacagaactccatgaactgtcttcttgatcttctgc	gcagaagatcaagaagacagttcatggagttctgtacacc
D504N	gtacagaactccatgaactatcttcttaatcttctgcatttcatcat	atgatgaaatgcagaagattaagaagatagttcatggagttctgtac
H507R	ctatcttcttgatcttctgcgtttcatcatggtcatcctgg	ccaggatgaccatgatgaaacgcagaagatcaagaagatag
F508Y	atcttcttgatcttctgcattatatcatggtcatcctggctcc	ggagccaggatgaccatgatataatgcagaagatcaagaagat
Y64N	ccaccaccagcccgttgactgctgtcaaaag	cttttgacagcagtcaacgggctggtggtgg
N144D	ctattgcaaatattgcagatttggccagtactgc	gcagtactggccaaatctgcaatatttgcaatag
Y333A	accacagggtacgccgccactcagggactgag	ctcagtccctgagtggcggcgtaccctgtggt
Y333F	cacagggtacgccttcactcagggactga	tcagtccctgagtgaaggcgtaccctgtg
F324A	tatatgactgtcctgggcgctgactgcatcaccacagg	cctgtggtgatgcagtcagcgcccaggacagtcatata
F324Y	tatgactgtcctgggctatgactgcatcaccac	gtggtgatgcagtcatagcccaggacagtcata
C326S	tcctgggcttgacagcatcaccacaggg	ccctgtggtgatgctgtcaaagcccagga

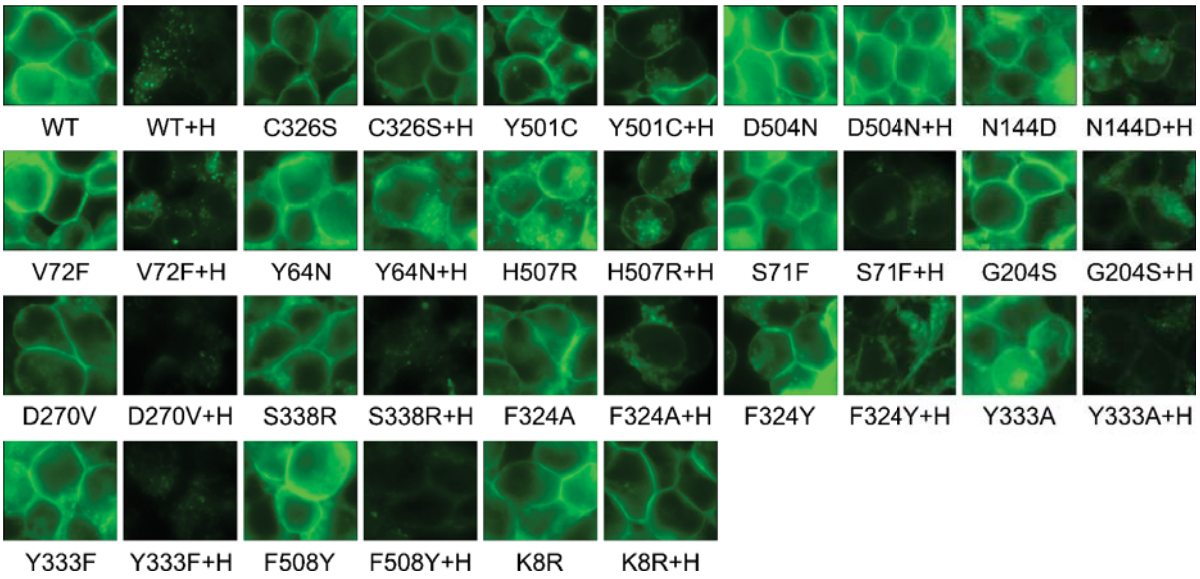


Figure S1: Microscopy of human Fpn (hFpn) mutant cells ± hepcidin treatment. HEK293T cells stably transfected with doxycycline (dox)-inducible hFpn-GFP mutants were induced with 100 ng/ml dox overnight. The cells were then washed, incubated with ±1 µg/ml hepcidin (0.4 µM) for 24 hours, and imaged by fluorescent microscopy.

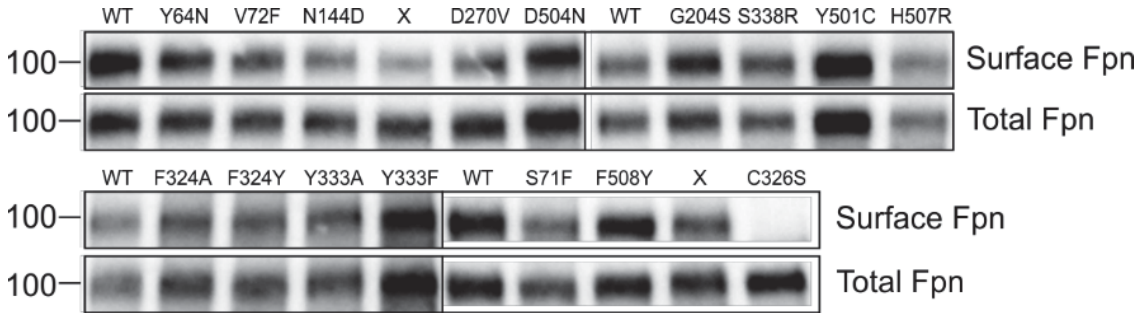


Figure S2: Representative Western blots: cell surface biotinylation of hFpn. HEK293T cells stably expressing doxycycline (dox)-inducible hFpn-GFP mutants were induced with dox to express Fpn, treated with maleimide-biotin for 30 minutes, immunoprecipitated using anti-GFP Ab, and immunoblotted with streptavidin-HRP or anti-GFP Ab. X denotes mutants not discussed in the paper.

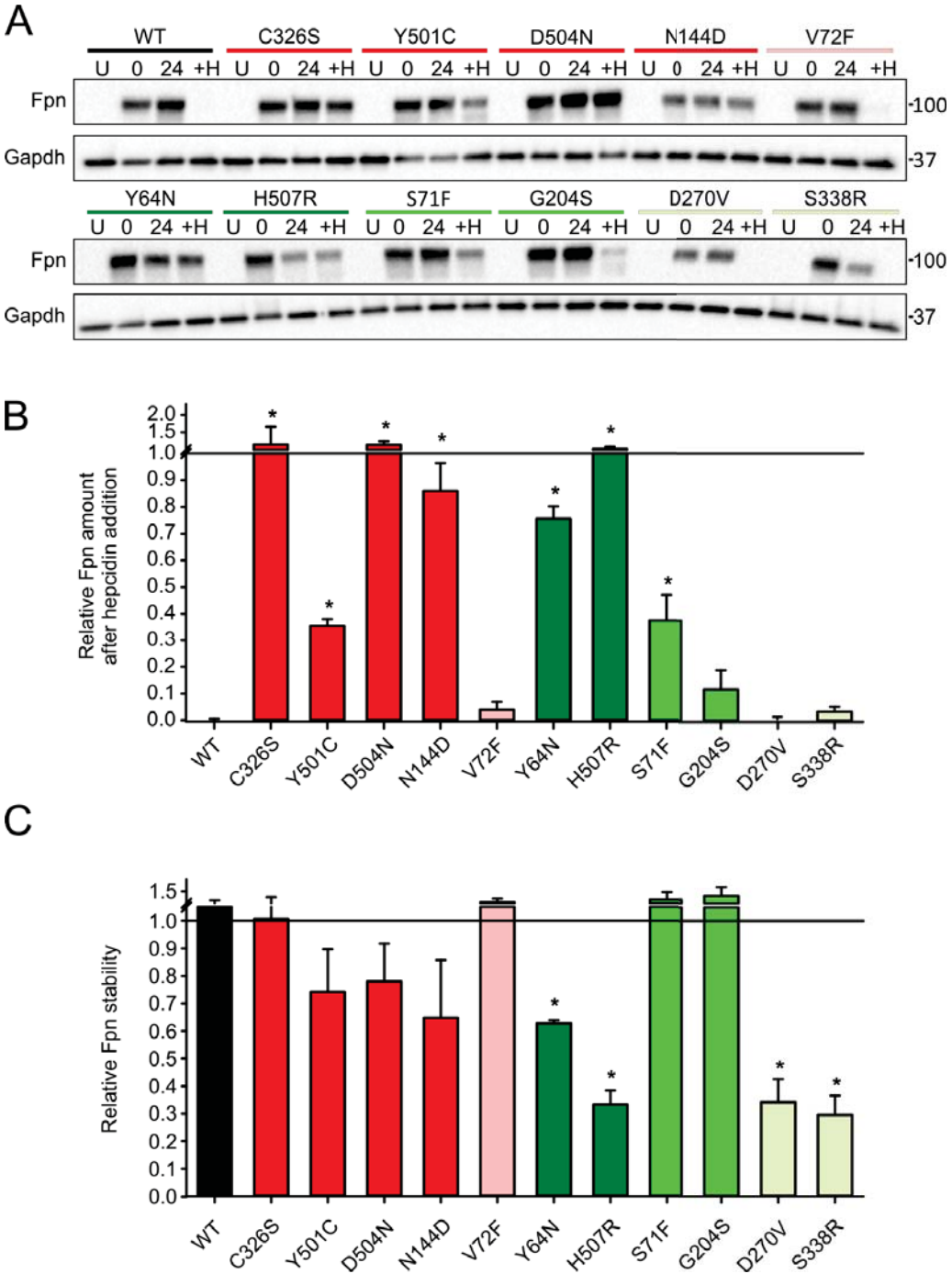

A
WT
C326S
Y501C
D504N
N144D
V72F
U 0 24 +H
Fpn
Gapdh
-100
-37
Y64N
H507R
S71F
G204S
D270V
S338R
B
Relative Fpn amount after hepcidin addition
2.0
1.5
1.0
0.9
0.8
0.7
0.6
0.5
0.4
0.3
0.2
0.1
0.0
WT
C326S
Y501C
D504N
N144D
V72F
Y64N
H507R
S71F
G204S
D270V
S338R
C
Relative Fpn stability

Figure S3: Stability and hepcidin-induced degradation of WT and mutant Fpn. Cells were induced overnight to express hFpn-GFP. The inducer was removed, the cells were washed, and some wells were harvested for the 0 h time point or incubated for another 24 hours ± 1 µg/ml hepcidin (0.4 µM). A) Representative Western blot of WT and mutant hFpn-GFP. Fpn was detected using anti-GFP Ab and GAPDH was used for normalization. U= uninduced Fpn cells, 0= 0 h time-point, 24= 24 h time-point without hepcidin treatment, and H= hepcidin treatment for 24 h. B) Quantification of Fpn degradation by hepcidin. Densitometry was performed on triplicate Western blots from A. GAPDH was used for normalization of the GFP signal. Values of hepcidin-treated samples were further normalized to their respective untreated 24 h control to express results as relative Fpn amount after hepcidin treatment. The two-tailed t-test comparing mutants to WT was employed and the FDR procedure was used to determine significance where * = significant. C) Quantification of Fpn stability. Densitometry was performed on triplicate Western blots from A, and GAPDH was used for normalization of GFP signal. Fpn values at 24 h (non-hepcidin treated) were expressed as a fraction of their respective controls at 0 h. 1= amount of Fpn at the 0 h time point for each respective mutant. Statistical analysis employed the two-tailed one-sample t-test using 1 as the comparison and the FDR procedure was used to determine significance where * = significant. Data shown are means ± SEM of 3-5 independent experiments.

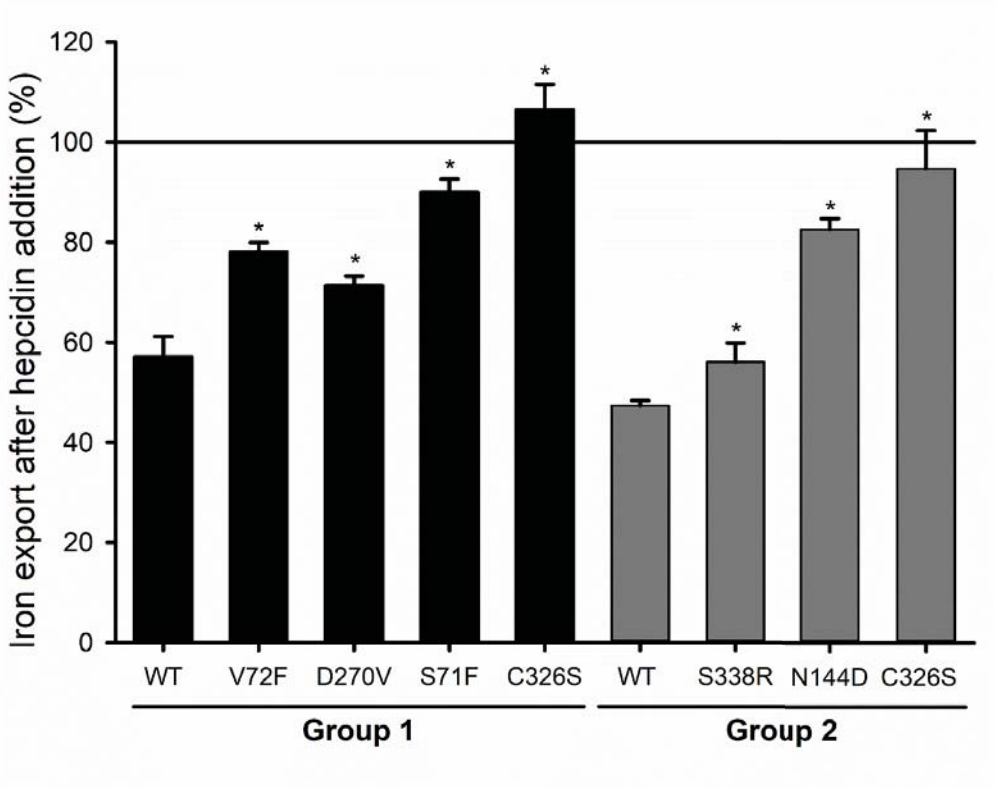


Figure S4: Iron export after hepcidin addition. Cells were loaded with 2mM ^{55}Fe for 48 hours, washed, re-plated, and either left uninduced or were induced by adding doxycycline overnight. Cells were washed again and medium was sampled at multiple time points to measure iron export up to 10 hours ± hepcidin (Group 1: 0.1 µg/ml, Group 2: 3 µg/ml). The "uninduced" measurement at each time point was subtracted as background. The slope for each "induced" and "induced + hepcidin" sample was determined, and % export after hepcidin treatment calculated. Data shown are means ± SEM of at least 4 biological replicates. Statistical analysis employed the two-tailed t-test if normally distributed and the two-tailed t-test on ranks if not, comparing each mutant to the WT Fpn analyzed within the same experiment. Once the P-values were determined, the FDR procedure was used to determine significance, which is indicated with *. C326S, a highly hepcidin-resistant mutant, was used in each experiment as a control for assay integrity.

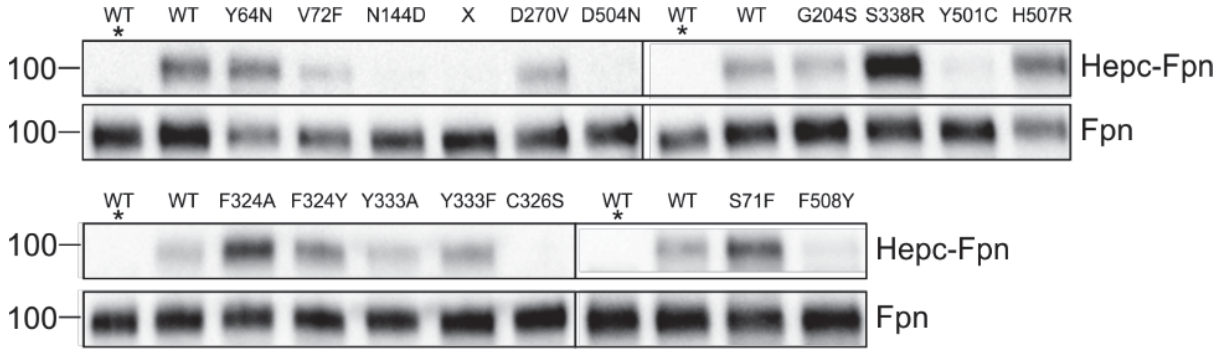


Figure S5: Representative Western blots: hepcidin binding to hFpn. Cells induced to express WT or mutant hFpn-GFP were treated with N-terminally biotinylated hepcidin for 30 minutes, immunoprecipitated with anti-GFP Ab, run under non-reducing conditions, and immunoblotted with streptavidin-HRP or anti-GFP Ab. Hepc-Fpn= hepcidin complexed with Fpn.*= WT with no hepcidin added. X denotes a mutant not discussed in the paper.

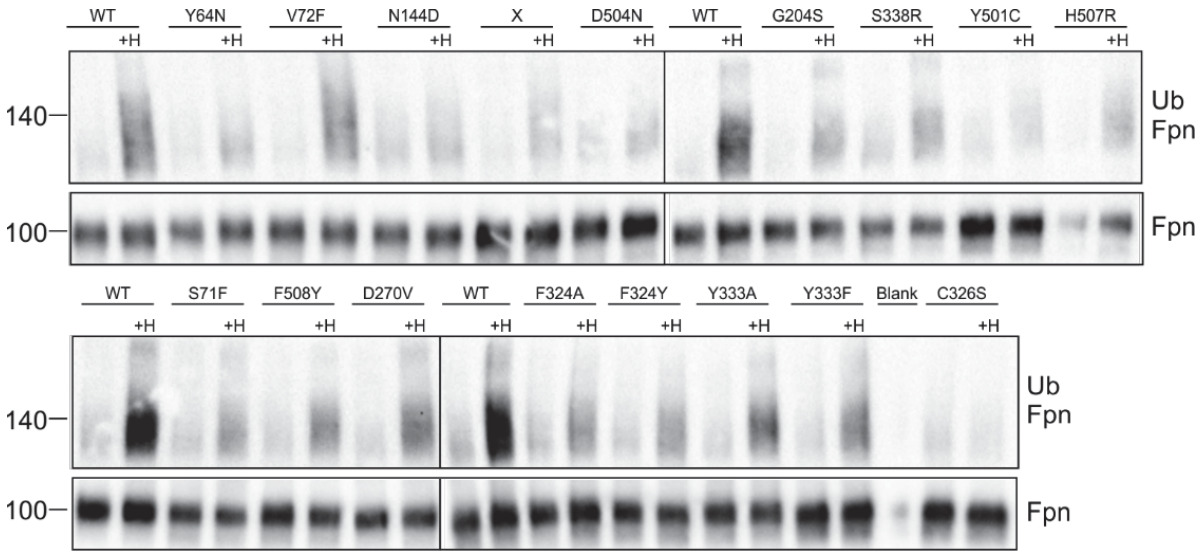


Figure S6: Representative Western blots: ubiquitination of hFpn. Cells expressing WT and mutant hFpn-GFP were treated with hepcidin for 30 minutes, immunoprecipitated with anti-GFP Ab, and immunoblotted with anti-poly/mono ubiquitin Ab (FK2) or anti-GFP Ab. X denotes a mutant not discussed in the paper.

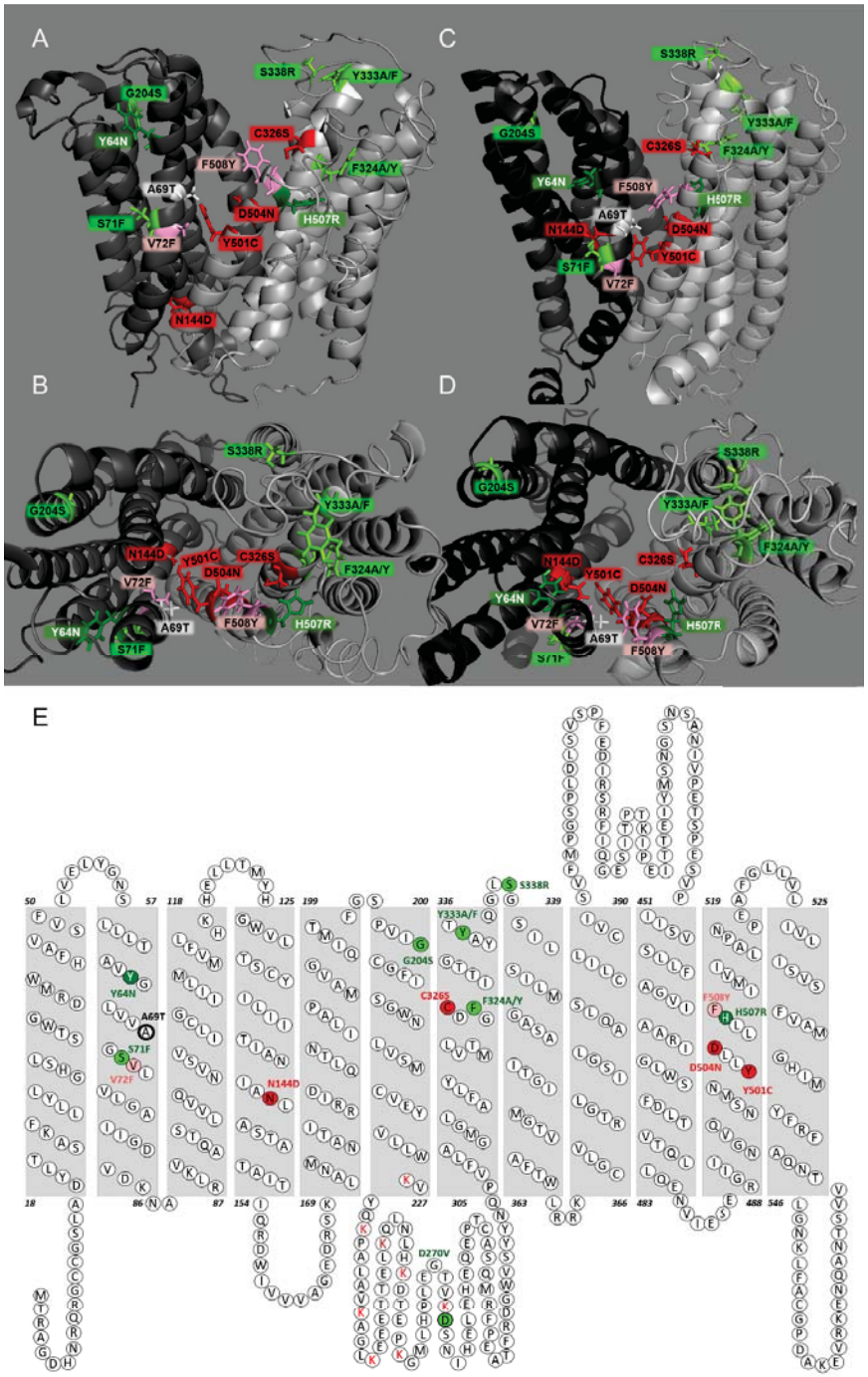

A
S338R
Y333A/F
G204S
Y64N
C326S
F508Y
F324A/Y
A69T
S71F
D504N
H507R
V72F
Y501C
N144D
C
S338R
G204S
Y333A/F
C326S
F324A/Y
Y64N
F508Y
H507R
A69T
N144D
D504N
S71F
Y501C
V72F
B
S338R
G204S
Y333A/F
N144D
Y501C
C326S
D504N
F324A/Y
V72F
Y64N
A69T
F508Y
H507R
S71F
D
S338R
G204S
Y333A/F
F324A/Y
N144D
Y501C
C326S
D504N
Y64N
V72F
A69T
H507R
F508Y
E
S338R
Y333A/F
G204S
C326S
F324A/Y
Y64N
A69T
S71F
V72F
N144D
F508Y
H507R
D504N
Y501C
D270V

Figure S7: hFpn I-TASSER modeling without or with BdFPN among templates. A,B) Model generated without the Bd2109 crystal structure; side-view and top-view of hFpn in its outward-facing state are shown. C,D) Model generated by including the Bd2109 crystal structure among templates; side-view and top-down view of hFpn in its outward-facing state are shown. D270V is not modeled because it is in the disordered intracellular loop of Fpn. Red/pink color denotes mutants with impaired hepcidin binding, and the green color denotes mutants with intact hepcidin binding but variably impaired ubiquitination. A69T, the white colored mutant, is a recently discovered clinical mutation causing non-classical ferroportin disease that was not experimentally examined in our study. E) 2D Fpn model of A and B. Red Ks (lysines) indicate the residues mutated in the K8R Fpn mutant. For A-E, the bold color denotes severe mutants and lighter color denotes mild and borderline mutants.

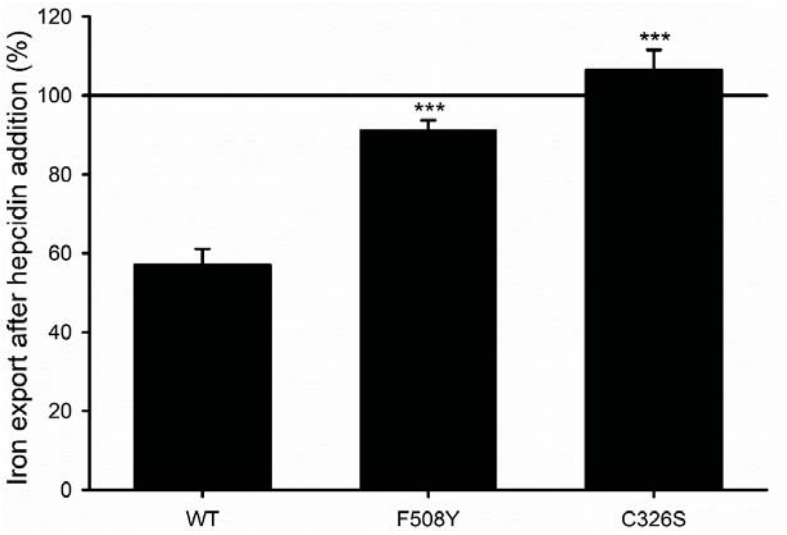


Figure S8: F508Y Fpn mutant is functionally resistant to hepcidin as determined by radiolabeled iron export. Cells were loaded with 2mM ^{55}Fe for 48 hours, washed, re-plated, and either left uninduced or were induced by adding doxycycline overnight. Cells were washed again, and medium sampled at multiple time points to measure iron export up to 10 hours ± 0.1 µg/ml hepcidin. The "uninduced" measurement at each time point was subtracted as background. The slope for each "induced" and "induced + hepcidin" sample was determined, and % export after hepcidin treatment calculated. Statistical analysis employed the two tailed t-test comparing each mutant to the WT. Data shown are means ± SEM of at least 4 biological replicates. *** $P < 0.0005$, **$P < 0.005$, *$P < 0.05$ by t-test or t-test on ranks if not normally distributed. C326S, a highly hepcidin-resistant mutant, was used in each experiment as a control for assay integrity.

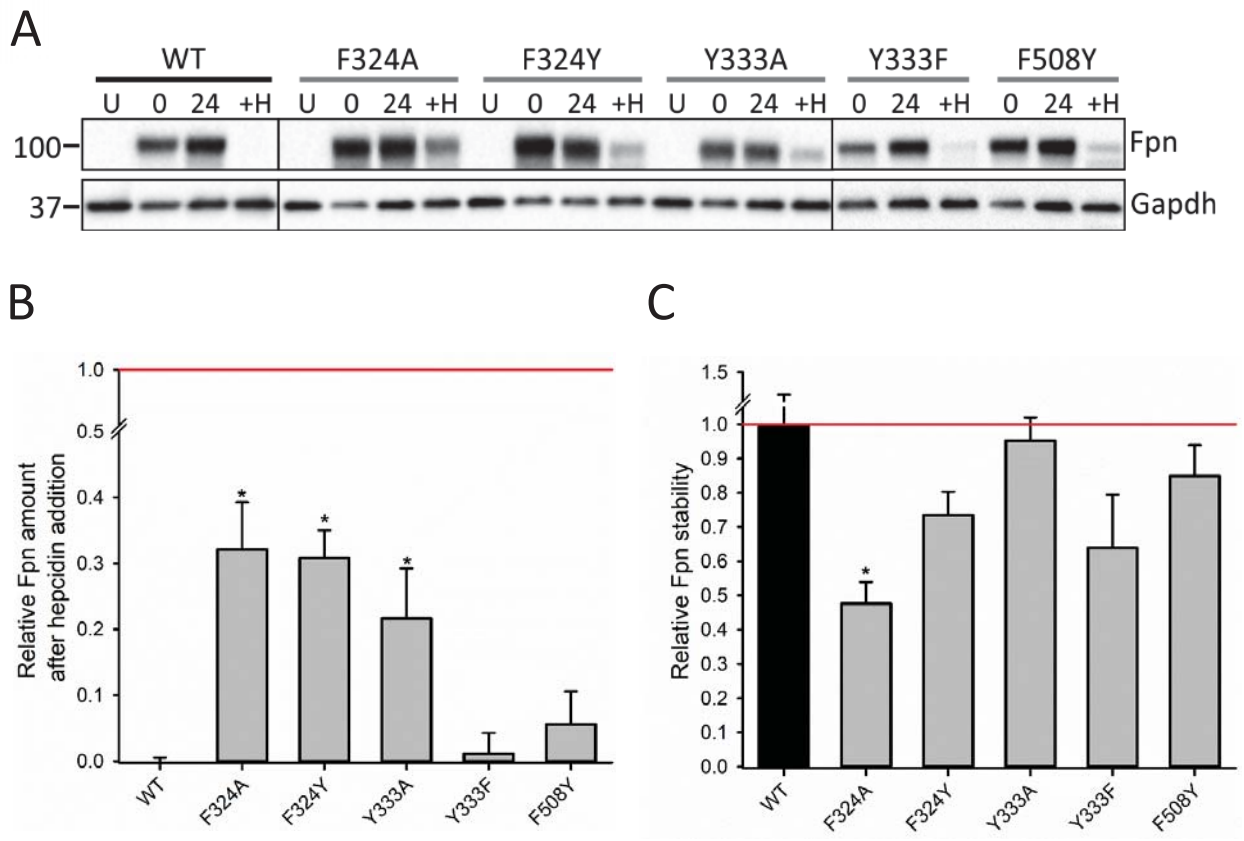


Figure S9: Stability and hepcidin-induced degradation of hFpn. Cells expressing inducible nonclinical Fpn mutants were analyzed with the same approaches as described in Figure S3. Cells were induced overnight to express WT and mutant hFpn-GFP. Doxycycline was removed and cells harvested for the 0 h time point or incubated for another 24 hours ±1 µg/ml hepcidin (0.4 µM) hepcidin. A) Representative Western blots. B) Quantification of Fpn degradation by hepcidin. C) Quantification of Fpn stability. Densitometry in B and C was performed on triplicate Western blots from A, and an average of two housekeeping proteins was used for normalization (GAPDH and actin). Statistical analysis employed the two-tailed t-test comparing the mutants to WT (B) or the two-tailed one-sample t-test using 1 as the comparison (C) Data shown are means ± SEM of 3 independent experiments. The FDR procedure was used to determine significance (* = significant).

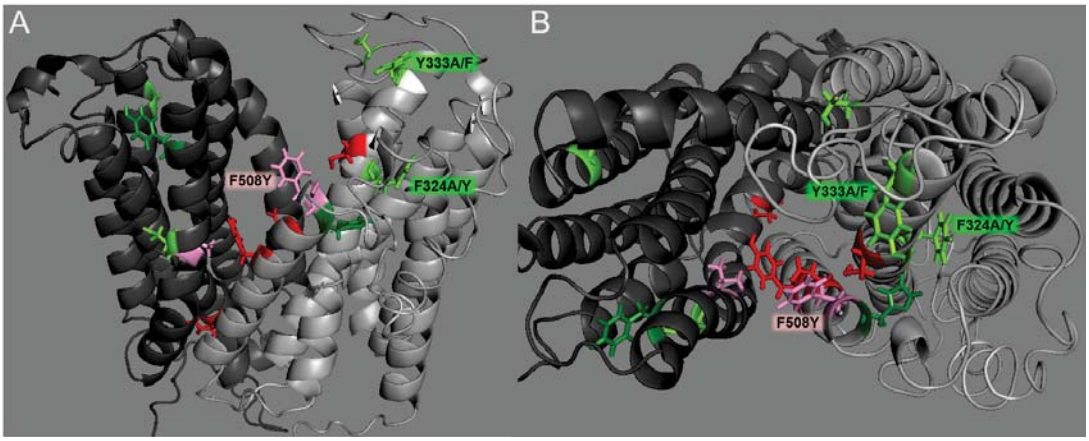


Figure S10: hFpn structure depicting nonclinical mutant residues. A) A side-view of hFpn in its outward-facing state, with the N-terminus on the left and C-terminus on the right. B) Top-down view of hFpn in its outward-facing state. All nonclinical mutants are mild mutants.

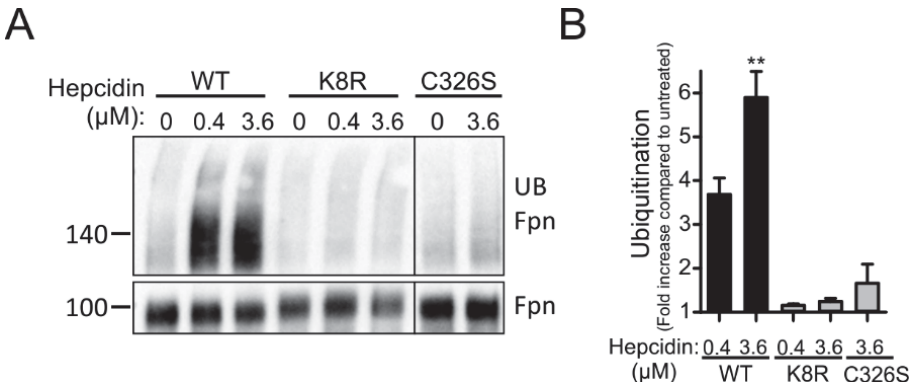
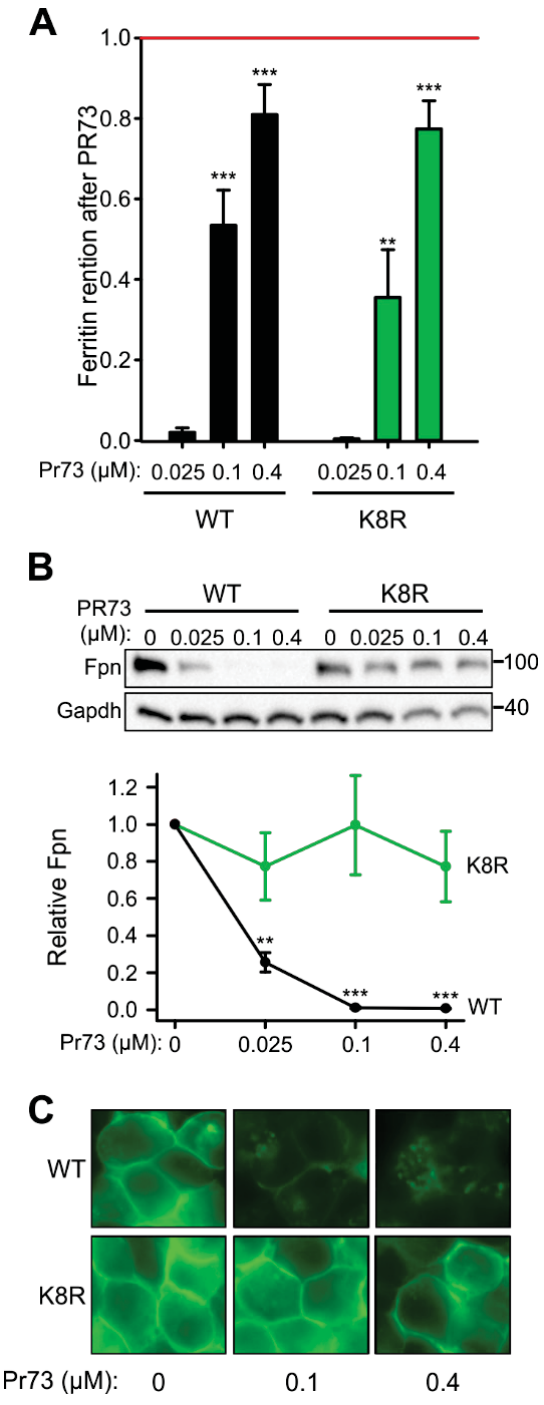


Figure S11: High concentrations of hepcidin do not cause ubiquitination of K8R Fpn. A) hFpn-GFP WT and mutants were treated with hepcidin for 30 minutes, immunoprecipated with anti-GFP Ab, and immunoblotted with anti-poly/mono ubiquitin Ab (FK2) or anti-GFP Ab. The C326S mutant, which does not bind hepcidin, was used as a control. B) Quantification of triplicate Western blots from A. Ubiquitination was normalized to total Fpn in each sample and then expressed as fold increase over hepcidin-untreated sample. 1= the amount of basal ubiquitination for each respective untreated mutant in the absence of hepcidin. Results are shown as the mean ± SEM of 3-5 independent experiments. Statistical significance for mutants was achieved only for the WT treated with 3.6 μM hepcidin when employing the two-tailed one-sample t-test using 1 as a comparison.

Figure S12: Evidence for Fpn occlusion by minihepcidin. Cells expressing inducible non-ubiquitinated K8R mutant were compared to those expressing WT Fpn. A) Ferritin retention after hepcidin addition was determined as in Figure 3A. Statistical analysis employed the two-tailed t-test using the respective untreated control for comparison (***P<0.001, **P<0.01, *P<0.05). Data shown are the mean ± SEM of 3 independent experiments. B) Lysates from A were analyzed by Western blotting. Top: representative Western blot. Bottom: densitometry of triplicate Western blots. Fpn signal was first normalized to GAPDH, then expressed as the fraction of respective untreated control (no hepcidin treatment). Data shown are the mean ± SEM of 3 independent experiments. For A and B, statistical analysis employed the two-tailed one-sample t-test using 1 as the comparison (***P<0.001, **P<0.01, *P<0.05). C) Microscopy of samples in A after 24 hours.



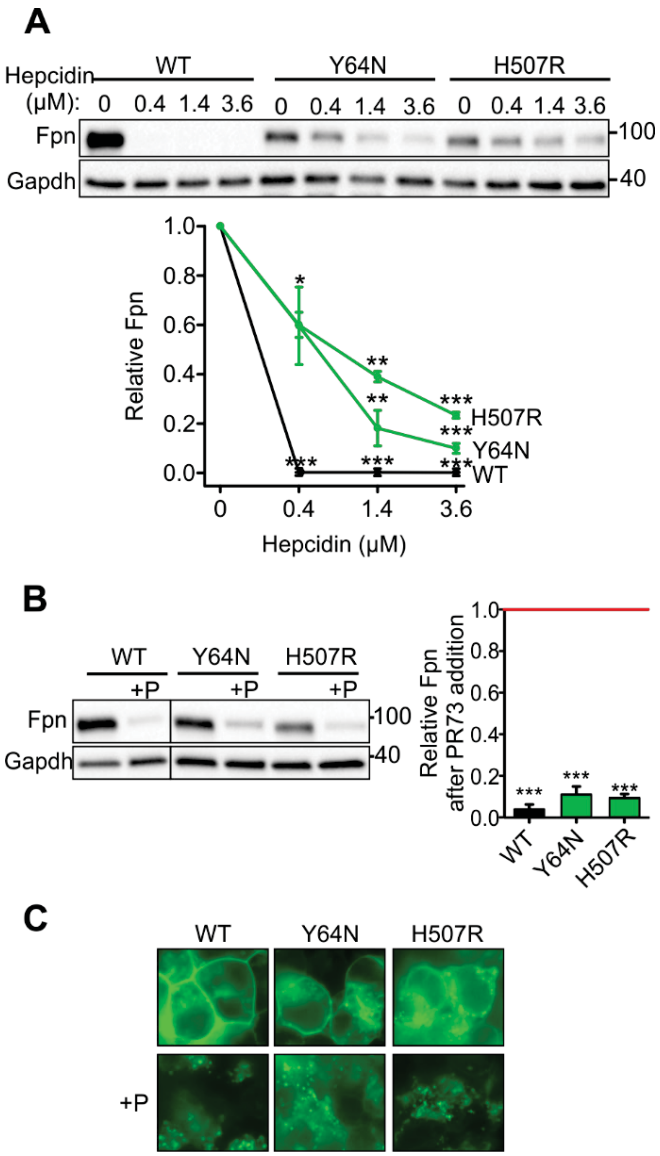


Figure S13: H507R and Y64N Fpn are degraded in the presence of high hepcidin or minihepcidin concentrations. A) Cells expressing inducible Y64N or H507R mutations were compared to those expressing WT Fpn in the presence of 0-3.6 μM hepcidin. Lysates were analyzed by Western blotting. Top: representative Western blot. Bottom: densitometry of triplicate Western blots. Fpn signal was first normalized to GAPDH, then

expressed as the fraction of respective untreated control (no hepcidin treatment). B) Cells expressing inducible Y64N or H507R mutations were compared to those expressing WT Fpn in the presence or absence of 3.6 μM PR73. Lysates were analyzed by Western blotting 24 hours after treatment. Left: representative Western blot. Right: densitometry of triplicate Western blots. Fpn signal was first normalized to GAPDH and then expressed as the fraction of respective untreated control (no PR73 treatment). Data shown are the mean ± SEM of 3 independent experiments. For A and B statistical analysis employed the two-tailed one-sample t-test using 1 as the comparison (***P<0.001, **P<0.01, *P<0.05). C) Microscopy of WT and mutant cells 24 hours ± PR73 treatment.

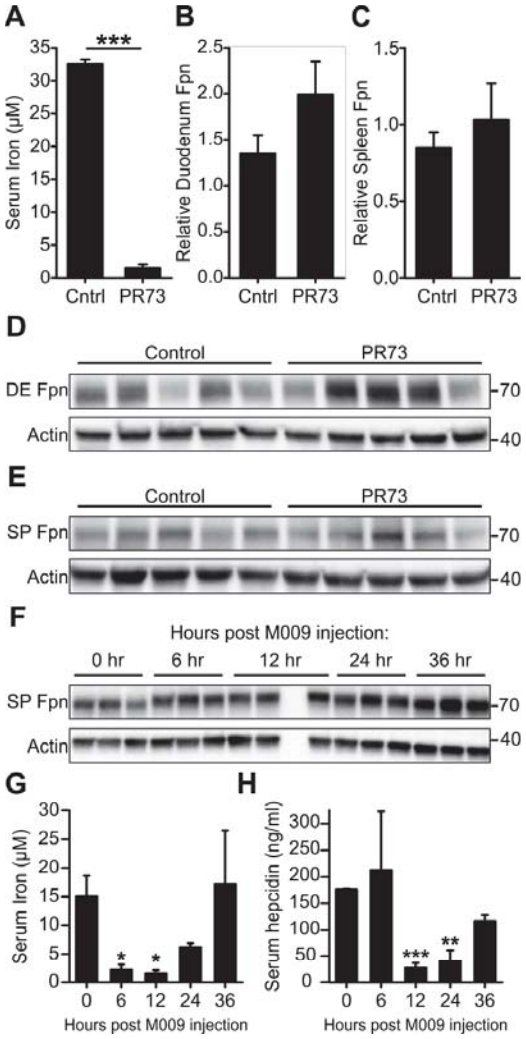


Figure S14: *In vivo* Fpn levels do not change after minihepcidin administration despite drastic decrease in serum iron. (A-E) WT mice were injected two times with 60 nmoles of PR73 and analyzed 4 hours after the second injection. A) Serum iron. B) Quantitation of duodenal Fpn levels (corresponding to the Western blot in D, normalized to actin). C) Quantitation of splenic Fpn levels (corresponding to the Western blot in E, normalized to actin). A-C) Cntrl= control. D) Western blot of Fpn and actin in duodenal enterocytes. E) Western blot of Fpn and actin in spleen. (F-H) th3 mice received a single injection of M009 minihepcidin, and tissues were harvested after 0, 6, 12, 24 and 36 h. F) Western blot of Fpn in the spleen. G) Serum iron. H) Serum hepcidin. Graphs show the

mean ± SEM. For A, B, C, G and H, statistical analysis employed the two-tailed t-test using either the control (A-C) or the zero hour time point (G,H) for comparison (***P<0.001, **P<0.01, *P<0.05).

SUPPLEMENTAL REFERENCES

S1. Lok CY, Merryweather-Clarke AT, Viprakasit V, Chinthammitr Y, Srichairatanakool S, Limwongse C, Oleesky D, et al. Iron overload in the Asian community. Blood 2009;114:20-25.

S2. Sham RL, Phatak PD, West C, Lee P, Andrews C, Beutler E. Autosomal dominant hereditary hemochromatosis associated with a novel ferroportin mutation and unique clinical features. Blood Cells, Molecules, and Diseases 2005;34:157-161.

S3. Letocart E, Le GG, Majore S, Ka C, Radio FC, Gourlaouen I, De BC, et al. A novel missense mutation in SLC40A1 results in resistance to hepcidin and confirms the existence of two ferroportin-associated iron overload diseases. Br.J Haematol. 2009;147:379-385.

S4. Callebaut I, Joubrel R, Pissard S, Kannengiesser C, Gérolami V, Ged C, Cadet E, et al. Comprehensive functional annotation of 18 missense mutations found in suspected hemochromatosis type 4 patients. Human Molecular Genetics 2014;23:4479-4490.

S5. Wallace DF, Clark RM, Harley HA, Subramaniam VN. Autosomal dominant iron overload due to a novel mutation of ferroportin1 associated with parenchymal iron loading and cirrhosis. J Hepatol 2004;40:710-713.

S6. Pelucchi S, Mariani R, Salvioni A, Bonfadini S, Riva A, Bertola F, Trombini P, et al. Novel mutations of the ferroportin gene (SLC40A1): analysis of 56 consecutive patients with unexplained iron overload. Clin Genet 2008;73:171-178.

S7. Rivard SR, Lanzara C, Grimard D, Carella M, Simard H, Ficarella R, Simard R, et al. Autosomal dominant reticuloendothelial iron overload (HFE type 4) due to a new missense mutation in the FERROPORTIN 1 gene (SLC11A3) in a large French-Canadian family. Haematologica 2003;88:824-826.

S8. Mayr R, Griffiths WJ, Hermann M, McFarlane I, Halsall DJ, Finkenstedt A, Douds A, et al. Identification of mutations in SLC40A1 that affect ferroportin function and phenotype of human ferroportin iron overload. Gastroenterology 2011;140:2056-2063, 2063.

S9. Yamakawa N, Oe K, Yukawa N, Murakami K, Nakashima R, Imura Y, Yoshifuji H, et al. A Novel Phenotype of a Hereditary Hemochromatosis Type 4 with Ferroportin-1 Mutation, Presenting with Juvenile Cataracts. Intern Med 2016;55:2697-2701.

S10. Le Lan C, Mosser A, Ropert M, Detivaud L, Loustaud-Ratti V, Vital-Durand D, Roget L, et al. Sex and acquired cofactors determine phenotypes of ferroportin disease. Gastroenterology 2011;140:1199-1207 e1191-1192.

S11. Santos PC, Cancado RD, Pereira AC, Schettert IT, Soares RA, Pagliusi RA, Hirata RD, et al. Hereditary hemochromatosis: mutations in genes involved in iron homeostasis in Brazilian patients. Blood Cells Mol Dis 2011;46:302-307.
S12. Zaahl MG, Merryweather-Clarke AT, Kotze MJ, van der Merwe S, Warnich L, Robson KJ. Analysis of genes implicated in iron regulation in individuals presenting with primary iron overload. Hum Genet 2004;115:409-417.
S13. Lee PL, Gaasterland T, Barton JC. Mild iron overload in an African American man with SLC40A1 D270V. Acta Haematol 2012;128:28-32.
S14. Wallace DF, Dixon JL, Ramm GA, Anderson GJ, Powell LW, Subramaniam VN. A novel mutation in ferroportin implicated in iron overload. J.Hepatol. 2007;46:921-926.
S15. Arezes J, Jung G, Gabayan V, Valore E, Ruchala P, Gulig PA, Ganz T, Nemeth E, Bulut Y. Hepcidin-induced hypoferremia is a critical host defense mechanism against the siderophilic bacterium Vibrio vulnificus. Cell Host Microbe. 2015 Jan 14;17(1):47-57. doi: 10.1016/j.chom.2014.12.001.
S16. Qiao B, Sugianto P, Fung E, et al. Hepcidin-induced endocytosis of ferroportin is dependent on ferroportin ubiquitination. *Cell Metab*. 2012;15(6):918-924.
S17. Mitchell CJ, Shawki A, Ganz T, Nemeth E, Mackenzie B. Functional properties of human ferroportin, a cellular iron exporter reactive also with cobalt and zinc. *Am J Physiol Cell Physiol*. 2014;306(5):C450-459.
S18 Stefanova D, Raychev A, Arezes J, Ruchala P, Gabayan V, Skurnik M, Dillon BJ, Horwitz MA, Ganz T, Bulut Y, Nemeth E. Endogenous hepcidin and its agonists mediate resistance to selected infections by clearing non-transferrin-bound iron. Blood. 2017 Jul 20;130(3):245-257. doi: 10.1182/blood-2017-03-772715.
S19. Casu C, Oikonomidou PR, Chen H, Nandi V, Ginzburg Y, Prasad P, Fleming RE, Shah YM, Valore EV, Nemeth E, Ganz T, MacDonald B, Rivella S. Minihepcidin peptides as disease modifiers in mice affected by β-thalassemia and polycythemia vera. Blood. 2016 Jul 14;128(2):265-76. doi: 10.1182/blood-2015-10-676742.
S20. Kautz L, Gabayan V, Wang X, et al. Testing the iron hypothesis in a mouse model of atherosclerosis. Cell Rep. 2013;5(5):1436-1442.
S21. Aschemeyer S, Gabayan V, Ganz T, Nemeth E, Kautz L. Erythroferrone and matriptase-2 independently regulate hepcidin expression. Am J Hematol. 2017;92(5):E61-E63.

Conclusion

This dissertation comprehensively examined the role of iron and hepcidin in different infection models ranging from extracellular to intracellular and biofilm-forming bacteria. We demonstrate that iron overload greatly increases susceptibility to infection with Gram-negative pathogens, and that hepcidin is essential for innate immune response in the context of nutritional immunity. Hepcidin, however, was not universally protective and played no role in infection with intracellular macrophage-tropic *M. tuberculosis* or extracellular biofilm-forming *S. aureus*.

Hepcidin-induced hypoferremia was protective against *Y. enterocolitica* systemic infection, *K. pneumoniae* dissemination during pneumonia, and *E. coli* sepsis and the associated mortality. We showed that the role of hepcidin was not to decrease total body iron or total serum iron, but rather to prevent formation of non-transferrin bound iron (NTBI) in the plasma. Therefore, we propose that a siderophilic pathogen should be defined by the enhancement of pathogenicity by NTBI.

We demonstrate that hepcidin-induced hypoferremia is an effective mechanism in combating not only the rare classic siderophilic pathogen *Y. enterocolitica* but also clinically common *E. coli* and *K. pneumoniae*. These results suggest that many more bacteria than previously appreciated may behave as siderophilic. Furthermore, we propose that siderophilicity is not promoted exclusively by the lack of siderophores. We showed that hepcidin agonist minihepcidin prevents infection-associated mortality in hepcidin-deficient mice infected with *Y. enterocolitica*, *K. pneumoniae* and *E. coli.* This indicates that manipulation of iron status may have therapeutic potential as an alternative

to antibiotic treatment. We further determined that the protective effect of minihepcidin was related to ablation of serum NTBI.

Lastly, we provide further understanding of ferroportin structure and the interaction between hepcidin and ferroportin with the potential to therapeutically target this complex. We believe that our work greatly enhances the understanding of the role of iron in infection and provides potential novel directions for anti-infection therapy.